



Elvio João Leonardo

PRODUTO E RAZÃO DE VARIÁVEIS GENERALIZADAS DE
DESVANECIMENTO E APLICAÇÕES EM DESEMPENHO DE
SISTEMAS DE COMUNICAÇÕES

PRODUCT AND RATIO OF GENERALIZED FADING VARIABLES
AND APPLICATIONS IN THE PERFORMANCE OF
COMMUNICATION SYSTEMS

Campinas
2013

Universidade Estadual de Campinas
Faculdade de Engenharia Elétrica e de Computação

Elvio João Leonardo

PRODUTO E RAZÃO DE VARIÁVEIS GENERALIZADAS DE DESVANECIMENTO E APLICAÇÕES
EM DESEMPENHO DE SISTEMAS DE COMUNICAÇÕES

PRODUCT AND RATIO OF GENERALIZED FADING VARIABLES AND APPLICATIONS IN THE
PERFORMANCE OF COMMUNICATION SYSTEMS

Tese de doutorado apresentada ao Programa de Pós-Graduação em Engenharia Elétrica da Faculdade de Engenharia Elétrica e de Computação da Universidade Estadual de Campinas, para a obtenção do título de Doutor em Engenharia Elétrica. Área de concentração: Telecomunicações e Telemática.

Doctorate thesis submitted to Graduate Program in Electrical Engineering of the School of Electrical and Computer Engineering of the State University of Campinas, in order to earn the degree of Doctor in Electrical Engineering. Concentration area: Telecommunications and Telematics.

Orientador (Supervisor): Prof. Dr. Michel Daoud Yacoub.

Este exemplar corresponde à versão final da tese defendida pelo aluno, e orientada pelo Prof. Dr. Michel Daoud Yacoub

FICHA CATALOGRÁFICA ELABORADA PELA
BIBLIOTECA DA ÁREA DE ENGENHARIA E ARQUITETURA - BAE - UNICAMP

L553p Leonardo, Elvio João
Produto e razão de variáveis generalizadas de desvanecimento e aplicações em desempenho de sistemas de comunicações / Elvio João Leonardo. -- Campinas, SP: [s.n.], 2013.

Orientador: Michel Daoud Yacoub.
Tese de Doutorado - Universidade Estadual de Campinas, Faculdade de Engenharia Elétrica e de Computação.

1. Sistema de comunicação sem fio. 2. Radio - Transmissores e transmissão - Desvanecimento. I. Yacoub, Michel Daoud, 1955-. II. Universidade Estadual de Campinas. Faculdade de Engenharia Elétrica e de Computação. III. Título.

Título em Inglês: Product and ratio of generalized fading variables and applications in the performance of communication systems

Palavras-chave em Inglês: Wireless communication system, Radio - Transmitters and transmission - Fading

Área de concentração: Telecomunicações e Telemática

Titulação: Doutor em Engenharia Elétrica

Banca examinadora: Dalton Soares Arantes, Ailton Akira Shinoda, José Antônio Martins, Paulo Cardieri

Data da defesa: 08-02-2013

Programa de Pós Graduação: Engenharia Elétrica

COMISSÃO JULGADORA - TESE DE DOUTORADO

Candidato: Elvio João Leonardo

Data da Defesa: 8 de fevereiro de 2013

Título da Tese: "Produto e Razão de Variáveis Generalizadas de Desvanecimento e Aplicações em Desempenho de Sistemas de Comunicações"

Prof. Dr. Michel Daoud Yacoub (Presidente):

Prof. Dr. Ailton Akira Shinoda:

Dr. José Antônio Martins:

Prof. Dr. Paulo Cardieri:

Prof. Dr. Dalton Soares Arantes:

TO MY PARENTS,
TO MY WIFE, AND
TO MY CHILDREN.

Agradecimentos

Agradeço,

a Deus pelas bênçãos que tenho recebido durante toda a minha vida;

ao Prof. Michel pela acolhida e valorosa orientação;

aos professores da Faculdade de Engenharia Elétrica e de Computação (FEEC) pelos valiosos cursos oferecidos;

aos meus pais, sogro, sogra e cunhadas pelo apoio a minha esposa no cuidado dos meus filhos, naqueles momentos em que eu não pude ajudar; e

à Universidade Estadual de Maringá (UEM) e ao Departamento de Informática (DIN) pela oportunidade oferecida.

Resumo

As estatísticas da razão e do produto de variáveis aleatórias (VAs) são importantes para caracterizar sistemas de comunicação sem fio, sendo fundamental para avaliar seus respectivos desempenhos. Por exemplo, muitos parâmetros de desempenho para comunicações sem fio envolvem o cálculo da razão entre as potências dos sinais, como a razão sinal-interferência (SIR, na sigla em inglês). Se o sistema de comunicação opera em um canal com desvanecimento, a SIR envolve a relação entre VAs, escolhidas de acordo com o modelo desejado para o canal. A análise do produto de VAs tem também grande importância. Por exemplo, em sistemas *multi-hop* em fio, o canal aleatório entre a origem e destino pode ser modelado como o produto das VAs que descrevem o ganho do canal a cada pulso, assumindo que estes ganhos sejam estatisticamente independentes. Nestes sistemas, a probabilidade de interrupção de serviço pode também ser modelada como o produto de VAs. Além disso, o produto de VAs é também útil para modelar o canal *keyhole* em sistemas de entrada e saída múltiplas (MIMO, na sigla em inglês).

Nesta tese, são derivadas expressões simples, exatas, genéricas, para a função densidade de probabilidade (FDP) e função de distribuição cumulativa (FDC) para a razão e o produto de distribuições independentes e não identicamente distribuídas. Especificamente, são considerados: razões Hoyt/ η - μ , Rice/ η - μ , Rice/ κ - μ , η - μ / η - μ , η - μ / κ - μ , κ - μ / κ - μ , κ - μ / η - μ , e α - μ / α - μ ; e produtos η - $\mu \times \eta$ - μ , κ - $\mu \times \kappa$ - μ , η - $\mu \times \kappa$ - μ , e α - $\mu \times \alpha$ - μ . Estes resultados são utilizados em alguns exemplos de aplicação. Entre eles, incluem-se a análise da vazão do CSMA (em inglês, *Carrier Sense Multiple Access*) em ambientes de desvanecimento Rice, Hoyt, Nakagami- m , Rice e Hoyt combinados, η - μ e κ - μ . Além disso, a vazão do DCF (em inglês, *Distributed Coordination Function*) do IEEE 802.11 em ambientes de desvanecimento Hoyt, Rice e Nakagami- m também é apresentada. Finalmente, a razão de variáveis aleatórias independentes α - μ e sua aplicação na análise da capacidade de sistemas de compartilhamento de espectro são apresentadas.

Palavras-chaves: Sistemas de comunicação sem fio. Canais com desvanecimento. Desvanecimento α - μ . Desvanecimento η - μ . Desvanecimento κ - μ . Razão de variáveis aleatórias. Produto de variáveis aleatórias. Desempenho de sistemas de comunicação sem fio.

Abstract

The statistics of the ratio and the product of random variables (RVs) are important to characterize the wireless communication systems and it is key to assess their performance. For instance, many wireless communication performance measures involve the calculation of the ratio between signal powers, e.g., the signal-to-interference ratio (SIR). In cases when the communication system is operating over a non-deterministic channel, such as a wireless fading channel, the SIR involves the ratio of RVs, selected according to the channel model assumed. The statistics of the product of RVs have also great importance. For instance, in a multi-hop wireless system, the random channel from source to destination may be modeled as the product of the RVs that describe the channel gain at each individual hop, assuming that these gains are statistically independent. For such a system, the overall outage probability may also be modeled as the product of RVs, each describing once more the channel gain for the individual hops. Moreover, the product of RVs is also useful to model the keyhole channel of Multiple-Input Multiple-Output (MIMO) systems. In this thesis, general, simple, exact, closed-form and infinite series form expressions for the probability density function (PDF) and cumulative distribution function (CDF) for the ratio and the product of independent non-identically distributed (i.n.i.d.) fading RVs are derived. Specifically, the following are considered: ratios Hoyt/ η - μ , Rice/ η - μ , Rice/ κ - μ , η - μ / η - μ , η - μ / κ - μ , κ - μ / κ - μ , κ - μ / η - μ , and α - μ / α - μ ; and products η - $\mu \times \eta$ - μ , κ - $\mu \times \kappa$ - μ , η - $\mu \times \kappa$ - μ , and α - $\mu \times \alpha$ - μ . These results are used in a few application examples. They include the analysis of the throughput of Carrier Sense Multiple Access (CSMA) in Rice, Hoyt, Nakagami- m , combined Ride and Hoyt, η - μ and κ - μ fading channels. In addition, it is presented the throughput of the Distributed Coordination Function (DCF) of IEEE 802.11 in Hoyt, Rice, and Nakagami- m Fading Channels. The ratio of independent alpha-mu random variables and its application in the capacity analysis of spectrum sharing systems is also presented.

Keywords: Wireless communication systems. Fading channels. Fading channel α - μ . Fading channel η - μ . Fading channel κ - μ . Ratio of random variables. Product of random variables. Performance of wireless communication systems.

List of Figures

2.1	PDF of the ratio of Hoyt and η - μ random variables.	17
2.2	CDF of the ratio of Hoyt and η - μ random variables.	19
2.3	PDF of the ratio of Rice and η - μ random variables.	22
2.4	CDF of the ratio of Rice and η - μ random variables.	24
2.5	PDF of the ratio of Rice and κ - μ random variables.	29
2.6	CDF of the ratio of Rice and κ - μ random variables.	30
2.7	PDF of the ratio of η - μ random variables.	34
2.8	CDF of the ratio of η - μ random variables.	38
2.9	PDF of the ratio of η - μ and κ - μ random variables.	41
2.10	CDF of the ratio of η - μ and κ - μ random variables.	43
2.11	PDF of the ratio of κ - μ random variables.	45
2.12	CDF of the ratio of κ - μ random variables.	49
2.13	PDF of the ratio of κ - μ and η - μ random variables.	52
2.14	CDF of the ratio of κ - μ and η - μ random variables.	55
2.15	PDF of the ratio of α - μ random variables.	57
2.16	CDF of the ratio of α - μ random variables.	58
3.1	PDF of the product of η - μ random variables.	63
3.2	CDF of the product of η - μ random variables.	64
3.3	PDF of the product of κ - μ random variables.	68
3.4	CDF of the product of κ - μ random variables.	69
3.5	PDF of the product of η - μ and κ - μ random variables.	73
3.6	CDF of the product of η - μ and κ - μ random variables.	75
3.7	PDF of the product of α - μ random variables.	78
3.8	CDF of the product of α - μ random variables.	79
4.1	Throughput curves assuming incoherent addition of Nakagami-fading interfering packets and constant mean packet power, with $m_s = m_n = 0.5$. The dotted lines correspond to the original (wireline) channel where $z_0 \rightarrow \infty$	88

4.2	Throughput curves assuming incoherent addition of Nakagami-fading interfering packets and constant mean packet power with $\tilde{z}_0 = 5$ and $a = 0.1$. The dashed line correspond to the Rayleigh channel where $m_s = m_n = 1$. The dotted line correspond to the original (wireline) channel where $z_0 \rightarrow \infty$	89
4.3	Normalised offered traffic density defined by (4.25).	90
4.4	Throughput curves assuming incoherent addition of Nakagami-fading interfering packets and spatial coverage, with $m_s = m_n = 0.5$. The dotted lines correspond to the original (wireline) channel where $z_0 \rightarrow \infty$	91
4.5	Throughput curves assuming incoherent addition of Nakagami-fading interfering packets and spatial coverage with $z_0 = 10$ and $a = 0.1$. The dashed line correspond to the Rayleigh channel where $m_s = m_n = 1$. The dotted line correspond to the original (wireline) channel where $z_0 \rightarrow \infty$	91
4.6	Throughput S for coherent Hoyt channel with $\eta = \eta_s = \eta_n$. The dashed lines correspond to the Rayleigh channel. The dotted lines correspond to the original (wireline) channel.	101
4.7	CDFs of (4.47) and (4.51) with $\eta = \eta_s = \eta_n$. For (4.47) only curves with $n = 1$ apply. The dashed lines correspond to the Rayleigh channel.	102
4.8	Conditional capture probability for incoherent Hoyt channel with $\eta = \eta_s = \eta_n$. The dashed lines correspond to the Rayleigh channel.	102
4.9	Throughput S for incoherent Hoyt channel with $\eta = \eta_s = \eta_n$. The dashed lines correspond to the Rayleigh channel. The dotted lines correspond to the original (wireline) channel.	103
4.10	Throughput S for coherent Rice channel with $\kappa = \kappa_s = \kappa_n$. The dashed lines correspond to the Rayleigh channel. The dotted lines correspond to the original (wireline) channel.	110
4.11	CDF of (4.72) with $\kappa = \kappa_s = \kappa_n$. The dashed lines correspond to the Rayleigh channel.	115
4.12	Conditional capture probability for incoherent Rice channel with $\kappa = \kappa_s = \kappa_n$. The dashed lines correspond to the Rayleigh channel.	115
4.13	Throughput S for incoherent Rice channel with $\kappa = \kappa_s = \kappa_n$. The dashed lines correspond to the Rayleigh channel. The dotted lines correspond to the original (wireline) channel.	116
4.14	CDF of (4.92) with $\mu = \mu_s = \mu_i = \mu_n/n$ and $\eta = \eta_s = \eta_i = \eta_n$. The dashed lines correspond to the Hoyt channel where $\mu = 1/2$. The dotted lines correspond to the Rayleigh channel where $\mu = 1/2$ and $\eta = 1$	125
4.15	Throughput S for incoherent $\eta - \mu$ channel. The dotted lines correspond to the wireline channel ($z_0 \rightarrow \infty$)	125
4.16	CDF of (4.109) with $\mu = \mu_s = \mu_i = \mu_n/n$ and $\kappa = \kappa_s = \kappa_i = \kappa_n$. The dashed lines correspond to the Rice and Rayleigh channels, as indicated.	136
4.17	Throughput S for incoherent $\kappa - \mu$ channel with $\mu = \mu_s = \mu_i = \mu_n/n$ and $\kappa = \kappa_s = \kappa_i = \kappa_n$. The dashed lines correspond to the Rice and Rayleigh channels, as indicated. The dotted lines correspond to the wireline channel ($z_0 \rightarrow \infty$). . .	137

4.18	Outage probability for incoherent combined Rice and Hoyt channel. The dashed lines correspond to the Rayleigh channel ($\kappa_s = 0$ and $\eta_n = 1$).	147
4.19	Throughput S for incoherent combined Rice and Hoyt channel with perfect power control. The dashed lines correspond to the Rayleigh channel ($\kappa_s = 0$ and $\eta_n = 1$). The dotted lines correspond to the wireline channel ($z_0 \rightarrow \infty$).	149
4.20	Outage probability versus Q_{pk} for different fading conditions.	158
4.21	Ergodic capacity versus Q_{avg} for different fading conditions.	159
4.22	Outage probability for incoherent Hoyt channel with $\eta = \eta_s = \eta_n$. The dashed lines correspond to the Rayleigh channel ($\eta = 1$).	187
4.23	Outage probability for incoherent Rice channel with $\kappa = \kappa_s = \kappa_n$. The dashed lines correspond to the Rayleigh channel ($\kappa = 0$).	188
4.24	Outage probability for incoherent Nakagami- m channel with $m = m_s = m_i$. The dashed lines correspond to the Rayleigh channel ($m = 1$).	188
4.25	Throughput S for IEEE 802.11 DCF with 2-way handshake, incoherent Hoyt channel, perfect power control and $\eta = \eta_s = \eta_i = \eta_n$. The dashed lines correspond to the Rayleigh channel ($\eta = 1$)	189
4.26	Throughput S for IEEE 802.11 DCF with 2-way handshake, incoherent Rice channel, perfect power control and $\kappa = \kappa_s = \kappa_i = \kappa_n$. The dashed lines correspond to the Rayleigh channel ($\kappa = 0$).	189
4.27	Throughput S for IEEE 802.11 DCF with 2-way handshake, incoherent Nakagami- m channel, perfect power control and $m = m_s = m_i = m_n/n$. The dashed lines correspond to the Rayleigh channel ($m = 1$).	190
4.28	Throughput S for IEEE 802.11 DCF with 2-way handshake, incoherent Hoyt, Rice, Nakagami- m and Rayleigh channels with perfect power control, $\eta = \eta_s = \eta_i = \eta_n$, $\kappa = \kappa_s = \kappa_i = \kappa_n$ and $m = m_s = m_i = m_n/n$, $\tilde{\tau} = 0.01$, $N = 4$, $\tilde{z}_0 = 6$ dB and $P_e = 0$	190
4.29	Throughput S for IEEE 802.11 DCF with 2-way handshake, incoherent Nakagami- m channel with spatial coverage, $m = m_s = m_i = m_n/n$ and $\tilde{\tau} = 0.01$. The dashed lines correspond to the Rayleigh channel ($m = 1$). The dotted lines correspond to CSMA/CA.	191
4.30	Throughput S for IEEE 802.11 DCF with 2-way handshake, incoherent Nakagami- m channel with spatial coverage, $m = m_s = m_i = m_n/n$, $\tilde{\tau} = 0.01$, $N = 10$, $\tilde{z}_0 = 6$ dB and $P_e = 0$. The dashed lines correspond to the Rayleigh channel ($m = 1$).	191

List of Tables

1.1	Path loss exponent values for different environments [1].	4
1.2	Sample of path loss exponent and log-normal shadowing standard deviation values for urban or suburban.	5
2.1	Relation between number of terms and accuracy in the infinite summation of (2.7) and (2.14).	18
2.2	Relation between number of terms and accuracy in the infinite summation of (2.19) and (2.29).	25
2.3	Relation between number of terms and accuracy in the infinite summation of (2.34) and (2.41).	30
2.4	Relation between number of terms and accuracy in the infinite summation of (2.46) and (2.54).	35
2.5	Relation between number of terms and accuracy in the infinite summation of (2.59) and (2.66).	40
2.6	Relation between number of terms and accuracy in the infinite summation of (2.71) and (2.78).	46
2.7	Relation between number of terms and accuracy in the infinite summation of (2.83) and (2.91).	51
3.1	Relation between number of terms and accuracy in the infinite summation of (3.9) and (3.10).	64
3.2	Relation between number of terms and accuracy in the infinite summation of (3.17) and (3.20).	69
3.3	Relation between number of terms and accuracy in the infinite summation of (3.27) and (3.30).	74
4.1	Relation between number of terms and accuracy in the summations of (4.47) and (4.51). For (4.47), only entries with $n = 1$ apply.	100
4.2	Relation between number of terms and accuracy in the infinite summation of (4.72).	113
4.3	Relation between number of terms and accuracy in the infinite summation of (4.92).	124
4.4	Relation between number of terms and accuracy in the infinite summation of (4.109).	134

4.5	Relation between number of terms and accuracy in the infinite summation of (4.134) and (4.137).	148
4.6	Relation between number of terms and accuracy in the infinite summation of (4.194).	185
4.7	Relation between number of terms and accuracy in the infinite summation of (4.201).	186
4.8	Typical network parameters.	187

Contents

1	Introduction	1
1.1	Mobile Radio Channel	2
1.1.1	Path Loss	3
1.1.2	Shadowing	4
1.1.3	Multipath Fading	5
1.2	Motivation	11
1.3	Literature Survey	12
1.4	Thesis Outline	14
2	Ratio of Random Variables	15
2.1	Introduction	15
2.2	Ratio Hoyt/ η - μ	16
2.2.1	Probability Density Function	16
2.2.2	Cumulative Distribution Function	19
2.3	Ratio Rice/ η - μ	21
2.3.1	Probability Density Function	22
2.3.2	Cumulative Distribution Function	26
2.4	Ratio Rice/ κ - μ	28
2.4.1	Probability Density Function	28
2.4.2	Cumulative Distribution Function	31
2.5	Ratio η - μ / η - μ	33
2.5.1	Probability Density Function	33
2.5.2	Cumulative Distribution Function	36
2.6	Ratio η - μ / κ - μ	38
2.6.1	Probability Density Function	39
2.6.2	Cumulative Distribution Function	42
2.7	Ratio κ - μ / κ - μ	44
2.7.1	Probability Density Function	44
2.7.2	Cumulative Distribution Function	47
2.8	Ratio κ - μ / η - μ	49
2.8.1	Probability Density Function	50

2.8.2	Cumulative Distribution Function	53
2.9	Ratio $\alpha\text{-}\mu/\alpha\text{-}\mu$	55
2.9.1	Probability Density Function	56
2.9.2	Cumulative Distribution Function	57
3	Product of Random Variables	61
3.1	Introduction	61
3.2	Product $\eta\text{-}\mu \times \eta\text{-}\mu$	62
3.2.1	Probability Density Function	62
3.2.2	Cumulative Distribution Function	65
3.3	Product $\kappa\text{-}\mu \times \kappa\text{-}\mu$	66
3.3.1	Probability Density Function	67
3.3.2	Cumulative Distribution Function	70
3.4	Product $\eta\text{-}\mu \times \kappa\text{-}\mu$	71
3.4.1	Probability Density Function	71
3.4.2	Cumulative Distribution Function	75
3.5	Product $\alpha\text{-}\mu \times \alpha\text{-}\mu$	77
3.5.1	Probability Density Function	77
3.5.2	Cumulative Distribution Function	79
4	Application Examples	81
4.1	Capacity of CSMA under Nakagami Fading	81
4.1.1	Introduction	81
4.1.2	Analytical Model	82
4.1.3	Analytical Results	86
4.1.4	Numerical Results	92
4.1.5	Conclusions	93
4.2	Throughput of CSMA in Hoyt Fading Channels	94
4.2.1	Introduction	94
4.2.2	Analytical Model	95
4.2.3	Results	100
4.2.4	Conclusion	105
4.3	Throughput of CSMA in Rice Fading Channels	106
4.3.1	Introduction	106
4.3.2	Analytical Model	107
4.3.3	Results	112
4.3.4	Conclusion	117
4.4	Throughput of CSMA in $\eta\text{-}\mu$ Fading Channels	118
4.4.1	Introduction	118
4.4.2	Analytical Model	119
4.4.3	Results	123
4.4.4	Conclusion	127
4.5	Throughput of CSMA in $\kappa\text{-}\mu$ Fading Channels	128

4.5.1	Introduction	128
4.5.2	Analytical Model	129
4.5.3	Results	133
4.5.4	Conclusion	137
4.5.5	Calculation	138
4.6	Throughput of CSMA in a Rice-Signal with Hoyt-Interference Environment . . .	139
4.6.1	Introduction	139
4.6.2	Analytical Model	140
4.6.3	Analytical Results	146
4.6.4	Numerical Results	150
4.6.5	Conclusions	151
4.7	The Ratio of Independent Arbitrary α - μ Random Variables and its Application in the Capacity Analysis of Spectrum Sharing Systems	151
4.7.1	Introduction	151
4.7.2	Ratio of Independent Arbitrary α - μ RVs	152
4.7.3	Application Example: Capacity Analysis of Spectrum Sharing Systems .	155
4.7.4	Numerical Results and Discussions	161
4.8	Exact Formulations for the Throughput of IEEE 802.11 DCF in Hoyt, Rice, and Nakagami- m Fading Channels	163
4.8.1	Introduction	163
4.8.2	Framework	166
4.8.3	System Model	169
4.8.4	Analytical Results	173
4.8.5	Numerical Results	181
4.8.6	Conclusions	184
5	Conclusions and Perspectives	193
5.1	Contributions	193
5.2	Future Works	194
	Bibliography	196

Introduction

The widespread use of mobile communications, made possible by the deployment of cellular telephone systems, has substantially altered and extended our capacity and opportunity to communicate with one another. It has become a technological milestone, capable of influencing directly our daily life, even in poorer communities where some basic services may still lack. Nowadays, for a large number of people, access to a wireless communication network has become indispensable, and a personal radio communication terminal part of their survival tool kit.

Given its importance, it is not a surprise to see that the mobile radio communication is a growing and very competitive industry. Consumers are enticed by an ever increasing range of services being offered, and they are demanding new applications and higher quality for the existing ones. In fact, mobile phones have grown from their original voice communication function to become a device delivering broad multimedia content, including, among others, music, games, video and internet.

The evolution of the industry has been stimulated by the remarkable advance in signal processing techniques, radio frequency circuit design, semiconductor fabrication technologies, software development methodologies, and system architectures. These technological advances have enabled increased user mobility, larger system capacity, and higher efficiency, allowing larger revenue for the service provider and lower rates for the consumer. As already hinted, the development of a personal radio communication system involves contributions from several fields of knowledge and it is indeed a complex task. In this work, a very important part of

this problem is considered, i.e., the wireless channel which connects the radio transmitter to the receiver.

1.1 Mobile Radio Channel

In mobile radio systems, the wireless channel is commonly considered to include a large number of scatterers, and the propagation between the transmitting antenna and the mobile terminal antenna occurs through multiple paths [2][3]. This situation may or may not include a component on a direct line-of-sight (LOS) path. In any case, along each path, the electromagnetic wave may interact with obstacles producing a component with its own amplitude, phase, distance (or delay) and direction. Possible interactions include reflection on large surfaces, scattering from small¹ objects, diffraction around small obstacles, transmission through walls or floors, and shadowing by trees and other obstructions [4]. At the receiver's antenna, these (mostly uncorrelated) components combine constructively or destructively to produce a signal that shows variations in both amplitude and phase. This scenario is aggravated if the receiver or the scatterers are moving, which is a likely situation, and a dynamic temporal behaviour should be added to the channel. At the end, a difficult receiving condition is established, with the presence of energy fading, inter-symbol-interference (ISI), cross-channel-interference (CCI) and Doppler effect, and where signal fades of 40 dB or more below the average signal level are not uncommon [5].

The received signal, produced by the combination at the receiver's antenna of waves arriving from different paths, can only be modelled deterministically in some simple cases. A precise mathematical description of this event, which almost certainly includes an unknown number of scatterers, is too complex for tractable analysis. Therefore, due to the complexity of the propagation phenomena and due to the statistical nature of the radio channel parameters, a reliable channel characterisation should make use of statistical analysis. The efforts towards this characterization have produced a number of relatively simple and accurate models which depend on the particular propagation environment. In general, the radio propagation analysis breaks

¹Large and small should be understood with respect to the wavelength of the carrier signal.

the problem in the following parts: path loss, shadowing or long-term fading, and multipath or short-term fading [2]. The path loss gives the mean received signal level, whereas the shadowing produces gradual but random changes in the local mean with granularity in the tens of meters. The multipath fading causes the received signal to vary rapidly, even with small displacements of the receiver terminal. In the following, each of these parts is described briefly.

1.1.1 Path Loss

Path loss refers to the attenuation of the electromagnetic wave while propagating through space, from the transmitter to the receiver antenna. It is caused by dissipation of the radiated power as well as other effects, such as absorption. The simplest of such model, the free space loss, considers the existence of only the direct LOS link between the transmitter and receiver. Under this model, the received signal power P_R is given as

$$P_R = P_T G_T G_R \left(\frac{\lambda}{4\pi d} \right)^2 \quad (1.1)$$

in which P_T is the transmitted power, G_T and G_R are the transmit and receive antennas gains, respectively, λ is the transmitted carrier wavelength, and d is the distance between the antennas. It can be seen that the received power decreases with the square of the distance under free space propagation. Also, shorter carrier wavelength, or equivalently higher carrier frequency, translates into higher path loss.

Although conveniently simple, the free space path loss alone is not an accurate model to describe most propagation scenarios. Additions to the basic model have been proposed by Okumura, Hata, among others [6][7], for propagation in urban, rural, and indoor areas. Also, experiments have indicated that the path loss exponent, i.e., the distance exponent in (1.1), depends on the specific propagation environment, as illustrated in Tables 1.1 [1] and 1.2, which shows higher attenuation than that found in free space propagation for most locations. In any case, it can be seen that the path loss given by (1.1) is constant at a given distance, which is a somewhat simplistic assumption.

Table 1.1: Path loss exponent values for different environments [1].

Environment	Path Loss Exponent
Free space	2
Urban area cellular radio	2.7 to 3.5
Shadowed urban cellular radio	3 to 5
In building, LOS	1.6 to 1.8
Obstructed in building	4 to 6

1.1.2 Shadowing

The presence of obstacles that are larger than the carrier wavelength, such as hills, buildings and trees, obstructs the direct path between transmitter and receiver. In such a case, the receiver is in the shadow of the transmitted signal, and only the diffracted waves are able to reach its antenna. Accordingly, this phenomenon is often called shadowing, and it results in changes of the signal strength, even if measured at points that are at equal distances from the transmitter.

Experimental results show that shadowing can be fairly accurately modelled as a log-normal random variable [2]. In other words, the envelope of the received signal under shadowing behaves as a Gaussian (Normal) random variable if the variable is expressed in the logarithmic scale, for instance, in dB. Thus, the probability density function (PDF) of the signal envelope r may be given by

$$f_R(r) = \frac{1}{\sqrt{2\pi}\sigma} \exp \left[-\frac{1}{2} \left(\frac{r - \mu}{\sigma} \right)^2 \right] \quad (1.2)$$

in which μ is the average value, σ is the standard deviation, with r , μ and σ expressed in dB. The value of μ usually represents the path loss estimates for the desired location, whereas the value of σ is often obtained by empirical measurements, with typical values in the range 5-12 dB [8], as shown in Table 1.2. In addition, measurements have indicated that shadowing exhibits spatial correlation, i.e., the fading is correlated over short distances, typically within 10 to 50 m [8].

Table 1.2: Sample of path loss exponent and log-normal shadowing standard deviation values for urban or suburban.

Environment	Path Loss Exponent	Standard Deviation
German cities [9]	2.4 to 3.8	7.1 to 13.1 dB
San Francisco Bay, USA [10]	2.6 to 2.7	7.7 to 9.3 dB
Residential, USA [11]	2.7 to 3.6	3.1 to 10.2 dB
Suburban, United States [12]	3.6 to 4.6	8.2 to 10.6 dB
Residential, Boulder, USA [13]	2.0 (LOS)	6.9 dB (LOS)
	3.5 (non LOS)	9.5 dB (non LOS)
Dense urban, Chicago, USA [14]	3.9	9.5 dB
Suburban, Helsinki, Finland [15]	4.0	6.1 dB

1.1.3 Multipath Fading

Multipath fading can cause deep fades in the signal strength within small distances or short periods of time and, accordingly, it is also referred to as short-term fading. Mainly, multipath fading can be caused by *(i)* multipath propagation, *(ii)* Doppler effect, and *(iii)* selective fading. Multipath propagation, with the combination at the receiver's antenna of different waves, each showing random amplitude and phase, can cause significant fluctuations of the received envelope. Also, the relative motion between the transmitter and the receiver can cause random frequency modulation, because of the effect of different Doppler shifts on each of the multipath components. The speed of surrounding objects may also alter the multipath components and their Doppler shifts, also significantly influencing the received signal. Finally, if the bandwidth of the transmitted signal is larger than the channel bandwidth, then selective fading might occur.

Multipath fading is usually modelled by a random variable with a certain probability distribution. A number of distributions, including the Rayleigh, Rice [16] (also known as Nakagami- n), Hoyt [17] (also known as Nakagami- q) and Nakagami- m [18], have been used for a few decades and are well established. In particular, the Nakagami- m distribution has attracted significant interest because of its analytical tractability and scope, although it was initially proposed without a physical model to support it. There have been, however, situations for which either of these distributions seems to provide only moderate statistical fit. As a result, work has been

done aimed at formulating broader models, able to include aspects of the channel that might have been neglected in these earlier efforts. Among the recent entries to the multipath family, the η - μ , κ - μ [19] and α - μ [20] distributions should be mentioned, which might be seen as generalizations of the traditional distributions. In the following, the multipath fading models relevant to this work are described briefly.

Rayleigh Fading Model

The Rayleigh fading [2] is, probably, the most used model for characterization of multipath fading in a non-frequency selective channel. It assumes a multipath propagation environment with a large number of scatterers and without LOS signal, resulting in a signal amplitude that follows the Rayleigh distribution.

Consider the received signal envelope, with amplitude R and phase Θ , defined as the sum of an arbitrary number n of scattered waves with random amplitudes and phases A_i and Θ_i , $i = 1, 2, \dots, n$, respectively. Clearly,

$$Re^{j\Theta} = \sum_{i=1}^n A_i e^{j\Theta_i} = X + jY \quad (1.3)$$

in which

$$X \triangleq \sum_{i=1}^n A_i \cos(\Theta_i), \text{ and } Y \triangleq \sum_{i=1}^n A_i \sin(\Theta_i) \quad (1.4)$$

are the in-phase and quadrature components of the signal envelope, respectively. If it is assumed that n is large and that the phases Θ_i are uniformly distributed between 0 and 2π , it results that, using the central limit theorem, X and Y are uncorrelated Gaussian variates with zero mean and equal variance σ^2 . In addition, knowing that $R^2 = X^2 + Y^2$, the density $f_R(r)$ can be calculated as the PDF of the Rayleigh distribution and expressed by

$$f_R(r) = \frac{r}{\sigma^2} \exp\left(-\frac{r^2}{2\sigma^2}\right). \quad (1.5)$$

Rice Fading Model

The Rice fading model assumes that the received signal is the result of a dominant component (such as a direct LOS signal) added to a large number of multipath scattered waves. Therefore, the analysis is similar to the Rayleigh fading channel introduced above, with the addition of the LOS component. Let the scattered components be represented by two independent Gaussian variates, denoted X and Y , both with zero mean and equal variance σ^2 . The in-phase and quadrature components of the signal envelope in a Rice fading channel can be expressed as $X + a$ and Y , respectively, where the constant a represents the envelope of the dominant signal (also, the mean value for the in-phase component). The PDF of the received signal envelope can be expressed as [16]

$$f_R(r) = \frac{r}{\sigma^2} \exp\left(-\frac{r^2 + a^2}{2\sigma^2}\right) I_0\left(\frac{ar}{\sigma^2}\right) \quad (1.6)$$

in which $I_\nu(\cdot)$ is the modified Bessel function of the first kind and ν -th order [21, Eq. 9.6.10].

Let $\kappa \triangleq \frac{a^2}{2\sigma^2}$ be defined as power ratio between the dominant and scattered signals. In addition, note that the mean square value $E(R^2) \triangleq \hat{r}^2 = a^2 + 2\sigma^2 = 2\sigma^2(\kappa + 1)$, in which $E(\cdot)$ is the expectation operator. Using the values above, the envelope PDF in (1.6) may be rewritten as

$$f_R(r) = \frac{2(\kappa + 1)}{e^\kappa} \frac{r}{\hat{r}^2} \exp\left[-(\kappa + 1)\frac{r^2}{\hat{r}^2}\right] I_0\left[2\sqrt{\kappa(\kappa + 1)}\frac{r}{\hat{r}}\right]. \quad (1.7)$$

It is easy to see that if κ is set to zero, thus eliminating the dominant component, (1.7) simplifies to the Rayleigh PDF; and if $\kappa \rightarrow \infty$, the non-fading situation is obtained.

Hoyt Fading Model

The Hoyt fading model assumes that the received signal is the result of the sum of a large number of multipath scattered waves, without the prevalence of a single component (for instance, the LOS signal). However, differently from the Rayleigh fading channel, the variances of the in-phase and quadrature components of the signal envelope may be different. Accordingly, let X and Y be two independent Gaussian variates with zero mean and variances σ_x^2 and σ_y^2 ,

respectively. The PDF of the received signal envelope can be expressed as [17]

$$f_R(r) = \frac{r}{\sigma_x \sigma_y} \exp \left[-\frac{r^2}{4} \left(\frac{1}{\sigma_x^2} + \frac{1}{\sigma_y^2} \right) \right] I_0 \left[\frac{r^2}{4} \left(\frac{1}{\sigma_y^2} - \frac{1}{\sigma_x^2} \right) \right]. \quad (1.8)$$

Let the power ratio between the in-phase and quadrature signals be defined as $\eta \triangleq \frac{\sigma_x^2}{\sigma_y^2}$. Also, let the parameters h and H be defined as

$$h \triangleq \frac{1}{4} \left(\frac{1}{\sqrt{\eta}} + \sqrt{\eta} \right)^2 \quad \text{and} \quad H \triangleq \frac{1}{4} \left(\frac{1}{\eta} - \eta \right). \quad (1.9)$$

In addition, note that the mean square value $E(R^2) \triangleq \hat{r}^2 = \sigma_x^2 + \sigma_y^2$. Using the values above, the envelope PDF in (1.8) may be rewritten as

$$f_R(r) = 2\sqrt{h} \frac{r}{\hat{r}^2} \exp \left(-h \frac{r^2}{\hat{r}^2} \right) I_0 \left(H \frac{r^2}{\hat{r}^2} \right). \quad (1.10)$$

It is easy to see that if η is set to unity, thus making $h = 1$ and $H = 0$, (1.10) simplifies to the Rayleigh PDF; and if $\eta \rightarrow 0$ or $\eta \rightarrow \infty$, the one-sided Gaussian PDF is obtained.

Nakagami- m Fading Model

The Nakagami- m fading model was inferred by Nakagami from experimental data. The PDF of the signal envelope R is given by [18]

$$f_R(r) = \frac{2r^{2m-1}}{\Gamma(m)} \left(\frac{m}{\hat{r}^2} \right)^m \exp \left(-\frac{mr^2}{\hat{r}^2} \right) \quad (1.11)$$

in which $\hat{r}^2 \triangleq E(R^2)$ is the mean square value, $m \triangleq \frac{E^2(R^2)}{\text{Var}(R^2)} > 0$ is a fading parameter, $\text{Var}(\cdot)$ is the variance operator, and $\Gamma(\cdot)$ is the gamma function [21, Eq. 6.1.1]. For $m = 1/2$, the Nakagami distribution reduces to the one-sided Gaussian PDF; for $m = 1$, it reduces to the Rayleigh PDF whereas $m \rightarrow \infty$ corresponds to a non-fading situation.

η - μ Fading Model

The η - μ fading model was introduced by Yacoub [19], and it is presented in two equivalent formats, numbered by the author 1 and 2. For the sake of simplicity, only the format 1 is considered here. The model considers a signal composed by an arbitrary number n of clusters of multipath waves propagating in a nonhomogeneous environment. The signal envelope R , written in terms of the in-phase and quadrature components, can be expressed as

$$R^2 = \sum_{i=1}^n (X_i^2 + Y_i^2) \quad (1.12)$$

in which X_i and Y_i are independent Gaussian variates with zero mean and variances σ_x^2 and σ_y^2 , respectively. The PDF of the received signal envelope can be expressed as [19]

$$f_R(r) = \frac{4\sqrt{\pi}\mu^{\mu+\frac{1}{2}}h^\mu r^{2\mu}}{\Gamma(\mu)H^{\mu-\frac{1}{2}}\hat{r}^{2\mu+1}} \exp\left(-2\mu h \frac{r^2}{\hat{r}^2}\right) I_{\mu-\frac{1}{2}}\left(2\mu H \frac{r^2}{\hat{r}^2}\right) \quad (1.13)$$

in which $\mu \triangleq \frac{E^2(R^2)}{\text{Var}(R^2)} \left(1 + \frac{H^2}{h^2}\right) > 0$ is the real extension of $\frac{n}{2}$, $\eta \triangleq \frac{\sigma_x^2}{\sigma_y^2}$ is the power ratio between the in-phase and quadrature signals, h and H are defined in (1.9), and $\hat{r}^2 \triangleq E(r^2)$ is the mean square value.

It is easy to see that if μ is set to $\frac{1}{2}$, (1.13) reduces to the Hoyt PDF; if $\eta \rightarrow 0$ or $\eta \rightarrow \infty$ it reduces to the Nakagami- m with $m = \mu$; and if $\mu = \frac{1}{2}$ and $\eta = 1$, it reduces to the Rayleigh PDF.

κ - μ Fading Model

Similarly to the η - μ model described above, the κ - μ fading model also considers a signal composed by an arbitrary number n of clusters of multipath waves propagating in a nonhomogeneous environment. The signal envelope R , written in terms of the in-phase and quadrature components, can be expressed as

$$R^2 = \sum_{i=1}^n [(X_i + p_i)^2 + (Y_i + q_i)^2] \quad (1.14)$$

in which X_i and Y_i are independent Gaussian variates with zero mean and equal variance σ^2 , and p_i and q_i are the mean values of the in-phase and quadrature components of cluster i , respectively. The PDF of the received signal envelope can be expressed as [19]

$$f_R(r) = \frac{2\mu(\kappa + 1)^{\frac{\mu+1}{2}} r^\mu}{\kappa^{\frac{\mu-1}{2}} e^{\mu\kappa\hat{r}^{\mu+1}}} \exp\left[-\mu(\kappa + 1)\frac{r^2}{\hat{r}^2}\right] I_{\mu-1}\left(2\mu\sqrt{\kappa(\kappa + 1)}\frac{r}{\hat{r}}\right) \quad (1.15)$$

in which $\mu \triangleq \frac{E^2(R^2)(2\kappa+1)}{\text{Var}(R^2)(\kappa+1)^2} > 0$ is the real extension of n , $\kappa \triangleq \frac{\sum_{i=1}^n (p_i^2 + q_i^2)}{2n\sigma^2} > 0$ is the ratio between the total power of the dominant components and the total power of the scattered waves, and $\hat{r}^2 \triangleq E(r^2)$ is the mean square value.

It is easy to see that if μ is set to unity, (1.15) reduces to the Rice PDF; if $\kappa \rightarrow 0$, it reduces to the Nakagami- m PDF with $m = \mu$; and if $\mu = 1$ and $\kappa \rightarrow 0$, it reduces to the Rayleigh PDF.

α - μ Fading Model

The α - μ fading model assumes that the received signal is composed by an arbitrary number n of multipath components, propagating over an environment in which the resulting signal envelope is a nonlinear summation of the modulus of these components. Also, suppose that the nonlinearity is given as a power parameter $\alpha > 0$. The resulting envelope R may be expressed by

$$R^\alpha = \sum_{i=1}^n (X_i^2 + Y_i^2) \quad (1.16)$$

in which X_i and Y_i are independent Gaussian variates with zero mean and equal mean square values $E(X_i^2) = E(Y_i^2) \triangleq \frac{\hat{r}^\alpha}{2n}$. The PDF of the received signal envelope can be expressed as [20]

$$f_R(r) = \frac{\alpha\mu^\mu r^{\alpha\mu-1}}{\Gamma(\mu)\hat{r}^{\alpha\mu}} \exp\left(-\mu\frac{r^\alpha}{\hat{r}^\alpha}\right) \quad (1.17)$$

in which $\mu \triangleq \frac{E^2(R^\alpha)}{\text{Var}(R^\alpha)} > 0$ is the real extension of n .

It is easy to see that if μ is set to unity, (1.17) reduces to the Weibull PDF; if $\mu = 1$ and $\alpha = 1$, it reduces to the negative exponential PDF; if $\mu = 1$ and $\alpha = 2$, it reduces to the Rayleigh PDF; and if $\alpha = 2$, it reduces to the Nakagami- m PDF with $m = \mu$.

1.2 Motivation

In wireless communications, the propagation phenomena involved are mostly described by fading models with parameters determined by experimental measurements. These models are used in the design and verification of wireless systems as well as in devising fading mitigation techniques. With increasing usage and growing range of services, the performance and reliability of wireless systems are becoming an ever greater challenge. Therefore, it is of fundamental importance the formulation of accurate channel models to be used in all phases of the system design and deployment, so that it would be possible to design optimal or near-optimal communications systems for the given restrictions.

In addition to the selection of the fading variables in accordance to the channel measurements, a number of issues require knowledge of the ratio and product of these variables. For instance, the statistical analysis of the ratio of random variables is a topic of interest in a wide number of fields beyond wireless communications, including biological and physical sciences, econometrics, and ranking and selection [22]. Particularly in wireless communications, many performance measures involve the calculation of the ratio between signal powers. A relation typically of interest is the signal-to-interference ratio (SIR), i.e., the quotient of the desired signal power and the interference power. In cases when the communication system is operating over a non-deterministic channel, such as a wireless fading channel, the SIR involves the ratio of random variables (RVs) [2][3].

The statistics of the product of RVs have also great importance. For instance, the product of the Rayleigh and Gamma variables is used to model high resolution synthetic aperture radar (SAR) clutter [23]. In addition, in wireless transmission, where the signal is subject to joint shadowing and multipath fading, the signal envelope can be modelled as the product of the two random variables involved [24]. Also, in a multi-hop wireless system, the random channel from source to destination may be modelled as the product of the RVs that describe the channel gain at each individual hop, assuming that these gains are statistically independent. For such a system, the overall outage probability may also be modelled as the product of RVs, each describing once more the channel gain for the individual hops. Moreover, the product of RVs is

also useful to model the keyhole channel of Multiple-Input Multiple-Output (MIMO) systems [25].

Consequently, it is fair to say that the statistics of the ratio and the product of RVs are important to characterize the wireless communication systems and it is key to assess their performance. In this thesis, general, simple, exact, closed-form and infinite series form expressions for the probability density function (PDF) and cumulative distribution function (CDF) for the ratio and the product of independent non-identically distributed (i.n.i.d.) fading RVs are derived. Specifically, the following distributions are considered: Rice [16], Hoyt [17], Nakagami- m [18], α - μ [20], η - μ and κ - μ [19]. These results find applicability in several performance analysis of wireless communication systems. As examples, a few of these applications are included in this thesis.

1.3 Literature Survey

The analysis of the ratio and the product of random variables has always been an active research topic. Considering only distributions important to wireless communications, a few of the relevant works are listed below, with emphasis to those published recently.

In [26], the authors investigate the product of i.i.d. random variables using the Mellin transform, with particular interest in Gaussian, negative exponential, Weibull and gamma distributions. The benefit of using the Mellin transform is that the product of i.i.d random variables is equal to the product of the Mellin transforms of the individual random variables. This artifice has also been explored in [27][28], among others. However, the inverse Mellin transform is a contour integral and it is usually of difficult solution.

In [29], the authors calculate the ratio of negative exponential variates and use the result to estimate the capacity slotted Aloha under Rayleigh fading channels. The follow up of this work is presented in [30], where the capacity of slotted Aloha under Nakagami- m fading channels is considered, using ratio of squared Nakagami- m random variables.

In [31], the authors derive the PDF of the ratio of two independent and same-family distributions of power-quadratic exponential type, such as the Gamma distribution. The PDF

and the CDF for the linear combination and the ratio of independent exponential and Rayleigh distributions is presented in [32]. In [33], the authors calculate the CDF of the ratio of weighted exponential random variables in order to assess the interference in broadcast systems. The PDF and CDF of the ratio $(\sum_{i=1}^L X_i)^2 / (\sum_{i=1}^L b_i X_i)$, in which b_i are positive scalars, and X_i , $i = 1, 2, \dots, L$, are i.i.d. exponential RVs, is considered in [34]. In [35], the author calculate the CDF of the ratio of Hoyt (numerator) and Rayleigh (denominator) random variables in order to assess outage probability of fading channels. Nadarajah derives the PDF and CDF of the ratio of independent Weibull random variables, and the ratio of independent gamma (numerator) and beta (denominator) random variables in [36] and [37], respectively. In [38], the authors derive an upper bound on the ratio of a Rayleigh random variable to a weighted sum of Rayleigh random variables, and apply their results to interference systems. In a work targeting the outage probability of fading channels, Paris [39] calculates the CDF of the ratio of η - μ random variables, and κ - μ (numerator) and η - μ (denominator) random variables, assuming that the μ parameter of the denominator is a positive integer.

The PDF and CDF of the product of n independent Rayleigh random variables is presented [40], with the authors using the Mellin transform. A similar work is presented in [41], except that the authors target the Nakagami- m distribution. In [42], an approximation of the product of two independent Nakagami- m random variables is presented, which is simpler to calculate compared to previous results. The magnitude of a Gaussian signal transmitted over a Rayleigh channel is investigated by [43]. In their analysis, the authors derive the PDF of the sum and product of two complex Gaussian variables. In [44], the authors introduce the complex double Gaussian distribution that describes the product of two independent, non-zero mean, complex Gaussian random variables, and discuss its application to blind time reversal detection systems. In [45], the authors derive approximations to the product of independent random variables, and the results are used to estimate the outage probability of cascaded fading channels and the rate offset of the hybrid automatic repeat request (H-ARQ) transmission. Finally, an approximation to the product of random variables using orthogonal polynomials for log-normal density is presented in [46].

1.4 Thesis Outline

The remainder of the thesis is divided into four additional chapters. The results of the ratio and product of random variables are presented in Chapters 2 and 3, respectively. The following are considered: ratios Hoyt/ η - μ , Rice/ η - μ , Rice/ κ - μ , η - μ / η - μ , η - μ / κ - μ , κ - μ / κ - μ , κ - μ / η - μ , and α - μ / α - μ ; and products η - $\mu \times \eta$ - μ , κ - $\mu \times \kappa$ - μ , η - $\mu \times \kappa$ - μ , and α - $\mu \times \alpha$ - μ . These results are used in a few application examples, which are presented in Chapter 4. They include the analysis of the throughput of Carrier Sense Multiple Access (CSMA) in Rice, Hoyt, Nakagami- m , combined Rice and Hoyt, η - μ and κ - μ fading channels. In addition, it is presented the throughput of the Distributed Coordination Function (DCF) of IEEE 802.11 in Hoyt, Rice, and Nakagami- m Fading Channels. The ratio of independent alpha-mu random variables and its application in the capacity analysis of spectrum sharing systems is also presented. Finally, in Chapter 5, a summary of the research contributions of this work are presented.

Ratio of Random Variables

In this chapter, the ratios of i.n.i.d. random variables are calculated. Specifically, the following are considered: Hoyt/ η - μ , Rice/ η - μ , Rice/ κ - μ , η - μ / η - μ , η - μ / κ - μ , κ - μ / κ - μ , κ - μ / η - μ , and α - μ / α - μ . After intricate and tedious calculations, the results are obtained with a single summation that converges with small or reasonably small number of terms for the desired accuracy in most cases of interest. The results for the first three sections can be obtained with simplifications from the later sections. However, they are included here because their results are used in the application examples provided in Chapter 4.

For the figures, given the flexibility of the distributions, values of the parameters have been selected in order to illustrate their possible shapes. The parameters for the accuracy tables have been selected at the vicinity of the upper and lower limits of their valid range.

2.1 Introduction

The analysis of the ratio of random variables is usually performed using standard analytical procedures. Let X and Y be two statistically independent random variables and $Z \triangleq \frac{X}{Y}$ their ratio. The resulting PDF can be expressed as [47]

$$f_Z(z) = \int_0^{\infty} y f_X(zy) f_Y(y) dy \quad (2.1)$$

in which $f_X(\cdot)$ and $f_Y(\cdot)$ are the PDFs of X and Y , respectively. The CDF is then expressed as

$$F_Z(z) = \text{Prob} \left\{ \frac{X}{Y} \leq Z \right\} = \int_0^z f_Z(t) dt. \quad (2.2)$$

2.2 Ratio Hoyt/ η - μ

Let (1.10) represent the PDF of the numerator X

$$f_X(x) = 2\sqrt{h_x} \frac{x}{\hat{x}^2} \exp\left(-h_x \frac{x^2}{\hat{x}^2}\right) I_0\left(H_x \frac{x^2}{\hat{x}^2}\right) \quad (2.3)$$

and (1.13) the PDF of the denominator Y

$$f_Y(y) = \frac{4\sqrt{\pi}\mu_y^{\mu_y+\frac{1}{2}} h_y^{\mu_y} y^{2\mu_y}}{\Gamma(\mu_y) H_y^{\mu_y-\frac{1}{2}} \hat{y}^{2\mu_y+1}} \exp\left(-2\mu_y h_y \frac{y^2}{\hat{y}^2}\right) I_{\mu_y-\frac{1}{2}}\left(2\mu_y H_y \frac{y^2}{\hat{y}^2}\right). \quad (2.4)$$

In the following, the PDF and the CDF of the ratio Z are calculated.

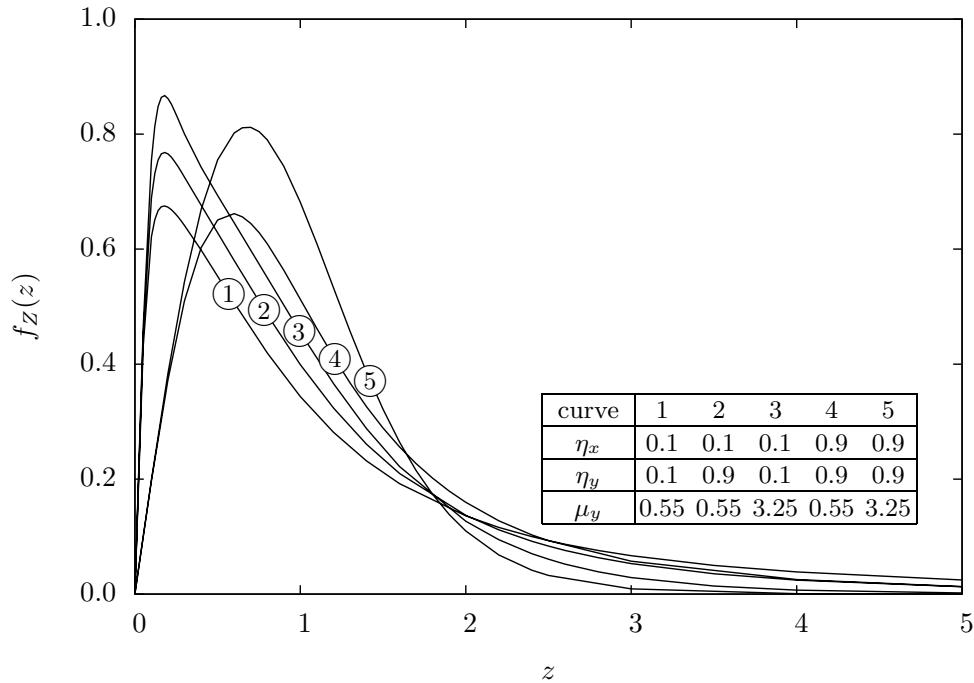
2.2.1 Probability Density Function

With (2.1), (2.3) and (2.4), the PDF of Z may be expressed as

$$\begin{aligned} f_Z(z) &= \int_0^\infty \frac{8\sqrt{\pi h_x} \mu_y^{\mu_y+\frac{1}{2}} h_y^{\mu_y}}{\Gamma(\mu_y) \hat{x}^2 \hat{y}^{2\mu_y+1} H_y^{\mu_y-\frac{1}{2}}} z y^{2\mu_y+2} \exp\left[-\frac{h_x (zy)^2}{\hat{x}^2}\right] \\ &\quad \times \exp\left(-2h_y \frac{\mu_y}{\hat{y}^2} y^2\right) I_0\left[\frac{H_x (zy)^2}{\hat{x}^2}\right] I_{\mu_y-\frac{1}{2}}\left(2H_y \frac{\mu_y}{\hat{y}^2} y^2\right) dy. \end{aligned} \quad (2.5)$$

Using [48, Eq. 8.445] to expand in series the function $I_{\mu_y-\frac{1}{2}}(\cdot)$, and making the integration variable $t = y^2$ results in

$$\begin{aligned} f_Z(z) &= \sum_{i=0}^{\infty} \int_0^\infty \frac{4\sqrt{\pi h_x} \mu_y^{2i+2\mu_y} h_y^{\mu_y} H_y^{2i}}{i! \Gamma(\mu_y) \Gamma\left(i + \mu_y + \frac{1}{2}\right) \hat{x}^2 \hat{y}^{4i+4\mu_y}} z t^{2i+2\mu_y} \\ &\quad \times \exp\left[-\left(\frac{h_x z^2}{\hat{x}^2} + 2h_y \frac{\mu_y}{\hat{y}^2}\right) t\right] I_0\left(\frac{H_x z^2 t}{\hat{x}^2}\right) dt. \end{aligned} \quad (2.6)$$

Figure 2.1: PDF of the ratio of Hoyt and η - μ random variables.

With the help of [48, Eq. 8.335.1] and [49, Eq. 2.15.3.2], the integral in (2.6) solves to

$$f_Z(z) = \frac{4}{z\sqrt{h_x h_y^{\mu_y}} (1 + uz^2)^{2\mu_y+1}} \sum_{i=0}^{\infty} \frac{1}{(i + \mu_y + \frac{1}{2}) B(\mu_y, i + 1) B(\mu_y + \frac{1}{2}, i + 1)} \times \left(\frac{H_x}{h_x} \frac{uz^2}{1 + uz^2} \right)^{2i} {}_2F_1 \left[i + \mu_y + \frac{1}{2}, i + \mu_y + 1, \mu_y + \frac{1}{2}, \left(\frac{H_y}{h_y} \frac{1}{1 + uz^2} \right)^2 \right] \quad (2.7)$$

in which $B(.,.)$ is the beta function [48, Eq. 8.384.1], ${}_2F_1(.,.)$ is the Gauss hypergeometric function [21, Eq. 15.1.1], and

$$u = \frac{h_x \hat{y}^2}{2\mu_y h_y \hat{x}^2}. \quad (2.8)$$

Although (2.7) includes an infinite summation, the evaluation of the PDF converges rapidly for cases of interest. In order to estimate the error if the summation in (2.7) is truncated, all summands whose absolute value is larger than 10^{-25} are calculated, and those smaller than this value are discarded because it was observed that they do not affect the desired accuracy. The error of the truncated summation may now be estimated and, of course, these results vary depending on the given set of parameters used. Let I be defined as the number of terms in a truncated summation, i.e., $0 \leq i < I$. Table 2.1 gives the value of I necessary to obtain a three-

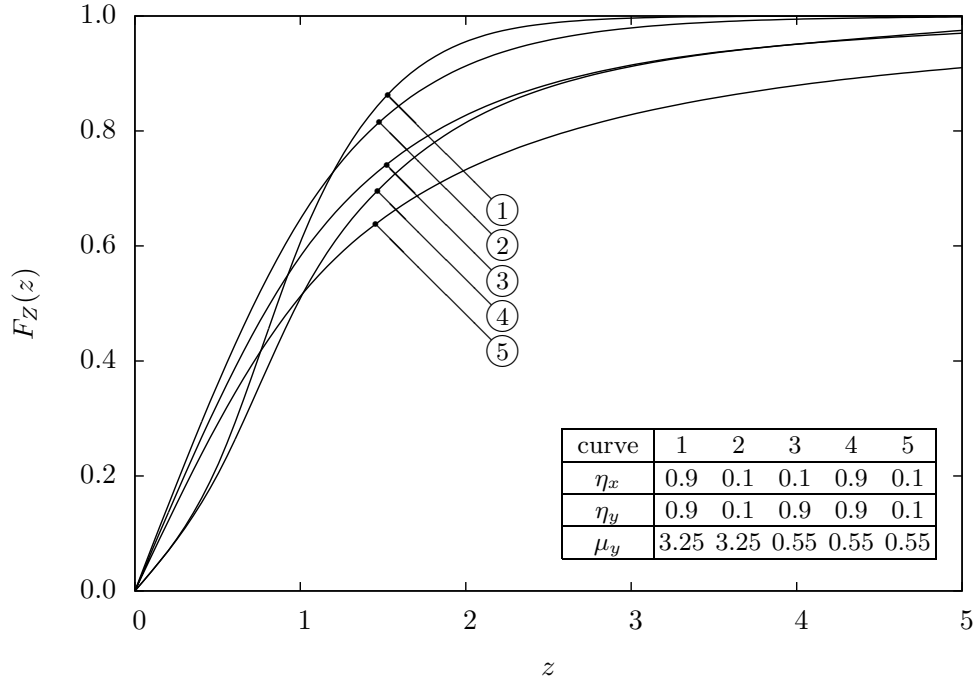
Table 2.1: Relation between number of terms and accuracy in the infinite summation of (2.7) and (2.14).

Parameters				smallest I for accuracy of			
η_x	η_y	μ_y	z	3-decimal-place		6-decimal-place	
				PDF	CDF	PDF	CDF
0.1	0.1	0.5	0.1	177	3	348	10
			1.0	81	308	168	643
			5.0	4	7656	12	15959
		1.0	0.1	213	3	391	7
			5.0	8	4807	23	9171
		5.0	0.1	408	2	625	5
	5.0		27	1994	115	3077	
	0.9	0.5	0.1	1	3	2	7
			5.0	0	4921	1	9542
		5.0	0.1	2	1	4	4
			5.0	0	1529	1	2179
	0.9	0.1	0.5	0.1	174	0	351
5.0				3	305	8	638
5.0			0.1	375	0	603	1
			5.0	0	83	65	130
0.9		0.5	0.1	1	0	3	2
			5.0	0	197	0	384
		5.0	0.1	1	0	3	1
			5.0	0	66	0	96

decimal-place accuracy (error < 0.0005) and a six-decimal-place accuracy (error < 0.0000005) for the infinite summation of (2.7). For the PDF accuracy, a smaller number of terms I is required for higher values of η_x , η_y or z , or lower values of μ_y .

Note that (2.7) may be reduced in the following situations: (i) if η_x is set to unity, thus making $h_x = 1$ and $H_x = 0$, the corresponding PDF reduces to Rayleigh; (ii) if μ_y is set to $\frac{1}{2}$, the corresponding PDF reduces to Hoyt; (iii) if $\eta_y \rightarrow 0$ or $\eta_y \rightarrow \infty$, the corresponding PDF reduces to Nakagami- m , with $m = \mu_y$; and (iv) if $\mu_y = \frac{1}{2}$ and $\eta_y = 1$, the corresponding PDF reduces to Rayleigh.

The PDF of Z is shown in Fig. 2.1 for various values of η_x , η_y and μ_y . It can be seen that increasing values of η_x shifts the curve away from the ordinate axis, making it assume, as expected, a shape closer to the familiar Rayleigh PDF. On the other hand, a PDF with smaller tail and a higher peak value is obtained for increasing values of η_y or μ_y .

Figure 2.2: CDF of the ratio of Hoyt and η - μ random variables.

2.2.2 Cumulative Distribution Function

With (2.2), (2.3) and (2.4), the CDF of Z may be expressed as

$$\begin{aligned}
 F_Z(z) &= \int_0^z \int_0^\infty \frac{8\sqrt{\pi h_x \mu_y^{\mu_y + \frac{1}{2}}} h_y^{\mu_y}}{\Gamma(\mu_y) \hat{x}^2 \hat{y}^{2\mu_y + 1} H_y^{\mu_y - \frac{1}{2}}} t y^{2\mu_y + 2} \exp\left[-\frac{h_x (ty)^2}{\hat{x}^2}\right] \exp\left(-2h_y \frac{\mu_y}{\hat{y}^2} y^2\right) \\
 &\quad \times I_0\left[\frac{H_x (ty)^2}{\hat{x}^2}\right] I_{\mu_y - \frac{1}{2}}\left(2H_y \frac{\mu_y}{\hat{y}^2} y^2\right) dy dt.
 \end{aligned} \tag{2.9}$$

Using [48, Eq. 8.445] to expand in series the function $I_0(\cdot)$, changing the integration order and the integration variable to $w = t^2$ leads to

$$\begin{aligned}
 F_Z(z) &= \sum_{i=0}^{\infty} \int_0^\infty \int_0^{z^2} \frac{4\sqrt{\pi h_x \mu_y^{\mu_y + \frac{1}{2}}} H_x^{2i} h_y^{\mu_y}}{i! \Gamma(\mu_y) \hat{x}^{4i+2} \hat{y}^{2\mu_y + 1} H_y^{\mu_y - \frac{1}{2}}} w^{2i} y^{4i+2\mu_y+2} \exp\left[-\frac{h_x w y^2}{\hat{x}^2}\right] \\
 &\quad \times \exp\left(-2h_y \frac{\mu_y}{\hat{y}^2} y^2\right) I_{\mu_y - \frac{1}{2}}\left(2H_y \frac{\mu_y}{\hat{y}^2} y^2\right) dw dy.
 \end{aligned} \tag{2.10}$$

Using [48, Eqs. 3.351.1, 8.356.3], the above integral in w solves to

$$F_Z(z) = \sum_{i=0}^{\infty} \int_0^{\infty} \frac{2^{-2i+2} \sqrt{\pi} \mu_y^{\mu_y + \frac{1}{2}} H_x^{2i} h_y^{\mu_y}}{i!^2 \Gamma(\mu_y) \hat{y}^{2\mu_y+1} h_x^{2i+\frac{1}{2}} H_y^{\mu_y-\frac{1}{2}}} y^{2\mu_y} \exp\left(-2h_y \frac{\mu_y}{\hat{y}^2} y^2\right) \times I_{\mu_y-\frac{1}{2}}\left(2H_y \frac{\mu_y}{\hat{y}^2} y^2\right) \left[\Gamma(2i+1) - \Gamma\left(2i+1, \frac{h_x z^2 y^2}{\hat{x}^2}\right) \right] dy \quad (2.11)$$

in which $\Gamma(.,.)$ is the incomplete gamma function [48, Eq. 8.350.2]. The integral in (2.11) can be split in two parts, with one of them carrying the function $\Gamma(.,.)$. Solving the simpler integral with [49, Eq. 2.15.3.2] and simplifying the summation leads to

$$F_Z(z) = 1 - \sum_{i=0}^{\infty} \int_0^{\infty} \frac{2^{-2i+2} \sqrt{\pi} \mu_y^{\mu_y + \frac{1}{2}} H_x^{2i} h_y^{\mu_y}}{i!^2 \Gamma(\mu_y) \hat{y}^{2\mu_y+1} h_x^{2i+\frac{1}{2}} H_y^{\mu_y-\frac{1}{2}}} y^{2\mu_y} \exp\left(-2h_y \frac{\mu_y}{\hat{y}^2} y^2\right) \times I_{\mu_y-\frac{1}{2}}\left(2H_y \frac{\mu_y}{\hat{y}^2} y^2\right) \Gamma\left(2i+1, \frac{h_x z^2 y^2}{\hat{x}^2}\right) dy. \quad (2.12)$$

With the help of [48, Eq. 8.335.1] and [50, Eq. 06.08.03.0009.01], the function $\Gamma(.,.)$ can be expanded in series and the CDF may be expressed as

$$F_Z(z) = 1 - \sum_{i=0}^{\infty} \int_0^{\infty} \frac{4\Gamma\left(i + \frac{1}{2}\right) \mu_y^{\mu_y + \frac{1}{2}} H_x^{2i} h_y^{\mu_y}}{i! \Gamma(\mu_y) \hat{y}^{2\mu_y+1} h_x^{2i+\frac{1}{2}} H_y^{\mu_y-\frac{1}{2}}} y^{2\mu_y} \exp\left(-2h_y \frac{\mu_y}{\hat{y}^2} y^2\right) \times I_{\mu_y-\frac{1}{2}}\left(2H_y \frac{\mu_y}{\hat{y}^2} y^2\right) \Gamma\left(2i+1, \frac{h_x z^2 y^2}{\hat{x}^2}\right) dy + \sum_{i=0}^{\infty} \sum_{j=2i}^{\infty} \int_0^{\infty} \frac{4\Gamma\left(i + \frac{1}{2}\right) \mu_y^{\mu_y + \frac{1}{2}} H_x^{2i} h_y^{\mu_y}}{i! \Gamma(j+2) \Gamma(\mu_y) \hat{x}^{2j+2} \hat{y}^{2\mu_y+1} h_x^{2i-j-\frac{1}{2}} H_y^{\mu_y-\frac{1}{2}}} z^{2j+2} y^{2j+2\mu_y+2} \times \exp\left[-\left(\frac{h_x}{\hat{x}^2} z^2 + h_y \frac{\mu_y}{\hat{y}^2}\right) y^2\right] I_{\mu_y-\frac{1}{2}}\left(2H_y \frac{\mu_y}{\hat{y}^2} y^2\right) dy. \quad (2.13)$$

Solving the above integrals with [49, Eq. 2.15.3.2] and simplifying the summations results in

$$F_Z(z) = \frac{uz^2}{h_y^{\mu_y} (1+uz^2)^{2\mu_y+1}} \sum_{i=0}^{\infty} \frac{(uz^2)^i}{(i+1)B(2\mu_y, i+1)(1+uz^2)^i} \times {}_2F_1\left[\frac{i}{2} + \mu_y + \frac{1}{2}, \frac{i}{2} + \mu_y + 1, \mu_y + \frac{1}{2}, \left(\frac{H_y}{h_y} \frac{1}{1+uz^2}\right)^2\right] \times \left\{ 1 - \frac{1}{i_c B\left(i_c, \frac{1}{2}\right) \sqrt{h_x}} \left(\frac{H_x}{h_x}\right)^{2i_c} {}_2F_1\left[i_c + \frac{1}{2}, 1, i_c + 1, \left(\frac{H_x}{h_x}\right)^2\right] \right\} \quad (2.14)$$

in which u is defined by (2.8), $i_c = \lceil \frac{i+1}{2} \rceil$, and $\lceil \cdot \rceil$ is the ceiling function.

Although (2.14) includes an infinite summation, the evaluation of the CDF converges rapidly for cases of interest. Let I be the number of terms in a truncated summation (as defined earlier). Table 2.1 gives the value of I necessary to obtain a three-decimal-place accuracy (error < 0.0005) and a six-decimal-place accuracy (error < 0.0000005) for the infinite summation of (2.14). For the CDF accuracy, a smaller number of terms I is required for higher values of η_x , η_y or μ_y , or lower values of z .

Note that (2.14) may be reduced in the following situations: (i) if η_x is set to unity, thus making $h_x = 1$ and $H_x = 0$, the corresponding CDF reduces to Rayleigh; (ii) if μ_y is set to $\frac{1}{2}$, the corresponding CDF reduces to Hoyt; (iii) if $\eta_y \rightarrow 0$ or $\eta_y \rightarrow \infty$, the corresponding CDF reduces to Nakagami- m , with $m = \mu_y$; and (iv) if $\mu_y = \frac{1}{2}$ and $\eta_y = 1$, the corresponding CDF reduces to Rayleigh.

The CDF of Z is shown in Fig. 2.2 for various values of η_x , η_y and μ_y . It can be seen that higher values of μ_y translate into steeper curves, approaching the unity faster. On the other hand, an opposite effect is obtained for lower values of η_y .

2.3 Ratio Rice/ η - μ

Let (1.7) represent the PDF of the numerator X

$$f_X(x) = \frac{2(\kappa_x + 1)}{e^{\kappa_x}} \frac{x}{\hat{x}^2} \exp \left[-(\kappa_x + 1) \frac{x^2}{\hat{x}^2} \right] I_0 \left[2\sqrt{\kappa_x(\kappa_x + 1)} \frac{x}{\hat{x}} \right] \quad (2.15)$$

and (1.13) the PDF of the denominator Y

$$f_Y(y) = \frac{4\sqrt{\pi}\mu_y^{\mu_y + \frac{1}{2}} h_y^{\mu_y} y^{2\mu_y}}{\Gamma(\mu_y) H_y^{\mu_y - \frac{1}{2}} \hat{y}^{2\mu_y + 1}} \exp \left(-2\mu_y h_y \frac{y^2}{\hat{y}^2} \right) I_{\mu_y - \frac{1}{2}} \left(2\mu_y H_y \frac{y^2}{\hat{y}^2} \right). \quad (2.16)$$

In the following, the PDF and the CDF of the ratio Z are calculated.

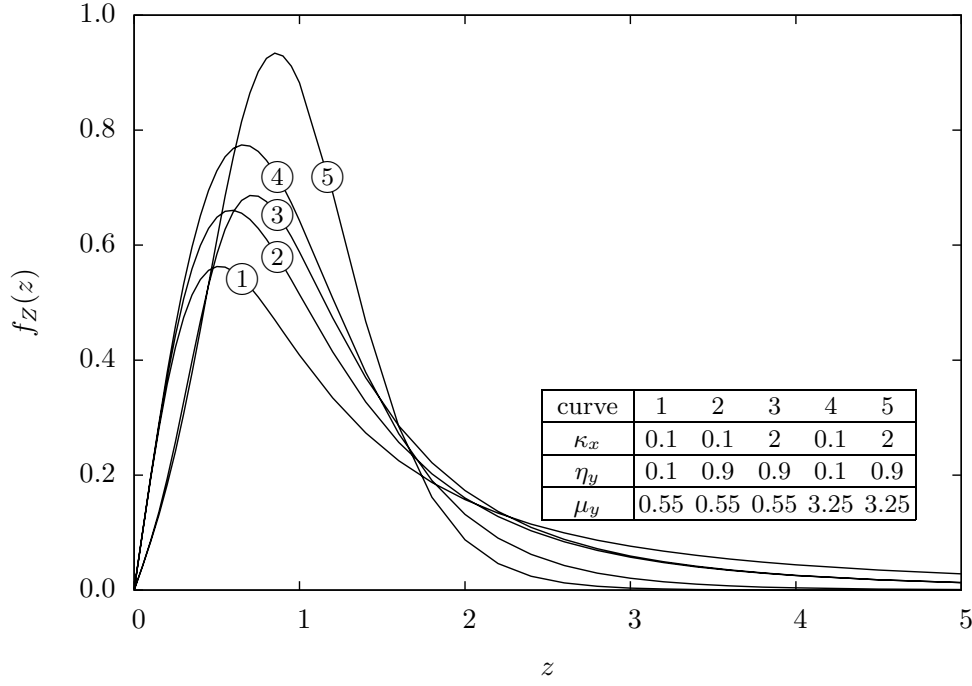


Figure 2.3: PDF of the ratio of Rice and η - μ random variables.

2.3.1 Probability Density Function

With (2.1), (2.15) and (2.16), the PDF of Z may be expressed as

$$\begin{aligned}
 f_Z(z) = & \int_0^\infty \frac{8\sqrt{\pi}(\kappa_x + 1)h_y^{\mu_y}}{e^{\kappa_x}\Gamma(\mu_y)\hat{x}^2 H_y^{\mu_y - \frac{1}{2}}} \left(\frac{\mu_y}{\hat{y}^2}\right)^{\mu_y + \frac{1}{2}} z y^{2\mu_y + 2} \exp\left[-\frac{\kappa_x + 1}{\hat{x}^2}(zy)^2\right] \\
 & \times \exp\left(-2h_y \frac{\mu_y}{\hat{y}^2} y^2\right) I_0\left(2\sqrt{\kappa_x \frac{\kappa_x + 1}{\hat{x}^2}} r y\right) I_{\mu_y - \frac{1}{2}}\left(2H_y \frac{\mu_y}{\hat{y}^2} y^2\right) dy.
 \end{aligned} \tag{2.17}$$

Using [48, Eq. 8.445] to expand in series the function $I_0(\cdot)$, and making the integration variable $t = y^2$ results in

$$\begin{aligned}
 f_Z(z) = & \sum_{i=0}^{\infty} \int_0^\infty \frac{4\sqrt{\pi}\kappa_x^i (\kappa_x + 1)^{i+1} \mu_y^{\mu_y + \frac{1}{2}} h_y^{\mu_y}}{i!^2 \Gamma(\mu_y) e^{\kappa_x} \hat{x}^{2i+2} \hat{y}^{2\mu_y + 1} H_y^{\mu_y - \frac{1}{2}}} z^{2i+1} t^{i + \mu_y + \frac{1}{2}} \\
 & \times \exp\left[-\left(\frac{\kappa_x + 1}{\hat{x}^2} z^2 + 2h_y \frac{\mu_y}{\hat{y}^2}\right) t\right] I_{\mu_y - \frac{1}{2}}\left(2H_y \frac{\mu_y}{\hat{y}^2} t\right) dt.
 \end{aligned} \tag{2.18}$$

Using [48, Eq. 8.335.1] and [49, Eq. 2.15.3.2], the above integral solves to

$$f_Z(z) = \frac{2uz}{(1+uz^2)^{2\mu_y+1} e^{\kappa_x} h_y^{\mu_y}} \sum_{i=0}^{\infty} \frac{(\kappa_x uz^2)^i}{i! B(i+1, 2\mu_y) (1+uz^2)^i} \times {}_2F_1 \left[\frac{i+2\mu_y+1}{2}, \frac{i+2\mu_y+2}{2}, \mu_y + \frac{1}{2}, \left(\frac{H_y}{h_y} \frac{1}{1+uz^2} \right)^2 \right] \quad (2.19)$$

in which

$$u = \frac{(\kappa_x + 1)\hat{y}^2}{2\mu_y \hat{x}^2 h_y}. \quad (2.20)$$

Although (2.19) includes an infinite summation, the evaluation of the PDF converges rapidly for cases of interest. Let I be the number of terms in a truncated summation (as defined earlier). Table 2.2 gives the value of I necessary to obtain a three-decimal-place accuracy (error < 0.0005) and a six-decimal-place accuracy (error < 0.0000005) for the infinite summation of (2.19). For the PDF accuracy, a smaller number of terms I is required for higher values of η_y , μ_y or z , or lower values of κ_x or μ_y .

Note that (2.19) may be reduced in the following situations: (i) if $\kappa_x \rightarrow 0$, the corresponding PDF reduces to Rayleigh; (ii) if μ_y is set to $\frac{1}{2}$, the corresponding PDF reduces to Hoyt; (iii) if $\eta_y \rightarrow 0$ or $\eta_y \rightarrow \infty$, the corresponding PDF reduces to Nakagami- m , with $m = \mu_y$; and (iv) if $\mu_y = \frac{1}{2}$ and $\eta_y = 1$, the corresponding PDF reduces to Rayleigh.

The PDF of Z is shown in Fig. 2.3 for various values of κ_x , η_y and μ_y . It can be seen that diminishing values of κ_x tends to spread out the probability density. On the other hand, a PDF with smaller tail and a higher peak value is obtained for increasing values of η_y or μ_y .

If μ_y is a positive integer, i.e., $\mu_y = 1, 2, \dots$, then the Bessel function of order $\mu_y - \frac{1}{2}$ in (2.17), with the help of [48, Eq. 8.467], may be expressed as

$$I_{n+\frac{1}{2}}(z) = \frac{1}{\sqrt{2\pi z}} \left[e^z \sum_{i=0}^n \frac{(-1)^i (n+i)!}{i! (n-i)! (2z)^i} + (-1)^{n+1} e^{-z} \sum_{i=0}^n \frac{(n+i)!}{i! (n-i)! (2z)^i} \right] \quad (2.21)$$

in which $n = 0, 1, 2, \dots = \mu_y - 1$. Using (2.21) in (2.17), and solving the integral in y using [49,

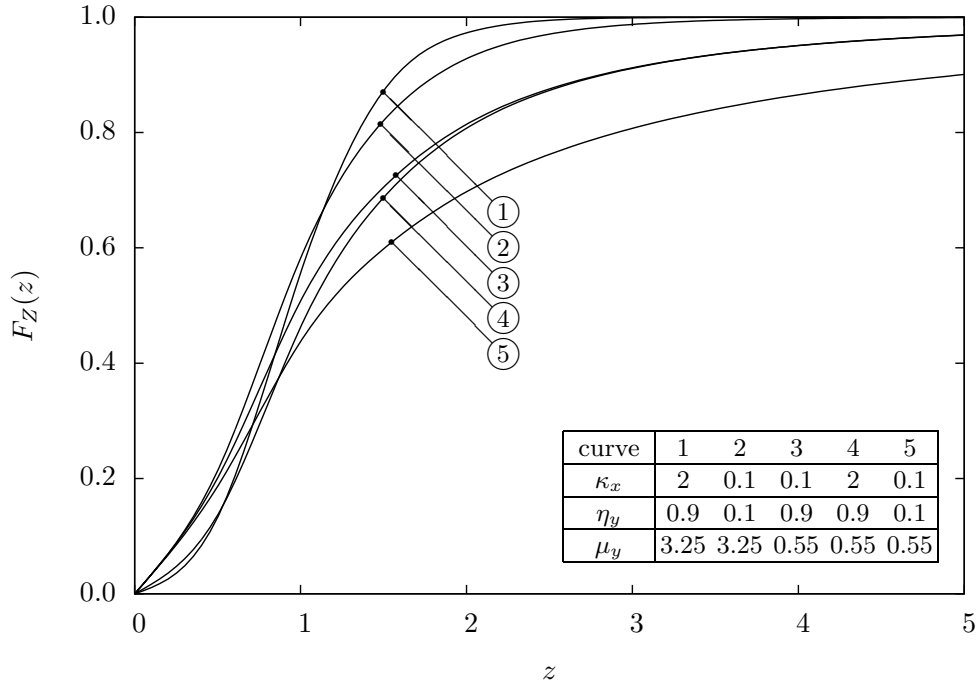


Figure 2.4: CDF of the ratio of Rice and η - μ random variables.

Eq. 2.15.5.4] leads to

$$\begin{aligned}
 f_Z(z) = & \frac{2h_y^{\mu_y} u_1 z}{e^{\kappa_x(1+u_1 z^2)}} \sum_{i=0}^{\mu_y-1} \frac{(-1)^i (-i + \mu_y)}{(i + \mu_y) B(\mu_y, i + 1) (2H_y)^{i+\mu_y} (h_y - H_y)^{-i+\mu_y} (1 + u_1 z^2)^{-i+\mu_y}} \\
 & \times {}_1F_1 \left(-i + \mu_y + 1, 1, \frac{\kappa_x u_1 z^2}{1 + u_1 z^2} \right) \\
 & + \frac{2h_y^{\mu_y} u_2 z}{e^{\kappa_x(1+u_2 z^2)}} \sum_{i=0}^{\mu_y-1} \frac{(-1)^{\mu_y} (-i + \mu_y)}{(i + \mu_y) B(\mu_y, i + 1) (2H_y)^{i+\mu_y} (h_y + H_y)^{-i+\mu_y} (1 + u_2 z^2)^{-i+\mu_y}} \\
 & \times {}_1F_1 \left(-i + \mu_y + 1, 1, \frac{\kappa_x u_2 z^2}{1 + u_2 z^2} \right)
 \end{aligned} \tag{2.22}$$

in which ${}_1F_1(\cdot)$ is the Kummer confluent hypergeometric function [21, Eq. 13.1.2], and

$$u_1 = \frac{(\kappa_x + 1)\hat{y}^2}{2\mu_y(h_y - H_y)\hat{x}^2}, \text{ and } u_2 = \frac{(\kappa_x + 1)\hat{y}^2}{2\mu_y(h_y + H_y)\hat{x}^2}. \tag{2.23}$$

Table 2.2: Relation between number of terms and accuracy in the infinite summation of (2.19) and (2.29).

Parameters				smallest I for accuracy of			
κ_x	η_y	μ_y	z	3-decimal-place		6-decimal-place	
				PDF	CDF	PDF	CDF
0.1	0.1	0.5	0.1	0	0	1	2
			1.0	2	15	4	32
			5.0	2	332	3	693
		1.0	0.1	0	0	1	2
			5.0	1	210	3	401
			5.0	0.1	0	0	1
	0.9	0.5	0.1	0	0	1	2
			5.0	1	214	3	417
			5.0	0.1	0	0	1
		5.0	0.1	0	0	1	1
			5.0	0	90	3	141
			5.0	0	0	0	0
10.0	0.1	0.5	0.1	1	0	8	5
			5.0	18	3303	26	6887
			5.0	0.1	0	0	4
		5.0	0.1	0	0	4	2
			5.0	0	863	19	1332
			5.0	0	0	0	0
	0.9	0.5	0.1	0	0	6	3
			5.0	17	2124	26	4119
		5.0	0.1	0	0	4	2
			5.0	0	663	0	946

2.3.2 Cumulative Distribution Function

With (2.2), (2.15) and (2.16), the CDF of Z may be expressed as

$$F_Z(z) = \int_0^z \int_0^\infty \frac{8\sqrt{\pi}(\kappa_x + 1)\mu_y^{\mu_y + \frac{1}{2}}h_y^{\mu_y}}{e^{\kappa_x}\Gamma(\mu_y)\hat{x}^2\hat{y}^{2\mu_y+1}H_y^{\mu_y - \frac{1}{2}}} ty^{2\mu_y+2} \exp\left[-\frac{\kappa_x + 1}{\hat{x}^2}(ty)^2\right] \\ \times \exp\left(-2h_y\frac{\mu_y}{\hat{y}^2}y^2\right) I_0\left(2\sqrt{\kappa_x\frac{\kappa_x + 1}{\hat{x}^2}}ty\right) I_{\mu_y - \frac{1}{2}}\left(2H_y\frac{\mu_y}{\hat{y}^2}y^2\right) dy dt. \quad (2.24)$$

Using [48, Eq. 8.445] to expand in series the function $I_0(\cdot)$, changing the integration order and the integration variable to $w = t^2$ leads to

$$F_Z(z) = \sum_{i=0}^{\infty} \int_0^\infty \int_0^{z^2} \frac{4\sqrt{\pi}\kappa_x^i(\kappa_x + 1)^{i+1}\mu_y^{\mu_y + \frac{1}{2}}h_y^{\mu_y}}{i!2e^{\kappa_x}\Gamma(\mu_y)\hat{x}^{2i+2}\hat{y}^{2\mu_y+1}H_y^{\mu_y - \frac{1}{2}}} w^i y^{2i+2\mu_y+2} \exp\left(-\frac{\kappa_x + 1}{\hat{x}^2}y^2w\right) \\ \times \exp\left(-2h_y\frac{\mu_y}{\hat{y}^2}y^2\right) I_{\mu_y - \frac{1}{2}}\left(2H_y\frac{\mu_y}{\hat{y}^2}y^2\right) dw dy. \quad (2.25)$$

Using [48, Eqs. 3.351.1, 8.356.3], the above integral in w solves to

$$F_Z(z) = \sum_{i=0}^{\infty} \int_0^\infty \frac{4\sqrt{\pi}\kappa_x^i\mu_y^{\mu_y + \frac{1}{2}}h_y^{\mu_y}}{i!e^{\kappa_x}\Gamma(\mu_y)\hat{y}^{2\mu_y+1}H_y^{\mu_y - \frac{1}{2}}} y^{2\mu_y} \exp\left(-2h_y\frac{\mu_y}{\hat{y}^2}y^2\right) \\ \times I_{\mu_y - \frac{1}{2}}\left(2H_y\frac{\mu_y}{\hat{y}^2}y^2\right) \left[1 - Q\left(i + 1, \frac{\kappa_x + 1}{\hat{x}^2}y^2z^2\right)\right] dy \quad (2.26)$$

in which $Q(a, z) = \frac{\Gamma(a, z)}{\Gamma(a)}$ is the regularized incomplete gamma function. The integral in (2.26) can be split in two parts, with one of them carrying the function $Q(\cdot, \cdot)$. Solving the simpler integral with [49, Eq. 2.15.3.2] and simplifying the summation leads to

$$F_Z(z) = 1 - \sum_{i=0}^{\infty} \int_0^\infty \frac{4\sqrt{\pi}\kappa_x^i\mu_y^{\mu_y + \frac{1}{2}}h_y^{\mu_y}}{i!e^{\kappa_x}\Gamma(\mu_y)\hat{y}^{2\mu_y+1}H_y^{\mu_y - \frac{1}{2}}} y^{2\mu_y} \exp\left(-2h_y\frac{\mu_y}{\hat{y}^2}y^2\right) \\ \times I_{\mu_y - \frac{1}{2}}\left(2H_y\frac{\mu_y}{\hat{y}^2}y^2\right) Q\left(i + 1, \frac{\kappa_x + 1}{\hat{x}^2}y^2z^2\right) dy. \quad (2.27)$$

Using [50, Eq. 06.08.03.0009.01] to represent $Q(.,.)$, the CDF may be expressed as

$$\begin{aligned}
F_Z(z) = & 1 - \sum_{i=0}^{\infty} \int_0^{\infty} \frac{4\sqrt{\pi}\kappa_x^i \mu_y^{\mu_y + \frac{1}{2}} h_y^{\mu_y}}{i! e^{\kappa_x} \Gamma(\mu_y) \hat{y}^{2\mu_y + 1} H_y^{\mu_y - \frac{1}{2}}} y^{2\mu_y} \exp\left(-2h_y \frac{\mu_y}{\hat{y}^2} y^2\right) \\
& \times I_{\mu_y - \frac{1}{2}}\left(2H_y \frac{\mu_y}{\hat{y}^2} y^2\right) dy \\
& + \sum_{i=0}^{\infty} \sum_{j=0}^i \int_0^{\infty} \frac{4\sqrt{\pi}\kappa_x^j \mu_y^{\mu_y + \frac{1}{2}} (\kappa_x + 1)^{i+1} h_y^{\mu_y} z^{2i+2}}{j!(i+1)! e^{\kappa_x} \Gamma(\mu_y) \hat{x}^{2i+2} \hat{y}^{2\mu_y + 1} H_y^{\mu_y - \frac{1}{2}}} y^{2i+2\mu_y+2} \\
& \times \exp\left[-\left(\frac{\kappa_x + 1}{\hat{x}^2} z^2 + 2\frac{\mu_y}{\hat{y}^2} h_y\right) y^2\right] I_{\mu_y - \frac{1}{2}}\left(2H_y \frac{\mu_y}{\hat{y}^2} y^2\right) dy
\end{aligned} \tag{2.28}$$

Solving the integrals with [49, Eq. 2.15.3.2] and simplifying the summation results in

$$\begin{aligned}
F_Z(z) = & \frac{uz^2}{h_y^{\mu_y} (1 + uz^2)^{2\mu_y + 1}} \sum_{i=0}^{\infty} \frac{Q(i+1, \kappa_x) (uz^2)^i}{(i+1)B(i+1, 2\mu_y) (1 + uz^2)^i} \\
& \times {}_2F_1\left[\frac{i+2\mu_y+1}{2}, \frac{i+2\mu_y+2}{2}, \mu_y + \frac{1}{2}, \left(\frac{H_y}{h_y} \frac{1}{1 + uz^2}\right)^2\right]
\end{aligned} \tag{2.29}$$

in which u is defined by (2.20).

Although (2.29) includes an infinite summation, the evaluation of the CDF converges rapidly for cases of interest. Let I be the number of terms in a truncated summation (as defined earlier). Table 2.2 gives the value of I necessary to obtain a three-decimal-place accuracy (error < 0.0005) and a six-decimal-place accuracy (error < 0.0000005) for the infinite summation of (2.29). For the CDF accuracy, a smaller number of terms I is required for higher values of η_y or μ_y , or lower values of κ_x or z .

Note that (2.29) may be reduced in the following situations: (i) if $\kappa_x \rightarrow 0$, the corresponding CDF reduces to Rayleigh; (ii) if μ_y is set to $\frac{1}{2}$, the corresponding CDF reduces to Hoyt; (iii) if $\eta_y \rightarrow 0$ or $\eta_y \rightarrow \infty$, the corresponding CDF reduces to Nakagami- m , with $m = \mu_y$; and (iv) if $\mu_y = \frac{1}{2}$ and $\eta_y = 1$, the corresponding CDF reduces to Rayleigh.

The CDF of Z is shown in Fig. 2.4 for various values of κ_x , η_y and μ_y . It can be seen that higher values of κ_x or μ_y tend to produce steeper curves, approaching the unity faster. On the other hand, a smoother CDF is obtained with smaller values of η_y .

2.4 Ratio Rice/ κ - μ

Let (1.7) represent the PDF of the numerator X

$$f_X(x) = \frac{2(\kappa_x + 1)}{e^{\kappa_x}} \frac{x}{\hat{x}^2} \exp \left[-(\kappa_x + 1) \frac{x^2}{\hat{x}^2} \right] I_0 \left[2\sqrt{\kappa_x(\kappa_x + 1)} \frac{x}{\hat{x}} \right] \quad (2.30)$$

and (1.15) the PDF of the denominator Y

$$f_Y(y) = \frac{2\mu_y(\kappa_y + 1) \frac{\mu_y+1}{2} y^{\mu_y}}{\kappa_y \frac{\mu_y-1}{2} e^{\mu_y \kappa_y} \hat{y}^{\mu_y+1}} \exp \left[-\mu_y(\kappa_y + 1) \frac{y^2}{\hat{y}^2} \right] I_{\mu_y-1} \left(2\mu_y \sqrt{\kappa_y(\kappa_y + 1)} \frac{y}{\hat{y}} \right). \quad (2.31)$$

In the following, the PDF and the CDF of the ratio Z are calculated.

2.4.1 Probability Density Function

With (2.1), (2.30) and (2.31), the PDF of Z may be expressed as

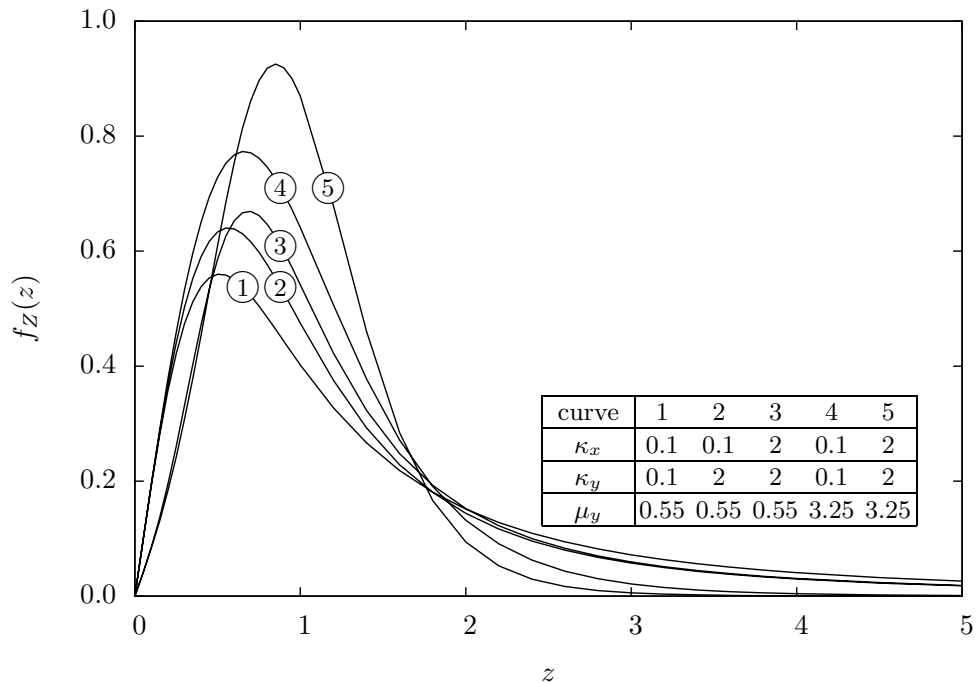
$$\begin{aligned} f_Z(z) &= \int_0^\infty \frac{4\mu_y(\kappa_x + 1)(\kappa_y + 1) \frac{\mu_y+1}{2}}{e^{\kappa_x + \mu_y \kappa_y} \kappa_y \frac{\mu_y-1}{2} \hat{x}^2 \hat{y}^{\mu_y+1}} z y^{\mu_y+2} \exp \left[-\frac{\kappa_x + 1}{\hat{x}^2} (zy)^2 \right] \exp \left(-\mu_y \frac{\kappa_y + 1}{\hat{y}^2} y^2 \right) \\ &\times I_0 \left(2\sqrt{\kappa_x \frac{\kappa_x + 1}{\hat{x}^2}} zy \right) I_{\mu_y-1} \left(2\mu_y \sqrt{\kappa_y \frac{\kappa_y + 1}{\hat{y}^2}} y \right) dy. \end{aligned} \quad (2.32)$$

Using [48, Eq. 8.445] to expand in series the function $I_0(\cdot)$ leads to

$$\begin{aligned} f_Z(z) &= \sum_{i=0}^{\infty} \int_0^\infty \frac{4\mu_y \kappa_x^i (\kappa_x + 1)^{i+1} (\kappa_y + 1) \frac{\mu_y+1}{2}}{i!^2 e^{\kappa_x + \mu_y \kappa_y} \kappa_y \frac{\mu_y-1}{2} \hat{x}^{2i+2} \hat{y}^{\mu_y+1}} z^{2i+1} y^{2i+\mu_y+2} \\ &\times \exp \left[-\left(\frac{\kappa_x + 1}{\hat{x}^2} z^2 + \mu_y \frac{\kappa_y + 1}{\hat{y}^2} \right) y^2 \right] I_{\mu_y-1} \left(2\mu_y \sqrt{\kappa_y \frac{\kappa_y + 1}{\hat{x}^2}} y \right) dy. \end{aligned} \quad (2.33)$$

Using [49, Eq. 2.15.5.4] to solve the above integral results in

$$\begin{aligned} f_Z(z) &= \frac{2uz}{e^{\kappa_x + \mu_y \kappa_y} (1 + uz^2)^{\mu_y+1}} \sum_{i=0}^{\infty} \frac{(\kappa_x uz^2)^i}{i! B(\mu_y, i+1) (1 + uz^2)^i} \\ &\times {}_1F_1 \left(i + \mu_y + 1, \mu_y, \frac{\mu_y \kappa_y}{1 + uz^2} \right) \end{aligned} \quad (2.34)$$

Figure 2.5: PDF of the ratio of Rice and κ - μ random variables.

in which

$$u = \frac{(\kappa_x + 1)\hat{y}^2}{\mu_y(\kappa_y + 1)\hat{x}^2}. \quad (2.35)$$

Although (2.34) includes an infinite summation, the evaluation of the PDF converges rapidly for cases of interest. Let I be the number of terms in a truncated summation (as defined earlier). Table 2.3 gives the value of I necessary to obtain a three-decimal-place accuracy (error < 0.0005) and a six-decimal-place accuracy (error < 0.0000005) for the infinite summation of (2.34). For the PDF accuracy, a smaller number of terms I is required for higher values of κ_x , κ_y , μ_y or z .

Note that (2.34) may be reduced in the following situations: (i) if $\kappa_x \rightarrow 0$, the corresponding PDF reduces to Rayleigh; (ii) if μ_y is set to unity, the corresponding PDF reduces to Rice; (iii) if $\kappa_y \rightarrow 0$, the corresponding PDF reduces to Nakagami- m , with $m = \mu_y$; and (iv) if $\mu_y = 1$ and $\kappa_y \rightarrow 0$, the corresponding PDF reduces to Rayleigh.

The PDF of Z is shown in Fig. 2.5 for various values of κ_x , κ_y and μ_y . It can be seen that diminishing values of κ_x tends to spread out the probability density. On the other hand, a PDF with smaller tail and a higher peak value is obtained for increasing values of κ_y or μ_y .

Table 2.3: Relation between number of terms and accuracy in the infinite summation of (2.34) and (2.41).

Parameters				smallest I for accuracy of					
κ_x	κ_y	μ_y	z	3-decimal-place		6-decimal-place			
				PDF	CDF	PDF	CDF		
0.1	0.1	0.5	0.1	2	0	3	2		
			1.0	1	15	3	32		
			5.0	0	331	1	685		
		1.0	0.1	2	0	4	2		
			5.0	0	209	1	397		
			5.0	0.1	4	0	6	1	
	10.0	0.5	0.1	13	0	19	1		
			5.0	3	108	7	170		
			5.0	0.1	72	0	86	1	
		5.0	5.0	0	55	0	73		
			10.0	0.1	0.1	0	0	2	5
					5.0	0	3296	1	6802
5.0	0.1	0			0	4	2		
5.0	5.0	0		863	1	1329			
	10.0	0.5		0.1	0	0	14	2	
				5.0	2	1045	5	1630	
5.0		0.1	0	0	73	2			
5.0	5.0	0	477	0	599				

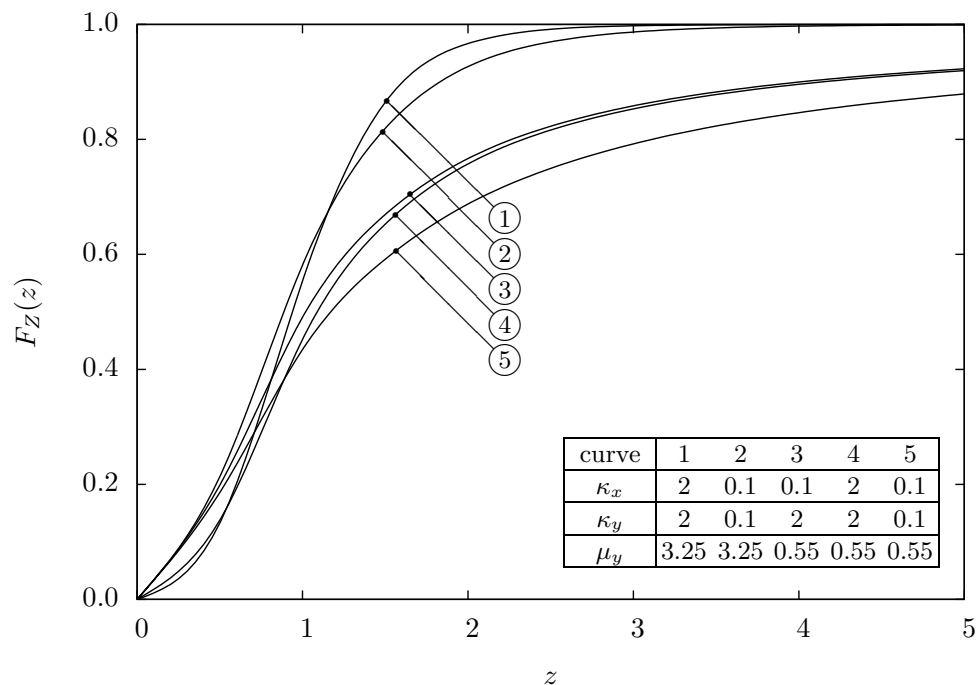


Figure 2.6: CDF of the ratio of Rice and κ - μ random variables.

2.4.2 Cumulative Distribution Function

With (2.2), (2.30) and (2.31), the CDF of Z may be expressed as

$$F_Z(z) = \int_0^z \int_0^\infty \frac{4\mu_y(\kappa_x + 1)(\kappa_y + 1)^{\frac{\mu_y+1}{2}}}{e^{\kappa_x + \mu_y \kappa_y} \kappa_y^{\frac{\mu_y-1}{2}} \hat{x}^2 \hat{y}^{\mu_y+1}} ty^{\mu_y+2} \exp\left[-\frac{\kappa_x + 1}{\hat{x}^2}(ty)^2\right] \times \exp\left(-\mu_y \frac{\kappa_y + 1}{\hat{y}^2} y^2\right) I_0\left(2\sqrt{\kappa_x \frac{\kappa_x + 1}{\hat{x}^2}} ty\right) I_{\mu_y-1}\left(2\mu_y \sqrt{\kappa_y \frac{\kappa_y + 1}{\hat{y}^2}} y\right) dy dt. \quad (2.36)$$

Using [48, Eq. 8.445] to expand in series the function $I_0(\cdot)$, changing the integration order and the integration variable to $w = t^2$ leads to

$$F_Z(z) = \sum_{i=0}^{\infty} \int_0^\infty \int_0^{z^2} \frac{2\mu_y \kappa_x^i (\kappa_x + 1)^{i+1} (\kappa_y + 1)^{\frac{\mu_y+1}{2}}}{i! e^{\kappa_x + \mu_y \kappa_y} \kappa_y^{\frac{\mu_y-1}{2}} \hat{x}^{2i+2} \hat{y}^{\mu_y+1}} w^k y^{2i+\mu_y+2} \times \exp\left[-\left(\frac{\kappa_x + 1}{\hat{x}^2} w + \mu_y \frac{\kappa_y + 1}{\hat{y}^2}\right) y^2\right] I_{\mu_y-1}\left(2\mu_y \sqrt{\kappa_y \frac{\kappa_y + 1}{\hat{y}^2}} y\right) dw dy \quad (2.37)$$

Using [48, Eqs. 3.351.1, 8.356.3], the above integral in w solves to

$$F_Z(z) = \sum_{i=0}^{\infty} \int_0^\infty \frac{2\mu_y \kappa_x^i (\kappa_y + 1)^{\frac{\mu_y+1}{2}}}{i! e^{\kappa_x + \mu_y \kappa_y} \kappa_y^{\frac{\mu_y-1}{2}} \hat{y}^{\mu_y+1}} y^{\mu_y} \exp\left[-\mu_y \frac{\kappa_y + 1}{\hat{y}^2} y^2\right] \times I_{\mu_y-1}\left(2\mu_y \sqrt{\kappa_y \frac{\kappa_y + 1}{\hat{y}^2}} y\right) \left[1 - Q\left(i + 1, \frac{\kappa_x + 1}{\hat{x}^2} z^2 y^2\right)\right] dy. \quad (2.38)$$

The integral in (2.38) can be split in two parts, with one of them carrying the function $Q(\cdot, \cdot)$.

Solving the simpler integral with [49, Eq. 2.15.5.4] and simplifying the summation leads to

$$F_Z(z) = 1 - \sum_{i=0}^{\infty} \int_0^\infty \frac{2\mu_y \kappa_x^i (\kappa_y + 1)^{\frac{\mu_y+1}{2}}}{i! e^{\kappa_x + \mu_y \kappa_y} \kappa_y^{\frac{-\mu_y+1}{2}} \hat{y}^{\mu_y+1}} y^{\mu_y} \exp\left[-\mu_y \frac{\kappa_y + 1}{\hat{y}^2} y^2\right] \times I_{\mu_y-1}\left(2\mu_y \sqrt{\kappa_y \frac{\kappa_y + 1}{\hat{y}^2}} y\right) Q\left(i + 1, \frac{\kappa_x + 1}{\hat{x}^2} z^2 y^2\right) dy. \quad (2.39)$$

Using [50, Eq. 06.08.03.0009.01] to represent $Q(.,.)$ leads to

$$\begin{aligned}
F_Z(z) = & 1 - \sum_{i=0}^{\infty} \int_0^{\infty} \frac{2\mu_y \kappa_x^i \kappa_y^{\frac{-\mu_y+1}{2}} (\kappa_y + 1)^{\frac{\mu_y+1}{2}}}{i! e^{\kappa_x + \mu_y \kappa_y} \hat{y}^{\mu_y+1}} y^{\mu_y} \exp\left(-\mu_y \frac{\kappa_y + 1}{\hat{y}} y^2\right) \\
& \times I_{\mu_y-1}\left(2\mu_y \sqrt{\kappa_y \frac{\kappa_y + 1}{\hat{y}}} y\right) dy \\
& + \sum_{i=0}^{\infty} \sum_{j=0}^i \int_0^{\infty} \frac{2\mu_y \kappa_x^j \kappa_y^{\frac{-\mu_y+1}{2}} (\kappa_x + 1)^{i+1} (\kappa_y + 1)^{\frac{\mu_y+1}{2}} z^{2i+2}}{(i+1)! j! e^{\kappa_x + \mu_y \kappa_y} \hat{x}^{2i+2} \hat{y}^{\mu_y+1}} y^{2i+\mu_y+2} \\
& \times \exp\left[-\left(\frac{\kappa_x + 1}{\hat{x}^2} z^2 + \mu_y \frac{\kappa_y + 1}{\hat{y}^2}\right) y^2\right] I_{\mu_y-1}\left(2\mu_y \sqrt{\kappa_y \frac{\kappa_y + 1}{\hat{y}}} y\right) dy.
\end{aligned} \tag{2.40}$$

Solving the integrals with [49, Eq. 2.15.5.4] and simplifying the summation results in

$$\begin{aligned}
F_Z(z) = & \frac{uz^2}{e^{\mu_y \kappa_y} (1 + uz^2)^{\mu_y+1}} \sum_{i=0}^{\infty} \frac{Q(i+1, \kappa_x)(uz^2)^i}{(i+1)B(i+1, \mu_y)(1 + uz^2)^i} \\
& \times {}_1F_1\left(i + \mu_y + 1, \mu_y, \frac{\mu_y \kappa_y}{1 + uz^2}\right)
\end{aligned} \tag{2.41}$$

in which u is defined by (2.35).

Although (2.41) includes an infinite summation, the evaluation of the CDF converges rapidly for cases of interest. Let I be the number of terms in a truncated summation (as defined earlier). Table 2.3 gives the value of I necessary to obtain a three-decimal-place accuracy (error < 0.0005) and a six-decimal-place accuracy (error < 0.0000005) for the infinite summation of (2.41). For the CDF accuracy, a smaller number of terms I is required for higher values of μ_x or κ_y , or lower values of κ_x or z .

Note that (2.41) may be reduced in the following situations: (i) if $\kappa_x \rightarrow 0$, the corresponding CDF reduces to Rayleigh; (ii) if μ_y is set to unity, the corresponding CDF reduces to Rice; (iii) if $\kappa_y \rightarrow 0$, the corresponding CDF reduces to Nakagami- m , with $m = \mu_y$; and (iv) if $\mu_y = 1$ and $\kappa_y \rightarrow 0$, the corresponding CDF reduces to Rayleigh.

The CDF of Z is shown in Fig. 2.6 for various values of κ_x , κ_y and μ_y . It can be seen that higher values of κ_x , κ_y or μ_y tend to produce steeper curves, approaching the unity faster. On the other hand, a smoother CDF is obtained with smaller values of these parameters.

2.5 Ratio $\eta\text{-}\mu/\eta\text{-}\mu$

Let (1.13) represent the PDF of the numerator X

$$f_X(x) = \frac{4\sqrt{\pi}\mu_x^{\mu_x+\frac{1}{2}}h_x^{\mu_x}x^{2\mu_x}}{\Gamma(\mu_x)H_x^{\mu_x-\frac{1}{2}}\hat{x}^{2\mu_x+1}} \exp\left(-2\mu_x h_x \frac{x^2}{\hat{x}^2}\right) I_{\mu_x-\frac{1}{2}}\left(2\mu_x H_x \frac{x^2}{\hat{x}^2}\right) \quad (2.42)$$

and the PDF of the denominator Y

$$f_Y(y) = \frac{4\sqrt{\pi}\mu_y^{\mu_y+\frac{1}{2}}h_y^{\mu_y}y^{2\mu_y}}{\Gamma(\mu_y)H_y^{\mu_y-\frac{1}{2}}\hat{y}^{2\mu_y+1}} \exp\left(-2\mu_y h_y \frac{y^2}{\hat{y}^2}\right) I_{\mu_y-\frac{1}{2}}\left(2\mu_y H_y \frac{y^2}{\hat{y}^2}\right). \quad (2.43)$$

In the following, the PDF and the CDF of the ratio Z are calculated.

2.5.1 Probability Density Function

With (2.1), (2.42) and (2.43), the PDF of Z may be expressed as

$$f_Z(z) = \int_0^\infty \frac{16\pi\mu_x^{\mu_x+\frac{1}{2}}\mu_y^{\mu_y+\frac{1}{2}}h_x^{\mu_x}h_y^{\mu_y}}{\Gamma(\mu_x)\Gamma(\mu_y)\hat{x}^{2\mu_x+1}\hat{y}^{2\mu_y+1}H_x^{\mu_x-\frac{1}{2}}H_y^{\mu_y-\frac{1}{2}}} z^{2\mu_x}y^{2\mu_x+2\mu_y+1} \exp\left[-2h_x \frac{\mu_x}{\hat{x}^2}(zy)^2\right] \\ \times \exp\left(-2h_y \frac{\mu_y}{\hat{y}^2}y^2\right) I_{\mu_x-\frac{1}{2}}\left[2H_x \frac{\mu_x}{\hat{x}^2}(zy)^2\right] I_{\mu_y-\frac{1}{2}}\left(2H_y \frac{\mu_y}{\hat{y}^2}y^2\right) dy. \quad (2.44)$$

Using [48, Eq. 8.445] to expand in series the second Bessel function in (2.44), and making the integration variable $t = y^2$ results in

$$f_Z(z) = \int_0^\infty \frac{8\pi\mu_x^{\mu_x+\frac{1}{2}}\mu_y^{2i+2\mu_y}h_x^{\mu_x}h_y^{\mu_y}H_y^{2i}}{i!\Gamma(\mu_x)\Gamma(\mu_y)\Gamma\left(i+\mu_y+\frac{1}{2}\right)\hat{x}^{2\mu_x+1}\hat{y}^{4i+4\mu_y}H_x^{\mu_x-\frac{1}{2}}} z^{2\mu_x}t^{2i+\mu_x+2\mu_y-\frac{1}{2}} \\ \times \exp\left[-2h_x \frac{\mu_x}{\hat{x}^2}(zy)^2\right] \exp\left(-2h_y \frac{\mu_y}{\hat{y}^2}y^2\right) I_{\mu_x-\frac{1}{2}}\left[2H_x \frac{\mu_x}{\hat{x}^2}(zy)^2\right] dt. \quad (2.45)$$

Using [48, Eq. 8.335.1] and [49, Eq. 2.15.3.2], the integral in (2.45) solves to

$$f_Z(z) = \frac{2u^{2\mu_x}z^{4\mu_x-1}}{h_x^{\mu_x}h_y^{\mu_y}(1+uz^2)^{2\mu_x+2\mu_y}} \sum_{i=0}^{\infty} \frac{1}{(i+\mu_y)B(\mu_y, i+1)B(2i+2\mu_y, \mu_x)} \\ \times \left[\frac{H_y}{h_y(1+uz^2)}\right]^{2i} {}_2F_1\left[i+\mu_x+\mu_y, i+\mu_x+\mu_y+\frac{1}{2}, \mu_x+\frac{1}{2}, \left(\frac{H_x}{h_x} \frac{uz^2}{1+uz^2}\right)^2\right] \quad (2.46)$$

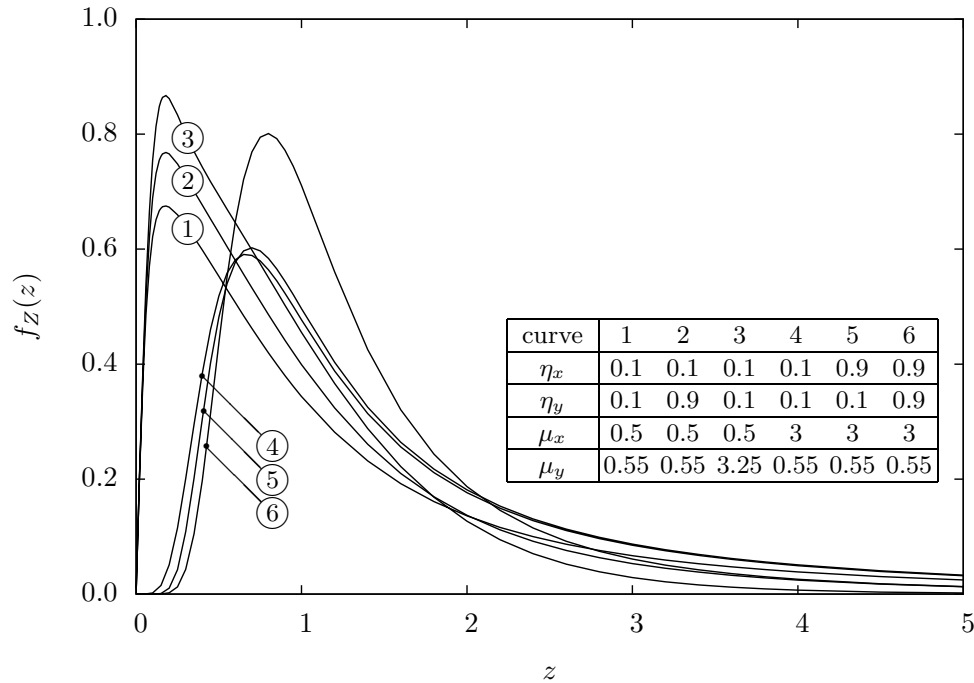


Figure 2.7: PDF of the ratio of η - μ random variables.

in which

$$u = \frac{\mu_x h_x \hat{y}^2}{\mu_y h_y \hat{x}^2}. \quad (2.47)$$

Although (2.46) includes an infinite summation, the evaluation of the PDF converges rapidly for cases of interest. Let I be the number of terms in a truncated summation (as defined earlier). Table 2.4 gives the value of I necessary to obtain a three-decimal-place accuracy (error < 0.0005) and a six-decimal-place accuracy (error < 0.0000005) for the infinite summation of (2.46). For the PDF accuracy, a smaller number of terms I is required for higher values of η_x , η_y or μ_x , or lower values of μ_y or z .

Note that (2.46) may be reduced in the following situations: (i) if μ_x (or μ_y) is set to $\frac{1}{2}$, the corresponding PDF reduces to Hoyt; (ii) if $\eta_x \rightarrow 0$ or $\eta_x \rightarrow \infty$ ($\eta_y \rightarrow 0$ or $\eta_y \rightarrow \infty$), the corresponding PDF reduces to Nakagami- m , with $m = \mu_x$ ($m = \mu_y$); and (iii) if $\mu_x = \frac{1}{2}$ and $\eta_x = 1$ ($\mu_y = \frac{1}{2}$ and $\eta_y = 1$), the corresponding PDF reduces to Rayleigh.

The PDF of Z is shown in Fig. 2.7 for various values of η_x , η_y , μ_x and μ_y . It can be seen that diminishing values of η_x tends to slightly spread out the probability density. On the other hand, a PDF with smaller tail and a higher peak value is obtained for increasing values of η_y or

Table 2.4: Relation between number of terms and accuracy in the infinite summation of (2.46) and (2.54).

Parameters					smallest I for accuracy of						
η_x	η_y	μ_x	μ_y	z	3-decimal-place		6-decimal-place				
					PDF	CDF	PDF	CDF			
0.1	0.1	0.5	0.5	0.1	177	3	348	10			
				1.0	81	308	168	643			
				5.0	4	7656	12	15959			
			1.0	0.1	213	3	391	7			
				5.0	8	4807	23	9171			
				5.0	0.1	408	2	625	5		
		5.0	0.5	0.1	0	0	312	21			
				5.0	2	75011	4	99915			
				5.0	0.1	0	0	0	0		
			5.0	0.1	0	0	19892	15	30687		
				0.9	0.5	0.5	0.1	1	3	2	7
							5.0	0	4921	1	9542
	5.0	0.1	2	2		4	4				
	5.0	0.5	0.5	0.1	0	0	1	0			
				5.0	0	49181	0	92606			
			5.0	0.1	0	0	0	0			
		5.0	0.1	0	0	15234	0	21690			
			0.9	0.5	0.5	0.1	174	0	351	2	
						5.0	3	305	8	638	
	5.0	0.1	375		0	603	1				
	5.0	0.5	0.5	0.1	0	0	0	0			
				5.0	2	3028	4	6322			
			5.0	0.1	0	0	0	0			
		5.0	0.1	0	0	784	9	1216			
0.9			0.5	0.5	0.1	1	0	3	2		
					5.0	0	197	0	384		
5.0	0.1	1		0	3	1					
5.0	0.5	0.5	0.1	0	0	0	0				
			5.0	0	66	0	96				
		5.0	0.1	0	0	0	0				
	5.0	0.9	0.5	0.5	0.1	0	0	0			
					5.0	0	1944	0	3778		
		5.0		0.1	0	0	0	0			
5.0	0.9	0.5	0.5	0.1	0	0	0				
				5.0	0	601	0	861			

μ_y , or diminishing value of μ_x .

2.5.2 Cumulative Distribution Function

With (2.2), (2.42) and (2.43), the CDF of Z may be expressed as

$$\begin{aligned}
 F_Z(z) &= \int_0^z \int_0^\infty \frac{16\pi\mu_x^{\mu_x+\frac{1}{2}}\mu_y^{\mu_y+\frac{1}{2}}h_x^{\mu_x}h_y^{\mu_y}}{\Gamma(\mu_x)\Gamma(\mu_y)\hat{x}^{2\mu_x+1}\hat{y}^{2\mu_y+1}H_x^{\mu_x-\frac{1}{2}}H_y^{\mu_y-\frac{1}{2}}} t^{2\mu_x}y^{2\mu_x+2\mu_y+1} \\
 &\quad \times \exp\left[-2\frac{\mu_x}{\hat{x}^2}h_x(ty)^2\right] \exp\left(-2h_y\frac{\mu_y}{\hat{y}^2}y^2\right) I_{\mu_x-\frac{1}{2}}\left[2H_x\frac{\mu_x}{\hat{x}^2}(ty)^2\right] \\
 &\quad \times I_{\mu_y-\frac{1}{2}}\left(2H_y\frac{\mu_y}{\hat{y}^2}y^2\right) dy dt.
 \end{aligned} \tag{2.48}$$

Using [48, Eq. 8.445] to expand in series the first Bessel function in (2.48), changing the integration order and the integration variable to $w = t^2$ leads to

$$\begin{aligned}
 F_Z(z) &= \sum_{i=0}^{\infty} \int_0^\infty \int_0^{z^2} \frac{8\pi\mu_x^{2i+2\mu_x}\mu_y^{\mu_y+\frac{1}{2}}h_x^{\mu_x}H_x^{2i}h_y^{\mu_y}}{i!\Gamma(\mu_x)\Gamma(\mu_y)\Gamma\left(i+\mu_x+\frac{1}{2}\right)\hat{x}^{4i+4\mu_x}\hat{y}^{2\mu_y+1}H_y^{\mu_y-\frac{1}{2}}} w^{2i+2\mu_x-1} \\
 &\quad \times y^{4i+4\mu_x+2\mu_y} \exp\left[-2\left(h_x\frac{\mu_x}{\hat{x}^2}w+h_y\frac{\mu_y}{\hat{y}^2}\right)y^2\right] I_{\mu_y-\frac{1}{2}}\left(2H_y\frac{\mu_y}{\hat{y}^2}y^2\right) dw dy.
 \end{aligned} \tag{2.49}$$

Using [48, Eqs. 3.381.1, 8.356.3], the above integral in w solves to

$$\begin{aligned}
 F_Z(z) &= \sum_{i=0}^{\infty} \int_0^\infty \frac{2^{-2i-2\mu_x+3}\pi\mu_y^{\mu_y+\frac{1}{2}}H_x^{2i}h_y^{\mu_y}}{i!\Gamma(\mu_x)\Gamma\left(i+\mu_x+\frac{1}{2}\right)\Gamma(\mu_y)\hat{y}^{2\mu_y+1}h_x^{2i+\mu_x}H_y^{\mu_y-\frac{1}{2}}} y^{2\mu_y} \exp\left(-2h_y\frac{\mu_y}{\hat{y}^2}y^2\right) \\
 &\quad \times I_{\mu_y-\frac{1}{2}}\left(2H_y\frac{\mu_y}{\hat{y}^2}y^2\right) \left[\Gamma(2i+2\mu_x) - \Gamma\left(2i+2m_x, h_x\frac{\mu_x}{\hat{x}^2}z^2y^2\right)\right] dy.
 \end{aligned} \tag{2.50}$$

The integral in (2.50) can be split in two parts, with one of them carrying the function $\Gamma(.,.)$.

Solving the simpler integral with [49, Eq. 2.15.3.2] and simplifying the summation leads to

$$\begin{aligned}
 F_Z(z) &= 1 - \sum_{i=0}^{\infty} \int_0^\infty \frac{2^{-2i-2\mu_x+3}\pi\mu_y^{\mu_y+\frac{1}{2}}H_x^{2i}h_y^{\mu_y}}{i!\Gamma(\mu_x)\Gamma\left(i+\mu_x+\frac{1}{2}\right)\Gamma(\mu_y)\hat{y}^{2\mu_y+1}h_x^{2i+\mu_x}H_y^{\mu_y-\frac{1}{2}}} y^{2\mu_y} \\
 &\quad \times \exp\left(-2h_y\frac{\mu_y}{\hat{y}^2}y^2\right) I_{\mu_y-\frac{1}{2}}\left(2H_y\frac{\mu_y}{\hat{y}^2}y^2\right) \Gamma\left(2i+2m_x, h_x\frac{\mu_x}{\hat{x}^2}z^2y^2\right) dy.
 \end{aligned} \tag{2.51}$$

With [50, Eq. 06.08.17.0003.02] and [21, Eqs. 6.5.3, 6.5.4, 6.5.29], the functions $\Gamma(\cdot, \cdot)$ and $Q(\cdot, \cdot)$ may be expressed as

$$\Gamma(a+n, z) = \Gamma(a+n) \left[Q(a, z) + e^{-z} \sum_{j=0}^{n-1} \frac{z^{j+a}}{\Gamma(j+a+1)} \right], \text{ and} \quad (2.52)$$

$$Q(a, z) = 1 - e^{-z} \sum_{j=0}^{\infty} \frac{z^{j+a}}{\Gamma(j+a+1)}.$$

Using (2.52) in (2.51) leads to

$$\begin{aligned} F_Z(z) = & 1 - \sum_{i=0}^{\infty} \int_0^{\infty} \frac{4\sqrt{\pi}\Gamma(i+\mu_x)\mu_y^{\mu_y+\frac{1}{2}}H_x^{2i}h_y^{\mu_y}}{i!\Gamma(\mu_x)\Gamma(\mu_y)\hat{y}^{2\mu_y+1}h_x^{2i+\mu_x}H_y^{\mu_y-\frac{1}{2}}} y^{2\mu_y} \exp\left(-2h_y\frac{\mu_y}{\hat{y}^2}y^2\right) \\ & \times I_{\mu_y-\frac{1}{2}}\left(2H_y\frac{\mu_y}{\hat{y}^2}y^2\right) \Gamma\left(2i+1, \frac{h_xz^2y^2}{\hat{x}^2}\right) dy \\ & + \sum_{i=0}^{\infty} \sum_{j=2i}^{\infty} \int_0^{\infty} \frac{2^{(j+2\mu_x+2)}\sqrt{\pi}\Gamma(i+\mu_x)\mu_x^{j+2\mu_x}\mu_y^{\mu_y+\frac{1}{2}}H_x^{2i}h_y^{\mu_y}}{i!\Gamma(\mu_x)\Gamma(j+2\mu_x+1)\Gamma(\mu_y)\hat{x}^{2j+4\mu_x}\hat{y}^{2\mu_y+1}h_x^{2i-j-\mu_x}H_y^{\mu_y-\frac{1}{2}}} z^{2j+4\mu_x} \\ & \times y^{2j+4\mu_x+2\mu_y} \exp\left[-\left(\frac{h_x}{\hat{x}^2}z^2+h_y\frac{\mu_y}{\hat{y}^2}\right)y^2\right] I_{\mu_y-\frac{1}{2}}\left(2H_y\frac{\mu_y}{\hat{y}^2}y^2\right) dy. \end{aligned} \quad (2.53)$$

Solving the integrals with [49, Eq. 2.15.3.2] and simplifying the summations results in

$$\begin{aligned} F_Z(z) = & \frac{(uz^2)^{2\mu_x}}{h_y^{\mu_y}(1+uz^2)^{2\mu_x+2\mu_y}} \sum_{i=0}^{\infty} \frac{(uz^2)^i}{(i+2\mu_x)B(i+2\mu_x, 2\mu_y)((1+uz^2))^i} \\ & \times {}_2F_1\left[\frac{i}{2}+\mu_x+\mu_y, \frac{i}{2}+\mu_x+\mu_y+\frac{1}{2}, \mu_y+\frac{1}{2}, \left(\frac{H_y}{h_y}\frac{1}{1+uz^2}\right)^2\right] \\ & \times \left\{1 - \frac{1}{i_c B(i_c, \mu_x) h_x^{\mu_x}} \left(\frac{H_x}{h_x}\right)^{2i_c} {}_2F_1\left[1, i_c+\mu_x, i_c+1, \left(\frac{H_x}{h_x}\right)^2\right]\right\} \end{aligned} \quad (2.54)$$

in which u is defined by (2.47), and $i_c = \lceil \frac{i+1}{2} \rceil$.

Although (2.54) includes an infinite summation, the evaluation of the CDF converges rapidly for cases of interest. Let I be the number of terms in a truncated summation (as defined earlier). Table 2.4 gives the value of I necessary to obtain a three-decimal-place accuracy (error < 0.0005) and a six-decimal-place accuracy (error < 0.0000005) for the infinite summation of (2.54). For the CDF accuracy, a smaller number of terms I is required for higher values of η_x , η_y , or μ_y , or lower values of μ_x or z .

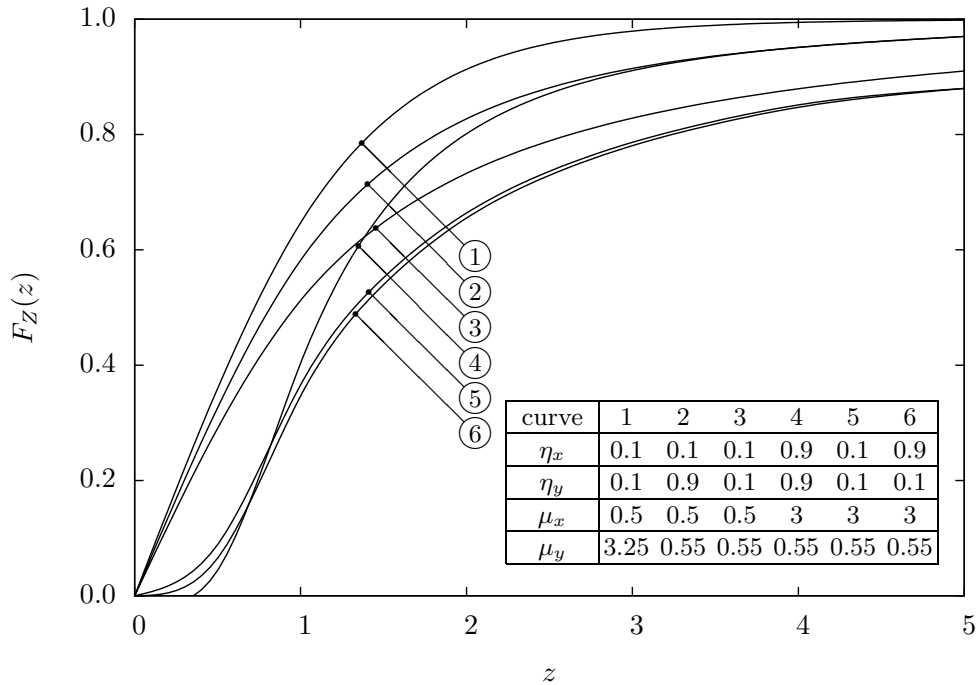


Figure 2.8: CDF of the ratio of η - μ random variables.

Note that (2.54) may be reduced in the following situations: (i) if μ_x (or μ_y) is set to $\frac{1}{2}$, the corresponding CDF reduces to Hoyt; (ii) if $\eta_x \rightarrow 0$ or $\eta_x \rightarrow \infty$ ($\eta_y \rightarrow 0$ or $\eta_y \rightarrow \infty$), the corresponding CDF reduces to Nakagami- m , with $m = \mu_x$ ($m = \mu_y$); and (iii) if $\mu_x = \frac{1}{2}$ and $\eta_x = 1$ ($\mu_y = \frac{1}{2}$ and $\eta_y = 1$), the corresponding CDF reduces to Rayleigh.

The CDF of Z is shown in Fig. 2.8 for various values of η_x , η_y , μ_x and μ_y . It can be seen that lower values of μ_x tends to smoothen the function. On the other hand, a CDF with steeper climb is obtained with higher values of η_x and η_y .

2.6 Ratio η - μ / κ - μ

Let (1.13) represent the PDF of the numerator X

$$f_X(x) = \frac{4\sqrt{\pi}\mu_x^{\mu_x+\frac{1}{2}}h_x^{\mu_x}x^{2\mu_x}}{\Gamma(\mu_x)H_x^{\mu_x-\frac{1}{2}}\hat{x}^{2\mu_x+1}} \exp\left(-2\mu_x h_x \frac{x^2}{\hat{x}^2}\right) I_{\mu_x-\frac{1}{2}}\left(2\mu_x H_x \frac{x^2}{\hat{x}^2}\right) \quad (2.55)$$

and (1.15) represent the PDF of the denominator Y

$$f_Y(y) = \frac{2\mu_y(\kappa_y + 1)^{\frac{\mu_y+1}{2}} y^{\mu_y}}{\kappa_y^{\frac{\mu_y-1}{2}} e^{\mu_y \kappa_y} \hat{y}^{\mu_y+1}} \exp \left[-\mu_y(\kappa_y + 1) \frac{y^2}{\hat{y}^2} \right] I_{\mu_y-1} \left(2\mu_y \sqrt{\kappa_y(\kappa_y + 1)} \frac{y}{\hat{y}} \right). \quad (2.56)$$

In the following, the PDF and the CDF of the ratio Z are calculated.

2.6.1 Probability Density Function

With (2.1), (2.55) and (2.56), the PDF of Z may be expressed as

$$f_Z(z) = \int_0^\infty \frac{8\sqrt{\pi} \mu_x^{\mu_x+\frac{1}{2}} \mu_y h_x^{\mu_x} (\kappa_y + 1)^{\frac{\mu_y+1}{2}}}{\Gamma(\mu_x) e^{\mu_y \kappa_y} \hat{x}^{2\mu_x+1} \hat{y}^{\mu_y+1} H_x^{\mu_x-\frac{1}{2}} \kappa_y^{\frac{\mu_y-1}{2}}} z^{2\mu_x} y^{2\mu_x+\mu_y+1} \exp \left[-2h_x \frac{\mu_x}{\hat{x}^2} (zy)^2 \right] \\ \times \exp \left(-(\kappa_y + 1) \frac{\mu_y}{\hat{y}^2} y^2 \right) I_{\mu_x-\frac{1}{2}} \left[2H_x \frac{\mu_x}{\hat{x}^2} (zy)^2 \right] I_{\mu_y-1} \left(2\sqrt{\kappa_y(\kappa_y + 1)} \frac{\mu_y}{\hat{y}} y \right) dy. \quad (2.57)$$

Using [48, Eq. 8.445] to expand in series the second Bessel function in (2.57), and making the integration variable $t = y^2$ results in

$$f_Z(z) = \sum_{i=0}^{\infty} \int_0^\infty \frac{4\sqrt{\pi} \mu_x^{\mu_x+\frac{1}{2}} \mu_y^{2i+\mu_y} h_x^{\mu_x} \kappa_y^i (\kappa_y + 1)^{i+\mu_y}}{i! \Gamma(\mu_x) \Gamma(i + \mu_y) e^{\mu_y \kappa_y} \hat{x}^{2\mu_x+1} \hat{y}^{2i+2\mu_y} H_x^{\mu_x-\frac{1}{2}}} z^{2\mu_x} t^{i+\mu_x+\mu_y-\frac{1}{2}} \\ \times \exp \left[-2 \left(h_x \frac{\mu_x}{\hat{x}^2} z^2 + (\kappa_y + 1) \frac{\mu_y}{\hat{y}^2} \right) t \right] I_{\mu_x-\frac{1}{2}} \left(2H_x \frac{\mu_x}{\hat{x}^2} z^2 t \right) dt. \quad (2.58)$$

Using [48, Eq. 8.335.1] and [49, Eq. 2.15.3.2], the integral in (2.58) solves to

$$f_Z(z) = \frac{2u^{2\mu_x} z^{4\mu_x-1}}{h_x^{\mu_x} e^{\mu_y \kappa_y} (1 + uz^2)^{2\mu_x+\mu_y}} \sum_{i=0}^{\infty} \frac{1}{i! B(2\mu_x, i + \mu_y)} \left(\frac{\mu_y \kappa_y}{1 + uz^2} \right)^i \\ \times {}_2F_1 \left[\frac{i + 2\mu_x + \mu_y}{2}, \frac{i + 2\mu_x + \mu_y + 1}{2}, \mu_x + \frac{1}{2}, \left(\frac{H_x}{h_x} \frac{uz^2}{1 + uz^2} \right)^2 \right] \quad (2.59)$$

in which

$$u = \frac{2\mu_x h_x \hat{y}^2}{\mu_y (\kappa_y + 1) \hat{x}^2}. \quad (2.60)$$

Although (2.59) includes an infinite summation, the evaluation of the PDF converges rapidly for cases of interest. Let I be the number of terms in a truncated summation (as defined earlier).

Table 2.5: Relation between number of terms and accuracy in the infinite summation of (2.59) and (2.66).

Parameters					smallest I for accuracy of						
η_x	κ_y	μ_x	μ_y	z	3-decimal-place		6-decimal-place				
					PDF	CDF	PDF	CDF			
0.1	0.1	0.5	0.5	0.1	2	7	4	16			
				1.0	1	231	3	540			
				5.0	0	317	1	896			
			1.0	0.1	2	5	4	11			
				5.0	0	331	2	932			
				5.0	0.1	4	3	7	7		
		5.0	0.1	4	3	7	7				
			5.0	0	102	2	1004				
			5.0	0.5	0.1	0	53	2	121		
				5.0	0	971	1	1841			
				5.0	0.1	0	10	0	23		
			5.0	0	0	1	1289				
	10.0	0.5	0.5	0.1	14	10	20	16			
				5.0	3	298	8	976			
				5.0	0.1	75	63	88	79		
			5.0	0.1	0	0	54	1071			
				0.5	0.1	0	8	0	28		
				5.0	2	661	5	1695			
		5.0	0.1	0	64	0	81				
			5.0	0	0	0	0				
			0.9	0.1	0.5	0.5	0.1	2	0	3	1
							5.0	0	1	1	4
							5.0	0.1	4	0	6
						5.0	5.0	0	0	2	3
0.5	0.1	0					0	0	0		
5.0	0	2					1	8			
5.0	0.1	0	0		0	0					
	5.0	0	0		0	2					
	10.0	0.5	0.5		0.1	13	7	19	14		
					5.0	3	3	7	6		
					5.0	0.1	72	50	86	72	
			5.0		5.0	0	13	0	30		
0.5				0.1	0	0	0	0			
5.0				2	2	5	6				
5.0	0.1	0	0	0	0						
	5.0	0	4	0	10						

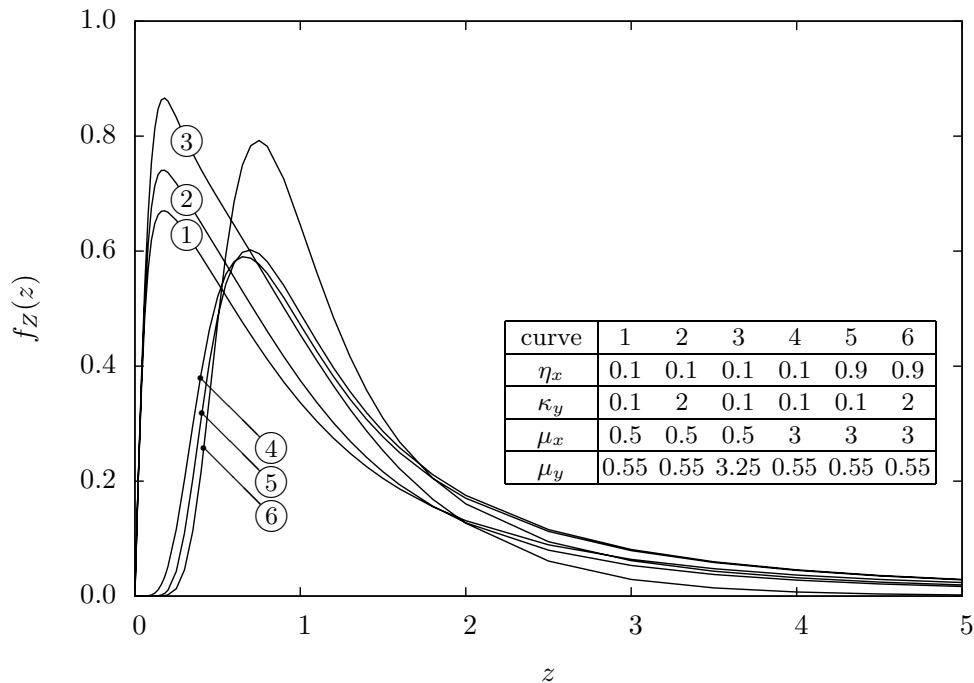


Figure 2.9: PDF of the ratio of $\eta\text{-}\mu$ and $\kappa\text{-}\mu$ random variables.

Table 2.5 gives the value of I necessary to obtain a three-decimal-place accuracy (error < 0.0005) and a six-decimal-place accuracy (error < 0.0000005) for the infinite summation of (2.59). For the PDF accuracy, a smaller number of terms I is required for higher values of η_x or μ_x , or lower values of κ_y , μ_y or z .

Note that (2.59) may be reduced in the following situations: (i) if μ_x is set to $\frac{1}{2}$, the corresponding PDF reduces to Hoyt; (ii) if μ_y is set to unity, the corresponding PDF reduces to Rice; (iii) if $\kappa_y \rightarrow 0$, the corresponding PDF reduces to Nakagami- m , with $m = \mu_y$; and (iv) if $\mu_y = 1$ and $\kappa_y \rightarrow 0$, the corresponding PDF reduces to Rayleigh.

The PDF of Z is shown in Fig. 2.9 for various values of η_x , κ_y , μ_x and μ_y . It can be seen that increasing values of μ_x shifts the curve away from the ordinate axis. Also, diminishing values of η_x tends to slightly spread out the probability density. On the other hand, a PDF with smaller tail and a higher peak value is obtained for increasing values of κ_y or μ_y , or diminishing value of μ_x .

If μ_x is a positive integer, i.e., $\mu_x = 1, 2, \dots$, then the Bessel function may be expressed by [48, Eq. 8.467], as illustrated in (2.21). Using (2.21) in (2.57), and solving the integral in y with

[49, Eq. 2.15.5.4] leads to

$$\begin{aligned}
f_Z(z) &= \frac{2h_x^{\mu_x}}{z\Gamma(\mu_x)\Gamma(\mu_y)e^{\kappa_y\mu_y}(1+u_1z^2)^{\mu_y}} \sum_{i=0}^{\mu_x-1} \frac{(-1)^i(i+\mu_x-1)!\Gamma(-i+\mu_x+\mu_y)}{i!(-i+\mu_x-1)!(2H_x)^{i+\mu_x}} \\
&\quad \times \left[\frac{u_1z^2}{(h_x-H_x)(1+u_1z^2)} \right]^{-i+\mu_x} {}_1F_1\left(-i+\mu_x+\mu_y, \mu_y, \frac{\mu_y\kappa_y}{1+u_1z^2}\right) \\
&+ \frac{2h_x^{\mu_x}}{z\Gamma(\mu_x)\Gamma(\mu_y)e^{\kappa_y\mu_y}(1+u_2z^2)^{\mu_y}} \sum_{i=0}^{\mu_x-1} \frac{(-1)^{\mu_x}(-i+\mu_y)}{(i+\mu_x-1)!\Gamma(-i+\mu_x+\mu_y)(2H_x)^{i+\mu_x}} \\
&\quad \times \left[\frac{u_2z^2}{(h_x+H_x)(1+u_2z^2)} \right]^{-i+\mu_x} {}_1F_1\left(-i+\mu_x+\mu_y, \mu_y, \frac{\mu_y\kappa_y}{1+u_2z^2}\right)
\end{aligned} \tag{2.61}$$

in which

$$u_1 = \frac{2\mu_x(h_x-H_x)\hat{y}^2}{\mu_y(\kappa_y+1)\hat{x}^2}, \quad \text{and} \quad u_2 = \frac{2\mu_x(h_x+H_x)\hat{y}^2}{\mu_y(\kappa_y+1)\hat{x}^2}. \tag{2.62}$$

2.6.2 Cumulative Distribution Function

With (2.2) and (2.59), the CDF of Z may be expressed as

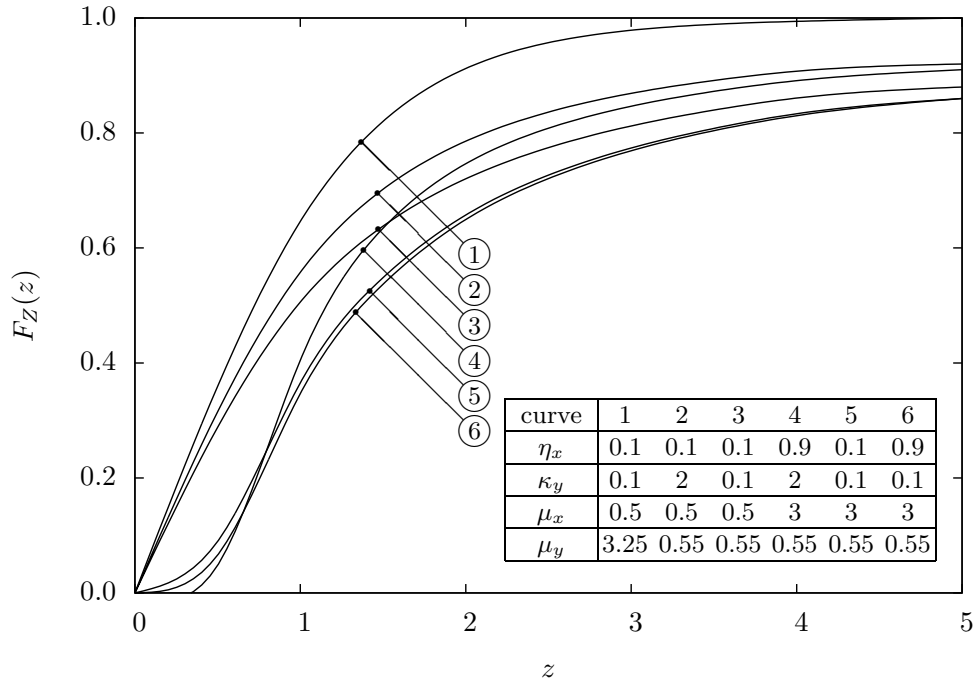
$$\begin{aligned}
F_Z(z) &= \int_0^z \frac{2u^{2\mu_x}t^{4\mu_x-1}}{h_x^{\mu_x}e^{\mu_y\kappa_y}(1+ut^2)^{2\mu_x+\mu_y}} \sum_{i=0}^{\infty} \frac{1}{i!B(2\mu_x, i+\mu_y)} \left(\frac{\mu_y\kappa_y}{1+ut^2}\right)^i \\
&\quad \times {}_2F_1\left[\frac{i+2\mu_x+\mu_y}{2}, \frac{i+2\mu_x+\mu_y+1}{2}, \mu_x+\frac{1}{2}, \left(\frac{H_x}{h_x} \frac{ut^2}{1+ut^2}\right)^2\right] dt.
\end{aligned} \tag{2.63}$$

Using in (2.63) the transformation of the hypergeometric function given by [50, Eq. 07.23.17.0116.01] leads to

$$\begin{aligned}
F_Z(z) &= \frac{2u^{2\mu_x}}{h_x^{\mu_x}e^{\mu_y\kappa_y}} \sum_{i=0}^{\infty} \int_0^z \frac{h_x^{2\mu_x+\mu_y}t^{4\mu_x-1}}{i!B(2\mu_x, i+\mu_y)[h_x+(h_x+H_x)ut^2]^{2\mu_x+\mu_y}} \\
&\quad \times \left[\frac{\mu_y\kappa_y h_x}{h_x+(h_x+H_x)ut^2} \right]^i {}_2F_1\left(i+2\mu_x+\mu_y, \mu_x, 2\mu_x, \frac{2H_x ut^2}{h_x+(h_x+H_x)ut^2}\right) dt.
\end{aligned} \tag{2.64}$$

Expanding in series the function ${}_2F_1(\cdot)$ with [48, Eq. 9.100], and using [48, Eq. 8.391] to integrate on t results in

$$F_Z(z) = \sum_{j=0}^{\infty} \sum_{i=0}^{\infty} \frac{2^j(i+2\mu_x+\mu_y)_j(\mu_x)_j}{i!j!(2\mu_x)_j B(2\mu_x, i+\mu_y)e^{\mu_y\kappa_y}} \frac{(\mu_y\kappa_y)^i h_x^{\mu_x} H_x^j}{(h_x+H_x)^{j+2\mu_x} B\left(\frac{uz^2}{1+uz^2}, j+2\mu_x, i+\mu_y\right)} \tag{2.65}$$

Figure 2.10: CDF of the ratio of η - μ and κ - μ random variables.

in which $(\cdot)_n$ is the Pochhammer symbol, and $B(\cdot, \cdot, \cdot)$ is the incomplete beta function [48, Eq. 8.391]. Using [50, Eqs. 06.18.17.0004.01, 06.21.17.0003.01] and [21, Eq. 6.6.3], (2.65) may be expressed as

$$\begin{aligned}
F_Z(z) = & I_{\frac{uz^2}{1+uz^2}}(2\mu_x, \mu_y) + \frac{(uz^2)^{2\mu_x}}{(1+uz^2)^{2\mu_x+\mu_y}} \sum_{i=0}^{\infty} \frac{1 - Q(i+1, \mu_y \kappa_y)}{(i+\mu_y)B(2\mu_x, i+\mu_y)(1+uz^2)^i} \\
& - \frac{2h_x^{\mu_x} H_x (uz^2)^{2\mu_x}}{e^{\mu_y \kappa_y} (h_x + H_x)^{2\mu_x+1} (1+uz^2)^{2\mu_x+\mu_y}} \sum_{i=0}^{\infty} \frac{1}{(i+1)(i+2\mu_x)} \\
& \times \frac{1}{B(\mu_x, i+1)B(i+2\mu_x, \mu_y)} \left[\frac{2H_x uz^2}{(h_x + H_x)(1+uz^2)} \right]^i \\
& \times {}_1F_1 \left(i+2\mu_x + \mu_y, \mu_y, \frac{\mu_y \kappa_y}{1+uz^2} \right) {}_2F_1 \left(1, i+\mu_x+1, i+2, \frac{2H_x}{h_x + H_x} \right)
\end{aligned} \tag{2.66}$$

in which $I_x(\cdot, \cdot)$ is the regularized incomplete beta function [48, Eq. 8.392], and u is given by (2.60).

Although (2.66) includes an infinite summation, the evaluation of the CDF converges rapidly for cases of interest. Let I be the number of terms in a truncated summation (as defined earlier). Table 2.5 gives the value of I necessary to obtain a three-decimal-place accuracy (error < 0.0005) and a six-decimal-place accuracy (error < 0.0000005) for the infinite summation of (2.66). For

the CDF accuracy, a smaller number of terms I is required for higher values of η_x or μ_y , or lower values of κ_y , μ_x or z .

Note that (2.66) may be reduced in the following situations: (i) if μ_x is set to $\frac{1}{2}$, the corresponding CDF reduces to Hoyt; (ii) if μ_y is set to unity, the corresponding CDF reduces to Rice; (iii) if $\kappa_y \rightarrow 0$, the corresponding CDF reduces to Nakagami- m , with $m = \mu_y$; and (iv) if $\mu_y = 1$ and $\kappa_y \rightarrow 0$, the corresponding CDF reduces to Rayleigh.

The CDF of Z is shown in Fig. 2.10 for various values of η_x , κ_y , μ_x and μ_y . It can be seen that lower values of μ_x tends to smoothen the function. On the other hand, a CDF with steeper climb is obtained with higher values of η_x and κ_y .

2.7 Ratio κ - μ/κ - μ

Let (1.15) represent the PDF of the numerator X

$$f_X(x) = \frac{2\mu_x(\kappa_x + 1)^{\frac{\mu_x+1}{2}} x^{\mu_x}}{\kappa_x^{\frac{\mu_x-1}{2}} e^{\mu_x \kappa_x} \hat{x}^{\mu_x+1}} \exp \left[-\mu_x(\kappa_x + 1) \frac{x^2}{\hat{x}^2} \right] I_{\mu_x-1} \left(2\mu_x \sqrt{\kappa_x(\kappa_x + 1)} \frac{x}{\hat{x}} \right) \quad (2.67)$$

and the PDF of the denominator Y

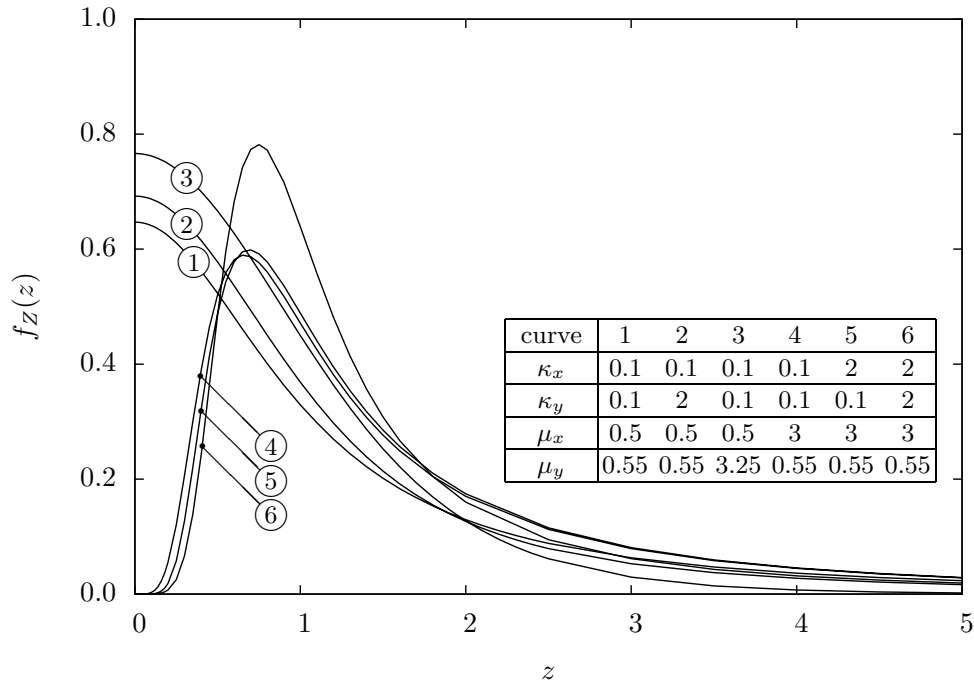
$$f_Y(y) = \frac{2\mu_y(\kappa_y + 1)^{\frac{\mu_y+1}{2}} y^{\mu_y}}{\kappa_y^{\frac{\mu_y-1}{2}} e^{\mu_y \kappa_y} \hat{y}^{\mu_y+1}} \exp \left[-\mu_y(\kappa_y + 1) \frac{y^2}{\hat{y}^2} \right] I_{\mu_y-1} \left(2\mu_y \sqrt{\kappa_y(\kappa_y + 1)} \frac{y}{\hat{y}} \right). \quad (2.68)$$

In the following, the PDF and the CDF of the ratio Z are calculated.

2.7.1 Probability Density Function

With (2.1), (2.67) and (2.68), the PDF of Z may be expressed as

$$\begin{aligned} f_Z(z) &= \int_0^\infty \frac{4\mu_x \mu_y (\kappa_x + 1)^{\frac{\mu_x+1}{2}} (\kappa_y + 1)^{\frac{\mu_y+1}{2}}}{\kappa_x^{\frac{\mu_x-1}{2}} \kappa_y^{\frac{\mu_y-1}{2}} e^{\mu_x \kappa_x + \mu_y \kappa_y} \hat{x}^{\mu_x+1} \hat{y}^{\mu_y+1}} z^{\mu_x} y^{\mu_x + \mu_y + 1} \\ &\quad \times \exp \left[-\mu_x \frac{\kappa_x + 1}{\hat{x}^2} (zy)^2 \right] \exp \left(-\mu_y \frac{\kappa_y + 1}{\hat{y}^2} y^2 \right) \\ &\quad \times I_{\mu_x-1} \left(2\mu_x \sqrt{\kappa_x \frac{\kappa_x + 1}{\hat{x}^2}} zy \right) I_{\mu_y-1} \left(2\mu_y \sqrt{\kappa_y \frac{\kappa_y + 1}{\hat{y}^2}} y \right) dy. \end{aligned} \quad (2.69)$$

Figure 2.11: PDF of the ratio of κ - μ random variables.

Using [48, Eq. 8.445] to expand in series the second Bessel function in (2.69) results in

$$\begin{aligned}
 f_Z(z) &= \sum_{i=0}^{\infty} \int_0^{\infty} \frac{4\mu_x\mu_y^{2i+\mu_y}(\kappa_x+1)^{\frac{\mu_x+1}{2}}(\kappa_y+1)^{i+\mu_y}}{i!\Gamma(i+\mu_y)\kappa_x^{\frac{\mu_x-1}{2}}\kappa_y^i e^{\mu_x\kappa_x+\mu_y\kappa_y}\hat{x}^{\mu_x+1}\hat{y}^{2i+2\mu_y}} z^{\mu_x}y^{2i+\mu_x+2\mu_y} \\
 &\times \exp\left[-\left(\mu_x\frac{\kappa_x+1}{\hat{x}^2}z^2+\mu_y\frac{\kappa_y+1}{\hat{y}^2}\right)y^2\right] I_{\mu_x-1}\left(2\mu_x\sqrt{\kappa_x\frac{\kappa_x+1}{\hat{x}^2}}ry\right) dy.
 \end{aligned} \tag{2.70}$$

Using [49, Eq. 2.15.5.4], the integral in y may be solved to

$$\begin{aligned}
 f_Z(z) &= \frac{2u^{\mu_x}z^{2\mu_x-1}}{e^{\mu_x\kappa_x+\mu_y\kappa_y}(1+uz^2)^{\mu_x+\mu_y}} \sum_{i=0}^{\infty} \frac{1}{i!B(i+\mu_y,\mu_x)} \left(\frac{\mu_y\kappa_y}{1+uz^2}\right)^i \\
 &\times {}_1F_1\left(i+\mu_x+\mu_y,\mu_x,\frac{\mu_x\kappa_x uz^2}{1+uz^2}\right)
 \end{aligned} \tag{2.71}$$

in which

$$u = \frac{\mu_x(\kappa_x+1)\hat{y}^2}{\mu_y(\kappa_y+1)\hat{x}^2}. \tag{2.72}$$

Although (2.71) includes an infinite summation, the evaluation of the PDF converges rapidly for cases of interest. Let I be the number of terms in a truncated summation (as defined earlier). Table 2.6 gives the value of I necessary to obtain a three-decimal-place accuracy (error < 0.0005)

Table 2.6: Relation between number of terms and accuracy in the infinite summation of (2.71) and (2.78).

Parameters					smallest I for accuracy of					
κ_x	κ_y	μ_x	μ_y	z	3-decimal-place		6-decimal-place			
					PDF	CDF	PDF	CDF		
0.1	0.1	0.5	0.5	0.1	2	0	4	2		
				1.0	1	9	3	19		
				5.0	0	167	1	345		
			1.0	0.1	2	0	4	2		
				5.0	0	106	2	202		
				5.0	0.1	4	0	7	2	
		5.0	5.0	0	47	2	75			
			0.5	0.1	0	0	2	0		
				5.0	0	1645	1	3400		
				5.0	0.1	0	0	1	0	
			10.0	0.5	0.5	0.1	14	0	20	2
						5.0	3	56	8	90
	5.0	0.1			75	0	88	2		
	5.0	5.0		0	31	54	42			
		0.5		0.1	0	0	10	0		
				5.0	2	521	5	815		
	5.0	5.0	0.1	0	0	0	0			
		5.0	0	239	0	304				
		10.0	0.1	0.5	0.1	1	1	3	4	
					5.0	0	1649	1	3404	
	5.0			0.1	3	0	6	3		
	5.0		5.0	0	434	1	670			
			0.5	0.1	0	0	0	0		
				5.0	0	16469	1	33982		
5.0	5.0	0.1	0	0	0	0				
	5.0	0	4295	0	6608					
	10.0	0.5	0.5	0.1	11	0	18	3		
				5.0	2	525	5	820		
5.0		0.1	66	0	83	3				
5.0	0.5	5.0	0	244	0	308				
		0.1	0	0	0	0				
	5.0	2	5205	4	8113					
	5.0	0.1	0	0	0	0				
5.0	0	2343	0	2922						

and a six-decimal-place accuracy (error < 0.0000005) for the infinite summation of (2.71). For the PDF accuracy, a smaller number of terms I is required for higher values of κ_x , μ_x or z , or lower values of κ_y or μ_y .

Note that (2.71) may be reduced in the following situations: (i) if μ_x (or μ_y) is set to unity, the corresponding PDF reduces to Rice; (ii) if $\kappa_x \rightarrow 0$ ($\kappa_y \rightarrow 0$), the corresponding PDF reduces to Nakagami- m , with $m = \mu_x$ ($m = \mu_y$); and (iii) if $\mu_x = 1$ and $\kappa_x \rightarrow 0$ ($\mu_y = 1$ and $\kappa_y \rightarrow 0$), the corresponding PDF reduces to Rayleigh.

The PDF of Z is shown in Fig. 2.11 for various values of κ_x , κ_y , μ_x and μ_y . It can be seen that diminishing values of κ_x tends to slightly spread out the probability density. On the other hand, a PDF with smaller tail and a higher peak value is obtained for increasing values of κ_y or μ_y , or diminishing value of μ_x . In the figure, it can be seen that the curves for $\mu_x = 0.5$ have the shape of a one-sided Gaussian, as expected.

2.7.2 Cumulative Distribution Function

With (2.2), (2.67) and (2.68), the CDF of Z may be expressed as

$$\begin{aligned}
 F_Z(z) &= \int_0^z \int_0^\infty \frac{4\mu_x\mu_y(\kappa_x+1)^{\frac{\mu_x+1}{2}}(\kappa_y+1)^{\frac{\mu_y+1}{2}}}{\kappa_x^{\frac{\mu_x-1}{2}}\kappa_y^{\frac{\mu_y-1}{2}}e^{\mu_x\kappa_x+\mu_y\kappa_y}\hat{x}^{\mu_x+1}\hat{y}^{\mu_y+1}} t^{\mu_x}y^{\mu_x+\mu_y+1} \\
 &\quad \times \exp\left[-\mu_x\frac{\kappa_x+1}{\hat{x}^2}(ty)^2\right] \exp\left(-\mu_y\frac{\kappa_y+1}{\hat{y}^2}y^2\right) \\
 &\quad \times I_{\mu_x-1}\left(2\mu_x\sqrt{\kappa_x\frac{\kappa_x+1}{\hat{x}^2}}ty\right) I_{\mu_y-1}\left(2\mu_y\sqrt{\kappa_y\frac{\kappa_y+1}{\hat{y}^2}}y\right) dy dt.
 \end{aligned} \tag{2.73}$$

Using [48, Eq. 8.445] to expand in series the first Bessel function in (2.73), changing the integration order and the integration variable to $w = t^2$ leads to

$$\begin{aligned}
 F_Z(z) &= \sum_{i=0}^{\infty} \int_0^\infty \int_0^{z^2} \frac{2\mu_x^{2i+\mu_x}\mu_y(\kappa_x+1)^{i+\mu_x}(\kappa_y+1)^{\frac{\mu_y+1}{2}}\kappa_x^i}{i!\Gamma(i+\mu_x)e^{\mu_x\kappa_x+\mu_y\kappa_y}\hat{x}^{2i+2\mu_x}\hat{y}^{\mu_y+1}\kappa_y^{\frac{\mu_y-1}{2}}} w^{i+\mu_x-1}y^{2i+2\mu_x+\mu_y} \\
 &\quad \times \exp\left(-\mu_x\frac{\kappa_x+1}{\hat{x}^2}wy^2\right) \exp\left(-\mu_y\frac{\kappa_y+1}{\hat{y}^2}y^2\right) I_{\mu_y-1}\left(2\mu_y\sqrt{\kappa_y\frac{\kappa_y+1}{\hat{y}^2}}y\right) dw dy
 \end{aligned} \tag{2.74}$$

Using [48, Eqs. 3.381.1, 8.356.3], the above integral in w solves to

$$F_Z(z) = \sum_{i=0}^{\infty} \int_0^{\infty} \frac{2\mu_y(\mu_x\kappa_x)^i(\kappa_y+1)^{\frac{\mu_y+1}{2}}}{i!e^{\mu_x\kappa_x+\mu_y\kappa_y}\kappa_y^{\frac{\mu_y-1}{2}}\hat{y}^{\mu_y+1}} y^{\mu_y} \exp\left[-\mu_y\frac{\kappa_y+1}{\hat{y}^2}y^2\right] \\ \times I_{\mu_y-1}\left(2\mu_y\sqrt{\kappa_y\frac{\kappa_y+1}{\hat{y}^2}}y\right) \left[1 - Q\left(i + \mu_x, \mu_x\frac{\kappa_x+1}{\hat{x}^2}z^2y^2\right)\right] dy. \quad (2.75)$$

The integral in (2.75) can be split in two parts, with one of them carrying the function $Q(\cdot, \cdot)$.

Solving the simpler integral with [49, Eq. 2.15.5.4] and simplifying the summation leads to

$$F_Z(z) = 1 - \sum_{i=0}^{\infty} \int_0^{\infty} \frac{2\mu_y(\mu_x\kappa_x)^i(\kappa_y+1)^{\frac{\mu_y+1}{2}}}{i!e^{\mu_x\kappa_x+\mu_y\kappa_y}\kappa_y^{\frac{\mu_y-1}{2}}\hat{y}^{\mu_y+1}} y^{\mu_y} \exp\left[-\mu_y\frac{\kappa_y+1}{\hat{y}^2}y^2\right] \\ \times I_{\mu_y-1}\left(2\mu_y\sqrt{\kappa_y\frac{\kappa_y+1}{\hat{y}^2}}y\right) Q\left(i + \mu_x, \mu_x\frac{\kappa_x+1}{\hat{x}^2}z^2y^2\right) dy. \quad (2.76)$$

Using (2.52) in (2.76) leads to

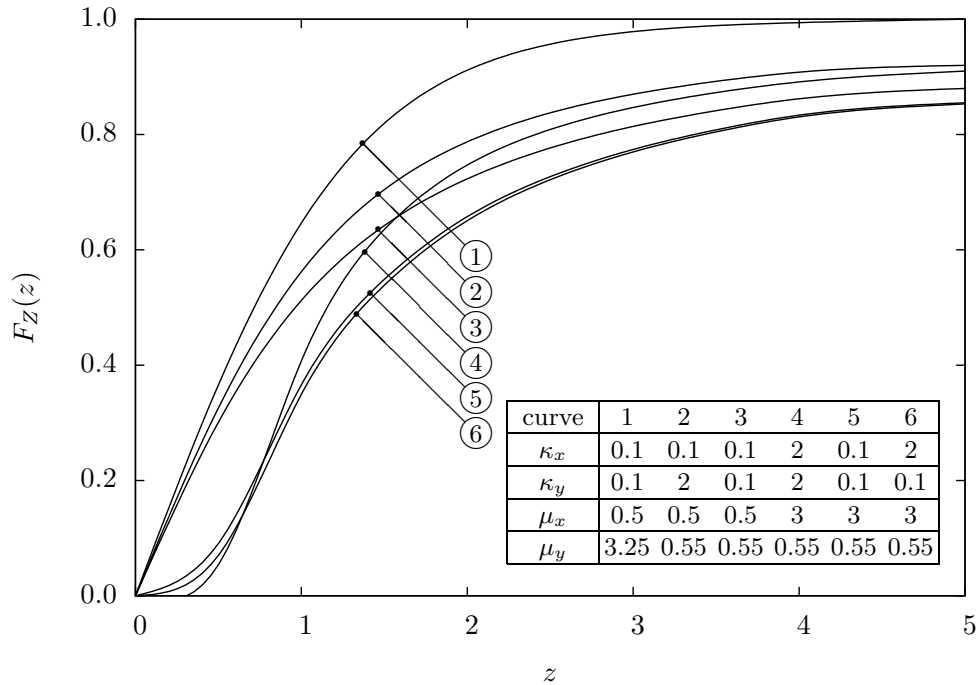
$$F_Z(z) = 1 - \sum_{i=0}^{\infty} \int_0^{\infty} \frac{2(\mu_x\kappa_x)^i\mu_y(\kappa_y+1)^{\frac{\mu_y+1}{2}}}{i!e^{\mu_x\kappa_x+\mu_y\kappa_y}\kappa_y^{\frac{\mu_y-1}{2}}\hat{y}^{\mu_y+1}} y^{\mu_y} \exp\left(-\mu_y\frac{\kappa_y+1}{\hat{y}^2}y^2\right) \\ \times I_{\mu_y-1}\left(2\mu_y\sqrt{\kappa_y\frac{\kappa_y+1}{\hat{y}^2}}y\right) \\ + \sum_{i=0}^{\infty} \sum_{j=0}^i \int_0^{\infty} \frac{2\mu_x^{i+j+\mu_x}\mu_y\kappa_x^j(\kappa_x+1)^{i+\mu_x}(\kappa_y+1)^{\frac{\mu_y+1}{2}}}{j!\Gamma(i+\mu_x+1)e^{\mu_x\kappa_x+\mu_y\kappa_y}\kappa_y^{\frac{\mu_y-1}{2}}\hat{x}^{2i+2\mu_x}\hat{y}^{\mu_y+1}} z^{2i+2\mu_x}y^{2i+2\mu_x+\mu_y} \\ \times \exp\left[-\left(\mu_x\frac{\kappa_x+1}{\hat{x}^2}z^2 + \mu_y\frac{\kappa_y+1}{\hat{y}^2}\right)y^2\right] I_{\mu_y-1}\left(2\mu_y\sqrt{\kappa_y\frac{\kappa_y+1}{\hat{y}^2}}y\right) \quad (2.77)$$

Solving the integrals with [49, Eq. 2.15.5.4] and simplifying the summation results in

$$F_Z(z) = \frac{(uz^2)^{\mu_x}}{e^{\mu_y\kappa_y}(1+uz^2)^{\mu_x+\mu_y}} \sum_{i=0}^{\infty} \frac{Q(i+1, \mu_x\kappa_x)(uz^2)^i}{(i+\mu_x)B(i+\mu_x, \mu_y)} {}_1F_1\left(i + \mu_x + \mu_y, \mu_y, \frac{\mu_y\kappa_y}{1+uz^2}\right) \quad (2.78)$$

in which u is defined by (2.72).

Although (2.78) includes an infinite summation, the evaluation of the CDF converges rapidly for cases of interest. Let I be the number of terms in a truncated summation (as defined earlier). Table 2.6 gives the value of I necessary to obtain a three-decimal-place accuracy (error < 0.0005) and a six-decimal-place accuracy (error < 0.0000005) for the infinite summation of (2.78). For

Figure 2.12: CDF of the ratio of κ - μ random variables.

the CDF accuracy, a smaller number of terms I is required for higher values of κ_y or μ_y , or lower values of κ_x , μ_x or z .

Note that (2.78) may be reduced in the following situations: (i) if μ_x (or μ_y) is set to unity, the corresponding CDF reduces to Rice; (ii) if $\kappa_x \rightarrow 0$ ($\kappa_y \rightarrow 0$), the corresponding CDF reduces to Nakagami- m , with $m = \mu_x$ ($m = \mu_y$); and (iii) if $\mu_x = 1$ and $\kappa_x \rightarrow 0$ ($\mu_y = 1$ and $\kappa_y \rightarrow 0$), the corresponding CDF reduces to Rayleigh.

The CDF of Z is shown in Fig. 2.12 for various values of κ_x , κ_y , μ_x and μ_y . It can be seen that lower values of μ_x tends to smoothen the function. On the other hand, a CDF with steeper climb is obtained with higher values of κ_x and κ_y .

2.8 Ratio κ - μ / η - μ

Let (1.15) represent the PDF of the numerator X

$$f_X(x) = \frac{2\mu_x(\kappa_x + 1)^{\frac{\mu_x+1}{2}} x^{\mu_x}}{\kappa_x^{\frac{\mu_x-1}{2}} e^{\mu_x \kappa_x} \hat{x}^{\mu_x+1}} \exp \left[-\mu_x(\kappa_x + 1) \frac{x^2}{\hat{x}^2} \right] I_{\mu_x-1} \left(2\mu_x \sqrt{\kappa_x(\kappa_x + 1)} \frac{x}{\hat{x}} \right) \quad (2.79)$$

and (1.13) the PDF of the denominator Y

$$f_Y(y) = \frac{4\sqrt{\pi}\mu_y^{\mu_y+\frac{1}{2}}h_y^{\mu_y}y^{2\mu_y}}{\Gamma(\mu_y)H_y^{\mu_y-\frac{1}{2}}\hat{y}^{2\mu_y+1}} \exp\left(-2\mu_y h_y \frac{y^2}{\hat{y}^2}\right) I_{\mu_y-\frac{1}{2}}\left(2\mu_y H_y \frac{y^2}{\hat{y}^2}\right). \quad (2.80)$$

In the following, the PDF and the CDF of the ratio Z are calculated.

2.8.1 Probability Density Function

With (2.1), (2.79) and (2.80), the PDF of Z may be expressed as

$$f_Z(z) = \int_0^\infty \frac{8\sqrt{\pi}\mu_x^{\mu_x+1}\mu_y^{\mu_y+\frac{1}{2}}(\kappa_x+1)^{\frac{\mu_x+1}{2}}h_y^{\mu_y}}{e^{\mu_x\kappa_x}\Gamma(\mu_y)\kappa_x^{\frac{\mu_x+1}{2}}\hat{x}^{\mu_x+1}\hat{y}^{2\mu_y+1}H_y^{\mu_y-\frac{1}{2}}} z^{\mu_x}y^{\mu_x+2\mu_y+1} \exp\left[-\mu_x\frac{\kappa_x+1}{\hat{x}^2}(zy)^2\right] \\ \times \exp\left(-2h_y\frac{\mu_y}{\hat{y}^2}y^2\right) I_{\mu_x-1}\left(2\mu_x\sqrt{\kappa_x\frac{\kappa_x+1}{\hat{x}^2}}zy\right) I_{\mu_y-\frac{1}{2}}\left(2H_y\frac{\mu_y}{\hat{y}^2}y^2\right) dy. \quad (2.81)$$

Using [48, Eq. 8.445] to expand in series the first Bessel function in (2.81), and making the integration variable $t = y^2$ results in

$$f_Z(z) = \sum_{i=0}^{\infty} \int_0^\infty \frac{4\sqrt{\pi}\mu_x^{2i+\mu_x}\mu_y^{\mu_y+\frac{1}{2}}\kappa_x^i(\kappa_x+1)^{i+\mu_x}h_y^{\mu_y}}{i!\Gamma(i+\mu_x)\Gamma(\mu_y)e^{\mu_x\kappa_x}\hat{x}^{2i+2\mu_x}\hat{y}^{\mu_y+\frac{1}{2}}H_y^{\mu_y-\frac{1}{2}}} z^{2i+2\mu_x-1}t^{i+\mu_x+\mu_y-\frac{1}{2}} \\ \times \exp\left[-\left(\mu_x\frac{\kappa_x+1}{\hat{x}^2}z^2+2h_y\frac{\mu_y}{\hat{y}^2}\right)t\right] I_{\mu_y-\frac{1}{2}}\left(2H_y\frac{\mu_y}{\hat{y}^2}t\right) dt. \quad (2.82)$$

Using [49, Eq. 2.15.3.2] to solve the above integral results in

$$f_Z(z) = \frac{2u^{\mu_x}z^{2\mu_x-1}}{e^{\mu_x\kappa_x}(1+uz^2)^{\mu_x+2\mu_y}} \sum_{i=0}^{\infty} \frac{1}{i!B(i+\mu_x, 2\mu_y)} \left(\frac{\mu_x\kappa_x uz^2}{1+uz^2}\right)^i \\ \times {}_2F_1\left[\frac{i+\mu_x+2\mu_y}{2}, \frac{i+\mu_x+2\mu_y+1}{2}, \mu_y+\frac{1}{2}, \left(\frac{H_y}{h_y}\frac{1}{1+uz^2}\right)^2\right] \quad (2.83)$$

in which

$$u = \frac{\mu_x(\kappa_x+1)\hat{y}^2}{2\mu_y h_y \hat{x}^2}. \quad (2.84)$$

Although (2.83) includes an infinite summation, the evaluation of the PDF converges rapidly for cases of interest. Let I be the number of terms in a truncated summation (as defined earlier).

Table 2.7: Relation between number of terms and accuracy in the infinite summation of (2.83) and (2.91).

Parameters					smallest I for accuracy of					
κ_x	η_y	μ_x	μ_y	z	3-decimal-place		6-decimal-place			
					PDF	CDF	PDF	CDF		
0.1	0.1	0.5	0.5	0.1	1	0	1	2		
				1.0	1	9	3	19		
				5.0	1	167	3	350		
			1.0	0.1	1	0	1	2		
				5.0	1	106	3	204		
				5.0	0	0	1	2		
		5.0	0.1	0	47	3	75			
			5.0	0.5	0.1	0	0	1	0	
				5.0	3	1649	6	3442		
				5.0	0.1	0	0	0	0	
			0.9	5.0	0.5	0.1	0	429	3	666
					0.5	0.1	1	0	1	2
	5.0	1				109	3	212		
	5.0	0.1		0		0	1	2		
	5.0	5.0		0.1	0	38	2	57		
				5.0	0.1	0	0	1	0	
			5.0		2	1059	5	2058		
		5.0	0.1		0	0	0	0		
		5.0	0	330	0	474				
		10.0	0.1	0.5	0.5	0.1	3	1	6	4
	5.0					11	1653	17	3446	
	5.0					0.1	2	0	4	3
					5.0	0	434	13	671	
					5.0	0.5	0.1	0	0	0
5.0	67					16506	83	34401		
5.0	0.1			0		0	0	0		
5.0	5.0			0.1	0	4291	61	6623		
				0.9	0.5	0.1	2	0	5	4
						5.0	10	1064	17	2063
	5.0					0.1	2	0	4	3
				5.0	0	335	0	479		
			5.0	5.0	0.1	0	0	0	0	
5.0	64				10607	81	20569			
5.0	0.1				0	0	0	0		
5.0	0.1			0	6623	0	4684			

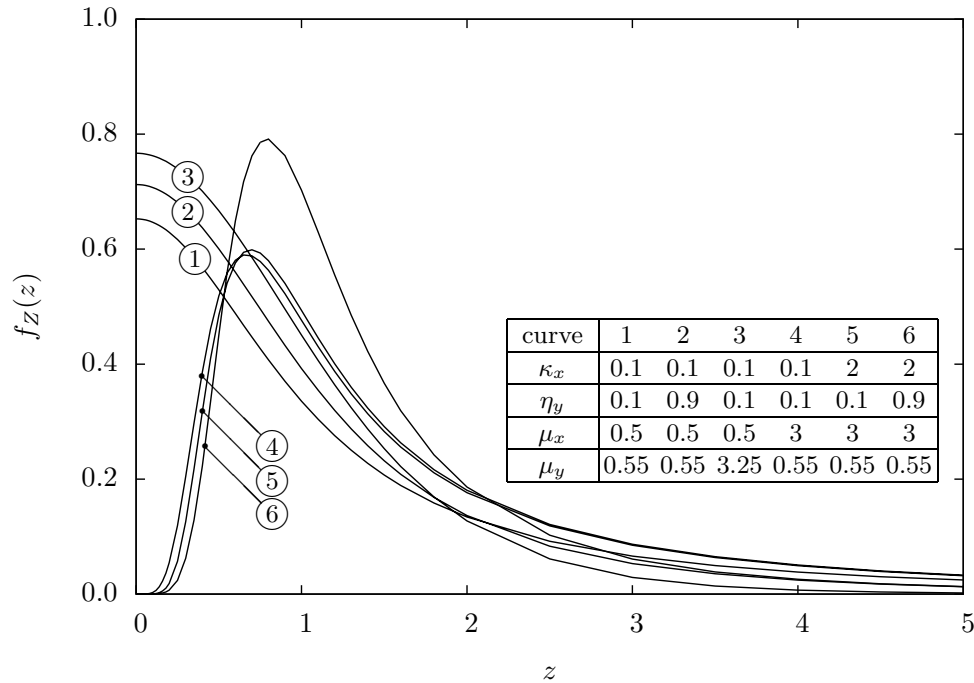


Figure 2.13: PDF of the ratio of κ - μ and η - μ random variables.

Table 2.7 gives the value of I necessary to obtain a three-decimal-place accuracy (error < 0.0005) and a six-decimal-place accuracy (error < 0.0000005) for the infinite summation of (2.83). For the PDF accuracy, a smaller number of terms I is required for higher values of η_y or μ_y , or lower values of κ_x , μ_x or z .

Note that (2.83) may be reduced in the following situations: (i) if μ_x is set to unity, the corresponding PDF reduces to Rice; (ii) if $\eta_y \rightarrow 0$ or $\eta_y \rightarrow \infty$, the corresponding PDF reduces to Nakagami- m , with $m = \mu_y$; and (iii) if $\mu_y = \frac{1}{2}$ and $\eta_y = 1$, the corresponding PDF reduces to Rayleigh.

The PDF of Z is shown in Fig. 2.13 for various values of κ_x , η_y , μ_x and μ_y . It can be seen that diminishing values of κ_x tends to slightly spread out the probability density. On the other hand, a PDF with smaller tail and a higher peak value is obtained for increasing values of η_y or μ_y , or diminishing value of μ_x . In the figure, it can be seen that the curves for $\mu_x = 0.5$ have the shape of a one-sided Gaussian, as expected.

If μ_y is a positive integer, i.e., $\mu_y = 1, 2, \dots$, then the Bessel function may be expressed by

(2.21). Using (2.21) in (2.81), and solving the integral in y with [49, Eq. 2.15.5.4] leads to

$$\begin{aligned}
f_Z(z) &= \frac{2h_y^{\mu_y} u_1^{\mu_x} z^{2\mu_x-1}}{e^{\mu_x \kappa_x} (1+u_1 z^2)^{\mu_x}} \sum_{i=0}^{\mu_y-1} \frac{(-1)^i}{2^{i+\mu_y} (i+\mu_y) B(\mu_y, i+1) B(\mu_x, -i+\mu_y) H_y^{i+\mu_y}} \\
&\quad \times \frac{1}{[(h_y - H_y)(1+u_1 z^2)]^{-i+\mu_y}} {}_1F_1 \left(-i + \mu_x + \mu_y, \mu_x, \frac{\mu_x \kappa_x u_1 z^2}{1+u_1 z^2} \right) \\
&+ \frac{2h_y^{\mu_y} u_2^{\mu_x} z^{2\mu_x-1}}{e^{\mu_x \kappa_x} (1+u_2 z^2)^{\mu_x}} \sum_{i=0}^{\mu_y-1} \frac{(-1)^{\mu_y}}{2^{i+\mu_y} (i+\mu_y) B(\mu_y, i+1) B(\mu_x, -i+\mu_y) H_y^{i+\mu_y}} \\
&\quad \times \frac{1}{[(h_y + H_y)(1+u_2 z^2)]^{-i+\mu_y}} {}_1F_1 \left(-i + \mu_x + \mu_y, \mu_x, \frac{\mu_x \kappa_x u_2 z^2}{1+u_2 z^2} \right)
\end{aligned} \tag{2.85}$$

in which

$$u_1 = \frac{\mu_x(\kappa_x + 1)\hat{y}^2}{2\mu_y(h_y - H_y)\hat{x}^2}, \quad \text{and} \quad u_2 = \frac{\mu_x(\kappa_x + 1)\hat{y}^2}{2\mu_y(h_y + H_y)\hat{x}^2}. \tag{2.86}$$

2.8.2 Cumulative Distribution Function

With (2.2), (2.79) and (2.80), the CDF of Z may be expressed as

$$\begin{aligned}
F_Z(z) &= \int_0^z \int_0^\infty \frac{8\sqrt{\pi} \mu_x^{\mu_x+1} \mu_y^{\mu_y+\frac{1}{2}} (\kappa_x + 1)^{\frac{\mu_x+1}{2}} h_y^{\mu_y}}{e^{\mu_x \kappa_x} \Gamma(\mu_y) \kappa_x^{\frac{\mu_x+1}{2}} \hat{x}^{\mu_x+1} \hat{y}^{2m_y+1} H_y^{\mu_y-\frac{1}{2}}} t^{\mu_x} y^{\mu_x+2\mu_y+1} \\
&\quad \times \exp \left[-\mu_x \frac{\kappa_x + 1}{\hat{x}^2} (ty)^2 \right] \exp \left(-2h_y \frac{\mu_y}{\hat{y}^2} y^2 \right) I_{\mu_x-1} \left(2\mu_x \sqrt{\kappa_x \frac{\kappa_x + 1}{\hat{x}^2}} ty \right) \\
&\quad \times I_{\mu_y-\frac{1}{2}} \left(2H_y \frac{\mu_y}{\hat{y}^2} y^2 \right) dy dt.
\end{aligned} \tag{2.87}$$

Using [48, Eq. 8.445] to expand in series the first Bessel function in (2.87), changing the integration order and the integration variable to $w = t^2$ leads to

$$\begin{aligned}
F_Z(z) &= \sum_{i=0}^{\infty} \int_0^\infty \int_0^{z^2} \frac{4\sqrt{\pi} \mu_x^{2i+\mu_x} \mu_y^{\mu_y+\frac{1}{2}} \kappa_x^i (\kappa_x + 1)^{i+\mu_x} h_y^{\mu_y}}{i! \Gamma(i+\mu_x) e^{\mu_x \kappa_x} \Gamma(\mu_y) \hat{x}^{2i+2\mu_x} \hat{y}^{2m_y+1} H_y^{\mu_y-\frac{1}{2}}} w^{i+\mu_x-1} y^{2i+2\mu_x+2\mu_y} \\
&\quad \times \exp \left[-\mu_x \frac{\kappa_x + 1}{\hat{x}^2} wy^2 \right] \exp \left(-2h_y \frac{\mu_y}{\hat{y}^2} y^2 \right) I_{\mu_y-\frac{1}{2}} \left(2H_y \frac{\mu_y}{\hat{y}^2} y^2 \right) dw dy
\end{aligned} \tag{2.88}$$

Using [48, Eqs. 3.381.1, 8.356.3], the above integral in w solves to

$$F_Z(z) = \sum_{i=0}^{\infty} \int_0^{\infty} \frac{4\sqrt{\pi}(\mu_x \kappa_x)^i \mu_y^{\mu_y + \frac{1}{2}} h_y^{\mu_y}}{i! e^{\mu_x \kappa_x} \Gamma(\mu_y) H_y^{\mu_y - \frac{1}{2}} \hat{y}^{2\mu_y + 1}} y^{2\mu_y} \exp\left(-2h_y \frac{\mu_y}{\hat{y}^2} y^2\right) I_{\mu_y - \frac{1}{2}}\left(2H_y \frac{\mu_y}{\hat{y}^2} y^2\right) \times \left[1 - Q\left(i + \mu_x, \mu_x \frac{\kappa_x + 1}{\hat{x}^2} y^2 z^2\right)\right] dy. \quad (2.89)$$

The integral in (2.89) can be split in two parts, with one of them carrying the function $Q(\cdot, \cdot)$.

Solving the simpler integral with [49, Eq. 2.15.3.2] and simplifying the summation leads to

$$F_Z(z) = 1 - \sum_{i=0}^{\infty} \int_0^{\infty} \frac{4\sqrt{\pi}(\mu_x \kappa_x)^i \mu_y^{\mu_y + \frac{1}{2}} h_y^{\mu_y}}{i! e^{\mu_x \kappa_x} \Gamma(\mu_y) H_y^{\mu_y - \frac{1}{2}} \hat{y}^{2\mu_y + 1}} y^{2\mu_y} \exp\left(-2h_y \frac{\mu_y}{\hat{y}^2} y^2\right) \times I_{\mu_y - \frac{1}{2}}\left(2H_y \frac{\mu_y}{\hat{y}^2} y^2\right) Q\left(i + \mu_x, \mu_x \frac{\kappa_x + 1}{\hat{x}^2} y^2 z^2\right) dy. \quad (2.90)$$

Using (2.52) in (2.90), solving the integrals with [49, Eq. 2.15.3.2] and simplifying the summation results in

$$F_Z(z) = \frac{(uz^2)^{\mu_x}}{h_y^{\mu_y} (1 + uz^2)^{\mu_x + 2\mu_y}} \sum_{i=0}^{\infty} \frac{Q(i + 1, \mu_x \kappa_x) (uz^2)^i}{(i + \mu_x) B(i + \mu_x, 2\mu_y) (1 + uz^2)^j} \times {}_2F_1\left[\frac{i + \mu_x + 2\mu_y}{2}, \frac{i + \mu_x + 2\mu_y + 1}{2}, \mu_y + \frac{1}{2}, \left(\frac{H_y}{h_y} \frac{1}{1 + uz^2}\right)^2\right] \quad (2.91)$$

in which u is defined by (2.84).

Although (2.91) includes an infinite summation, the evaluation of the CDF converges rapidly for cases of interest. Let I be the number of terms in a truncated summation (as defined earlier). Table 2.7 gives the value of I necessary to obtain a three-decimal-place accuracy (error < 0.0005) and a six-decimal-place accuracy (error < 0.0000005) for the infinite summation of (2.91). For the CDF accuracy, a smaller number of terms I is required for higher values of η_y or μ_y , or lower values of κ_x , μ_x or z .

Note that (2.91) may be reduced in the following situations: (i) if μ_x is set to unity, the corresponding CDF reduces to Rice; (ii) if $\eta_y \rightarrow 0$ or $\eta_y \rightarrow \infty$, the corresponding CDF reduces to Nakagami- m , with $m = \mu_y$; and (iii) if $\mu_y = \frac{1}{2}$ and $\eta_y = 1$, the corresponding CDF reduces to Rayleigh.

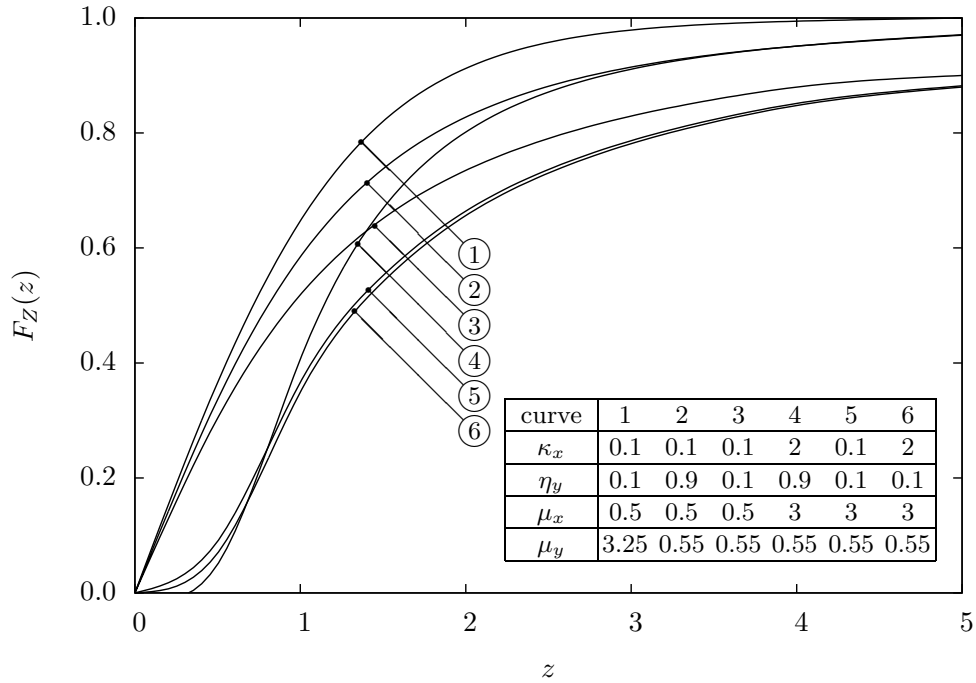


Figure 2.14: CDF of the ratio of $\kappa\text{-}\mu$ and $\eta\text{-}\mu$ random variables.

The CDF of Z is shown in Fig. 2.14 for various values of κ_x , η_y , μ_x and μ_y . It can be seen that lower values of μ_x tends to smoothen the function. On the other hand, a CDF with steeper climb is obtained with higher values of κ_x and η_y .

2.9 Ratio $\alpha\text{-}\mu/\alpha\text{-}\mu$

Let (1.17) represent the PDF of the numerator X

$$f_X(x) = \frac{\alpha_x \mu_x^{\mu_x} x^{\alpha_x \mu_x - 1}}{\Gamma(\mu_x) \hat{x}^{\alpha_x \mu_x}} \exp\left(-\mu_x \frac{x^{\alpha_x}}{\hat{x}^{\alpha_x}}\right) \quad (2.92)$$

and the PDF of the denominator Y

$$f_Y(y) = \frac{\alpha_y \mu_y^{\mu_y} y^{\alpha_y \mu_y - 1}}{\Gamma(\mu_y) \hat{y}^{\alpha_y \mu_y}} \exp\left(-\mu_y \frac{y^{\alpha_y}}{\hat{y}^{\alpha_y}}\right). \quad (2.93)$$

In the following, the PDF and the CDF of the ratio Z are calculated.

2.9.1 Probability Density Function

With (2.1), (2.92) and (2.93), the PDF of Z may be expressed as

$$f_Z(z) = \int_0^\infty \frac{\alpha_x \alpha_y \mu_x^{\mu_x} \mu_y^{\mu_y}}{\Gamma(\mu_x) \Gamma(\mu_y) \hat{x}^{\alpha_x \mu_x} \hat{y}^{\alpha_y \mu_y}} z^{\alpha_x \mu_x - 1} y^{\alpha_x \mu_x + \alpha_y \mu_y - 1} \times \exp \left[-\frac{\mu_x}{\hat{x}^{\alpha_x}} (zy)^{\alpha_x} \right] \exp \left(-\frac{\mu_y}{\hat{y}^{\alpha_y}} y^{\alpha_y} \right) dy. \quad (2.94)$$

Let us assume that $\frac{\alpha_x}{\alpha_y} = \frac{p}{q}$ in which p and q are coprime positive integers. With the integration variable changed to $t = y^{\alpha_x}$, the integral in (2.94) can be solved with the help of [51, Eq. 2.3.2.13]. If $p > q$, it results in

$$f_Z(z) = \frac{\alpha_y}{\Gamma(\mu_x) \Gamma(\mu_y)} \sum_{i=0}^{p-1} \frac{(-1)^i u^{-\alpha_y(i+\mu_y)} z^{-\alpha_y(i+\mu_y)-1}}{i!} \Gamma \left[\mu_x + (i + \mu_y) \frac{q}{p} \right] \times {}_{(q+1)}F_{(p)} \left[1, \Delta \left(\mu_x + (i + \mu_y) \frac{q}{p}, q \right); \Delta(i + 1, p); \frac{q^q}{(-p)^p} (uz)^{-p\alpha_y} \right] \quad (2.95)$$

in which

$$\Delta(a, n) = \left(\frac{a}{n}, \frac{a+1}{n}, \dots, \frac{a+n-1}{n} \right) \quad (2.96)$$

and

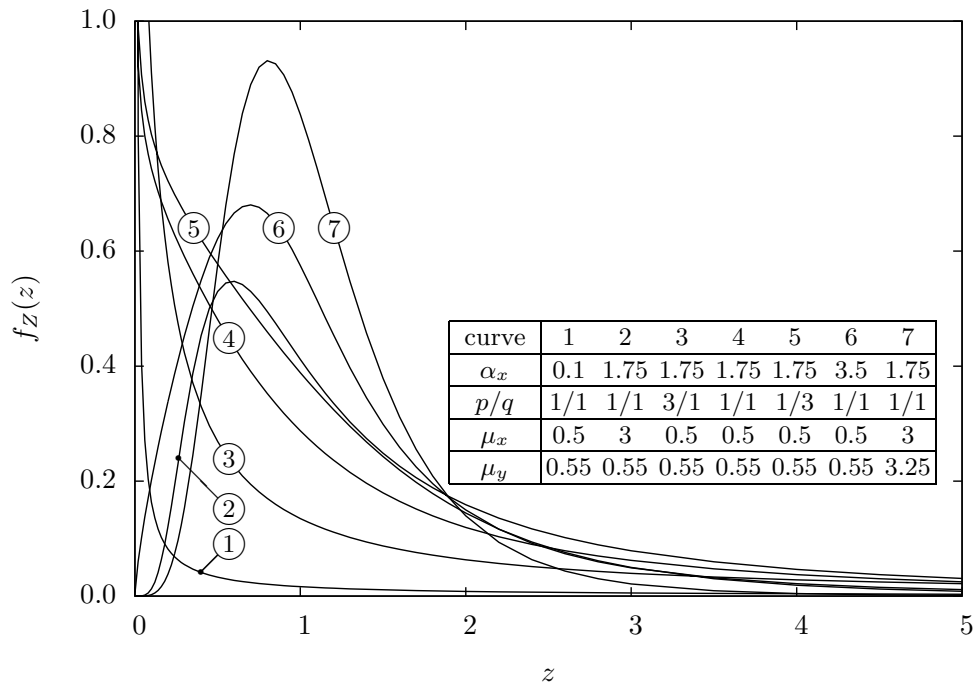
$$u = \frac{\mu_x^{\frac{1}{\alpha_x}} \hat{y}}{\mu_y^{\frac{1}{\alpha_y}} \hat{x}}. \quad (2.97)$$

On the other hand, if $p < q$, solving the integral in (2.94) results in

$$f_Z(z) = \frac{\alpha_x}{\Gamma(\mu_x) \Gamma(\mu_y)} \sum_{i=0}^{q-1} \frac{(-1)^i u^{\alpha_x(i+\mu_x)} z^{\alpha_x(i+\mu_x)-1}}{i!} \Gamma \left[\mu_y + (i + \mu_x) \frac{p}{q} \right] \times {}_{(p+1)}F_{(q)} \left[1, \Delta \left(\mu_y + (i + \mu_x) \frac{p}{q}, p \right); \Delta(i + 1, q); \frac{p^p}{(-q)^q} (uz)^{q\alpha_x} \right]. \quad (2.98)$$

Finally, if $p = q$ (thus making $\alpha_x = \alpha_y = \alpha$), then

$$\begin{aligned} f_Z(z) &= \frac{\alpha u^{-\alpha \mu_y} z^{-\alpha \mu_y - 1}}{B(\mu_x, \mu_y) [1 + (uz)^{-\alpha}]^{\mu_x + \mu_y}} \\ &= \frac{\alpha u^{\alpha \mu_x} z^{-\alpha \mu_x - 1}}{B(\mu_x, \mu_y) [1 + (uz)^\alpha]^{\mu_x + \mu_y}}. \end{aligned} \quad (2.99)$$

Figure 2.15: PDF of the ratio of α - μ random variables.

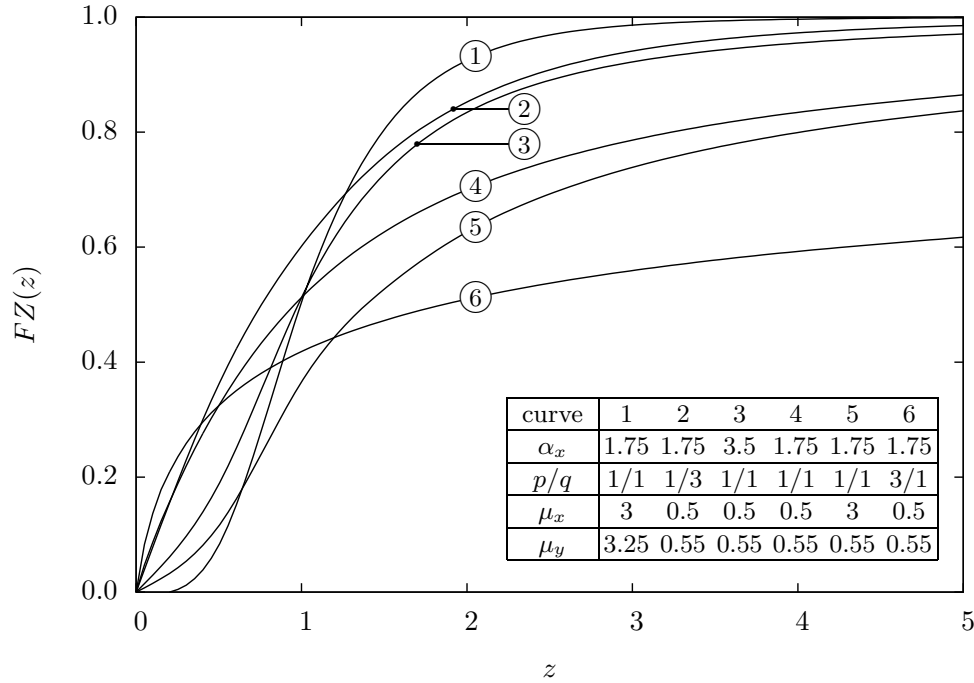
Note that (2.95), (2.98) and (2.99) may be reduced in the following situations: (i) if μ_x (or μ_y) is set to unity, the corresponding PDF reduces to Weibull; (ii) if $\mu_x = 1$ and $\alpha_x = 1$ ($\mu_y = 1$ and $\alpha_y = 1$), the corresponding PDF reduces to negative exponential; and (iii) if $\mu_x = 1$ and $\alpha_x = 2$ ($\mu_y = 1$ and $\alpha_y = 2$), the corresponding PDF reduces to Nakagami- m PDF with $m = \mu_x$ ($m = \mu_y$).

The PDF of Z is shown in Fig. 2.15 for various values of α_x , p , q , μ_x and μ_y . It can be seen that the curves have different shapes, varying from close to the negative exponential (smaller α_x) to closer to Rayleigh (larger α_x). Also, a PDF with smaller tail is obtained for increasing values of μ_y , or diminishing values of α_x or the ratio $\frac{p}{q}$.

2.9.2 Cumulative Distribution Function

With (2.2), (2.92) and (2.93), the CDF of Z may be expressed as

$$\begin{aligned}
 F_Z(z) = & \int_0^z \int_0^\infty \frac{\alpha_x \alpha_y \mu_x^{\mu_x} \mu_y^{\mu_y}}{\Gamma(\mu_x) \Gamma(\mu_y) \hat{x}^{\alpha_x \mu_x} \hat{y}^{\alpha_y \mu_y}} t^{\alpha_x \mu_x - 1} y^{\alpha_x \mu_x + \alpha_y \mu_y - 1} \\
 & \times \exp \left[-\frac{\mu_x}{\hat{x}^{\alpha_x}} (ty)^{\alpha_x} \right] \exp \left(-\frac{\mu_y}{\hat{y}^{\alpha_y}} y^{\alpha_y} \right) dy dt.
 \end{aligned} \tag{2.100}$$

Figure 2.16: CDF of the ratio of α - μ random variables.

Using [48, Eq. 1.211.1] to expand in series the first exponential function in (2.100), solving the integral on y results in

$$F_Z(z) = \sum_{i=0}^{\infty} \int_0^z \frac{(-1)^i \alpha_y}{i! \Gamma(\mu_x) \Gamma(\mu_y)} \Gamma \left[\mu_x + (i + \mu_y) \frac{\alpha_y}{\alpha_x} \right] \left[\left(\frac{\hat{x}}{\hat{y}} \right)^{\alpha_y} \frac{\mu_y}{\mu_x \frac{\alpha_y}{\alpha_x}} \right]^{i + \mu_y} t^{-\alpha_y(i + \mu_y) - 1} dt. \quad (2.101)$$

With $\frac{\alpha_x}{\alpha_y} = \frac{p}{q}$ as already defined, assuming $p > q$, and solving the integral in (2.101) results in

$$F_Z(z) = 1 - \frac{1}{\Gamma(\mu_x) \Gamma(\mu_y)} \sum_{i=0}^{p-1} \frac{(-1)^i (uz)^{-\alpha_y(i + \mu_y)}}{i!(i + \mu_y)} \Gamma \left[\mu_x + (i + \mu_y) \frac{q}{p} \right] \\ \times {}_{(q+2)}F_{(p+1)} \left[1, \frac{i + \mu_y}{p}, \Delta \left(\mu_x + (i + \mu_y) \frac{q}{p}, q \right); \right. \\ \left. \frac{i + \mu_y}{p} + 1, \Delta(i + 1, p); \frac{q^q}{(-p)^p} (uz)^{-p\alpha_y} \right] \quad (2.102)$$

in which u is given by (2.97). Using [48, Eq. 1.211.1] to expand in series the second exponential function in (2.100), solving the integral on y results in

$$F_Z(z) = \sum_{i=0}^{\infty} \int_0^z \frac{(-1)^i \alpha_x}{i! \Gamma(\mu_x) \Gamma(\mu_y)} \Gamma \left[\mu_y + (i + \mu_x) \frac{\alpha_x}{\alpha_y} \right] \left[\left(\frac{\hat{y}}{\hat{x}} \right)^{\alpha_x} \frac{\mu_x}{\mu_y \frac{\alpha_x}{\alpha_y}} \right]^{i + \mu_x} t^{\alpha_x(i + \mu_x) - 1} dt. \quad (2.103)$$

With $\frac{\alpha_x}{\alpha_y} = \frac{p}{q}$ as already defined, assuming $p < q$, and solving the integral in (2.103) results in

$$\begin{aligned}
F_Z(z) = & 1 - \frac{1}{\Gamma(\mu_x)\Gamma(\mu_y)} \sum_{i=0}^{q-1} \frac{(-1)^i (uz)^{-\alpha_x(i+\mu_x)}}{i!(i+\mu_x)} \Gamma \left[\mu_y + (i+\mu_x) \frac{p}{q} \right] \\
& \times {}_{(p+2)}F_{(q+1)} \left[1, \frac{i+\mu_x}{q}, \Delta \left(\mu_y + (i+\mu_x) \frac{p}{q}, p \right); \right. \\
& \left. \frac{i+\mu_x}{p} + 1, \Delta(i+1, q); \frac{p^p}{(-q)^q} (uz)^{q\alpha_x} \right]
\end{aligned} \tag{2.104}$$

in which u is given by (2.97). If $p = q$ (thus making $\alpha_x = \alpha_y = \alpha$), then

$$\begin{aligned}
F_Z(z) = & 1 - \frac{(uz)^{-\alpha\mu_y}}{\mu_y B(\mu_x, \mu_y)} {}_2F_1 [\mu_y, \mu_x + \mu_y, \mu_y + 1, -(uz)^{-\alpha}] \\
= & \frac{(uz)^{-\alpha\mu_x}}{\mu_x B(\mu_x, \mu_y)} {}_2F_1 [\mu_x, \mu_x + \mu_y, \mu_x + 1, -(uz)^{\alpha}].
\end{aligned} \tag{2.105}$$

Note that (2.102), (2.104), and (2.105) may be reduced in the following situations: (i) if μ_x (or μ_y) is set to unity, the corresponding CDF reduces to Weibull; (ii) if $\mu_x = 1$ and $\alpha_x = 1$ ($\mu_y = 1$ and $\alpha_y = 1$), the corresponding CDF reduces to negative exponential; and (iii) if $\mu_x = 1$ and $\alpha_x = 2$ ($\mu_y = 1$ and $\alpha_y = 2$), the corresponding CDF reduces to Nakagami- m CDF with $m = \mu_x$ ($m = \mu_y$).

The CDF of Z is shown in Fig. 2.16 for various values of α_x , p , q , μ_x and μ_y . It can be seen that higher values of μ_y , α_x or α_y tend to produce a steeper curve. On the other hand, lower values of μ_x or μ_y result in a smoother CDF.

Product of Random Variables

In this chapter, the products of i.n.i.d. random variables are calculated. Specifically, the following are considered: $\eta\text{-}\mu \times \eta\text{-}\mu$, $\kappa\text{-}\mu \times \kappa\text{-}\mu$, $\eta\text{-}\mu \times \kappa\text{-}\mu$, and $\alpha\text{-}\mu \times \alpha\text{-}\mu$. After intricate and tedious calculations, the results are obtained with a single summation that converges with small or reasonably small number of terms for the desired accuracy in most cases of interest.

For the figures, given the flexibility of the distributions, values of the parameters have been selected in order to illustrate their possible shapes. The parameters for the accuracy tables have been selected at the vicinity of the upper and lower limits of their valid range.

3.1 Introduction

The analysis of the product of random variables may be performed using standard analytical procedures. Let X and Y be two statistically independent random variables and $W \triangleq X \times Y$ their ratio. The resulting PDF can be expressed as [47]

$$f_W(w) = \int_0^\infty \frac{1}{y} f_X\left(\frac{w}{y}\right) f_Y(y) dy \quad (3.1)$$

in which $f_X(\cdot)$ and $f_Y(\cdot)$ are the PDFs of X and Y , respectively. The CDF is then expressed as

$$F_W(w) = \text{Prob}\{XY \leq W\} = \int_0^w f_W(t) dt. \quad (3.2)$$

3.2 Product η - $\mu \times \eta$ - μ

Let (1.13) represent the PDF of X

$$f_X(x) = \frac{4\sqrt{\pi}\mu_x^{\mu_x+\frac{1}{2}}h_x^{\mu_x}x^{2\mu_x}}{\Gamma(\mu_x)H_x^{\mu_x-\frac{1}{2}}\hat{x}^{2\mu_x+1}} \exp\left(-2\mu_x h_x \frac{x^2}{\hat{x}^2}\right) I_{\mu_x-\frac{1}{2}}\left(2\mu_x H_x \frac{x^2}{\hat{x}^2}\right) \quad (3.3)$$

and the PDF of Y

$$f_Y(y) = \frac{4\sqrt{\pi}\mu_y^{\mu_y+\frac{1}{2}}h_y^{\mu_y}y^{2\mu_y}}{\Gamma(\mu_y)H_y^{\mu_y-\frac{1}{2}}\hat{y}^{2\mu_y+1}} \exp\left(-2\mu_y h_y \frac{y^2}{\hat{y}^2}\right) I_{\mu_y-\frac{1}{2}}\left(2\mu_y H_y \frac{y^2}{\hat{y}^2}\right). \quad (3.4)$$

In the following, the PDF and the CDF of the product W are calculated.

3.2.1 Probability Density Function

With (3.1), (3.3) and (3.4), the PDF of W may be expressed as

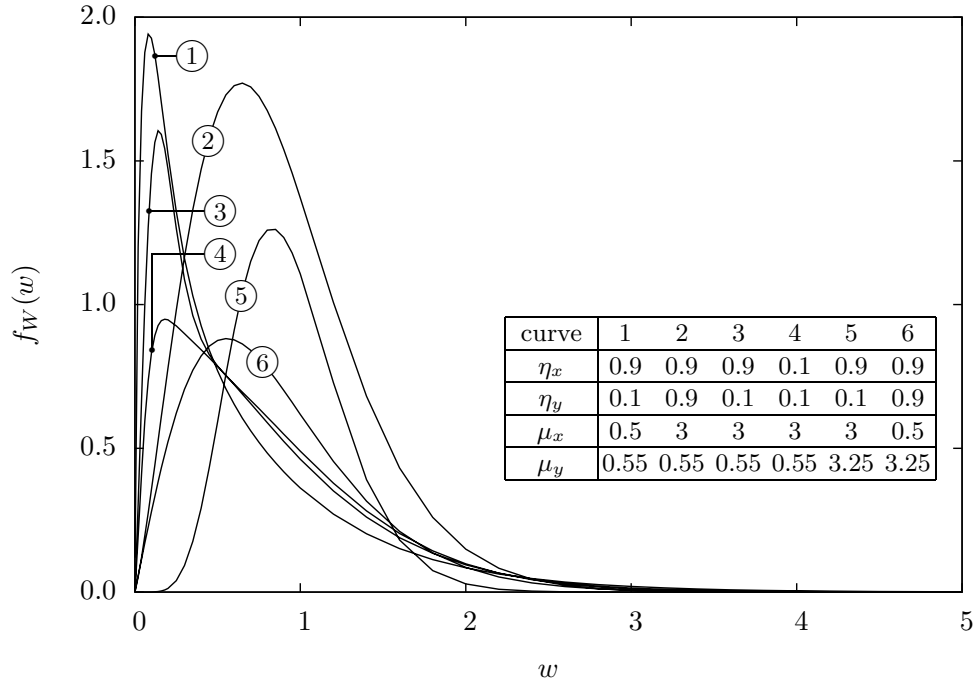
$$f_W(w) = \int_0^\infty \frac{16\pi\mu_x^{\mu_x+\frac{1}{2}}\mu_y^{\mu_y+\frac{1}{2}}h_x^{\mu_x}h_y^{\mu_y}}{\Gamma(\mu_x)\Gamma(\mu_y)H_x^{\mu_x-\frac{1}{2}}H_y^{\mu_y-\frac{1}{2}}\hat{x}^{2\mu_x+1}\hat{y}^{2\mu_y+1}} w^{2\mu_x}y^{-2\mu_x+2\mu_y-1} \times \exp\left(-2h_x \frac{\mu_x w^2}{\hat{x}^2} - 2h_y \frac{\mu_y}{\hat{y}^2} y^2\right) I_{\mu_x-\frac{1}{2}}\left(2H_x \frac{\mu_x w^2}{\hat{x}^2} y^2\right) I_{\mu_y-\frac{1}{2}}\left(2H_y \frac{\mu_y}{\hat{y}^2} y^2\right) dy. \quad (3.5)$$

Using [48, Eq. 8.445] to expand in series the Bessel functions, and making the integration variable $t = y^2$ results in

$$f_W(w) = \sum_{i=0}^{\infty} \sum_{j=0}^{\infty} \int_0^\infty \frac{8\pi\mu_x^{2i+2\mu_x}\mu_y^{2j+2\mu_y}h_x^{\mu_x}H_x^{2i}h_y^{\mu_y}H_y^{2j}}{i!j!\Gamma(\mu_x)\Gamma(\mu_y)\Gamma(i+\mu_x+\frac{1}{2})\Gamma(j+\mu_y+\frac{1}{2})\hat{x}^{4i+4\mu_x}\hat{y}^{4j+4\mu_y}} \times w^{4i+4\mu_x-1}t^{-2i+2j-2\mu_x+2\mu_y-1} \exp\left(-2h_x \frac{\mu_x w^2}{\hat{x}^2} \frac{t}{t} - 2h_y \frac{\mu_y}{\hat{y}^2} t\right) dt. \quad (3.6)$$

Using [48, Eq. 3.471.9], the integral in (3.6) solves to

$$f_W(w) = \sum_{i=0}^{\infty} \sum_{j=0}^{\infty} \frac{16\pi}{i!j!\Gamma(\mu_x)\Gamma(\mu_y)\Gamma(i+\mu_x+\frac{1}{2})\Gamma(j+\mu_y+\frac{1}{2})h_x^{\mu_x}h_y^{\mu_y}} \left(\frac{H_x}{h_x}\right)^{2i} \left(\frac{H_y}{h_y}\right)^{2j} \times u^{i+j+\mu_x+\mu_y} w^{2i+2j+2\mu_x+2\mu_y-1} K_{2i-2j+2\mu_x-2\mu_y}(4\sqrt{uw}) \quad (3.7)$$

Figure 3.1: PDF of the product of $\eta\text{-}\mu$ random variables.

in which $K_\nu(\cdot)$ is the modified Bessel function of the second kind and ν -th order [21, Eq. 9.6.2], and

$$u = \frac{h_x h_y \mu_x \mu_y}{\hat{x}^2 \hat{y}^2}. \quad (3.8)$$

After some algebraic manipulation, the double summation in (3.7) may be simplified to

$$\begin{aligned}
f_W(w) = & \frac{2^{-2\mu_x - 2\mu_y + 3} \pi^2 \csc[(2\mu_x - 2\mu_y)\pi]}{w \Gamma(\mu_x) \Gamma(\mu_y) h_x^{\mu_x} h_y^{\mu_y}} \sum_{i=0}^{\infty} \frac{(2\sqrt{uw})^{2i}}{i!} \\
& \times \left\{ \frac{(2\sqrt{uw})^{4\mu_y}}{\Gamma(i - 2\mu_x + 2\mu_y + 1)} {}_2\tilde{F}_1 \left[-\frac{i}{2}, -\frac{i+2}{2}, \mu_y + \frac{1}{2}, \left(\frac{H_y}{h_y}\right)^2 \right] \right. \\
& \quad \times {}_2\tilde{F}_1 \left[-\frac{i}{2} + \mu_x - \mu_y, -\frac{i}{2} + \mu_x - \mu_y + \frac{1}{2}, \mu_x + \frac{1}{2}, \left(\frac{H_x}{h_x}\right)^2 \right] \\
& \quad - \frac{(2\sqrt{uw})^{4\mu_x}}{\Gamma(i + 2\mu_x - 2\mu_y + 1)} {}_2\tilde{F}_1 \left[-\frac{i}{2}, -\frac{i+1}{2}, \mu_x + \frac{1}{2}, \left(\frac{H_x}{h_x}\right)^2 \right] \\
& \quad \left. \times {}_2\tilde{F}_1 \left[-\frac{i}{2} - \mu_x + \mu_y, -\frac{i}{2} - \mu_x + \mu_y + \frac{1}{2}, \mu_y + \frac{1}{2}, \left(\frac{H_y}{h_y}\right)^2 \right] \right\} \quad (3.9)
\end{aligned}$$

in which ${}_2\tilde{F}_1(\cdot)$ is the regularized Gauss hypergeometric function [50, Eq. 07.24.02.0001.01].

Although (3.9) includes an infinite summation, the evaluation of the PDF converges rapidly

Table 3.1: Relation between number of terms and accuracy in the infinite summation of (3.9) and (3.10).

Parameters					smallest I for accuracy of				
η_x	η_y	μ_x	μ_y	z	3-decimal-place		6-decimal-place		
					PDF	CDF	PDF	CDF	
0.1	0.1	0.5	0.5	0.1	113	11	258	15	
				1.0	133	134	291	137	
				5.0	70	682	262	686	
			1.0	0.1	142	19	299	22	
				5.0	52	971	282	974	
				5.0	0.1	351	40	557	43
		5.0	0		2176	401	2180		
		0.9	0.5		0.5	0.1	71	2	208
				5.0		88	100	269	104
				5.0	0.1	2	2	4	12
			5.0		0	338	298	341	

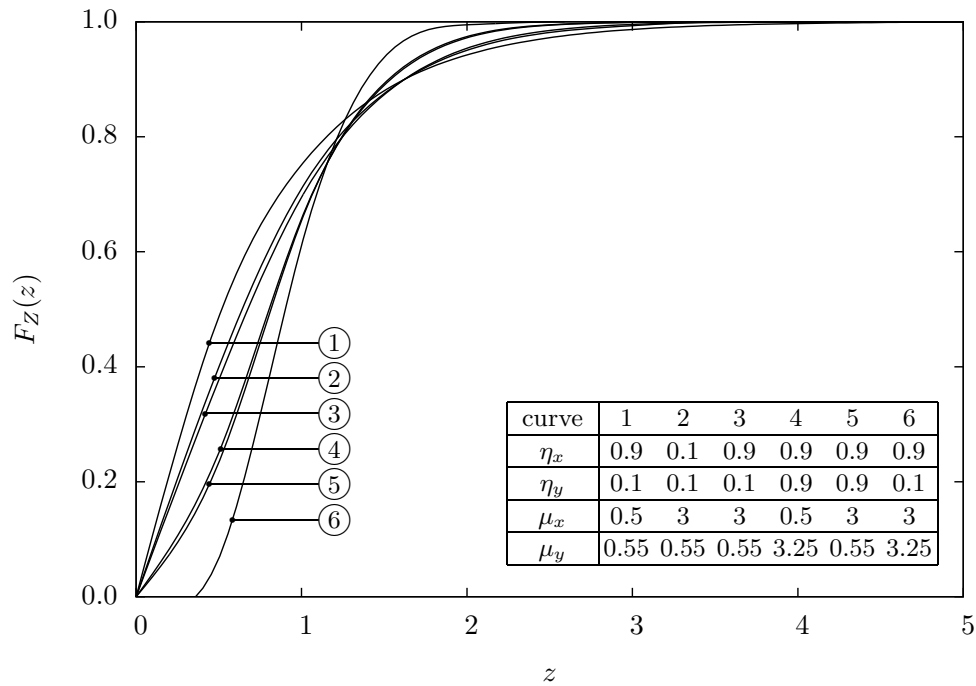


Figure 3.2: CDF of the product of η - μ random variables.

for cases of interest. Let I be the number of terms in a truncated summation (as defined earlier). Table 3.1 gives the value of I necessary to obtain a three-decimal-place accuracy (error < 0.0005) and a six-decimal-place accuracy (error < 0.0000005) for the infinite summation of (3.9). For the PDF accuracy, a smaller number of terms I is required for higher values of η_x , η_y or z , or lower values of μ_x or μ_y .

The PDF of Z is shown in Fig. 3.1 for various values of η_x , η_y , μ_x and μ_y . It can be seen that increasing values of μ_x or μ_y shifts the curve away from the ordinate axis. On the other hand, a PDF with smaller tail and a higher peak value is obtained for increasing values of η_y , η_y , μ_x or μ_y .

Note that (3.9) may be reduced in the following situations: (i) if μ_x (or μ_y) is set to $\frac{1}{2}$, the corresponding PDF reduces to Hoyt; (ii) if $\eta_x \rightarrow 0$ or $\eta_x \rightarrow \infty$ ($\eta_y \rightarrow 0$ or $\eta_y \rightarrow \infty$), the corresponding PDF reduces to Nakagami- m , with $m = \mu_x$ ($m = \mu_y$); and (iii) if $\mu_x = \frac{1}{2}$ and $\eta_x = 1$ ($\mu_y = \frac{1}{2}$ and $\eta_y = 1$), the corresponding PDF reduces to Rayleigh.

3.2.2 Cumulative Distribution Function

With (3.2) and (3.9), the CDF of W may be calculate as

$$\begin{aligned}
 F_W(w) = & \frac{2^{-2\mu_x - 2\mu_y + 2} \pi^2 \csc[(2\mu_x - 2\mu_y)\pi]}{\Gamma(\mu_x)\Gamma(\mu_y)h_x^{\mu_x}h_y^{\mu_y}} \sum_{i=0}^{\infty} \frac{(2\sqrt{uw})^{2i}}{i!} \\
 & \times \left\{ \frac{(2\sqrt{uw})^{4\mu_y}}{(i + 2\mu_y)\Gamma(i - 2\mu_x + 2\mu_y + 1)} {}_2\tilde{F}_1 \left[-\frac{i}{2}, -\frac{i+1}{2}, \mu_y + \frac{1}{2}, \left(\frac{H_y}{h_y}\right)^2 \right] \right. \\
 & \quad \times {}_2\tilde{F}_1 \left[-\frac{i}{2} + \mu_x - \mu_y, -\frac{i}{2} + \mu_x - \mu_y + \frac{1}{2}, \mu_x + \frac{1}{2}, \left(\frac{H_x}{h_x}\right)^2 \right] \\
 & \quad - \frac{(2\sqrt{uw})^{4\mu_x}}{(i + 2\mu_x)\Gamma(i + 2\mu_x - 2\mu_y + 1)} {}_2\tilde{F}_1 \left[-\frac{i}{2}, -\frac{i+1}{2}, \mu_x + \frac{1}{2}, \left(\frac{H_x}{h_x}\right)^2 \right] \\
 & \quad \left. \times {}_2\tilde{F}_1 \left[-\frac{i}{2} - \mu_x + \mu_y, -\frac{i}{2} - \mu_x + \mu_y + \frac{1}{2}, \mu_y + \frac{1}{2}, \left(\frac{H_y}{h_y}\right)^2 \right] \right\} \quad (3.10)
 \end{aligned}$$

in which u is defined by (3.8).

Although (3.10) includes an infinite summation, the evaluation of the CDF converges rapidly for cases of interest. Let I be the number of terms in a truncated summation (as defined earlier).

Table 3.1 gives the value of I necessary to obtain a three-decimal-place accuracy (error < 0.0005) and a six-decimal-place accuracy (error < 0.0000005) for the infinite summation of (3.10). For the CDF accuracy, a smaller number of terms I is required for higher values of η_x , η_y or μ_y , or lower values of μ_x or μ_y .

Note that (3.10) may be reduced in the following situations: (i) if μ_x (or μ_y) is set to $\frac{1}{2}$, the corresponding CDF reduces to Hoyt; (ii) if $\eta_x \rightarrow 0$ or $\eta_x \rightarrow \infty$ ($\eta_y \rightarrow 0$ or $\eta_y \rightarrow \infty$), the corresponding CDF reduces to Nakagami- m , with $m = \mu_x$ ($m = \mu_y$); and (iii) if $\mu_x = \frac{1}{2}$ and $\eta_x = 1$ ($\mu_y = \frac{1}{2}$ and $\eta_y = 1$), the corresponding CDF reduces to Rayleigh.

The CDF of Z is shown in Fig. 3.2 for various values of η_x , η_y , μ_x and μ_y . It can be seen that increasing values of μ_x or μ_y tend to produce steeper curves. On the other hand, lower values of η_x or η_y tend to produce curves that reach the unity for higher values of z .

3.3 Product κ - $\mu \times \kappa$ - μ

Let (1.15) represent the PDF of X

$$f_X(x) = \frac{2\mu_x(\kappa_x + 1)^{\frac{\mu_x+1}{2}} x^{\mu_x}}{\kappa_x^{\frac{\mu_x-1}{2}} e^{\mu_x \kappa_x} \hat{x}^{\mu_x+1}} \exp \left[-\mu_x(\kappa_x + 1) \frac{x^2}{\hat{x}^2} \right] I_{\mu_x-1} \left(2\mu_x \sqrt{\kappa_x(\kappa_x + 1)} \frac{x}{\hat{x}} \right). \quad (3.11)$$

and the PDF of Y

$$f_Y(y) = \frac{2\mu_y(\kappa_y + 1)^{\frac{\mu_y+1}{2}} y^{\mu_y}}{\kappa_y^{\frac{\mu_y-1}{2}} e^{\mu_y \kappa_y} \hat{y}^{\mu_y+1}} \exp \left[-\mu_y(\kappa_y + 1) \frac{y^2}{\hat{y}^2} \right] I_{\mu_y-1} \left(2\mu_y \sqrt{\kappa_y(\kappa_y + 1)} \frac{y}{\hat{y}} \right). \quad (3.12)$$

In the following, the PDF and the CDF of the ratio W are calculated.

3.3.1 Probability Density Function

With (3.1), (3.11) and (3.12), the PDF of W may be expressed as

$$\begin{aligned}
f_W(w) &= \int_0^\infty \frac{4\mu_x\mu_y(\kappa_x+1)^{\frac{\mu_x+1}{2}}(\kappa_y+1)^{\frac{\mu_y+1}{2}}}{\kappa_x^{\frac{\mu_x-1}{2}}\kappa_y^{\frac{\mu_y-1}{2}}e^{\mu_x\kappa_x+\mu_y\kappa_y}\hat{x}^{\mu_x+1}\hat{y}^{\mu_y+1}} w^{\mu_x}y^{-\mu_x+\mu_y-1} \\
&\quad \times \exp\left[-\mu_x\frac{\kappa_x+1}{\hat{x}^2}\left(\frac{w}{y}\right)^2\right] \exp\left(-\mu_y\frac{\kappa_y+1}{\hat{y}^2}y^2\right) \\
&\quad \times I_{\mu_x-1}\left(2\mu_x\sqrt{\kappa_x(\kappa_x+1)}\frac{w}{y\hat{x}}\right) I_{\mu_y-1}\left(2\mu_y\sqrt{\kappa_y(\kappa_y+1)}\frac{y}{\hat{y}}\right) dy.
\end{aligned} \tag{3.13}$$

Using [48, Eq. 8.445] to expand in series the Bessel functions, and making the integration variable $t = y^2$ results in

$$\begin{aligned}
f_W(w) &= \sum_{i=0}^{\infty} \sum_{j=0}^{\infty} \int_0^\infty \frac{2\mu_x^{2i+\mu_x}\mu_y^{2j+\mu_y}\kappa_x^i\kappa_y^j(\kappa_x+1)^{i+\mu_x}(\kappa_y+1)^{j+\mu_y}}{i!j!\Gamma(i+\mu_x)\Gamma(j+\mu_y)e^{\mu_x\kappa_x+\mu_y\kappa_y}\hat{x}^{2i+2\mu_x}\hat{y}^{2j+2\mu_y}} \\
&\quad \times w^{2i+2\mu_x-1}t^{-i+j-\mu_x+\mu_y-1} \exp\left(-\mu_x\frac{\kappa_x+1}{\hat{x}^2}\frac{w^2}{t} - \mu_y\frac{\kappa_y+1}{\hat{y}^2}t\right) dt.
\end{aligned} \tag{3.14}$$

Using [48, Eq. 3.471.9], the integral in (3.14) solves to

$$\begin{aligned}
f_W(w) &= \sum_{i=0}^{\infty} \sum_{j=0}^{\infty} \frac{4(\mu_x\kappa_x)^i(\mu_y\kappa_y)^j}{i!j!\Gamma(i+\mu_x)\Gamma(j+\mu_y)e^{\mu_x\kappa_x+\mu_y\kappa_y}} \\
&\quad \times u^{\frac{i+j+\mu_x+\mu_y}{2}} w^{i+j+\mu_x+\mu_y-1} K_{i-j+\mu_x-\mu_y}(2\sqrt{uw})
\end{aligned} \tag{3.15}$$

in which

$$u = \frac{\mu_x\mu_y(\kappa_x+1)(\kappa_y+1)}{\hat{x}^2\hat{y}^2}. \tag{3.16}$$

After some algebraic manipulation, the double summation in (3.15) may be simplified to

$$\begin{aligned}
f_W(w) &= \frac{4u^{\frac{\mu_x+\mu_y}{2}}w^{\mu_x+\mu_y-1}}{e^{\mu_x\kappa_x+\mu_y\kappa_y}} K_{\mu_x-\mu_y}(2\sqrt{uw}) {}_0\tilde{F}_3\left(1, \mu_x, \mu_y, \mu_x\kappa_x\mu_y\kappa_yuw^2\right) \\
&\quad + \frac{4u^{\frac{\mu_x+\mu_y}{2}}w^{\mu_x+\mu_y-1}}{e^{\mu_x\kappa_x+\mu_y\kappa_y}} \sum_{i=1}^{\infty} (\sqrt{uw})^i \\
&\quad \times \left[(\mu_x\kappa_x)^i K_{i+\mu_x-\mu_y}(2\sqrt{uw}) {}_0\tilde{F}_3\left(i+1, i+\mu_x, \mu_y, \mu_x\kappa_x\mu_y\kappa_yuw^2\right) \right. \\
&\quad \left. + (\mu_y\kappa_y)^i K_{-i+\mu_x-\mu_y}(2\sqrt{uw}) {}_0\tilde{F}_3\left(i+1, \mu_x, i+\mu_y, \mu_x\kappa_x\mu_y\kappa_yuw^2\right) \right]
\end{aligned} \tag{3.17}$$

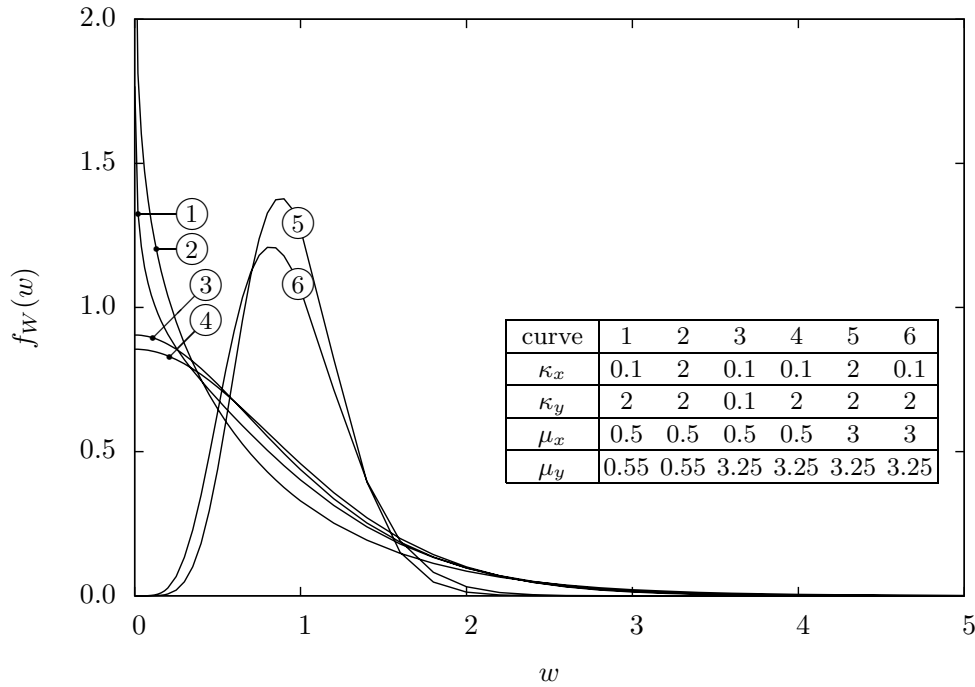


Figure 3.3: PDF of the product of κ - μ random variables.

in which ${}_p\tilde{F}_q(\cdot)$ is the regularized generalized hypergeometric function [50, Eq. 07.32.02.0001.01].

Although (3.17) includes an infinite summation, the evaluation of the PDF converges rapidly for cases of interest. Let I be the number of terms in a truncated summation (as defined earlier). Table 3.2 gives the value of I necessary to obtain a three-decimal-place accuracy (error < 0.0005) and a six-decimal-place accuracy (error < 0.0000005) for the infinite summation of (3.17). For the PDF accuracy, a smaller number of terms I is required for higher values of z , or lower values of κ_x , κ_y , μ_x or μ_y .

The PDF of Z is shown in Fig. 3.3 for various values of κ_x , κ_y , μ_x and μ_y . It can be seen that the values of μ_x and μ_y influence significantly the shape of the curves, from curves with shape similar to the negative exponential to curves with shape similar to Rayleigh. Also, a PDF with smaller tail and a higher peak value is obtained for increasing values of κ_x or κ_y .

Note that (3.17) may be reduced in the following situations: (i) if μ_x (or μ_y) is set to unity, the corresponding PDF reduces to Rice; (ii) if $\kappa_x \rightarrow 0$ ($\kappa_y \rightarrow 0$), the corresponding PDF reduces to Nakagami- m , with $m = \mu_x$ ($m = \mu_y$); and (iii) if $\mu_x = 1$ and $\kappa_x \rightarrow 0$ ($\mu_y = 1$ and $\kappa_y \rightarrow 0$), the corresponding PDF reduces to Rayleigh.

Table 3.2: Relation between number of terms and accuracy in the infinite summation of (3.17) and (3.20).

Parameters					smallest I for accuracy of				
κ_x	κ_y	μ_x	μ_y	z	3-decimal-place		6-decimal-place		
					PDF	CDF	PDF	CDF	
0.1	0.1	0.5	0.5	0.1	2	0	3	1	
				1.0	2	2	3	4	
				5.0	1	7	3	9	
			1.0	0.1	21	0	29	1	
				5.0	0	10	23	12	
				5.0	0.1	4	0	7	2
		10.0	0.5	0.5	0.1	13	1	19	2
					5.0	0	22	15	26
					5.0	0.1	74	0	87
				5.0	5.0	0	61	69	65

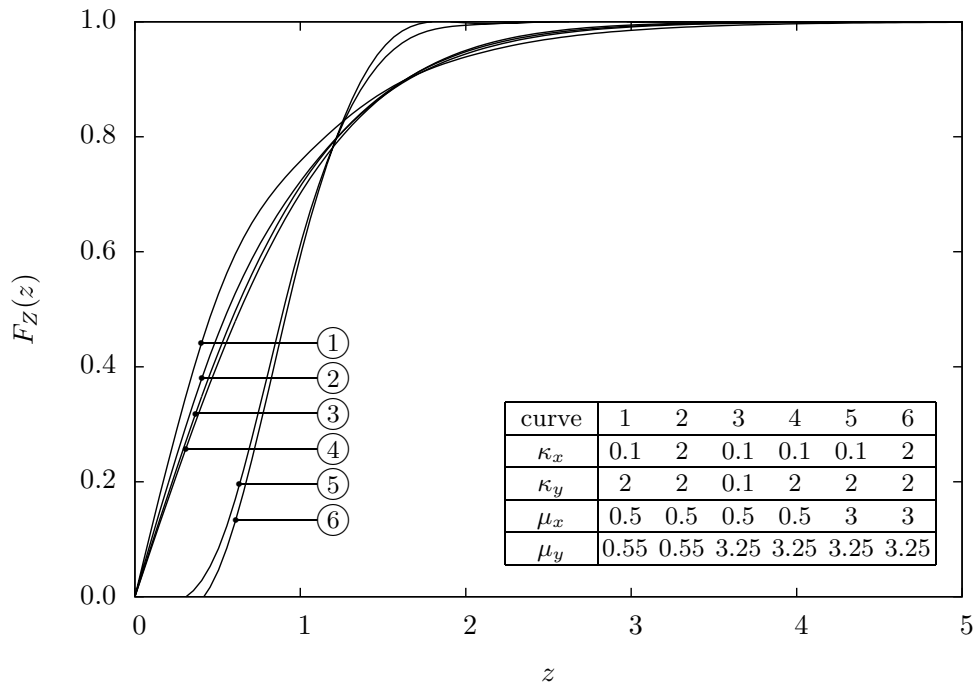


Figure 3.4: CDF of the product of κ - μ random variables.

3.3.2 Cumulative Distribution Function

With (3.2) and (3.15), the CDF of W may be expressed as

$$F_W(w) = \sum_{i=0}^{\infty} \sum_{j=0}^{\infty} \int_0^w \frac{4(\mu_x \kappa_x)^i (\mu_y \kappa_y)^j}{i! j! \Gamma(i + \mu_x) \Gamma(j + \mu_y) e^{\mu_x \kappa_x + \mu_y \kappa_y}} \times u^{\frac{i+j+\mu_x+\mu_y}{2}} t^{i+j+\mu_x+\mu_y-1} K_{i-j+\mu_x-\mu_y}(2\sqrt{ut}) dt. \quad (3.18)$$

With the help of [49, Eq. 2.16.2.3], the above integral solves to

$$F_W(w) = \sum_{i=0}^{\infty} \sum_{j=0}^{\infty} \frac{\pi \csc[(i-j+\mu_x-\mu_y)\pi] (\mu_x \kappa_x)^i (\mu_y \kappa_y)^j}{i! j! \Gamma(i + \mu_x) e^{\mu_x \kappa_x + \mu_y \kappa_y}} (uw^2)^{j+\mu_y} \times {}_1\tilde{F}_2(j + \mu_y, j + \mu_y + 1, -i + j - \mu_x + \mu_y + 1, uw^2) - \sum_{i=0}^{\infty} \sum_{j=0}^{\infty} \frac{\pi \csc[(i-j+\mu_x-\mu_y)\pi] (\mu_x \kappa_x)^i (\mu_y \kappa_y)^j}{i! j! \Gamma(j + \mu_y) e^{\mu_x \kappa_x + \mu_y \kappa_y}} (uw^2)^{i+\mu_x} \times {}_1\tilde{F}_2(i + \mu_x, i + \mu_x + 1, i - j + \mu_x - \mu_y + 1, uw^2) \quad (3.19)$$

in which u is defined by (3.16). After some algebraic manipulation, the double summations in (3.19) may be simplified to

$$F_W(w) = \frac{\csc[(\mu_x - \mu_y)\pi] \pi}{e^{\mu_x \kappa_x + \mu_y \kappa_y}} \sum_{i=0}^{\infty} \frac{(uw^2)^i}{i!} \times \left\{ \frac{(uw^2)^{\mu_y}}{(i + \mu_y) \Gamma(i - \mu_x + \mu_y + 1)} {}_1\tilde{F}_1(-i, \mu_y, \mu_y \kappa_y) {}_1\tilde{F}_1(-i + \mu_x - \mu_y, \mu_x, \mu_x \kappa_x) - \frac{(uw^2)^{\mu_x}}{(i + \mu_x) \Gamma(i + \mu_x - \mu_y + 1)} {}_1\tilde{F}_1(-i, \mu_x, \mu_x \kappa_x) {}_1\tilde{F}_1(-i - \mu_x + \mu_y, \mu_y, \mu_y \kappa_y) \right\}. \quad (3.20)$$

Although (3.20) includes an infinite summation, the evaluation of the CDF converges rapidly for cases of interest. Let I be the number of terms in a truncated summation (as defined earlier). Table 3.2 gives the value of I necessary to obtain a three-decimal-place accuracy (error < 0.0005) and a six-decimal-place accuracy (error < 0.0000005) for the infinite summation of (3.20). For the CDF accuracy, a smaller number of terms I is required for lower values of κ_x , κ_y , μ_x , μ_y or z .

Note that (3.20) may be reduced in the following situations: (i) if μ_x (or μ_y) is set to unity,

the corresponding CDF reduces to Rice; (ii) if $\kappa_x \rightarrow 0$ ($\kappa_y \rightarrow 0$), the corresponding CDF reduces to Nakagami- m , with $m = \mu_x$ ($m = \mu_y$); and (iii) if $\mu_x = 1$ and $\kappa_x \rightarrow 0$ ($\mu_y = 1$ and $\kappa_y \rightarrow 0$), the corresponding CDF reduces to Rayleigh.

The CDF of Z is shown in Fig. 3.4 for various values of κ_x , κ_y , μ_x and μ_y . It can be seen that increasing values of μ_x or μ_y tend to produce steeper curves. On the other hand, lower values of κ_x or κ_y tend to produce curves that reach the unity for higher values of z .

3.4 Product $\eta\text{-}\mu \times \kappa\text{-}\mu$

Let (1.13) represent the PDF of X

$$f_X(x) = \frac{4\sqrt{\pi}\mu_x^{\mu_x+\frac{1}{2}}h_x^{\mu_x}x^{2\mu_x}}{\Gamma(\mu_x)H_x^{\mu_x-\frac{1}{2}}\hat{x}^{2\mu_x+1}} \exp\left(-2\mu_x h_x \frac{x^2}{\hat{x}^2}\right) I_{\mu_x-\frac{1}{2}}\left(2\mu_x H_x \frac{x^2}{\hat{x}^2}\right) \quad (3.21)$$

and (1.15) the PDF of Y

$$f_Y(y) = \frac{2\mu_y(\kappa_y+1)^{\frac{\mu_y+1}{2}}y^{\mu_y}}{\kappa_y^{\frac{\mu_y-1}{2}}e^{\mu_y\kappa_y}\hat{y}^{\mu_y+1}} \exp\left[-\mu_y(\kappa_y+1)\frac{y^2}{\hat{y}^2}\right] I_{\mu_y-1}\left(2\mu_y\sqrt{\kappa_y(\kappa_y+1)}\frac{y}{\hat{y}}\right). \quad (3.22)$$

In the following, the PDF and the CDF of the ratio W are calculated.

3.4.1 Probability Density Function

With (3.1), (3.21) and (3.22), the PDF of W may be expressed as

$$\begin{aligned} f_W(w) &= \int_0^\infty \frac{8\sqrt{\pi}\mu_x^{\mu_x+\frac{1}{2}}\mu_y(\kappa_y+1)^{\frac{\mu_y+1}{2}}h_x^{\mu_x}}{\Gamma(\mu_x)e^{\mu_y\kappa_y}\kappa_y^{\frac{\mu_y-1}{2}}H_x^{\mu_x-\frac{1}{2}}\hat{x}^{2\mu_x+1}\hat{y}^{\mu_y+1}} w^{2\mu_x}y^{-2\mu_x+\mu_y-1} \\ &\quad \times \exp\left[-2h_x\frac{\mu_x}{\hat{x}^2}\left(\frac{w}{y}\right)^2\right] \exp\left(-\mu_y\frac{\kappa_y+1}{\hat{y}^2}y^2\right) \\ &\quad \times I_{\mu_x-\frac{1}{2}}\left[2H_x\frac{\mu_x}{\hat{x}^2}\left(\frac{w}{y}\right)^2\right] I_{\mu_y-1}\left(2\mu_y\sqrt{\kappa_y(\kappa_y+1)}\frac{y}{\hat{y}}\right) dy. \end{aligned} \quad (3.23)$$

Using [48, Eq. 8.445] to expand in series the Bessel functions, and making the integration variable $t = y^2$ results in

$$f_W(w) = \sum_{i=0}^{\infty} \sum_{j=0}^{\infty} \int_0^{\infty} \frac{4\sqrt{\pi}\mu_x^{2i+2\mu_x}\mu_y^{2j+\mu_y}\kappa_y^j(\kappa_y+1)^{j+\mu_y}h_x^{\mu_x}H_x^{2i}}{i!j!\Gamma[\mu_x]\Gamma(i+\mu_x+\frac{1}{2})\Gamma(j+\mu_y)e^{\mu_y\kappa_y}\hat{x}^{4i+4\mu_x}\hat{y}^{2j+2\mu_y}} \times w^{4i+4\mu_x-1}t^{-2i+j-2\mu_x+\mu_y-1} \exp\left(-2h_x\frac{\mu_x}{\hat{x}^2}\frac{w^2}{t} - \mu_y\frac{\kappa_y+1}{\hat{y}^2}t\right) dt. \quad (3.24)$$

Using [51, Eq. 2.3.16.1], the integral in (3.24) solves to

$$f_W(w) = \sum_{i=0}^{\infty} \sum_{j=0}^{\infty} \frac{2^{-2i-2\mu_x+3}\sqrt{\pi}(\mu_y\kappa_y)^j}{i!j!\Gamma(\mu_x)\Gamma(i+\mu_x+\frac{1}{2})\Gamma(j+\mu_y)e^{\mu_y\kappa_y}h_x^{\mu_x}} \times \left(\frac{H_x}{h_x}\right)^{2i} u^{\frac{2i+j+2\mu_x+\mu_y}{2}} w^{2i+j+2\mu_x+\mu_y-1} K_{-2i+j-2\mu_x+\mu_y}(2\sqrt{uw}) \quad (3.25)$$

in which

$$u = \frac{2\mu_x\mu_y h_x(\kappa_y+1)}{\hat{x}^2\hat{y}^2}. \quad (3.26)$$

After some algebraic manipulation, the double summation in (3.25) may be simplified to

$$f_W(w) = \frac{4u^{\mu_x+\frac{\mu_y}{2}}w^{2\mu_x+\mu_y-1}}{\Gamma(2\mu_x)\Gamma(\mu_y)e^{\mu_y\kappa_y}h_x^{\mu_x}} K_{-2\mu_x+\mu_y}(2\sqrt{uw}) \times {}_0\tilde{F}_5\left[\frac{1}{2}, 1, \mu_x + \frac{1}{2}, \frac{\mu_y}{2}, \frac{\mu_y+1}{2}, \left(\frac{1}{8}\frac{H_x}{h_x}\mu_y\kappa_y uw^2\right)^2\right] + \frac{4u^{\mu_x+\frac{\mu_y}{2}}w^{2\mu_x+\mu_y-1}}{e^{\mu_y\kappa_y}h_x^{\mu_x}} \sum_{i=1}^{\infty} \left\{ \frac{(\mu_y\kappa_y\sqrt{uw})^i}{i!\Gamma(2\mu_x)\Gamma(i+\mu_y)} K_{i-2\mu_x+\mu_y}(2\sqrt{uw}) \times {}_0\tilde{F}_5\left[\frac{i+1}{2}, \frac{i}{2}+1, \mu_x + \frac{1}{2}, \frac{i+\mu_y}{2}, \frac{i+\mu_y+1}{2}, \left(\frac{1}{8}\frac{H_x}{h_x}\mu_y\kappa_y uw^2\right)^2\right] \right. \quad (3.27) \\ \left. + \frac{1}{i_c(-i+2i_c)!B(\mu_x, i_c)\Gamma(2\mu_x+2i_c)\Gamma(-i+\mu_y+2i_c)(\mu_y\kappa_y\sqrt{uw})^i} \times \left(\frac{H_x}{h_x}\mu_y\kappa_y uw^2\right)^{2i_c} K_{-i-2\mu_x+\mu_y}(2\sqrt{uw}) \times {}_1\tilde{F}_6\left[1, i_c+1, -\frac{i}{2}+i_c+\frac{1}{2}, -\frac{i}{2}+i_c+1, \mu_x+i_c+\frac{1}{2}, \right. \\ \left. \left. -\frac{-i+\mu_y}{2}+i_c, -\frac{-i+\mu_y}{2}+i_c+\frac{1}{2}, \left(\frac{1}{8}\frac{H_x}{h_x}\mu_y\kappa_y uw^2\right)^2\right] \right\}$$

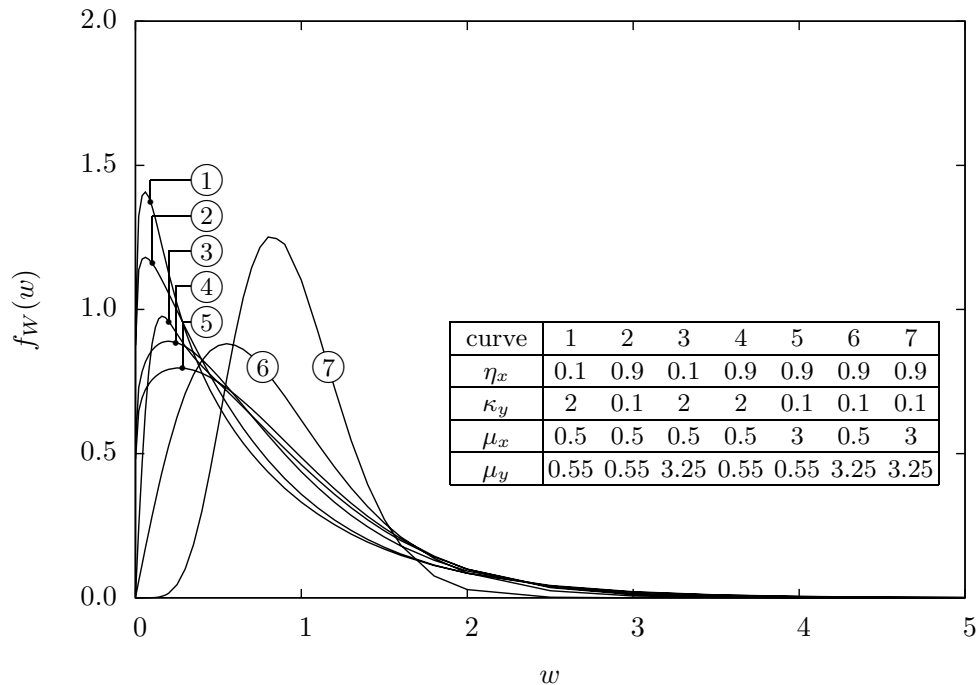


Figure 3.5: PDF of the product of η - μ and κ - μ random variables.

in which $i_c = \lceil \frac{i}{2} \rceil$.

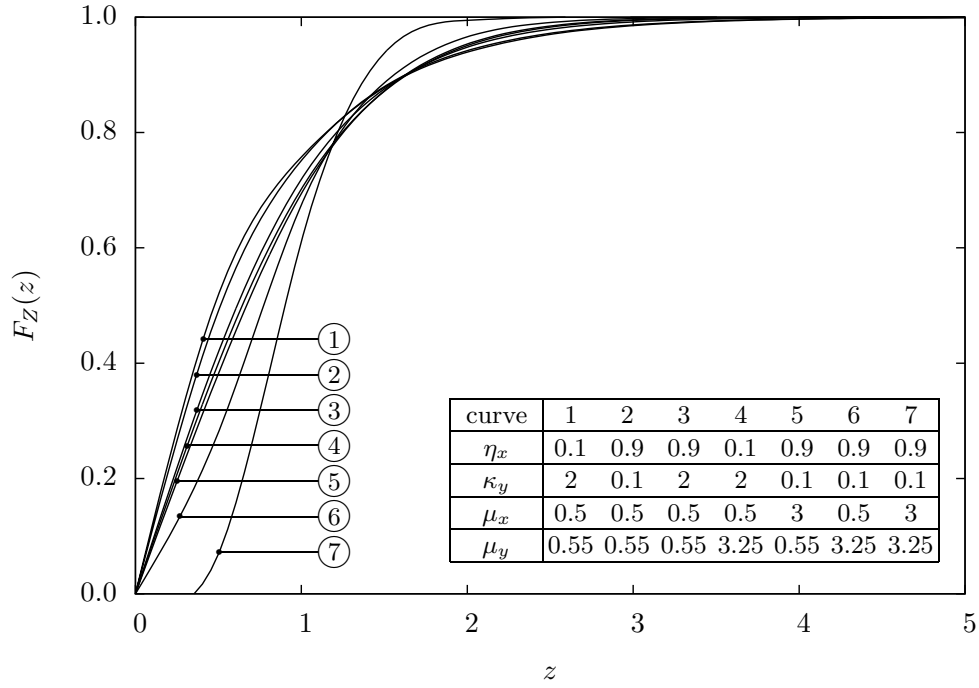
Although (3.27) includes an infinite summation, the evaluation of the PDF converges rapidly for cases of interest. Let I be the number of terms in a truncated summation (as defined earlier). Table 3.3 gives the value of I necessary to obtain a three-decimal-place accuracy (error < 0.0005) and a six-decimal-place accuracy (error < 0.0000005) for the infinite summation of (3.27). For the PDF accuracy, a smaller number of terms I is required for higher values of η_x , κ_y , μ_y or z , or lower values of μ_x .

The PDF of Z is shown in Fig. 3.5 for various values of η_x , κ_y , μ_x and μ_y . It can be seen that combined low κ_y and high μ_y shifts the curve away from the ordinate axis, making it assume, as expected, a shape closer to the familiar Rayleigh PDF. This is also seen, to a lesser degree, with high μ_x . On the other hand, a PDF with smaller tail and a higher peak value is obtained for diminishing values of e_x or increasing values of κ_y .

Note that (3.27) may be reduced in the following situations: (i) if μ_x is set to $\frac{1}{2}$, the corresponding PDF reduces to Hoyt; (ii) if $\kappa_y \rightarrow 0$, the corresponding PDF reduces to Nakagami- m , with $m = \mu_y$; and (iii) if $\mu_y = 1$ and $\kappa_y \rightarrow 0$, the corresponding PDF reduces to Rayleigh.

Table 3.3: Relation between number of terms and accuracy in the infinite summation of (3.27) and (3.30).

Parameters					smallest I for accuracy of				
η_x	κ_y	μ_x	μ_y	z	3-decimal-place		6-decimal-place		
					PDF	CDF	PDF	CDF	
0.1	0.1	0.5	0.5	0.1	236	1	544	3	
				1.0	234	11	544	16	
				5.0	176	70	518	73	
			1.0	0.1	140	2	416	4	
				5.0	176	100	538	103	
				5.0	0.1	4	7	14	9
		5.0	5.0	0	233	580	237		
			5.0	0.5	0.1	728	0	1148	2
				5.0	0	225	966	229	
				5.0	0.1	604	0	1024	11
			10.0	5.0	5.0	0	723	846	726
					0.5	0.1	90	3	374
	5.0	0				223	561	226	
	5.0	0.1		74	2	87	5		
		5.0		0	707	568	710		
		5.0		0.1	0	0	0	0	
	0.9	0.1	0.5	0.5	0.1	2	0	4	1
					5.0	0	10	4	13
				5.0	0.1	3	0	6	2
			5.0		0	40	4	43	
			5.0	0.5	0.1	4	0	7	1
					5.0	0	42	3	45
		5.0		0.1	0	0	0	0	
		10.0	5.0	5.0	0	120	0	123	
0.5				0.1	11	1	17	2	
				5.0	0	33	14	35	
5.0			0.1	70	0	85	1		
				5.0	0	97	0	99	
	5.0		0.5	0.1	2	0	5	2	
5.0	0.1	5.0	0	116	0	120			
		5.0	0	0	0	0	0		
5.0	0	338	0	341					

Figure 3.6: CDF of the product of $\eta\text{-}\mu$ and $\kappa\text{-}\mu$ random variables.

3.4.2 Cumulative Distribution Function

With (3.2) and (3.25), the CDF of W may be expressed as

$$\begin{aligned}
 F_W(w) &= \sum_{i=0}^{\infty} \sum_{j=0}^{\infty} \int_0^w \frac{2^{-2i-2\mu_x+3} \sqrt{\pi} (\mu_y \kappa_y)^j}{i! j! \Gamma(\mu_x) \Gamma(i + \mu_x + \frac{1}{2}) \Gamma(j + \mu_y) e^{\mu_y \kappa_y} h_x^{\mu_x}} \\
 &\quad \times \left(\frac{H_x}{h_x} \right)^{2i} u^{\frac{2i+j+2\mu_x+\mu_y}{2}} t^{2i+j+2\mu_x+\mu_y-1} K_{-2i+j-2\mu_x+\mu_y}(2\sqrt{ut}) dt.
 \end{aligned} \tag{3.28}$$

With the help of [49, Eq. 2.16.3.2], the above integral solves to

$$\begin{aligned}
 F_W(w) &= \sum_{i=0}^{\infty} \sum_{j=0}^{\infty} \frac{\Gamma(-2i+j-2\mu_x+\mu_y) \Gamma(i+\mu_x) (\mu_y \kappa_y)^j}{i! j! (2i+2\mu_x) \Gamma(\mu_x) \Gamma(2i+2\mu_x) \Gamma(j+\mu_y) e^{\mu_y \kappa_y} h_x^{\mu_x}} \left(\frac{H_x}{h_x} \right)^{2i} \\
 &\quad \times (uw^2)^{2i+2\mu_x} {}_1F_2(2i+2\mu_x, 2i+2\mu_x+1, 2i-j+2\mu_x-\mu_y+1, uw^2) \\
 &+ \sum_{i=0}^{\infty} \sum_{j=0}^{\infty} \frac{\Gamma(2i-j+2\mu_x-\mu_y) \Gamma(i+\mu_x) (\mu_y \kappa_y)^j}{i! j! (j+\mu_y) \Gamma(\mu_x) \Gamma(2i+2\mu_x) \Gamma(j+\mu_y) e^{\mu_y \kappa_y} h_x^{\mu_x}} \left(\frac{H_x}{h_x} \right)^{2i} \\
 &\quad \times (uw^2)^{j+\mu_y} {}_1F_2(j+\mu_y, j+\mu_y+1, -2i+j-2\mu_x+\mu_y+1, uw^2)
 \end{aligned} \tag{3.29}$$

in which u is defined by (3.26). After some algebraic manipulation, the double summations in (3.29) may be simplified to

$$\begin{aligned}
F_W(w) &= \frac{\pi}{\Gamma(\mu_y) e^{\mu_y \kappa_y} h_x^{\mu_x}} \sum_{i=0}^{\infty} \frac{\csc[(2\mu_x - \mu_y)\pi]}{i! \Gamma(2\mu_x)} \\
&\times \left\{ \frac{(uw^2)^{i+\mu_y}}{(i+\mu_y)\Gamma(i-2\mu_x+\mu_y+1)} {}_1F_1(-i, \mu_y, \mu_y \kappa_y) \right. \\
&\quad \times {}_2F_1 \left[-\frac{i}{2} + \mu_x - \frac{\mu_y}{2}, -\frac{i}{2} + \mu_x - \frac{\mu_y}{2} + \frac{1}{2}, \mu_x + \frac{1}{2}, \left(\frac{H_x}{h_x} \right)^2 \right] \\
&\quad - \frac{(uw^2)^{i+2\mu_x}}{(i+2\mu_x)\Gamma(i+2\mu_x-\mu_y+1)} {}_1F_1(-i-2\mu_x+\mu_y, \mu_y, \mu_y \kappa_y) \\
&\quad \left. \times {}_2F_1 \left[-\frac{i}{2}, -\frac{i+1}{2}, \mu_x + \frac{1}{2}, \left(\frac{H_x}{h_x} \right)^2 \right] \right\} \\
&+ \sum_{i=0}^{\infty} \frac{\csc[(2\mu_x - \mu_y + 2i_f)\pi] (uw^2)^{i+2\mu_x}}{8i_f(i+2\mu_x)(i-2i_f)! B(\mu_x, i_f) \Gamma(2\mu_x + 2i_f) \Gamma(i+2\mu_x - \mu_y + 1)} \\
&\quad \times {}_1F_1(-i-2\mu_x+\mu_y, \mu_y, \mu_y \kappa_y) \left(\frac{H_x}{h_x} \right)^{2i_f} \\
&\quad \times {}_3F_2 \left[1, -\frac{i}{2} + i_f, -\frac{i}{2} + i + f + \frac{1}{2}, i_f + 1, \mu_x + i_f + \frac{1}{2}, \left(\frac{H_x}{h_x} \right)^2 \right]
\end{aligned} \tag{3.30}$$

in which $i_f = \lfloor \frac{i}{2} \rfloor + 1$, and $\lfloor \cdot \rfloor$ is the floor function.

Although (3.30) includes an infinite summation, the evaluation of the CDF converges rapidly for cases of interest. Let I be the number of terms in a truncated summation (as defined earlier). Table 3.3 gives the value of I necessary to obtain a three-decimal-place accuracy (error < 0.0005) and a six-decimal-place accuracy (error < 0.0000005) for the infinite summation of (3.30). For the CDF accuracy, a smaller number of terms I is required for higher values of μ_y , or lower values of η_x , κ_y , μ_x or z .

Note that (3.30) may be reduced in the following situations: (i) if μ_x is set to $\frac{1}{2}$, the corresponding CDF reduces to Hoyt; (ii) if $\kappa_y \rightarrow 0$, the corresponding CDF reduces to Nakagami- m , with $m = \mu_y$; and (iii) if $\mu_y = 1$ and $\kappa_y \rightarrow 0$, the corresponding CDF reduces to Rayleigh.

The CDF of Z is shown in Fig. 3.6 for various values of η_x , κ_y , μ_x and μ_y . It can be seen that increasing values of μ_x or μ_y tend to produce steeper curves. On the other hand, lower values of η_x or κ_y tend to produce curves that reach the unity for higher values of z .

3.5 Product α - $\mu \times \alpha$ - μ

Let (1.17) represent the PDF of X

$$f_X(x) = \frac{\alpha_x \mu_x^{\mu_x} x^{\alpha_x \mu_x - 1}}{\Gamma(\mu_x) \hat{x}^{\alpha_x \mu_x}} \exp\left(-\mu_x \frac{x^{\alpha_x}}{\hat{x}^{\alpha_x}}\right) \quad (3.31)$$

and the PDF of Y

$$f_Y(y) = \frac{\alpha_y \mu_y^{\mu_y} y^{\alpha_y \mu_y - 1}}{\Gamma(\mu_y) \hat{y}^{\alpha_y \mu_y}} \exp\left(-\mu_y \frac{y^{\alpha_y}}{\hat{y}^{\alpha_y}}\right). \quad (3.32)$$

In the following, the PDF and the CDF of the ratio W are calculated.

3.5.1 Probability Density Function

With (3.1), (3.31) and (3.32), the PDF of W may be expressed as

$$f_W(w) = \int_0^\infty \frac{\alpha_x \alpha_y \mu_x^{\mu_x} \mu_y^{\mu_y} w^{\alpha_x \mu_x - 1} y^{-\alpha_x \mu_x + \alpha_y \mu_y - 1}}{\Gamma(\mu_x) \Gamma(\mu_y) \hat{x}^{\alpha_x \mu_x} \hat{y}^{\alpha_y \mu_y}} \times \exp\left[-\frac{\mu_x}{\hat{x}^{\alpha_x}} \left(\frac{w}{y}\right)^{\alpha_x}\right] \exp\left(-\frac{\mu_y}{\hat{y}^{\alpha_y}} y^{\alpha_y}\right) dy. \quad (3.33)$$

Let us assume that $\frac{\alpha_x}{\alpha_y} = \frac{p}{q}$ in which p and q are coprime positive integers. With the integration variable changed to $t = y^{\alpha_x}$, the integral in (3.33) can be solved with the help of [51, Eq. 2.3.2.14]. If $p \neq q$, it results in

$$\begin{aligned} f_W(w) = & \frac{1}{\Gamma(\mu_x) \Gamma(\mu_y)} \left\{ \alpha_y \sum_{i=0}^{p-1} \frac{(-1)^i}{i!} u^{\frac{i+\mu_y}{p}} w^{\alpha_y(i+\mu_y)-1} \Gamma\left[\mu_x - (i+\mu_y)\frac{q}{p}\right] \right. \\ & \times {}_1F_{p+q}\left[1, \Delta(i+1, p), \Delta\left(-\mu_x + (i+\mu_y)\frac{q}{p} + 1, q\right), \frac{(-1)^{p+q}}{p^p q^q} u w^{q\alpha_x}\right] \\ & + \alpha_x \sum_{i=0}^{q-1} \frac{(-1)^i}{i!} u^{\frac{i+\mu_x}{q}} w^{\alpha_x(i+\mu_x)-1} \Gamma\left[-(i+\mu_x)\frac{p}{q} + \mu_y\right] \\ & \left. \times {}_1F_{p+q}\left[1, \Delta(i+1, q), \Delta\left[-\mu_y + (i+\mu_x)\frac{p}{q}, p\right], \frac{(-1)^{p+q}}{p^p q^q} u w^{q\alpha_x}\right] \right\} \end{aligned} \quad (3.34)$$

in which

$$u = \left(\frac{\mu_x}{\hat{x}^{\alpha_x}}\right)^q \left(\frac{\mu_y}{\hat{y}^{\alpha_y}}\right)^p. \quad (3.35)$$

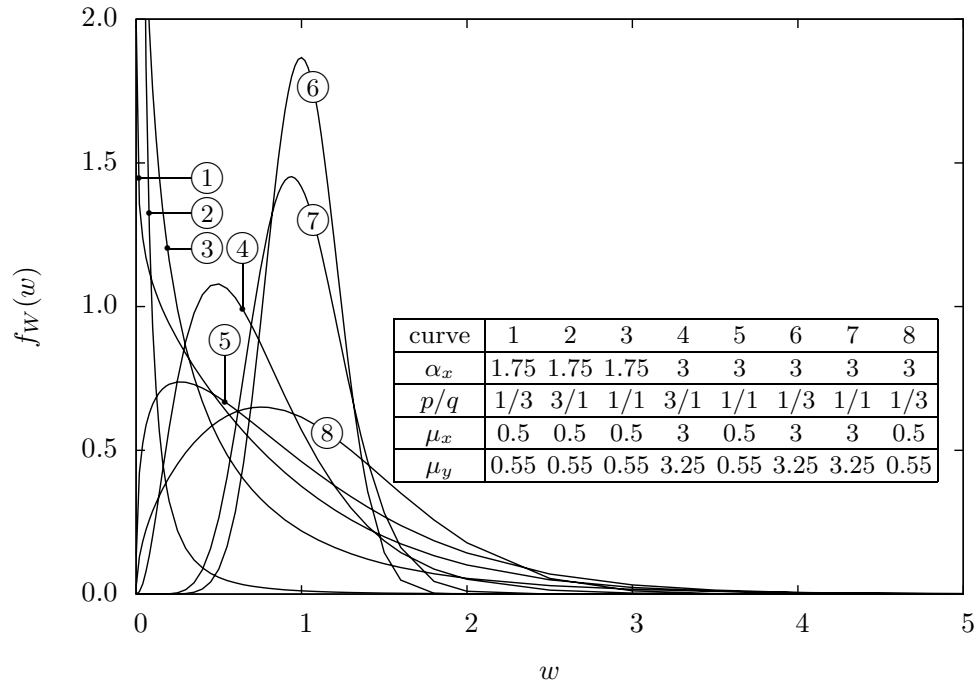


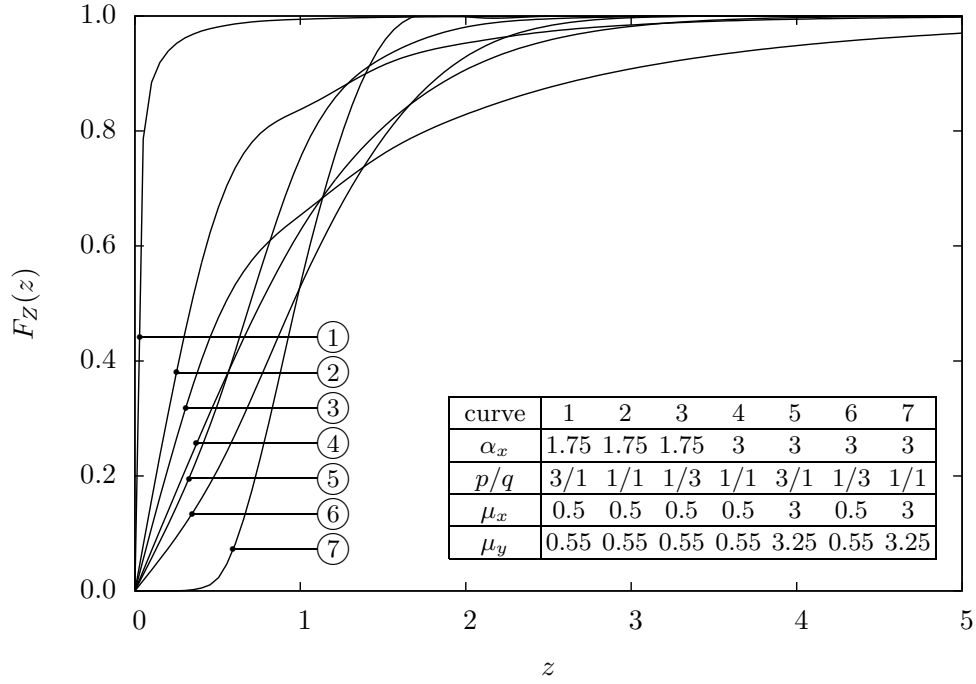
Figure 3.7: PDF of the product of α - μ random variables.

If $p = q$ (thus making $\alpha_x = \alpha_y = \alpha$),

$$f_W(w) = \frac{2\alpha}{\Gamma(\mu_x)\Gamma(\mu_y)} u^{\frac{\mu_x+\mu_y}{2}} w^{\alpha\frac{\mu_x+\mu_y}{2}-1} K_{\mu_x-\mu_y} \left(2\sqrt{uw^\alpha} \right). \quad (3.36)$$

The PDF of Z is shown in Fig. 3.7 for various values of α_x , p , q , μ_x and μ_y . It can be seen that the curves have different shapes, varying from close to the negative exponential (smaller α_x) to closer to Rayleigh and Rice (larger α_x). Also, a PDF with smaller tail is obtained for increasing values of μ_y .

Note that (3.34) and (3.36) may be reduced in the following situations: (i) if μ_x (or μ_y) is set to unity, the corresponding PDF reduces to Weibull; (ii) if $\mu_x = 1$ and $\alpha_x = 1$ ($\mu_y = 1$ and $\alpha_y = 1$), the corresponding PDF reduces to negative exponential; and (iii) if $\mu_x = 1$ and $\alpha_x = 2$ ($\mu_y = 1$ and $\alpha_y = 2$), the corresponding PDF reduces to Nakagami- m PDF with $m = \mu_x$ ($m = \mu_y$)

Figure 3.8: CDF of the product of α - μ random variables.

3.5.2 Cumulative Distribution Function

Let $\frac{\alpha_x}{\alpha_y} = \frac{p}{q}$ as already defined. Assuming that $p \neq q$, with (3.2) and (3.34), and using [52, Eq. 1.16.1.1] to solve the integral leads to

$$\begin{aligned}
F_W(w) &= \frac{1}{\Gamma(\mu_x)\Gamma(\mu_y)} \left\{ \sum_{i=0}^{p-1} \frac{(-1)^i}{i!(i+\mu_y)} u^{\frac{i+\mu_y}{p}} w^{\alpha_y(i+\mu_y)} \Gamma \left[\mu_x - (i+\mu_y) \frac{q}{p} \right] \right. \\
&\times {}_2F_{p+q+1} \left[1, \frac{i+\mu_y}{p}, \Delta(i+1, p), \Delta \left[-\mu_x + (i+\mu_y) \frac{q}{p} + 1, q \right], \frac{i+\mu_y}{p} + 1, \frac{(-1)^{p+q}}{p^p q^q} u w^{\alpha_x q} \right] \\
&+ \sum_{i=0}^{q-1} \frac{(-1)^i}{i!(i+\mu_x)} u^{\frac{i+\mu_x}{q}} w^{\alpha_x(i+\mu_x)} \Gamma \left[-(i+\mu_x) \frac{p}{q} + \mu_y \right] \\
&\times {}_2F_{p+q+1} \left[1, \frac{i+\mu_x}{q}, \Delta(i+1, q), \Delta \left[(i+\mu_x) \frac{p}{q} - \mu_y + 1, p \right], \frac{i+\mu_x}{q} + 1, \frac{(-1)^{p+q}}{p^p q^q} u w^{\alpha_x q} \right] \left. \right\}. \tag{3.37}
\end{aligned}$$

If $p = q$ (thus making $\alpha_x = \alpha_y = \alpha$),

$$\begin{aligned}
f_W(w) &= \frac{1}{\Gamma(\mu_x)\Gamma(\mu_y)} \left\{ \frac{\Gamma(\mu_x - \mu_y)}{\mu_y} (u w^\alpha)^{\mu_y} {}_1F_2(\mu_y, -\mu_x + \mu_y + 1, \mu_y + 1, u w^\alpha) \right. \\
&+ \left. \frac{\Gamma(-\mu_x + \mu_y)}{\mu_x} (u w^\alpha)^{\mu_x} {}_1F_2(\mu_x, \mu_x - \mu_y + 1, \mu_x + 1, u w^\alpha) \right\} \tag{3.38}
\end{aligned}$$

in which u is given by (3.35)

Note that (3.37) and (3.38) may be reduced in the following situations: (i) if μ_x (or μ_y) is set to unity, the corresponding CDF reduces to Weibull; (ii) if $\mu_x = 1$ and $\alpha_x = 1$ ($\mu_y = 1$ and $\alpha_y = 1$), the corresponding CDF reduces to negative exponential; and (iii) if $\mu_x = 1$ and $\alpha_x = 2$ ($\mu_y = 1$ and $\alpha_y = 2$), the corresponding CDF reduces to Nakagami- m CDF with $m = \mu_x$ ($m = \mu_y$)

The CDF of Z is shown in Fig. 3.8 for various values of α_x , p , q , μ_x and μ_y . It can be seen that higher values of μ_y , α_x or α_y tend to produce a steeper curve. On the other hand, lower values of μ_x or μ_y result in a smoother CDF.

Application Examples

In this chapter, application examples based on results from previous chapters are presented. Specifically, the following are studied: *(i)* analysis of the throughput of Carrier Sense Multiple Access (CSMA) in Rice, Hoyt, Nakagami- m , combined Ride and Hoyt, η - μ and κ - μ fading channels; *(ii)* analysis of the throughput of the Distributed Coordination Function (DCF) of IEEE 802.11 in Hoyt, Rice, and Nakagami- m Fading Channels; and *(iii)* ratio of independent alpha-mu random variables and its application in the capacity analysis of spectrum sharing systems.

These examples are introduced as a collection of articles presented in conferences or published or submitted to scientific journals. For the sake of convenience, the introductory parts explaining the motivation and presenting the analytical model are repeated in every application.

4.1 Capacity of CSMA under Nakagami Fading¹

4.1.1 Introduction

Wireless local area networks (WLANs) are experiencing rapid development in part stimulated by the deployment of systems compatible to the IEEE 802.11 standards. They offer data communication between terminals within radio range while allowing a certain degree of mobility. In order to serve terminals exhibiting bursty traffic behaviour, WLANs make use of

¹This material was presented at [53].

packet radio techniques with random access to a transmission channel shared by multiple users. Specifically, variations of carrier sense multiple access (CSMA) is generally used to access the wireless medium [54, 55, 56, 57]. The capacity of the channel is then influenced by the probability of packet collision and by the signal degradation due to mutual interference and signal attenuation. In other words, it is influenced by the medium contention resolution algorithm and by the channel characteristics.

Intuitively one might expect that original (wireline) CSMA systems show better system performance than wireless systems because of more hostile channel characteristics found in the latter. However, this is not necessarily the case. For instance, in a channel model that takes into account the effects of fading, competing packets arriving at a common radio receiver antenna will not always destroy each other because they may show different and independent fading and attenuation levels [58, 59]. This leads to expect that wireless systems may actually exhibit successful reception rate higher than that of original (wireline) systems. In fact, Arnbak and Blitterswijk have shown this to happen with slotted Aloha over Rayleigh fading channels [29].

In this application example, we investigate the throughput performance of CSMA in a packet radio network with Nakagami fading environment. The performance of the original (wireline) CSMA is presented in [60] and is here extended to the wireless environment, for which the Nakagami- m fading conditions are assumed. A number of closed form as well as series expressions are found. To the best of the authors' knowledge, these results are novel contributions.

This application example is organized as follows. Section 4.1.2 describes the analytical model. Section 4.1.3 considers the case of incoherent packet addition at the receiver's antenna, and extends the model to include spatial coverage such as in a cell. Comments and conclusions are given in Sections 4.1.4 and 4.1.5, respectively.

4.1.2 Analytical Model

Nonpersistent CSMA

For nonpersisting CSMA, a terminal ready to transmit first senses the channel. If it senses the channel idle, it transmits the packet. Otherwise, it schedules the (re)transmission of the

packet to a later time according to some randomly distributed retransmission delay. After the retransmission delay has elapsed, the terminal repeats the procedure described above. In this application example, the channel is considered to be memoryless, i.e., failures to capture the channel and future attempts are uncorrelated. In addition, all packets are assumed to have fixed length and to require p seconds to transmit. Finally, each packet is assumed to have a single destination.

Probability of Capture

Given the transmission of an arbitrary test packet over a wireline channel, it is generally assumed that a successful reception can only occur if no other transmission attempt is made during the test packet reception, i.e., if there is no signal overlap at the receiver. However, in wireless systems the radio receiver may be able to be captured by a test packet, even in the presence of n interfering packets, provided that the power ratio between the test signal and the joint interfering signal exceeds a certain threshold during a given portion of the transmission period t_w , $0 < t_w < p$, to lock the receiver [61, 62]. In such a case, a test packet is only destroyed if $w_s/w_n \leq z$ during t_w , with $n > 0$, where z is the capture ratio, and w_s and w_n are the test packet power and the joint interference power at the receiver's antenna, respectively. Values for z and the capture window t_w depend on the modulation and the coding employed by the network, among other things. For a typical narrowband FM receiver, a z value of 6 dB is suggested in [63]. The details about estimation of the values of z and t_w are beyond the scope of this application example.

Let the random variable Z be defined as the signal-to-interference ratio

$$Z \triangleq \frac{W_s}{W_n}, \quad Z \geq 0 \quad (4.1)$$

where $W_s \geq 0$ and $W_n \geq 0$ are random variables representing the desired signal power and the interference power, respectively. Assuming that W_s and W_n are statistically independent, the

resulting probability density function (PDF) can be expressed as [47]

$$f_Z(z) = \int_0^\infty y f_{W_s}(zy) f_{W_n}(y) dy \quad (4.2)$$

where $f_{W_s}(\cdot)$ and $f_{W_n}(\cdot)$ are the PDFs of the desired signal power and the interference power, respectively. The cumulative distribution function (CDF) is then expressed as

$$F_Z(z_0) = \text{Prob} \left\{ \frac{W_s}{W_n} \leq z_0 \right\} = \int_0^{z_0} f_Z(z) dz. \quad (4.3)$$

Let the number of packets generated in the network for new messages plus retransmissions be Poisson distributed, with mean generation rate of λ packets per second. The mean offered traffic is then expressed as $G = p\lambda$ packets per transmission period. Given the transmission of an arbitrary test packet, the probability of it being overlap by n other packets is given by [47]

$$R_n = \frac{(Ga)^n}{n!} e^{-Ga} \quad (4.4)$$

where τ is the worst case propagation delay and $a = \tau/p$ its normalised version. Finally, the unconditional probability of a test packet being able to capture the receiver in an arbitrary transmission period may be expressed by

$$P_{capt}(z_0) = 1 - \sum_{n=1}^{\infty} R_n F_Z(z_0). \quad (4.5)$$

Channel Throughput

Let U , B and I be random variables representing, respectively, the duration of the successful transmission, the duration of the busy period and the duration of the idle period. Let $E\{U\}$, $E\{B\}$ and $E\{I\}$ be their respective expected values. Clearly, the channel throughput can be expressed by $S = E\{U\}/(E\{B\} + E\{I\})$. For nonpersistent CSMA, Kleinrock and Tobagi have shown that [60]

$$E\{B\} = p + 2\tau - \frac{p}{G} (1 - e^{-Ga}) \quad \text{and} \quad E\{I\} = \frac{p}{G}. \quad (4.6)$$

It can also be seen that

$$E\{U\} = p P_{capt}(z_0) \quad (4.7)$$

where $P_{capt}(\cdot)$ is the probability of receiver's capture and also it represents the probability of a successful transmission. Using the results of (4.6)-(4.7), the throughput can be written as

$$S = \frac{GP_{capt}(z_0)}{G(1 + 2a) + e^{-Ga}} \quad (4.8)$$

Nakagami Fading Channel

In a Nakagami fading channel, PDF of the signal envelope r is given by [18]

$$f_R(r) = \frac{2r^{2m-1}}{\Gamma(m)} \left(\frac{m}{\bar{w}}\right)^m \exp\left(-\frac{mr^2}{\bar{w}}\right) \quad (4.9)$$

where $\bar{w} = E\{r^2\}$ is the mean square value, m is a fading parameter, and $\Gamma(\cdot)$ is the gamma function [21, Eq. 6.1.1]. For $m=1$, the Nakagami distribution reduces to the Rayleigh PDF while $m \rightarrow \infty$ corresponds to a non-fading situation. If we define the signal power $w = r^2$, its PDF can be expressed as

$$f_W(w) = \frac{w^{m-1}}{\Gamma(m)} \left(\frac{m}{\bar{w}}\right)^m \exp\left(-\frac{mw}{\bar{w}}\right) \quad (4.10)$$

where $\bar{w} = E\{w\}$ is the mean power.

Interference Signal

In a wireless system, interference typically results from (supposedly uncorrelated) signals arriving at the receiver's antenna from multiple transmitters. Depending on how these random signals combine during the observation interval, one of two scenarios might occur [1]: coherent addition or incoherent addition.

Coherent addition occurs if the carrier frequencies are equal and if the random phase fluctuations are small during the capture time t_w . For instance, coherent addition might happen when the deviation caused by the phase modulation is very small, and the observation interval is short

compared to the modulation rate. For the Nakagami channel, analysis of coherent addition of signals is rather intricate and it is a matter still under investigation by the authors.

Incoherent addition occurs if the phases of the individual signals fluctuate significantly due to mutually independent modulation [29, 64]. In this case, the interference power w_n experienced during the observation interval is the sum of the individual signals' powers w_i , i.e.,

$$w_n = \sum_{i=1}^n w_i = \sum_{i=1}^n \overline{x_i(t)x_i^*(t)} \quad (4.11)$$

where $x_i^*(\cdot)$ is the complex conjugate of phasor $x_i(\cdot)$. Considering the current work, where the signal power is a random variable, the PDF of the joint interference power is therefore the convolution of the PDFs of all contributing signal powers.

4.1.3 Analytical Results

For the calculations presented in this section, let (4.10) represent the desired signal power PDF as well as, with different parameters, the signal power PDF of an individual component of the interference signal. Note that due to the lack of space, some intermediate steps in the derivation of the formulae presented below may be omitted. Also, for the remaining of this application example and wherever applicable, the subscripts s , i and n are used to represent the desired signal variables, the interference signal's individual component variables, and the joint interference signal variables, respectively. Finally, let \tilde{z}_0 be defined as $\tilde{z}_0 \triangleq z_0/(\bar{w}_s/\bar{w}_n)$.

Incoherent Interference

For the incoherent addition, assume that the interference signal is composed of n i.i.d. variables. As a result, the joint interference signal power PDF is the n -fold convolution of the individual signal power PDF which, on its turn, is expressed by (4.10). This calculation gives that

$$f_{W_n}(w_n) = \frac{w_n^{m_n-1}}{\Gamma(m_n)} \left(\frac{m_n}{\bar{w}_n}\right)^{m_n} \exp\left(-\frac{m_n w_n}{\bar{w}_n}\right) \quad (4.12)$$

where m_i and $m_n = nm_i$ are the individual and the joint fading parameters, respectively, and $\bar{w}_n = E\{w_n\} = nE\{w_i\}$ is the joint mean power. It can be seen from (4.10) and (4.12) that both signal power and interference power are described by the same distribution, except that they have distinct parameters.

Using the appropriated expressions in (4.2), and after some manipulation, the signal-to-interference PDF may be expressed as

$$f_Z(z) = \frac{1}{B(m_s, m_n)} \frac{1}{z} \left(\frac{m_s \bar{w}_n}{m_n \bar{w}_s} z \right)^{m_s} \left(1 + \frac{m_s \bar{w}_n}{m_n \bar{w}_s} z \right)^{-m_n - m_s} \quad (4.13)$$

where $B(\cdot)$ is the beta function [21, Eq. 6.2.2]. The corresponding CDF may be expressed as [30]

$$F_Z(z_0) = I_{x_0}(m_s, m_n) \quad (4.14)$$

where $I_x(\cdot)$ is the regularized incomplete beta function [21, Eq. 6.6.2], and

$$x_0 = \left(1 + \frac{m_n \bar{w}_s}{m_s \bar{w}_n} \frac{1}{z_0} \right)^{-1}. \quad (4.15)$$

As a special case, for Rayleigh fading channels $m_s = m_i = 1$ (which results in $m_n = n$). Using these values in (4.14), it can be shown that

$$F_Z(z_0) = 1 - \left(\frac{n}{n + z_0 \bar{w}_n / \bar{w}_s} \right)^n. \quad (4.16)$$

If the result above is further simplified by assuming that $\bar{w}_s = \bar{w}_i = \bar{w}_n/n$, then the same expression presented in [29] is found.

Spatial Coverage

The analysis presented so far assumes that the components of the interference signal have equal mean power \bar{w}_i , $i = 1, \dots, n$. This restriction limits the results to systems where perfect power control is employed or to terminals placed at a fixed distance from the receiving antenna (i.e., on a circular ring) and in an environment without any shadowing effects. Let us now

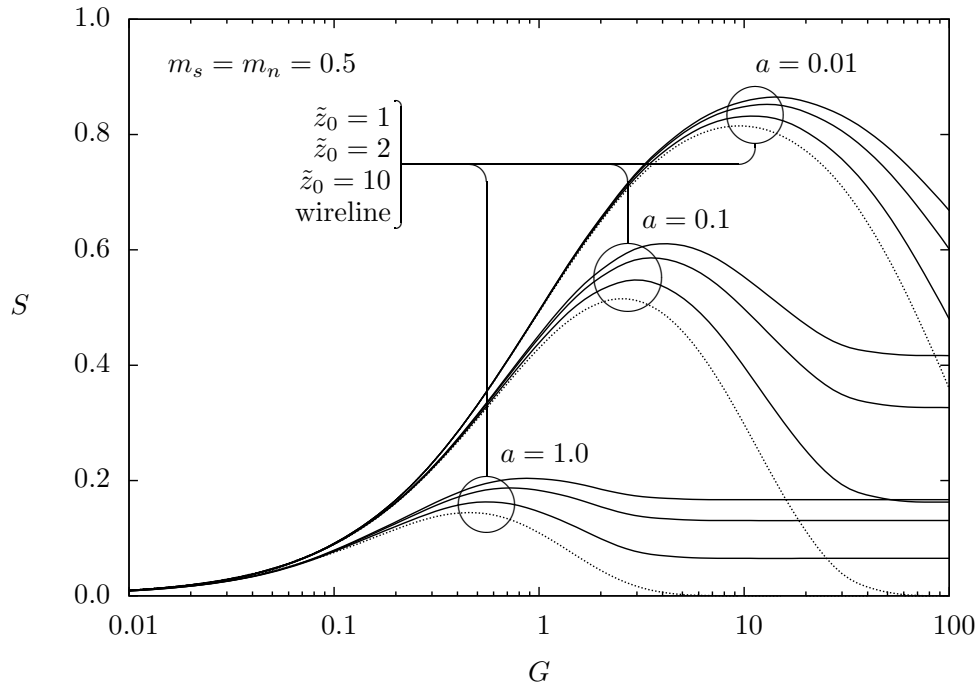


Figure 4.1: Throughput curves assuming incoherent addition of Nakagami-fading interfering packets and constant mean packet power, with $m_s = m_n = 0.5$. The dotted lines correspond to the original (wireline) channel where $z_0 \rightarrow \infty$.

extend the model presented above to include the case of packets arriving with different mean power, e.g., from terminals spread across a radio cell and at different transmission distances to the receiver's antenna. Therefore, the statistical behaviour of the packet mean power needs to be specified and taken into account.

The mean power of a packet received from a terminal at a distance d is of the general form [2]

$$\bar{w} = k d^{-\alpha} \quad (4.17)$$

where α gives the channel attenuation with the distance, and k is a value that depends on, among other things, the transmit power and the height and gain of the antennas. Typical values of the exponent α are $\alpha = 2$ in free space and $\alpha = 4$ in urban land mobile cellular systems. Using a similar approach to that presented in [29], let $\rho \triangleq d k^{-1/\alpha}$ be defined and used to rewrite (4.17) as

$$\bar{w} = \rho^{-\alpha}. \quad (4.18)$$

Let the offered traffic density function $G(\rho)$ be defined as the number of packets offered per

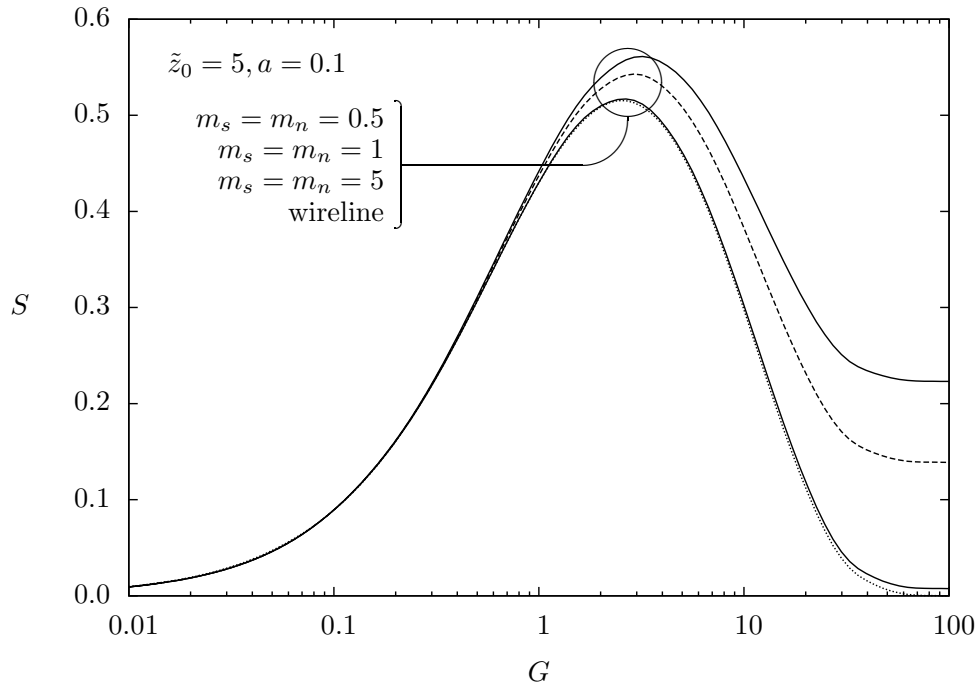


Figure 4.2: Throughput curves assuming incoherent addition of Nakagami-fading interfering packets and constant mean packet power with $\tilde{z}_0 = 5$ and $a = 0.1$. The dashed line correspond to the Rayleigh channel where $m_s = m_n = 1$. The dotted line correspond to the original (wireline) channel where $z_0 \rightarrow \infty$.

transmission period per unit of area at distance ρ . The total offered traffic can be calculated by

$$G_t = 2\pi \int_0^\infty \rho G(\rho) d\rho. \quad (4.19)$$

The spatial CDF of the offered traffic as a function of the distance ρ can be expressed as

$$\begin{aligned} F_G(\rho) &= \text{Prob}\{\text{packet generated within distance } \rho\} \\ &= \frac{2\pi}{G_t} \int_0^\rho u G(u) du \end{aligned} \quad (4.20)$$

and the corresponding PDF is

$$f_G(\rho) = \frac{2\pi}{G_t} \rho G(\rho). \quad (4.21)$$

The PDF of the received packet mean power

$$f_{\bar{w}}(\bar{w}) = f_G(\rho) \left| \frac{d\rho}{d\bar{w}} \right| \quad (4.22)$$

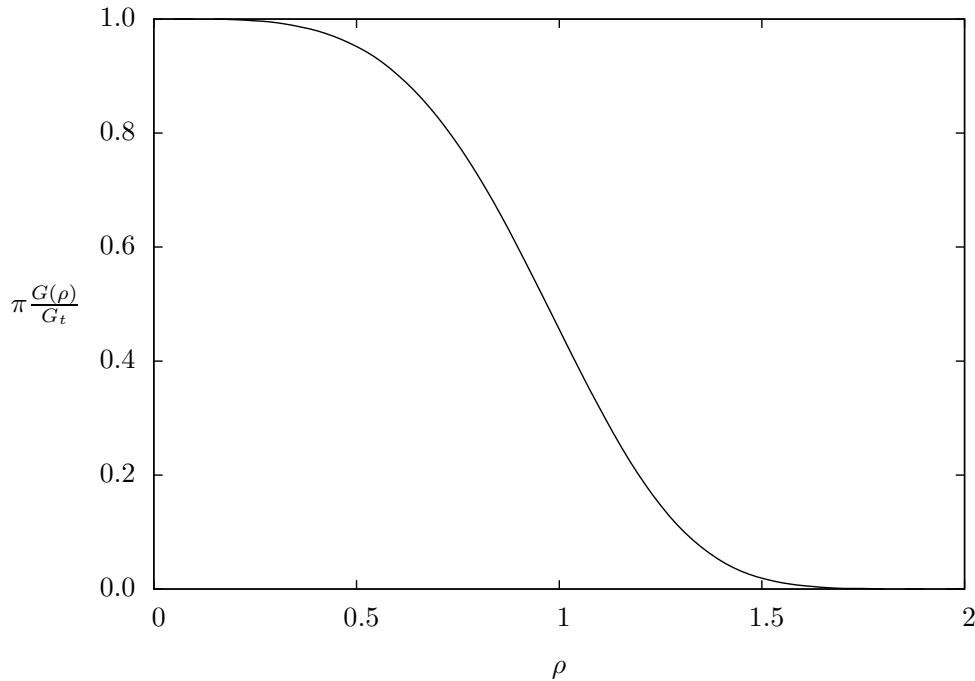


Figure 4.3: Normalised offered traffic density defined by (4.25).

is calculated using (4.18) and (4.21) and can be expressed as

$$f_{\bar{W}}(\bar{w}) = \frac{2\pi}{\alpha G_t} \frac{G(\bar{w}^{-1/\alpha})}{\bar{w}^{1+2/\alpha}}. \quad (4.23)$$

The capture probability for spatial coverage is now considered. Given an arbitrary spatial traffic density $G(\rho)$, (4.23) can be used to calculate the PDF of the test packet mean power $f_{\bar{W}_s}(\bar{w}_s)$. The PDF of the mean interference power of n packets $f_{\bar{W}_n}(\bar{w}_n)$ is calculated by convolving (4.23) n times. With these results and assuming that the signal power and the interference power are statistically independent, the CDF of the signal-to-interference ratio can be calculated as

$$F_Z(z_0) = \int_0^{z_0} dz \int_0^\infty d\bar{w}_n \int_0^\infty f_Z(z) f_{\bar{W}_n}(\bar{w}_n) f_{\bar{W}_s}(\bar{w}_s) d\bar{w}_s \quad (4.24)$$

where $f_Z(\cdot)$ is given by (4.2). With (4.5) and (4.24), the capture probability is then calculated. As an example, let us use the quasi-constant traffic density given in [29], expressed as

$$G(\rho) = \frac{G_t}{\pi} \exp\left(-\frac{\pi}{4}\rho^4\right), \quad \rho \geq 0, \quad (4.25)$$

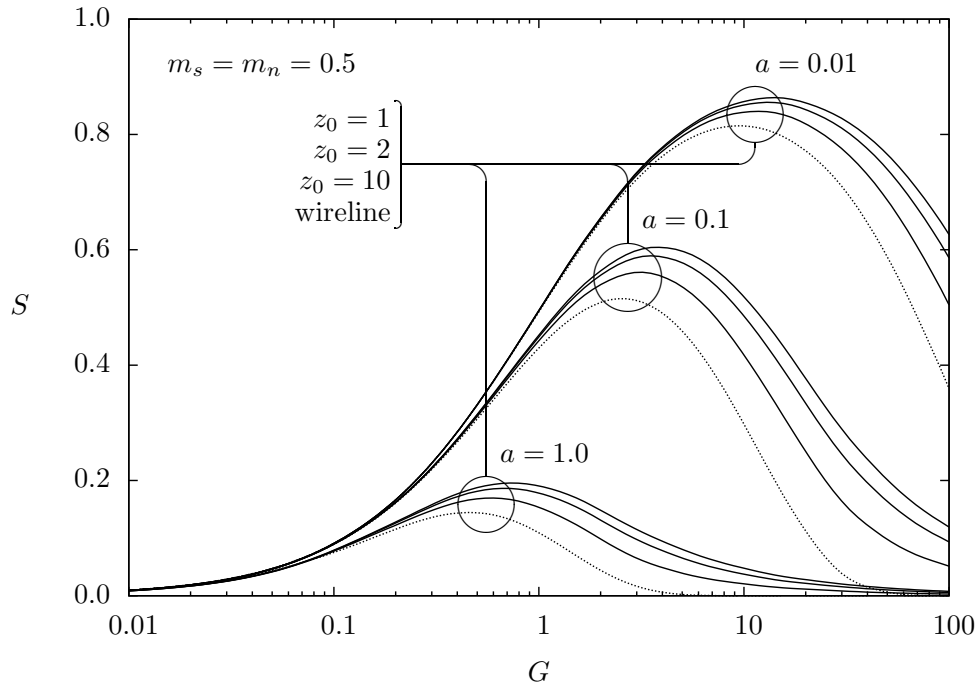


Figure 4.4: Throughput curves assuming incoherent addition of Nakagami-fading interfering packets and spatial coverage, with $m_s = m_n = 0.5$. The dotted lines correspond to the original (wireline) channel where $z_0 \rightarrow \infty$.

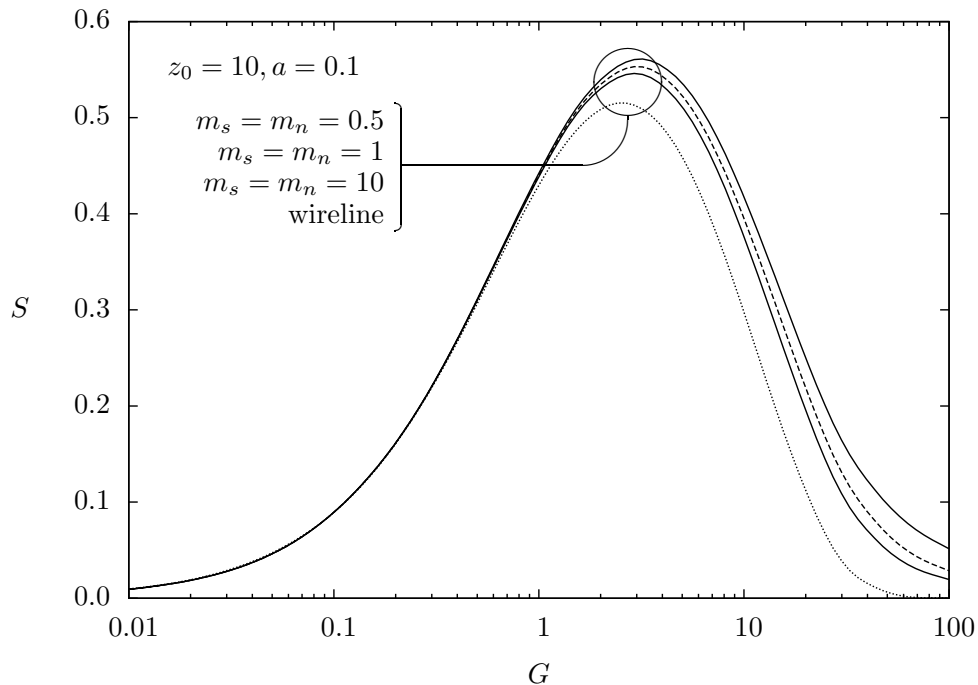


Figure 4.5: Throughput curves assuming incoherent addition of Nakagami-fading interfering packets and spatial coverage with $z_0 = 10$ and $a = 0.1$. The dashed line correspond to the Rayleigh channel where $m_s = m_n = 1$. The dotted line correspond to the original (wireline) channel where $z_0 \rightarrow \infty$.

and depicted in Fig. 4.3. Note that the traffic density is roughly constant inside the cell of radius $\rho = 1$, falling rapidly beyond the cell boundary. If we select $\alpha = 4$, it can be seen that

$$f_{\bar{w}_s}(\bar{w}_s) = \frac{1}{2\bar{w}_s^{3/2}} \exp\left(-\frac{\pi}{4\bar{w}_s}\right) \quad (4.26)$$

and

$$f_{\bar{w}_n}(\bar{w}_n) = \frac{n}{2\bar{w}_n^{3/2}} \exp\left(-\frac{\pi n^2}{4\bar{w}_n}\right). \quad (4.27)$$

Using these results in (4.24), and considering $f_Z(\cdot)$ given by (4.13), the signal-to-interference CDF is given by

$$F_Z(z_0) = \sec(m_s \pi) \left[\frac{c_0^{m_s}}{m_s} \frac{{}_2F_1(m_s, m_s + m_n, m_s + 1, c_0)}{B(m_s, m_n)} - 2\sqrt{c_0} \frac{\Gamma(m_n + \frac{1}{2})}{\Gamma(m_s)\Gamma(m_n)\Gamma(-m_s + \frac{3}{2})} {}_3F_2\left(\frac{1}{2}, 1, m_n + \frac{1}{2}, \frac{3}{2}, -m_s + \frac{3}{2}, c_0\right) \right] \quad (4.28)$$

where ${}_2F_1(\cdot)$ is the Gauss hypergeometric function [21, Eq. 15.1.1], ${}_3F_2(\cdot)$ is a generalized hypergeometric function [48, Eq. 9.14.1], and

$$c_0 = n^2 z_0 \frac{m_s}{m_n}. \quad (4.29)$$

4.1.4 Numerical Results

Perfect Power Control

With the results obtained in Section 4.1.3, using (4.5), (4.8) and (4.14), it is possible to calculate the capture probability and the channel throughput considering the perfect power control. Figs. 4.1 and 4.2 present the channel throughput for a number of different conditions. As expected, lower values for the propagation delay a brings higher throughput figures. Throughput is also higher with lower values for the capture threshold z_0 , which is related to the receiver's ability to cope with the interference. A lower value for z_0 means that the receiver is able to detect the test signal even in the presence of higher interference power levels. The fading parameter m has also an impact on the throughput. Less severe fading conditions (indicated by higher values

of m) result in lower throughput figures. In other words, higher m values push the throughput results closer to those obtained for the original (wireline) channel model.

Spatial Coverage

With the results obtained in Section 4.1.3, applying the results of (4.4) and (4.28) in (4.5), and the latter in (4.8), the throughput can be calculated. Fig. 4.4 presents the throughput for $m_s = m_n = 0.5$ and various values of the capture threshold z_0 and the propagation delay a . As expected, the lower the value of z_0 , the higher the throughput obtained. The same behaviour is also observed with the value of a . Fig. 4.5 presents the curves of throughput for various values of m_s and m_n . In a way similar to the result presented above, the lower fading intensity also translates into lower throughput. However, for the current analysis it seems that m has a somewhat minor impact on the throughput.

4.1.5 Conclusions

This application example investigates the throughput performance of CSMA in a packet radio network and Nakagami fading environment. Analytical and numerical results are presented considering the signal capture model with incoherent addition of interfering signals, as well as the case of unequal average power levels. The results showed that lower values for the capture threshold z_0 result in higher throughput figures. This is an expected outcome since z_0 is related to the ability of a receiver to detect the intended signal among the interfering signals. Also, the results showed that the fading intensity, represented by the Nakagami distribution m parameter, has a somewhat smaller influence in the throughput performance.

4.2 Throughput of CSMA in Hoyt Fading Channels²

4.2.1 Introduction

Wireless local area networks (WLANs) are experiencing rapid development in part stimulated by the deployment of systems compatible to the IEEE 802.11 standards. They offer data communication between terminals within radio range while allowing a certain degree of mobility.

In order to serve terminals exhibiting bursty traffic behaviour, WLANs make use of packet radio techniques with random access to a transmission channel shared by multiple users. Specifically, variations of carrier sense multiple access (CSMA) is generally used to access the wireless medium [54, 55, 56, 57]. The capacity of the channel is then influenced by the probability of packet collision and by the signal degradation due to mutual interference and signal attenuation. In other words, it is influenced by the medium contention resolution algorithm and by the channel characteristics.

Intuitively one might expect that original (wireline) CSMA systems show better system performance than wireless systems because of more hostile channel characteristics found in the latter. However, this is not necessarily the case. For instance, in a channel model that takes into account the effects of fading, competing packets arriving at a common radio receiver antenna will not always destroy each other because they may show different and independent fading and attenuation levels [58, 59]. This leads to expect that wireless systems may actually exhibit successful reception rate higher than that of original (wireline) systems. In fact, Arnbak and Blitterswijk have shown this to happen with slotted Aloha over Rayleigh fading channels [29].

In this application example, we investigate the throughput performance of CSMA in a packet radio network with Hoyt fading environment. The performance of the original (wireline) CSMA is presented in [60] and is here extended to this fading scenario. The channel model considered in this work is among those commonly used to describe the short-term signal statistics of wireless communications links subject to fading [66, 67]. The Hoyt model (also known as Nakagami- q) applies to the cases when there is not a dominant signal and the variances of the in-phase and

²This material was presented at [65].

quadrature components of the received signal are different or correlated.

This application example is organized as follows. Section 4.2.2 describes the analytical model and considers the cases of coherent and incoherent packet addition at the receiver's antenna. Section 4.2.3 presents the results obtained. Comments and conclusions are given in Section 4.2.4.

4.2.2 Analytical Model

Nonpersistent CSMA

For nonpersisting CSMA, a terminal ready to transmit first senses the channel. If it senses the channel idle, it transmits the packet. Otherwise, it schedules the (re)transmission of the packet to a later time according to some randomly distributed retransmission delay. After the retransmission delay has elapsed, the terminal repeats the procedure described above. In this application example, the channel is considered to be memoryless, i.e., failures to capture the channel and future attempts are uncorrelated. In addition, all packets are assumed to have fixed length and to require p seconds to transmit. Finally, each packet is assumed to have a single destination.

Probability of Capture

Given the transmission of an arbitrary test packet over a wireline channel, it is generally assumed that a successful reception can only occur if no other transmission attempt is made during the test packet reception, i.e., if there is no signal overlap at the receiver'. However, in wireless systems the radio receiver may be able to be captured by a test packet, even in the presence of n interfering packets, provided the power ratio between the test signal and the joint interfering signal exceeds a certain threshold during a given portion of the transmission period t_w , $0 < t_w < p$, to lock the receiver [61, 62]. In such a case, a test packet is only destroyed if

$$\frac{w_s}{w_n} \leq z \quad \text{during } t_w, \text{ with } n > 0, \quad (4.30)$$

where z is the capture ratio, and w_s and w_n are the test packet power and the joint interference power at the receiver's antenna, respectively. Values for z and the capture window t_w depend on the modulation and the coding employed by the network, among other things. For a typical narrowband FM receiver, a z value of 6 dB is suggested in [63]. The details about estimation of the values of z and t_w are beyond the scope of this application example.

Let the random variable Z be defined as the signal-to-interference ratio (SIR)

$$Z \triangleq \frac{W_s}{W_n}, \quad Z \geq 0 \quad (4.31)$$

where $W_s \geq 0$ and $W_n \geq 0$ are random variables representing the desired signal power and the interference power, respectively. Assuming that W_s and W_n are statistically independent, the resulting cumulative distribution function (CDF) can be expressed as [47]

$$\begin{aligned} F_Z(z_0|n) &= \text{Prob} \left\{ \frac{W_s}{W_n} \leq z_0|n \right\} \\ &= \int_0^{z_0} dz \int_0^\infty y f_{W_s}(zy) f_{W_n}(y) dy \end{aligned} \quad (4.32)$$

where $f_{W_s}(\cdot)$ and $f_{W_n}(\cdot)$ are the probability density functions (PDFs) of the desired signal power and the interference power, respectively.

If n is known and fixed, the conditional capture probability may be expressed as

$$P_{\text{capt}}(z_0|n) = 1 - F_Z(z_0|n). \quad (4.33)$$

Let the number of packets generated in the network for new messages plus retransmissions be Poisson distributed, with mean generation rate of λ packets per second. The mean offered traffic is then expressed as $G = p\lambda$ packets per transmission period. Given the transmission of an arbitrary test packet, the probability of it being overlap by n other packets is given by [47]

$$R_n = \frac{(G\tilde{\tau})^n}{n!} e^{-G\tilde{\tau}} \quad (4.34)$$

where τ is the worst case propagation delay and $\tilde{\tau} = \tau/p$ its normalised version. Finally, the

unconditional probability of a test packet being able to capture the receiver in an arbitrary transmission period may be expressed by

$$P_{capt}(z_0) = 1 - \sum_{n=1}^{\infty} R_n F_Z(z_0|n). \quad (4.35)$$

Channel Throughput

Let U , B and I be random variables representing, respectively, the duration of the successful transmission, the duration of the busy period and the duration of the idle period. Let $E\{U\}$, $E\{B\}$ and $E\{I\}$ be their respective expected values. Clearly, the channel throughput can be expressed by

$$S = \frac{E\{U\}}{E\{B\} + E\{I\}}. \quad (4.36)$$

For nonpersistent CSMA, Kleinrock and Tobagi have shown that [60]

$$E\{B\} = p + 2\tau - \frac{p}{G} (1 - e^{-G\tau}) \quad (4.37)$$

and

$$E\{I\} = \frac{p}{G}. \quad (4.38)$$

It can also be seen that

$$E\{U\} = p P_{capt}(z_0) \quad (4.39)$$

where $P_{capt}(\cdot)$ is the probability of receiver's capture and also it represents the probability of a successful transmission. Using the results of (4.37)-(4.39), the throughput can be written as

$$S = \frac{GP_{capt}(z_0)}{G(1 + 2\tau) + e^{-G\tau}} \quad (4.40)$$

Hoyt Fading Channel

The Hoyt fading model assumes that the received signal is the result of the sum of a large number of multipath scattered waves. Let x and y be two independent Gaussian processes with

zero mean and variances σ_x^2 and σ_y^2 , respectively. The PDF of the received signal envelope can be expressed as [17]

$$f_R(r) = \frac{r}{\sigma_x \sigma_y} \exp \left[-\frac{r^2}{4} \left(\frac{1}{\sigma_x^2} + \frac{1}{\sigma_y^2} \right) \right] I_0 \left[\frac{r^2}{4} \left(\frac{1}{\sigma_y^2} - \frac{1}{\sigma_x^2} \right) \right]. \quad (4.41)$$

Let $\eta \triangleq \sigma_x^2 / \sigma_y^2$ be defined as power ratio between the in-phase and quadrature signals. Also, let the parameters h and H be defined as

$$h \triangleq \frac{1}{4} \left(\frac{1}{\sqrt{\eta}} + \sqrt{\eta} \right)^2 \quad \text{and} \quad H \triangleq \frac{1}{4} \left(\frac{1}{\eta} - \eta \right). \quad (4.42)$$

In addition, note that $\hat{r}^2 \triangleq E\{r^2\} = \sigma_x^2 + \sigma_y^2$. Using the values above, the envelope PDF in (4.41) may be rewritten as

$$f_R(r) = 2\sqrt{h} \frac{r}{\hat{r}^2} \exp \left(-h \frac{r^2}{\hat{r}^2} \right) I_0 \left(H \frac{r^2}{\hat{r}^2} \right). \quad (4.43)$$

It is easy to see that if η is set to unity, thus making $h = 1$ and $H = 0$, (4.43) simplifies to the Rayleigh distribution with $\hat{r}^2 = 2\sigma_x^2 = 2\sigma_y^2$.

Let $w = r^2$ be the signal power and $\bar{w} = \hat{r}^2$ its average value. The signal power PDF may be expressed as

$$f_W(w) = \frac{\sqrt{h}}{\bar{w}} \exp \left(-h \frac{w}{\bar{w}} \right) I_0 \left(H \frac{w}{\bar{w}} \right). \quad (4.44)$$

Knowing that $\eta > 0$, it can be seen that the PDF in (4.44) is symmetrical around $\eta = 1$ [19]. Therefore, as far as the signal power distribution is concerned, considering either of the ranges $\eta \leq 1$ or $\eta \geq 1$ suffices.

Interference Signal

In a wireless system, interference typically results from (supposedly uncorrelated) signals arriving at the receiver's antenna from multiple transmitters. Depending on how these random signals combine during the observation interval, one of two scenarios might occur [1]: coherent addition or incoherent addition.

Coherent addition occurs if the carrier frequencies are equal and if the random phase fluctuations are small during the capture time t_w . For instance, coherent addition might happen when the deviation caused by the phase modulation is very small, and the observation interval is short compared to the modulation rate. Although the conditions for the coherent addition of signals to occur are difficult to meet, which makes it a rather unlikely scenario, the analysis are still presented here for the sake of completeness.

Let the phasor $x(t) = \text{Re}\{r(t) e^{j[w_c t + \theta(t)]}\}$ represent a signal reaching the receiver's antenna, where $r(t)$ and $\theta(t)$ are the random envelope and phase, respectively, and w_c is the carrier's angular frequency. For the coherent addition of n signals, the resulting phasor is [29]

$$x_n(t) = \sum_{i=1}^n x_i(t) \quad (4.45)$$

where the subscripts n and i represent the aggregate and individual variables, respectively.

Consider the Hoyt channel model described earlier, with its in-phase and quadrature Gaussian components. Since such channel is generated by the sum of Gaussian processes, further adding same-type phasors changes the parameters of the channel without changing its nature. In other words, the interference signal, assuming coherent addition, behaves as a Hoyt phasor, with the aggregate mean value equal to the sum of the individual mean values. If the n phasors are independent and identically distributed (i.i.d.), the resulting phasor has $\bar{w}_n = n\bar{w}_i$, $\sigma_{x,n}^2 = n\sigma_{x,i}^2$, $\sigma_{y,n}^2 = n\sigma_{y,i}^2$, and $\eta_n = \eta_i$.

Incoherent addition occurs if the phases of the individual signals fluctuate significantly due to mutually independent modulation [29, 64]. In this case, the interference power w_n experienced during the observation interval is the sum of the individual signals' powers w_i , i.e.,

$$w_n = \sum_{i=1}^n w_i = \sum_{i=1}^n \overline{x_i(t)x_i^*(t)} \quad (4.46)$$

where $x_i^*(\cdot)$ is the complex conjugate of phasor $x_i(\cdot)$. Considering the current work, where the signal power is a random variable, the PDF of the joint interference power is therefore the convolution of the PDFs of all contributing signal powers. If the individual components

Table 4.1: Relation between number of terms and accuracy in the summations of (4.47) and (4.51). For (4.47), only entries with $n = 1$ apply.

n	Parameters			smallest J for accuracy of			
	η_s	η_n	\tilde{z}_0	3-decimal-place	6-decimal-place		
1	0.1	0.1	0.1	5	10		
			1.0	13	30		
			5.0	18	44		
	0.9	1.0	5.0	0.9	13	26	
				1.0	19	44	
				1.0	1	3	
		0.1	5.0	0.9	2	3	
				1.0	1	3	
				5.0	1	4	
	10	0.1	0.1	1.0	10	17	
				5.0	21	38	
				1.0	10	16	
0.9			5.0	1.0	21	36	
				0.1	2	3	
				5.0	1	4	
0.9		0.1	5.0	1.0	2	3	
				1.0	2	3	
				5.0	1	4	
		50	0.1	0.1	5.0	21	32
					0.9	21	31
					5.0	1	3
0.9	0.1		5.0	0.9	1	3	
				5.0	1	4	
				5.0	1	4	

are i.i.d., then the interference power is expressed as the n -fold convolution of the PDF of the individual signal power.

4.2.3 Results

For the calculations presented in this section, let (4.44) represent the desired signal power PDF as well as, with different parameters, the signal power PDF of an individual component of the interference signal. Also, for the remaining of this application example and wherever applicable, the subscripts s , i and n are used to represent the desired signal variables, the interference signal's individual component variables, and the joint interference signal variables, respectively. Finally, let \tilde{z}_0 be defined as $\tilde{z}_0 \triangleq z_0/(\bar{w}_s/\bar{w}_n)$ where the ratio \bar{w}_s/\bar{w}_n is commonly denoted as average SIR.

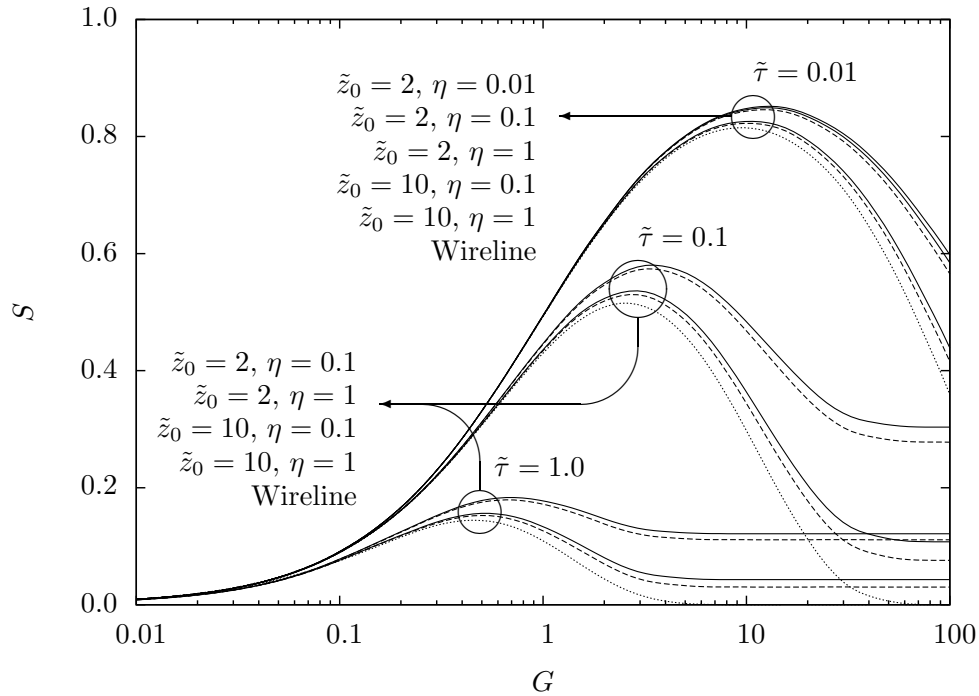


Figure 4.6: Throughput S for coherent Hoyt channel with $\eta = \eta_s = \eta_n$. The dashed lines correspond to the Rayleigh channel. The dotted lines correspond to the original (wireline) channel.

Coherent Addition

If coherent addition of phasors is assumed, then (4.44) should be used to represent the joint interference signal power PDF. Using the appropriated expressions in (4.32), and after some manipulation, the signal-to-interference CDF may be expressed as

$$\begin{aligned}
 F_Z(\tilde{z}_0|n) = & 1 - \frac{v_1}{\sqrt{\pi}\sqrt{h_s h_n}} \sum_{j=0}^{\infty} (1 - v_1)^j {}_2F_1 \left[\frac{j+1}{2}, \frac{j}{2} + 1, 1, \left(v_1 \frac{H_n}{h_n} \right)^2 \right] \\
 & \times \left(\frac{H_s^2}{h_s^2} \right)^{\lceil \frac{j}{2} \rceil} \frac{\Gamma(\lceil \frac{j}{2} \rceil + \frac{1}{2})}{\Gamma(\lceil \frac{j}{2} \rceil + 1)} {}_2F_1 \left[1, \lceil \frac{j}{2} \rceil + \frac{1}{2}, \lceil \frac{j}{2} \rceil + 1, \left(\frac{H_s}{h_s} \right)^2 \right]
 \end{aligned} \tag{4.47}$$

where $\Gamma(\cdot)$ is the gamma function [21, Eq. 6.1.1], ${}_2F_1(\cdot)$ is the Gauss hypergeometric function [21, Eq. 15.1.1], $\lceil \cdot \rceil$ is the ceiling function (defined as $\lceil x \rceil = n$, with $x \in \mathbb{R}$ and n is the smallest integer such that $x \leq n$), and

$$v_1 = \frac{h_n}{h_n + h_s \tilde{z}_0}. \tag{4.48}$$

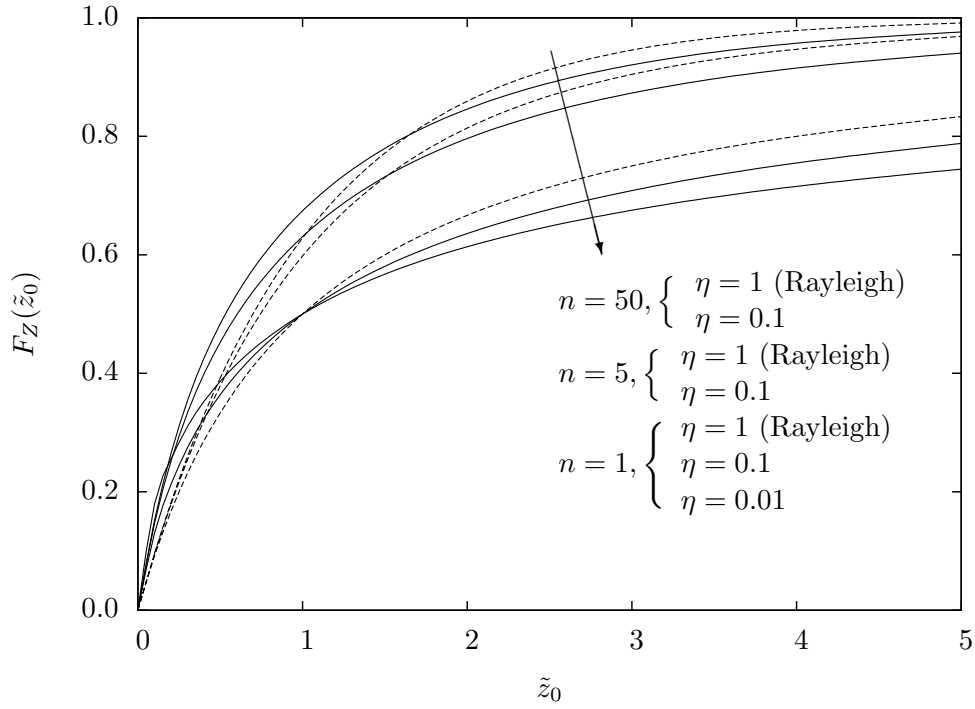


Figure 4.7: CDFs of (4.47) and (4.51) with $\eta = \eta_s = \eta_n$. For (4.47) only curves with $n = 1$ apply. The dashed lines correspond to the Rayleigh channel.

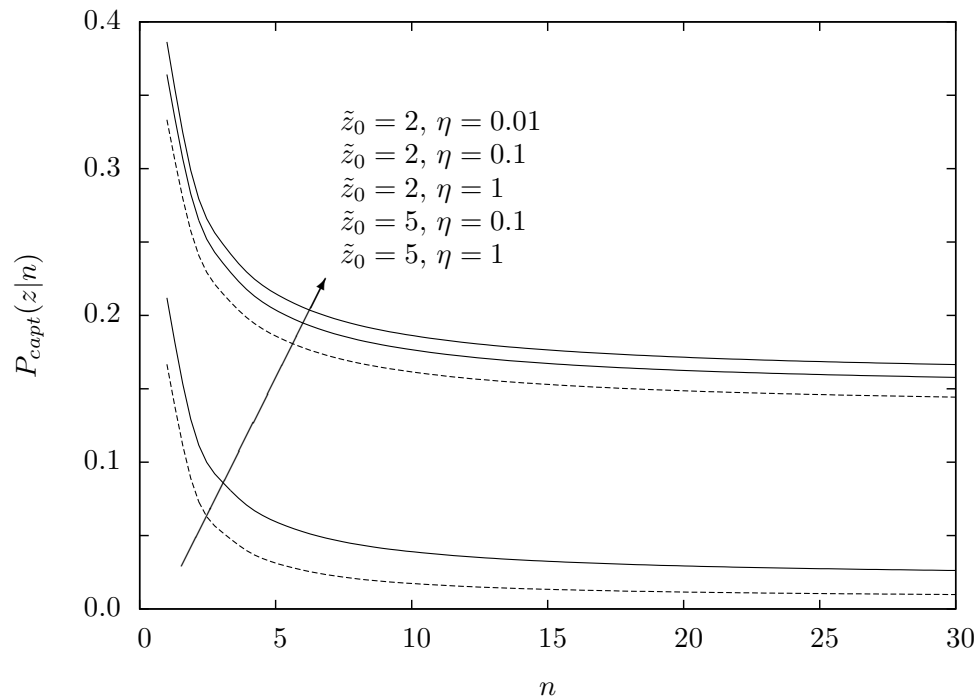


Figure 4.8: Conditional capture probability for incoherent Hoyt channel with $\eta = \eta_s = \eta_n$. The dashed lines correspond to the Rayleigh channel.

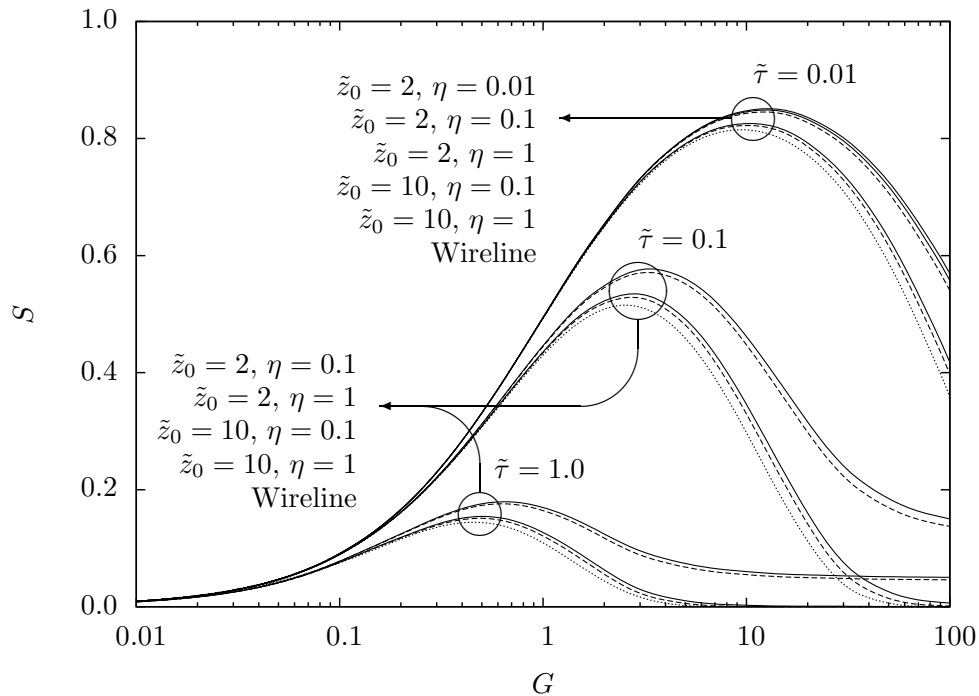


Figure 4.9: Throughput S for incoherent Hoyt channel with $\eta = \eta_s = \eta_n$. The dashed lines correspond to the Rayleigh channel. The dotted lines correspond to the original (wireline) channel.

It is interesting to note that (4.47) does not depend directly on the value of n . In other words, the statistics of the joint interference signal can be described using only the parameters η_n and \bar{w}_n , which is expected since this signal follows the Hoyt distribution.

Note also that if both η_s and η_n are set to unity in (4.47), the CDF simplifies to the Rayleigh channel model and it can be expressed as

$$F_Z(\tilde{z}_0|n) = \frac{\tilde{z}_0}{1 + \tilde{z}_0}. \quad (4.49)$$

If the result above is further simplified by assuming that $\bar{w}_s = \bar{w}_i = \bar{w}_n/n$, then the same expression presented in [29] is produced.

Although (4.47) includes an infinite summation, the evaluation of the CDF converges rapidly for most cases of interest. Let J be defined as the maximum value for the index variable j in a truncated summation, i.e., $0 \leq j \leq J$. The entries for $n = 1$ in Table 4.1 give the value of J necessary to obtain a three-decimal-place accuracy (error < 0.0005) and a six-decimal-place accuracy (error < 0.0000005) for the summation of (4.47).

With the results obtained so far, using (4.35), (4.40) and (4.47), it is possible to calculate the channel throughput, which is presented in Fig. 4.6. Assuming that $\eta = \eta_s = \eta_n$ and that the n interfering signals are i.i.d., the curves for $n = 1$ in Fig. 4.7 illustrate the CDF of (4.47).

Incoherent Addition

For the incoherent addition, assume that the interference signal is composed of n i.i.d. variables. As a result, the joint interference signal power PDF is the n -fold convolution of the individual signal power PDF which, on its turn, is expressed by (4.44). This calculation gives that

$$f_{W_n}(w_n) = \frac{\sqrt{n\pi} (nh_n)^{\frac{n}{2}}}{\Gamma(\frac{n}{2}) \bar{w}_n} \left(\frac{w_n}{2H_n \bar{w}_n} \right)^{\frac{n-1}{2}} \exp\left(-nh_n \frac{w_n}{\bar{w}_n}\right) I_{\frac{n-1}{2}}\left(nH_n \frac{w_n}{\bar{w}_n}\right) \quad (4.50)$$

where $\bar{w}_n = n\bar{w}_i$, $h_n = h_i$ and $H_n = H_i$. It can be seen that the n -fold convolution used to obtain (4.50) produced the $\eta - \mu$ distribution presented in [19].

Using the appropriated expressions in (4.32), and after some manipulation, the signal-to-interference CDF may be expressed as

$$\begin{aligned} F_Z(\tilde{z}_0|n) &= 1 - \frac{v_n^n}{\sqrt{\pi} \sqrt{h_s h_n^n}} \sum_{j=0}^{\infty} \frac{(1-v_n)^j}{(j+n)B(j+1, n)} \\ &\times {}_2F_1\left[\frac{j+n}{2}, \frac{j+n+1}{2}, \frac{n+1}{2}, \left(v_n \frac{H_n}{h_n}\right)^2\right] \\ &\times \left(\frac{H_s^2}{h_s^2}\right)^{\lceil \frac{j}{2} \rceil} \frac{\Gamma(\lceil \frac{j}{2} \rceil + \frac{1}{2})}{\Gamma(\lceil \frac{j}{2} \rceil + 1)} {}_2F_1\left[1, \lceil \frac{j}{2} \rceil + \frac{1}{2}, \lceil \frac{j}{2} \rceil + 1, \left(\frac{H_s}{h_s}\right)^2\right] \end{aligned} \quad (4.51)$$

where

$$v_n = \frac{nh_n}{nh_n + h_s \tilde{z}_0} \quad (4.52)$$

with $\bar{w}_n = n\bar{w}_i$, $\eta_n = \eta_i$, $h_n = h_i$ and $H_n = H_i$ since the n interfering signals are i.i.d.. It is interesting to note that if n is set to unity in (4.51), the CDF simplifies to the coherent addition case of (4.47).

Although (4.51) includes an infinite summation, the evaluation of the CDF converges rapidly for most cases of interest. Let J be the maximum value of the index variable j (as defined

earlier). Table 4.1 gives the value of J necessary to obtain a three-decimal-place accuracy (error < 0.0005) and a six-decimal-place accuracy (error < 0.0000005) for the summation of (4.47).

Fig. 4.7 depicts the CDF of (4.51) for $\eta = \eta_s = \eta_n$ and various values of n . With the results obtained so far, using (4.35), (4.40) and (4.51), it is now possible to calculate the capture probability and the channel throughput, which are presented in Figs. 4.8 and 4.9, respectively.

4.2.4 Conclusion

This application example investigates the throughput performance of CSMA in a packet radio network and Hoyt fading environment. Analytical and numerical results are presented considering the signal capture model with coherent and incoherent addition of interfering signals.

Fig. 4.7 presents the CDF of the capture threshold z_0 for incoherent addition of signals and, if $n = 1$, coherent addition of signals as well. It can be seen that for values of η closer to unity, the distribution shows a somewhat smaller variance. This is indicated by the steeper climb from zero that these curves exhibit. A similar, although stronger, effect can also be seen for higher values of n .

The throughput graphics clearly indicate the important role the normalised worst case propagation delay $\tilde{\tau}$ plays to determine the channel throughput. Also, the higher the capture threshold is, the closer the curve is to the original (wireline) results, which is expected since it indicates a diminished ability of receiver detection of the intended signal among the interfering signals. When compared to the Rayleigh channel, Hoyt results show only minor differences in the throughput performance, with lower values of η producing slightly higher throughput. Larger differences in throughput figures can be seen when results are compared against those obtained for the original (wireline) channel.

4.3 Throughput of CSMA in Rice Fading Channels³

4.3.1 Introduction

Wireless local area networks (WLANs) are experiencing rapid development in part stimulated by the deployment of systems compatible to the IEEE 802.11 standards. They offer data communication between terminals within radio range while allowing a certain degree of mobility.

In order to serve terminals exhibiting bursty traffic behaviour, WLANs make use of packet radio techniques with random access to a transmission channel shared by multiple users. Specifically, variations of carrier sense multiple access (CSMA) is generally used to access the wireless medium [54, 55, 56, 57]. The capacity of the channel is then influenced by the probability of packet collision and by the signal degradation due to mutual interference and signal attenuation. In other words, it is influenced by the medium contention resolution algorithm and by the channel characteristics.

Intuitively one might expect that original (wireline) CSMA systems show better system performance than wireless systems because of more hostile channel characteristics found in the latter. However, this is not necessarily the case. For instance, in a channel model that takes into account the effects of fading, competing packets arriving at a common radio receiver antenna will not always destroy each other because they may show different and independent fading and attenuation levels [58, 59]. This leads to expect that wireless systems may actually exhibit successful reception rate higher than that of original (wireline) systems. In fact, Arnbak and Blitterswijk have shown this to happen with slotted Aloha over Rayleigh fading channels [29].

In this application example, we investigate the throughput performance of CSMA in a packet radio network with Rice fading environment. The performance of the original (wireline) CSMA is presented in [60] and is here extended to this fading scenario. The Rice fading environment is relevant to model a situation where the random multipath signals are superimposed on a nonfading dominant signal, for instance, when a line-of-sight (LOS) component is present [2].

This application example is organized as follows. Section 4.3.2 describes the analytical model

³This material was presented at [68].

and considers the cases of coherent and incoherent packet addition at the receiver's antenna. Section 4.3.3 presents the results obtained. Comments and conclusions are given in Section 4.3.4.

4.3.2 Analytical Model

Nonpersistent CSMA

For nonpersisting CSMA, a terminal ready to transmit first senses the channel. If it senses the channel idle, it transmits the packet. Otherwise, it schedules the (re)transmission of the packet to a later time according to some randomly distributed retransmission delay. After the retransmission delay has elapsed, the terminal repeats the procedure described above. In this application example, the channel is considered to be memoryless, i.e., failures to capture the channel and future attempts are uncorrelated. In addition, all packets are assumed to have fixed length and to require p seconds to transmit. Finally, each packet is assumed to have a single destination.

Probability of Capture

Given the transmission of an arbitrary test packet over a wireline channel, it is generally assumed that a successful reception can only occur if no other transmission attempt is made during the test packet reception, i.e., if there is no signal overlap at the receiver. However, in wireless systems the radio receiver may be able to be captured by a test packet, even in the presence of n interfering packets, provided the power ratio between the test signal and the joint interfering signal exceeds a certain threshold during a given portion of the transmission period t_w , $0 < t_w < p$, to lock the receiver [61, 62]. In such a case, a test packet is only destroyed if

$$\frac{w_s}{w_n} \leq z \quad \text{during } t_w, \text{ with } n > 0, \quad (4.53)$$

where z is the capture ratio, and w_s and w_n are the test packet power and the joint interference power at the receiver's antenna, respectively. Values for z and the capture window t_w depend

on the modulation and the coding employed by the network, among other things. For a typical narrowband FM receiver, a z value of 6 dB is suggested in [63]. The details about estimation of the values of z and t_w are beyond the scope of this application example.

Let the random variable Z be defined as the signal-to-interference ratio (SIR)

$$Z \triangleq \frac{W_s}{W_n}, \quad Z \geq 0 \quad (4.54)$$

where $W_s \geq 0$ and $W_n \geq 0$ are random variables representing the desired signal power and the interference power, respectively. Assuming that W_s and W_n are statistically independent, the resulting cumulative distribution function (CDF) can be expressed as [47]

$$\begin{aligned} F_Z(z_0) &= \text{Prob} \left\{ \frac{W_s}{W_n} \leq z_0 \right\} \\ &= \int_0^{z_0} dz \int_0^\infty y f_{W_s}(zy) f_{W_n}(y) dy \end{aligned} \quad (4.55)$$

where $f_{W_s}(\cdot)$ and $f_{W_n}(\cdot)$ are the probability density functions (PDFs) of the desired signal power and the interference power, respectively.

Let the number of packets generated in the network for new messages plus retransmissions be Poisson distributed, with mean generation rate of λ packets per second. The mean offered traffic is then expressed as $G = p\lambda$ packets per transmission period. Given the transmission of an arbitrary test packet, the probability of it being overlap by n other packets is given by [47]

$$R_n = \frac{(G\tilde{\tau})^n}{n!} e^{-G\tilde{\tau}} \quad (4.56)$$

where τ is the worst case propagation delay and $\tilde{\tau} = \tau/p$ its normalised version. Finally, the unconditional probability of a test packet being able to capture the receiver in an arbitrary transmission period may be expressed by

$$P_{capt}(z_0) = 1 - \sum_{n=1}^{\infty} R_n F_Z(z_0). \quad (4.57)$$

Channel Throughput

Let U , B and I be random variables representing, respectively, the duration of the successful transmission, the duration of the busy period and the duration of the idle period. Let $E\{U\}$, $E\{B\}$ and $E\{I\}$ be their respective expected values. Clearly, the channel throughput can be expressed by

$$S = \frac{E\{U\}}{E\{B\} + E\{I\}}. \quad (4.58)$$

For nonpersistent CSMA, Kleinrock and Tobagi have shown that [60]

$$E\{B\} = p + 2\tau - \frac{p}{G} (1 - e^{-G\bar{\tau}}) \quad (4.59)$$

and

$$E\{I\} = \frac{p}{G}. \quad (4.60)$$

It can also be seen that

$$E\{U\} = p P_{capt}(z_0) \quad (4.61)$$

where $P_{capt}(\cdot)$ is the probability of receiver's capture and also it represents the probability of a successful transmission. Using the results of (4.59)-(4.61), the throughput can be written as

$$S = \frac{GP_{capt}(z_0)}{G(1 + 2\bar{\tau}) + e^{-G\bar{\tau}}} \quad (4.62)$$

Rice Fading Channel

The Rice fading model assumes that the received signal is the result of a dominant component added to a large number of multipath scattered waves. Let x and y be two independent Gaussian processes with zero mean and variances σ_x^2 and σ_y^2 , respectively. The in-phase and quadrature components of the signal envelope in a Rice fading channel can be expressed as $x + a$ and y , respectively, where the constant a represents the envelope of the LOS signal (also, the mean value for the in-phase component). Assuming that $\sigma^2 \triangleq \sigma_x^2 = \sigma_y^2$, the PDF of the received signal

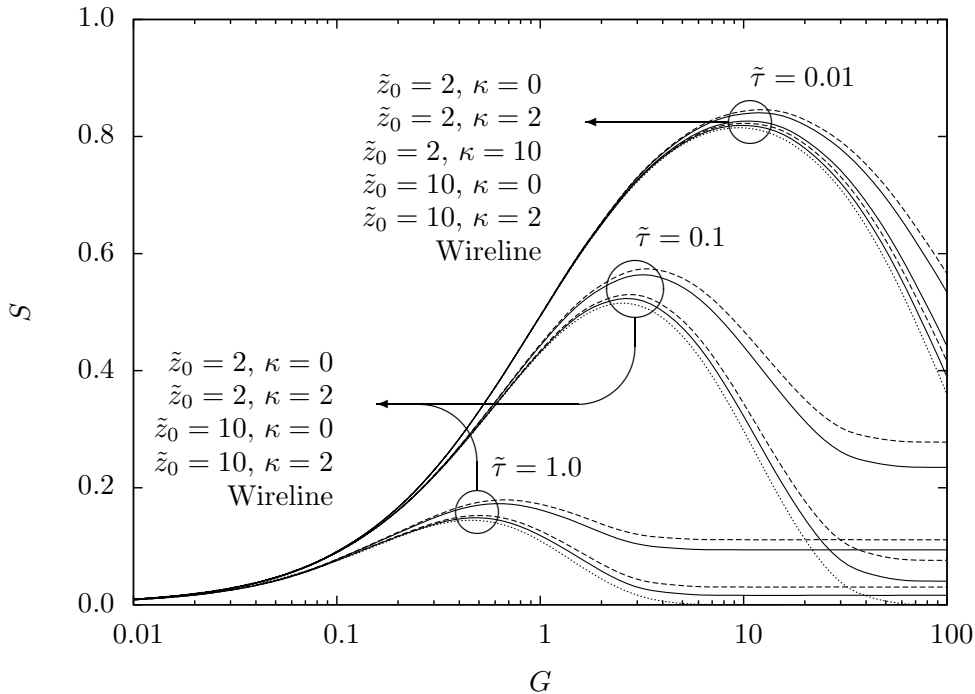


Figure 4.10: Throughput S for coherent Rice channel with $\kappa = \kappa_s = \kappa_n$. The dashed lines correspond to the Rayleigh channel. The dotted lines correspond to the original (wireline) channel.

envelope r can be expressed as [2]

$$f_R(r) = \frac{r}{\sigma^2} \exp\left(-\frac{r^2 + a^2}{2\sigma^2}\right) I_0\left(\frac{ar}{\sigma^2}\right) \quad (4.63)$$

where $I_\nu(\cdot)$ is the modified Bessel function of the first kind and ν -th order [21, Eq. 9.6.10].

Let $\kappa \triangleq a^2/(2\sigma^2)$ be defined as power ratio between the LOS and scattered signals. Also, note that $\hat{r}^2 \triangleq E\{r^2\} = a^2 + 2\sigma^2 = 2\sigma^2(\kappa + 1)$, where $E\{\cdot\}$ represents expected value. Using the values above, the envelope PDF in (4.63) may be rewritten as

$$f_R(r) = \frac{2(\kappa + 1)}{e^\kappa} \frac{r}{\hat{r}^2} \exp\left(-(\kappa + 1)\frac{r^2}{\hat{r}^2}\right) I_0\left(2\sqrt{\kappa(\kappa + 1)}\frac{r}{\hat{r}}\right). \quad (4.64)$$

It is easy to see that if κ is set to zero, thus eliminating the LOS component, (4.64) simplifies to the Rayleigh distribution with $\hat{r}^2 = 2\sigma^2$.

Let $w = r^2$ be the signal power and $\bar{w} = \hat{r}^2$ its average value. The signal power PDF may

be expressed as

$$f_W(w) = \frac{\kappa + 1}{\bar{w} e^\kappa} \exp\left(-(\kappa + 1)\frac{w}{\bar{w}}\right) I_0\left(2\sqrt{\kappa(\kappa + 1)}\frac{w}{\bar{w}}\right). \quad (4.65)$$

Interference Signal

In a wireless system, interference typically results from (supposedly uncorrelated) signals arriving at the receiver's antenna from multiple transmitters. Depending on how these random signals combine during the observation interval, one of two scenarios might occur [1]: coherent addition or incoherent addition.

Coherent addition occurs if the carrier frequencies are equal and if the random phase fluctuations are small during the capture time t_w . For instance, coherent addition might happen when the deviation caused by the phase modulation is very small, and the observation interval is short compared to the modulation rate. Although the conditions for the coherent addition of signals to occur are difficult to meet, which makes it a rather unlikely scenario, the analysis are still presented here for the sake of completeness.

Let the phasor $x(t) = \text{Re}\{r(t) e^{j[w_c t + \theta(t)]}\}$ represent a signal reaching the receiver's antenna, where $r(t)$ and $\theta(t)$ are the random envelope and phase, respectively, and w_c is the carrier's angular frequency. For the coherent addition of n signals, the resulting phasor is [29]

$$x_n(t) = \sum_{i=1}^n x_i(t) \quad (4.66)$$

where the subscripts n and i represent the aggregate and individual variables, respectively.

Consider the Rice channel model described earlier, with its in-phase and quadrature Gaussian components. Since such channel is generated by the sum of Gaussian processes, further adding same-type phasors changes the parameters of the channel without changing its nature. In other words, the interference signal, assuming coherent addition, behaves as a Rice phasor, with the aggregate mean value equal to the sum of the individual mean values. As a result, the coherent addition of n uncorrelated Rice phasors produces a Rice phasor with mean value $\bar{w}_n = \sum_{i=1}^n \bar{w}_i$, LOS signal power $a_n^2 = \sum_{i=1}^n a_i^2$, and scattered signal power $\sigma_n^2 = \sum_{i=1}^n \sigma_i^2$. If the n phasors are independent and identically distributed (i.i.d.), the resulting phasor has $\bar{w}_n = n\bar{w}_i$, $a_n^2 = na_i^2$,

$\sigma_n^2 = n\sigma_i^2$, and $\kappa_n = \kappa_i$.

Incoherent addition occurs if the phases of the individual signals fluctuate significantly due to mutually independent modulation [29, 64]. In this case, the interference power w_n experienced during the observation interval is the sum of the individual signals' powers w_i , i.e.,

$$w_n = \sum_{i=1}^n w_i = \sum_{i=1}^n \overline{x_i(t)x_i^*(t)} \quad (4.67)$$

where $x_i^*(\cdot)$ is the complex conjugate of phasor $x_i(\cdot)$. Considering the current work, where the signal power is a random variable, the PDF of the joint interference power is therefore the convolution of the PDFs of all contributing signal powers. If the individual components are i.i.d., then the interference power is expressed as the n -fold convolution of the PDF of the individual signal power.

4.3.3 Results

For the calculations presented in this section, let (4.65) represent the desired signal power PDF as well as, with different parameters, the signal power PDF of an individual component of the interference signal. Also, for the remaining of this application example and wherever applicable, the subscripts s , i and n are used to represent the desired signal variables, the interference signal's individual component variables, and the joint interference signal variables, respectively. Finally, let \tilde{z}_0 be defined as $\tilde{z}_0 \triangleq z_0/(\bar{w}_s/\bar{w}_n)$ where the ratio \bar{w}_s/\bar{w}_n is commonly denoted as average SIR.

Coherent Addition

If coherent addition of phasors is assumed, then (4.65) should be used to represent the joint interference signal power PDF. Using the appropriated expressions in (4.55), and after some manipulation, the signal-to-interference CDF may be expressed as

$$F_Z(\tilde{z}_0) = \frac{u_1}{e^{\kappa_n}} \sum_{j=0}^{\infty} (1 - u_1)^j Q(j, \kappa_s) {}_1F_1(j + 1, 1, \kappa_n u_1) \quad (4.68)$$

Table 4.2: Relation between number of terms and accuracy in the infinite summation of (4.72).

Parameters				smallest J for accuracy of	
n	κ_s	κ_n	\tilde{z}_0	3-decimal-place	6-decimal-place
1	0.01	0.01	0.1	2	2
			1.0	2	3
			5.0	2	3
		1.0	1.0	2	2
		10.0	1.0	1	2
	1.0	0.01	1.0	5	8
		1.0	1.0	3	5
		10.0	1.0	2	4
	10.0	0.01	1.0	18	26
		1.0	1.0	10	16
		10.0	1.0	4	7
	10	0.01	0.01	1.0	1
1.0			1.0	2	3
10.0			1.0	2	3
1.0		0.01	1.0	0	8
		1.0	1.0	5	8
		10.0	1.0	4	5
10.0		0.01	1.0	0	19
		1.0	1.0	19	24
		10.0	1.0	9	13
50	0.01	1.0	1.0	1	3
		10.0	1.0	2	3
	1.0	1.0	1.0	5	9
		10.0	1.0	5	7
	10.0	1.0	1.0	0	0
		10.0	1.0	18	23

where ${}_1F_1(\cdot)$ is the Kummer confluent hypergeometric function [21, Eq. 13.1.2], $Q(\cdot)$ is the regularized incomplete gamma function defined as $Q(a, b) = \Gamma(a, b)/\Gamma(a)$, $\Gamma(\cdot)$ is the gamma function [21, Eq. 6.1.1], $\Gamma(\cdot, \cdot)$ is the incomplete gamma function [21, Eq. 6.5.3], and

$$u_1 = \frac{(\kappa_n + 1)}{(\kappa_n + 1) + (\kappa_s + 1) \tilde{z}_0}. \quad (4.69)$$

It is interesting to note that (4.68) does not depend directly on the value of n . In other words, the statistics of the joint interference signal can be described using only the parameters κ_n and \bar{w}_n , which is expected since this signal follows the Rice distribution.

If both κ_s and κ_n are set to zero in (4.68), the CDF simplifies to the Rayleigh channel model and it can be expressed as

$$F_Z(\tilde{z}_0) = \frac{\tilde{z}_0}{1 + \tilde{z}_0}. \quad (4.70)$$

If the result above is further simplified by assuming that $\bar{w}_s = \bar{w}_i = \bar{w}_n/n$, then the same expression presented in [29] is produced.

Although (4.68) includes an infinite summation, the evaluation of the CDF converges rapidly for most cases of interest. Let J be defined as the maximum value for the index variable j in a truncated summation, i.e., $1 \leq j \leq J$. The entries for $n = 1$ in Tb. 4.2 give the value J necessary to obtain a three-decimal-place accuracy (error < 0.0005) and a six-decimal-place accuracy (error < 0.0000005) for the infinite summation of (4.68).

With the results obtained so far, using (4.57), (4.62) and (4.68), it is possible to calculate the channel throughput, which is presented in Fig. 4.10. Assuming that $\kappa = \kappa_s = \kappa_n$ and that the n interfering signals are i.i.d., the curves for $n = 1$ in Fig. 4.11 illustrate the CDF of (4.68).

Incoherent Addition

For the incoherent addition, assume that the interference signal is composed of n i.i.d. variables. As a result, the joint interference signal power PDF is the n -fold convolution of the individual signal power PDF which, on its turn, is expressed by (4.65). This calculation gives

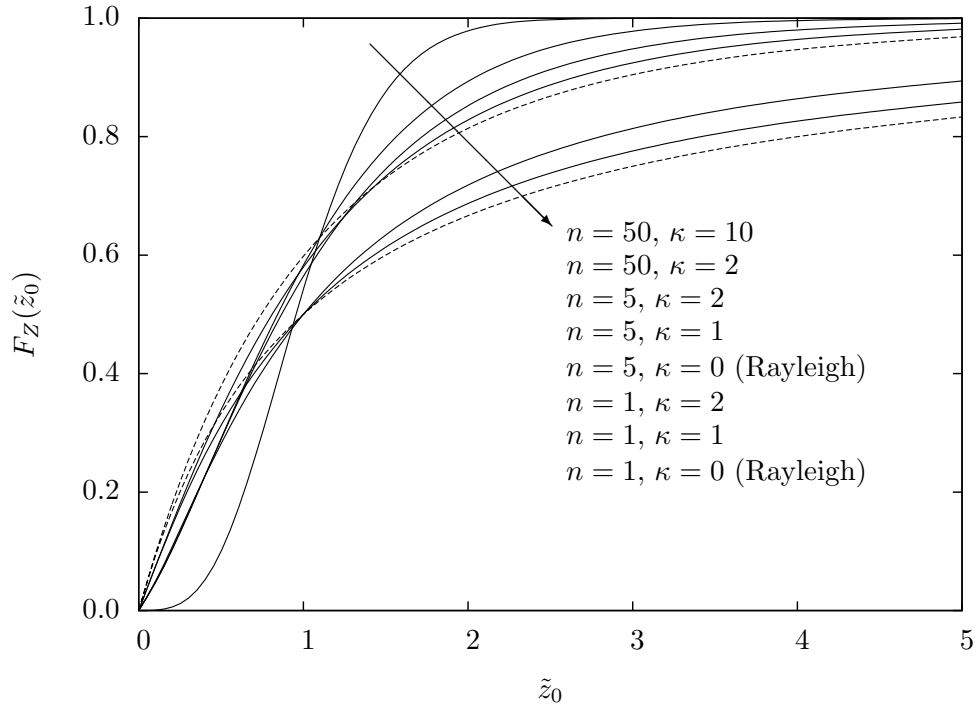


Figure 4.11: CDF of (4.72) with $\kappa = \kappa_s = \kappa_n$. The dashed lines correspond to the Rayleigh channel.

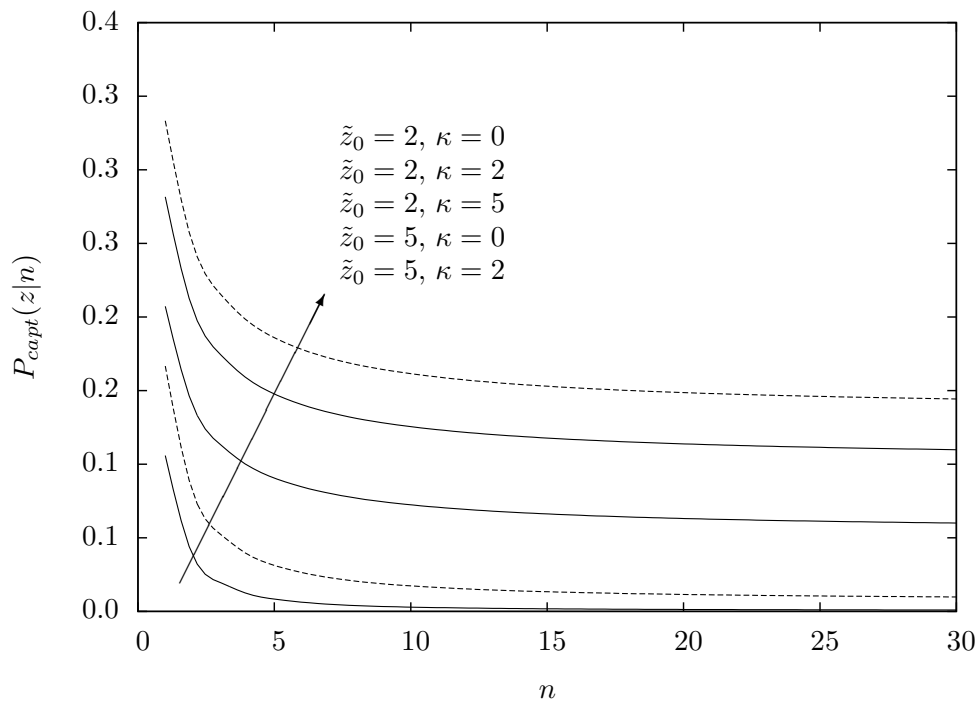


Figure 4.12: Conditional capture probability for incoherent Rice channel with $\kappa = \kappa_s = \kappa_n$. The dashed lines correspond to the Rayleigh channel.

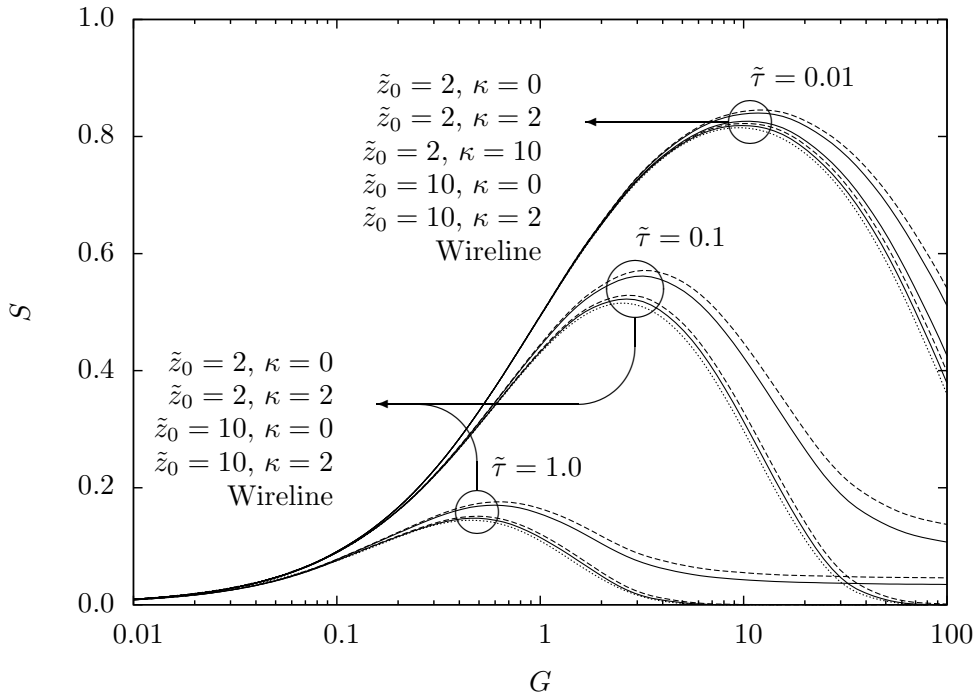


Figure 4.13: Throughput S for incoherent Rice channel with $\kappa = \kappa_s = \kappa_n$. The dashed lines correspond to the Rayleigh channel. The dotted lines correspond to the original (wireline) channel.

that

$$f_{W_n}(w_n) = \frac{n}{e^{n\kappa_n}} \left(\frac{\kappa_n + 1}{\bar{w}_n} \right)^{\frac{n+1}{2}} \left(\frac{w_n}{\kappa_n} \right)^{\frac{n-1}{2}} \exp \left(-n(\kappa_n + 1) \frac{w_n}{\bar{w}_n} \right) \times I_{n-1} \left(2n \sqrt{\kappa_n(\kappa_n + 1)} \frac{w_n}{\bar{w}_n} \right) \quad (4.71)$$

where $\bar{w}_n = n\bar{w}_i$, and $\kappa_n = \kappa_i$. It can be seen that the n -fold convolution used to obtain (4.71) produced the $\kappa - \mu$ distribution presented in [19].

Using the appropriated expressions in (4.55), and after some manipulation, the signal-to-interference CDF may be expressed as

$$F_Z(\tilde{z}_0) = \frac{u_n^n}{e^{n\kappa_n}} \sum_{j=0}^{\infty} \frac{(1-u_n)^j Q(j, \kappa_s)}{(j+n)B(j+1, n)} {}_1F_1(j+n, n, n\kappa_n u_n) \quad (4.72)$$

where $B(\cdot)$ is the beta function [21, Eq. 6.2.2], and

$$u_n = \frac{n(\kappa_n + 1)}{n(\kappa_n + 1) + (\kappa_s + 1)\tilde{z}_0}, \quad (4.73)$$

with $\bar{w}_n = n\bar{w}_i$ and $\kappa_n = \kappa_i$ since the n interfering signals are i.i.d.. If both κ_s and κ_n are set to zero in (4.72), the CDF simplifies to the Rayleigh channel model and it can be expressed as

$$F_Z(\tilde{z}_0) = 1 - \left(\frac{n}{n + \tilde{z}_0} \right)^n. \quad (4.74)$$

If the result above is further simplified by assuming that $\bar{w}_s = \bar{w}_i = \bar{w}_n/n$, then the same expression presented in [29] is found. Also, it is interesting to note that if n is set to unity in (4.72) or (4.74), the corresponding CDF simplifies to the coherent addition cases.

Although (4.72) includes an infinite summation, the evaluation of the CDF converges rapidly for most cases of interest. Let J be the maximum value of the index variable j (as defined earlier). Tb. 4.2 gives the value of J necessary to obtain a three-decimal-place accuracy (error < 0.0005) and a six-decimal-place accuracy (error < 0.0000005) for the infinite summation of (4.72).

Fig. 4.11 depicts the CDF of (4.72) for $\kappa = \kappa_s = \kappa_n$ and various values of n . With the results obtained so far, using (4.57), (4.62) and (4.72), it is now possible to calculate the capture probability and the channel throughput, which are presented in Figs. 4.12 and 4.13, respectively.

4.3.4 Conclusion

This application example investigates the throughput performance of CSMA in a packet radio network and Rice fading environment. Analytical and numerical results are presented considering the signal capture model with coherent and incoherent addition of interfering signals.

Fig. 4.11 presents the CDF of the capture threshold z_0 for incoherent addition of signals and, if $n = 1$, coherent addition of signals as well. First, it can be seen that larger values of κ concentrates the random outcomes around $\tilde{z}_0 = 1$. This is indicated by the sharp increase of the CDF around this value and it is an expected result since larger values of κ mean that the deterministic LOS component dominates over the random Gaussian components. In addition, larger values of n tend to produce a distribution with lower variance. This is indicated by the steeper climb from zero that curves with larger n experience.

The throughput graphics clearly indicate the important role the normalised worst case propagation delay $\tilde{\tau}$ plays to determine the channel throughput. Also, the higher the capture threshold

is, the closer the curve is to the original (wireline) results, which is expected since it indicates a diminished ability of receiver detection of the intended signal among the interfering signals.

Compared to the Rayleigh channel results, higher values of κ in Rice channels produce slightly lower throughput. The reason behind it might be that higher values of κ increase the dominance of the deterministic components. However, when compared to the Rayleigh channel, Rice results show only minor differences in the throughput performance.

4.4 Throughput of CSMA in η - μ Fading Channels⁴

4.4.1 Introduction

Wireless local area networks (WLANs) are experiencing rapid development in part stimulated by the deployment of systems compatible to the IEEE 802.11 standards. They offer data communication between terminals within radio range while allowing a certain degree of mobility.

In order to serve terminals exhibiting bursty traffic behaviour, WLANs make use of packet radio techniques with random access to a transmission channel shared by multiple users. Specifically, variations of carrier sense multiple access (CSMA) is generally used to access the wireless medium [54, 55, 56, 57]. The capacity of the channel is then influenced by the probability of packet collision and by the signal degradation due to mutual interference and signal attenuation. In other words, it is influenced by the medium contention resolution algorithm and by the channel characteristics.

Intuitively one might expect that original (wireline) CSMA systems show better system performance than wireless systems because of more hostile channel characteristics found in the latter. However, this is not necessarily the case. For instance, in a channel model that takes into account the effects of fading, competing packets arriving at a common radio receiver antenna will not always destroy each other because they may show different and independent fading and attenuation levels [58, 59]. This leads to expect that wireless systems may actually exhibit successful reception rate higher than that of original (wireline) systems. In fact, Arnbak and

⁴This material was presented at [69].

Blitterswijk have shown this to happen with slotted Aloha over Rayleigh fading channels [29].

In this application example, we investigate the throughput performance of CSMA in a packet radio network with η - μ fading environment. The performance of the original (wireline) CSMA is presented in [60] and is here extended to this fading scenario. The η - μ fading environment is a general fading model that can be used to better represent the small-scale variation of the fading signal in a non-line-of-sight condition [19]. The distribution has the Hoyt (Nakagami- q), the Nakagami- m , the Rayleigh, and the One-Sided Gaussian distributions as special cases. As an intermediate outcome of the calculation, results for the outage probability for this environment is also presented. Analysis of the outage probability for fading channels has been an active investigation topic for the last few years [70, 71, 72, 35, 73, 74], in part because it may be used to estimate performance of spectrum sharing systems. The work presented here offers contributions in this area and introduces some original results.

This application example is organized as follows. Section 4.4.2 describes the analytical model and considers the incoherent packet addition at the receiver's antenna. Section 4.4.3 presents the results obtained. Comments and conclusions are given in Section 4.4.4.

4.4.2 Analytical Model

Nonpersistent CSMA

For nonpersisting CSMA, a terminal ready to transmit first senses the channel. If it senses the channel idle, it transmits the packet. Otherwise, it schedules the (re)transmission of the packet to a later time according to some randomly distributed retransmission delay. After the retransmission delay has elapsed, the terminal repeats the procedure described above. In this application example, the channel is considered to be memoryless, i.e., failures to capture the channel and future attempts are uncorrelated. In addition, all packets are assumed to have fixed length and to require p seconds to transmit. Finally, each packet is assumed to have a single destination.

Probability of Capture

Given the transmission of an arbitrary test packet over a wireline channel, it is generally assumed that a successful reception can only occur if no other transmission attempt is made during the test packet reception, i.e., if there is no signal overlap at the receiver. However, in wireless systems the radio receiver may be able to be captured by a test packet, even in the presence of n interfering packets, provided the power ratio between the test signal and the joint interfering signal exceeds a certain threshold during a given portion of the transmission period t_w , $0 < t_w < p$, to lock the receiver [61, 62]. In such a case, a test packet is only destroyed if

$$\frac{w_s}{w_n} \leq z \quad \text{during } t_w, \text{ with } n > 0, \quad (4.75)$$

where z is the capture ratio, and w_s and w_n are the test packet power and the joint interference power at the receiver's antenna, respectively. Values for z and the capture window t_w depend on the modulation and the coding employed by the network, among other things. For a typical narrowband FM receiver, a z value of 6 dB is suggested in [63]. The details about estimation of the values of z and t_w are beyond the scope of this application example.

Let the random variable Z be defined as the signal-to-interference ratio (SIR)

$$Z \triangleq \frac{W_s}{W_n}, \quad Z \geq 0 \quad (4.76)$$

where $W_s \geq 0$ and $W_n \geq 0$ are random variables representing the desired signal power and the interference power, respectively. Assuming that W_s and W_n are statistically independent, the resulting cumulative distribution function (CDF) can be expressed as [47]

$$\begin{aligned} F_Z(z_0, n) &= \text{Prob} \left\{ \frac{W_s}{W_n} \leq z_0 \right\} \\ &= \int_0^{z_0} dz \int_0^\infty y f_{W_s}(zy) f_{W_n}(y) dy \end{aligned} \quad (4.77)$$

where $f_{W_s}(\cdot)$ and $f_{W_n}(\cdot)$ are the probability density functions (PDFs) of the desired signal power and the interference power, respectively.

Let the number of packets generated in the network for new messages plus retransmissions be Poisson distributed, with mean generation rate of λ packets per second. The mean offered traffic is then expressed as $G = p\lambda$ packets per transmission period. Given the transmission of an arbitrary test packet, the probability of it being overlap by n other packets is given by [47]

$$R_n = \frac{(G\tilde{\tau})^n}{n!} e^{-G\tilde{\tau}} \quad (4.78)$$

where τ is the worst case propagation delay and $\tilde{\tau} = \tau/p$ its normalised version. Finally, the unconditional probability of a test packet being able to capture the receiver in an arbitrary transmission period may be expressed by

$$P_{capt}(z_0) = 1 - \sum_{n=1}^{\infty} R_n F_Z(z_0, n). \quad (4.79)$$

Outage Probability

The CDF in (4.77) also represents another important measure of performance for wireless systems: the outage probability. It is defined as the probability that the SIR at the reference receiver falls below a certain specified threshold required for successful reception. Therefore

$$P_{out}(z_0, n) = F_Z(z_0, n) \quad (4.80)$$

where z_0 is the successful reception threshold.

Channel Throughput

Let U , B and I be random variables representing, respectively, the duration of the successful transmission, the duration of the busy period and the duration of the idle period. Let $E\{U\}$, $E\{B\}$ and $E\{I\}$ be their respective expected values. Clearly, the channel throughput can be expressed by

$$S = \frac{E\{U\}}{E\{B\} + E\{I\}}. \quad (4.81)$$

For nonpersistent CSMA, Kleinrock and Tobagi have shown that [60]

$$E\{B\} = p + 2\tau - \frac{p}{G} (1 - e^{-G\tilde{\tau}}) \quad (4.82)$$

and

$$E\{I\} = \frac{p}{G}. \quad (4.83)$$

It can also be seen that

$$E\{U\} = p P_{capt}(z_0) \quad (4.84)$$

where $P_{capt}(\cdot)$ is the probability of receiver's capture and also it represents the probability of a successful transmission. Using the results of (4.82)-(4.84), the throughput can be written as

$$S = \frac{GP_{capt}(z_0)}{G(1 + 2\tilde{\tau}) + e^{-G\tilde{\tau}}} \quad (4.85)$$

η - μ Fading Channel

The η - μ fading model [19] considers clusters of multipath waves propagating in a nonhomogeneous environment. The probability density function (PDF) of the signal envelope r may be expressed as

$$f_R(r) = \frac{4\sqrt{\pi}\mu^{\mu+\frac{1}{2}}h^\mu}{\hat{r}\Gamma(\mu)H^{\mu-\frac{1}{2}}} \left(\frac{r}{\hat{r}}\right)^{2\mu} \exp\left[-2\mu h \left(\frac{r}{\hat{r}}\right)^2\right] I_{\mu-\frac{1}{2}}\left[2\mu H \left(\frac{r}{\hat{r}}\right)^2\right] \quad (4.86)$$

where $\hat{r} = \sqrt{E(R^2)}$ is the rms value of R , $\Gamma(\cdot)$ is the Gamma function [21, Eq. 6.1.1], $I_\nu(\cdot)$ is the modified Bessel function of the first kind and ν -th order [21, Eq. 9.6.10], $\eta > 0$ is the scattered-wave power ratio between the in-phase and quadrature components, $\mu > 0$ is given by $\mu \triangleq \frac{E^2(R^2)}{2V(R^2)} \left[1 + \left(\frac{H}{h}\right)^2\right]$, $E(\cdot)$ and $V(\cdot)$ are the expectation and variance operator, respectively, and

$$h = \frac{2 + \frac{1}{\eta} + \eta}{4} \text{ and } H = \frac{\frac{1}{\eta} - \eta}{4}. \quad (4.87)$$

Let $W = R^2$ be the signal power and $\bar{w} = \hat{r}^2$ its average value. The signal power PDF may

be expressed as

$$f_W(w) = \frac{2\sqrt{\pi}\mu^{\mu+\frac{1}{2}}h^\mu}{w\Gamma(\mu)H^{\mu-\frac{1}{2}}} \left(\frac{w}{w}\right)^{\mu-\frac{1}{2}} \exp\left(-2\mu h\frac{w}{w}\right) I_{\mu-\frac{1}{2}}\left[2\mu H\frac{w}{w}\right]. \quad (4.88)$$

Interference Signal

In a wireless system, interference typically results from signals arriving at the receiver's antenna from multiple transmitters. Depending on how these random signals combine during the observation interval, one of two scenarios might occur [1]: coherent addition or incoherent addition.

Coherent addition occurs if the carrier frequencies are equal and if the random phase fluctuations are small during the capture time t_w . The conditions for the coherent addition of signals to occur are difficult to meet, which makes it a rather unlikely scenario, and will not be considered at this moment.

Incoherent addition occurs if the phases of the individual signals fluctuate significantly due to mutually independent modulation [29, 64]. In this case, the interference power W_n experienced during the observation interval is the sum of the individual signals' powers W_i , i.e.,

$$W_n = \sum_{i=1}^n W_i = \sum_{i=1}^n \overline{X_i(t)X_i^*(t)} \quad (4.89)$$

where $X_i^*(\cdot)$ is the complex conjugate of phasor $X_i(\cdot)$. Considering the current work, where the signal power is a random variable, the PDF of the joint interference power is therefore the convolution of the PDFs of all contributing signal powers. If the individual components are independent and identically distributed (i.i.d.), then the interference power is expressed as the n -fold convolution of the PDF of the individual signal power.

4.4.3 Results

For the calculations presented in this section, let (4.88) represent the desired signal power PDF as well as, with different parameters, the signal power PDF of an individual component

Table 4.3: Relation between number of terms and accuracy in the infinite summation of (4.92).

Parameters					smallest J for accuracy of			
μ_s	μ_n	η_s	η_n	\tilde{z}_0	3-decimal-place	6-decimal-place		
0.5	0.5	0.01	0.01	0.1	32	69		
				1.0	309	644		
				5.0	1534	3197		
		0.5	0.99	1.0	1.0	1.0	197	377
						0.01	16	34
						0.99	11	22
						0.01	15	31
						0.99	10	20
0.5	1.0	0.01	0.01	1.0	195	373		
				0.99	131	230		
		0.5	0.01	1.0	1.0	11	22	
					0.99	9	16	
		0.99	0.01	1.0	1.0	10	20	
					0.99	8	15	
5.0	0.01	0.01	1.0	84	132			
1.0	0.5	0.01	0.01	1.0	614	1281		
	1.0	0.01	0.01	1.0	387	739		
	5.0	0.01	0.01	1.0	163	254		
5.0	0.5	0.01	0.01	1.0	3056	6379		
	1.0	0.01	0.01	1.0	1916	3664		
	5.0	0.01	0.01	1.0	792	1228		

of the interference signal. Also, for the remaining of this application example and wherever applicable, the subscripts s , i and n are used to represent the desired signal variables, the interference signal's individual component variables, and the joint interference signal variables, respectively. Finally, let \tilde{z}_0 be defined as $\tilde{z}_0 \triangleq z_0/(\bar{w}_s/\bar{w}_n)$ where the ratio \bar{w}_s/\bar{w}_n is commonly denoted as average SIR.

For the incoherent addition, assume that the interference signal is composed of n i.i.d. variables. As a result, the joint interference signal power PDF is the n -fold convolution of the individual signal power PDF which, on its turn, is expressed by (4.88). If the Laplace transform of the PDF is used, then the n -fold convolution can be converted to a n -times product. Using [21, Eqs. 29.2.12, 29.3.60], the Laplace transform $F_W(s) = L[f_W(w)]$ of (4.88) can be calculated

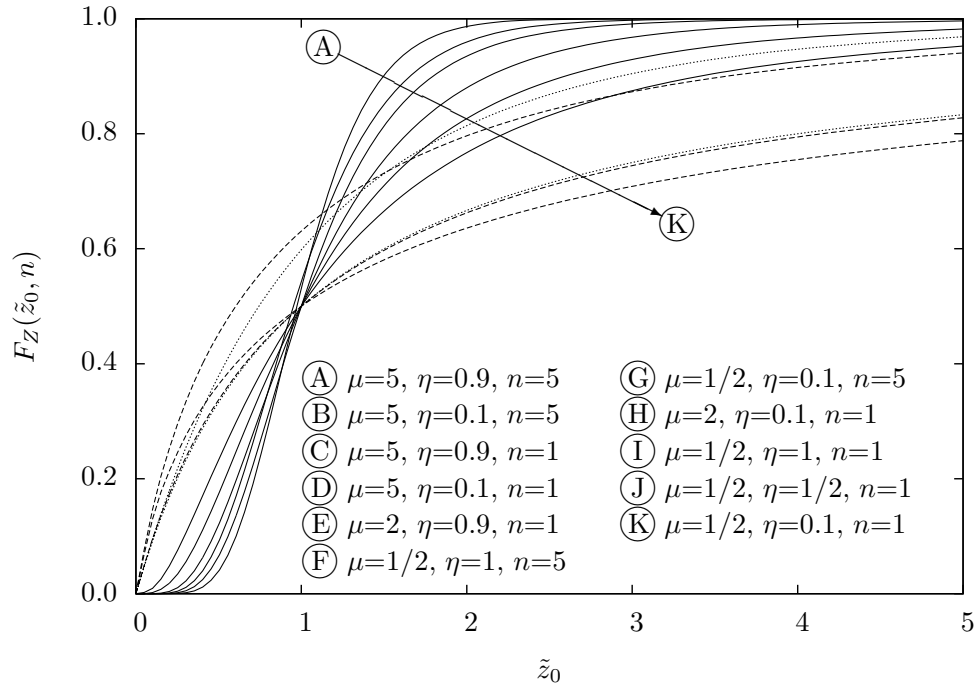


Figure 4.14: CDF of (4.92) with $\mu = \mu_s = \mu_i = \mu_n/n$ and $\eta = \eta_s = \eta_i = \eta_n$. The dashed lines correspond to the Hoyt channel where $\mu = 1/2$. The dotted lines correspond to the Rayleigh channel where $\mu = 1/2$ and $\eta = 1$.

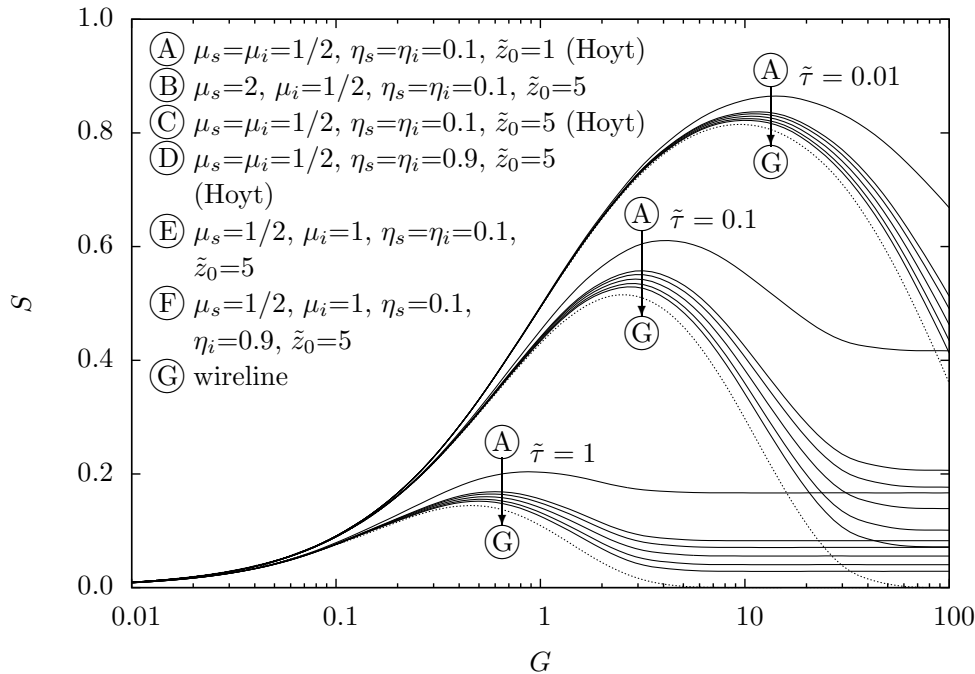


Figure 4.15: Throughput S for incoherent $\eta - \mu$ channel. The dotted lines correspond to the wireline channel ($z_0 \rightarrow \infty$)

as

$$F_W(s) = \left[4h \left(\frac{\mu}{\bar{w}} \right)^2 \right]^\mu \left[\frac{1}{(s + a_1)^2 - a_2^2} \right]^\mu \quad (4.90)$$

where $a_1 \triangleq 2h\mu/\bar{w}$ and $a_2 \triangleq 2H\mu/\bar{w}$. Raising (4.90) to the n -th power and using [21, Eqs. 29.2.3, 29.2.12, 29.3.60] to calculate its inverse Laplace transform gives the joint interference signal power PDF, which can be expressed as

$$f_{W_n}(w_n) = \frac{2\sqrt{\pi}}{\Gamma(\mu_n)} h_n^{\mu_n} \left(\frac{\mu_n}{\bar{w}_n} \right)^{\mu_n + \frac{1}{2}} \left(\frac{w_n}{H_n} \right)^{\mu_n - \frac{1}{2}} \times \exp \left(-2\mu_n h_n \frac{w_n}{\bar{w}_n} \right) I_{\mu_n - \frac{1}{2}} \left(2\mu_n H_n \frac{w_n}{\bar{w}_n} \right). \quad (4.91)$$

It can be seen that the joint interference signal power PDF and the individual signal power PDF follow the same distribution, with $\mu_n = n\mu_i$, $\eta_n = \eta_i$ (thus making $h_n = h_i$ and $H_n = H_i$), and $\bar{w}_n = n\bar{w}_i$.

Using the appropriated expressions in (4.77), and after some manipulation, the signal-to-interference CDF may be expressed as ⁵

$$F_Z(\tilde{z}_0, n) = \frac{u^{2\mu_n}}{h_n^{\mu_n}} \sum_{j=0}^{\infty} \frac{(1-u)^{j+2\mu_s}}{(j+2\mu_s)B(j+2\mu_s, 2\mu_n)} {}_2F_1 \left[j_\mu, j_\mu + \frac{1}{2}, \mu_n + \frac{1}{2}, \left(\frac{H_n}{h_n} u \right)^2 \right] \times \left\{ 1 - \frac{1}{m_j h_s^{\mu_s} B(\mu_s, \mu_n)} \left(\frac{H_s}{h_s} \right)^{2m_j} {}_2F_1 \left[1, m_j + \mu_s, m_j + 1, \left(\frac{H_s}{h_s} \right)^2 \right] \right\} \quad (4.92)$$

where $j_\mu = \frac{j}{2} + \mu_s + \mu_n$, $m_j = \lceil \frac{j+1}{2} \rceil$, $\lceil \cdot \rceil$ is the ceiling function, $B(\cdot)$ is the beta function [21, Eq. 6.2.2], ${}_2F_1(\cdot)$ is the Gauss hypergeometric function [21, Eq. 15.1.1], and

$$u = \frac{\mu_n h_n}{\mu_n h_n + \mu_s h_s \tilde{z}_0}. \quad (4.93)$$

Although (4.92) includes an infinite summation, the evaluation of the CDF converges rapidly for most cases of interest. Let J be defined as the number of terms in a truncated summation, i.e., $0 \leq j < J$. Table 4.3 gives the value of J necessary to obtain a three-decimal-place accuracy (error < 0.0005) and a six-decimal-place accuracy (error < 0.0000005) for the infinite summation

⁵This expression corrects a typo in Eq. (18) of [69].

of (4.92).

Fig. 4.14 depicts the CDF of (4.92) for $\mu = \mu_s = \mu_i = \mu_n/n$ and $\eta = \eta_s = \eta_i = \eta_n$ and a couple of values of n . The curves for Hoyt and Rayleigh channels are indicated. The Rayleigh channel is obtained when [19] $\mu = 1/2$ and $\eta = 1$, and the Hoyt channel is obtained when $\mu = 1/2$ with the Hoyt parameter b given by $b = -\frac{1-\eta}{1+\eta}$. First, it can be seen that larger values of μ concentrate the random outcomes around $\tilde{z}_0 = 1$. This is indicated by the sharp increase of the CDF around this value. Also, larger values of n tend to produce a distribution with lower variance. This is indicated by the steeper climb from zero that curves with larger n experience.

With the results obtained so far, using (4.79), (4.85) and (4.92), it is now possible to calculate the channel throughput, which are presented in Fig. 4.15. The graphics clearly indicate the important role the normalised worst case propagation delay $\tilde{\tau}$ plays to determine the channel throughput. Also, the higher the capture threshold is (indicated by higher \tilde{z}_0), the lower the throughput is, which is expected since it indicates a diminished ability of receiver detection of the intended signal among the interfering signals. For instance, with $\tilde{\tau} = 0.1$, $\mu_s = \mu_i = 1/2$ and $\eta_s = \eta_i = 0.1$, there is an throughput increase of 3% at $G = 10$ if the capture threshold changes from $\tilde{z}_0 = 5$ to 1. This gain is larger for heavier traffic (higher G). The fading intensity may be the reason behind the influence of μ_s , where lower values of μ_s (i.e., higher fading intensity) produce higher throughput. The parameters η_s and η_i play a somewhat smaller influence on the throughput. It can be seen that values of η_s and η_i close to zero produce higher fading intensity and, as a result, higher throughput.

4.4.4 Conclusion

This application example investigates the throughput performance of CSMA in a packet radio network and η - μ fading environment. Analytical and numerical results are presented considering the signal capture model with incoherent addition of interfering signals. The approach used here includes the signal capture model with uniform attenuation for all terminals (or perfect power control). The results indicate that higher fading intensity, lower capture threshold or lower propagation delay contributes to higher channel throughput.

The formulations for the statistics of the ratio of η - μ variates, although used here for the evaluation of the CSMA technique, are general and can be applied to any communication system in which interference is an issue. Wireless communications networks in general in which reuse frequency is deployed are certainly possible targets. More specifically, cooperative communications with relay and/or destination nodes being interfered with unwanted faded Hoyt, Nakagami- m , Rayleigh, or η - μ signals can be investigated. Also, in spectrum sensing applications the effect of the interference of the secondary users with the primary users in η - μ scenario can be explored.

4.5 Throughput of CSMA in κ - μ Fading Channels⁶

4.5.1 Introduction

Wireless local area networks (WLANs) are experiencing rapid development in part stimulated by the deployment of systems compatible to the IEEE 802.11 standards. They offer data communication between terminals within radio range while allowing a certain degree of mobility.

In order to serve terminals exhibiting bursty traffic behaviour, WLANs make use of packet radio techniques with random access to a transmission channel shared by multiple users. Specifically, variations of carrier sense multiple access (CSMA) are generally used to access the wireless medium [54, 55, 56, 57]. The capacity of the channel is then influenced by the probability of packet collision and by the signal degradation due to mutual interference and signal attenuation. In other words, it is influenced by the medium contention resolution algorithm and by the channel characteristics.

Intuitively one might expect that original (wireline) CSMA systems show better system performance than wireless systems because of more hostile channel characteristics found in the latter. However, this is not necessarily the case. For instance, in a channel model that takes into account the effects of fading, competing packets arriving at a common radio receiver antenna will not always destroy each other because they may show different and independent fading

⁶This material was presented at [75].

and attenuation levels [58, 59]. This leads to expect that wireless systems may actually exhibit successful reception rate higher than that of original (wireline) systems. In fact, Arnbak and Blitterswijk have shown this to happen with slotted Aloha over Rayleigh fading channels [29].

In this application example, we investigate the throughput performance of CSMA in a packet radio network with κ - μ fading environment. The performance of the original (wireline) CSMA is presented in [60] and is here extended to this fading scenario. The κ - μ fading environment is relevant to model a situation where the random multipath signals are superimposed on a nonfading dominant signal, for instance, when a line-of-sight (LOS) component is present [19]. The distribution has the Rice (Nakagami- n), the Nakagami- m , the Rayleigh, and the One-Sided Gaussian distributions as special cases.

This application example is organized as follows. Section 4.5.2 describes the analytical model and considers the incoherent packet addition at the receiver's antenna. Section 4.5.3 presents the results obtained. Comments and conclusions are given in Section 4.5.4.

4.5.2 Analytical Model

Nonpersistent CSMA

For nonpersisting CSMA, a terminal ready to transmit first senses the channel. If it senses the channel idle, it transmits the packet. Otherwise, it schedules the (re)transmission of the packet to a later time according to some randomly distributed retransmission delay. After the retransmission delay has elapsed, the terminal repeats the procedure described above. In this application example, the channel is considered to be memoryless, i.e., failures to capture the channel and future attempts are uncorrelated. In addition, all packets are assumed to have fixed length and to require p seconds to transmit. Finally, each packet is assumed to have a single destination.

Probability of Capture

Given the transmission of an arbitrary test packet over a wireline channel, it is generally assumed that a successful reception can only occur if no other transmission attempt is made

during the test packet reception, i.e., if there is no signal overlap at the receiver. However, in wireless systems the radio receiver may be able to be captured by a test packet, even in the presence of n interfering packets, provided the power ratio between the test signal and the joint interfering signal exceeds a certain threshold during a given portion of the transmission period t_w , $0 < t_w < p$, to lock the receiver [61, 62]. In such a case, a test packet is only destroyed if

$$\frac{w_s}{w_n} \leq z \quad \text{during } t_w, \text{ with } n > 0, \quad (4.94)$$

where z is the capture ratio, and w_s and w_n are the test packet power and the joint interference power at the receiver's antenna, respectively. Values for z and the capture window t_w depend on the modulation and the coding employed by the network, among other things. For a typical narrowband FM receiver, a z value of 6 dB is suggested in [63]. The details about estimation of the values of z and t_w are beyond the scope of this application example.

Let the random variable Z be defined as the signal-to-interference ratio (SIR)

$$Z \triangleq \frac{W_s}{W_n}, \quad Z \geq 0 \quad (4.95)$$

where $W_s \geq 0$ and $W_n \geq 0$ are random variables representing the desired signal power and the interference power, respectively. Assuming that W_s and W_n are statistically independent, the resulting cumulative distribution function (CDF) can be expressed as [47]

$$\begin{aligned} F_Z(z_0) &= \text{Prob} \left\{ \frac{W_s}{W_n} \leq z_0 \right\} \\ &= \int_0^{z_0} dz \int_0^\infty y f_{W_s}(zy) f_{W_n}(y) dy \end{aligned} \quad (4.96)$$

where $f_{W_s}(\cdot)$ and $f_{W_n}(\cdot)$ are the probability density functions (PDFs) of the desired signal power and the interference power, respectively.

Let the number of packets generated in the network for new messages plus retransmissions be Poisson distributed, with mean generation rate of λ packets per second. The mean offered traffic is then expressed as $G = p\lambda$ packets per transmission period. Given the transmission of

an arbitrary test packet, the probability of it being overlap by n other packets is given by [47]

$$R_n = \frac{(G\tilde{\tau})^n}{n!} e^{-G\tilde{\tau}} \quad (4.97)$$

where τ is the worst case propagation delay and $\tilde{\tau} = \tau/p$ its normalised version. Finally, the unconditional probability of a test packet being able to capture the receiver in an arbitrary transmission period may be expressed by

$$P_{capt}(z_0) = 1 - \sum_{n=1}^{\infty} R_n F_Z(z_0). \quad (4.98)$$

Channel Throughput

Let U , B and I be random variables representing, respectively, the duration of the successful transmission, the duration of the busy period and the duration of the idle period. Let $E\{U\}$, $E\{B\}$ and $E\{I\}$ be their respective expected values. Clearly, the channel throughput can be expressed by

$$S = \frac{E\{U\}}{E\{B\} + E\{I\}}. \quad (4.99)$$

For nonpersistent CSMA, Kleinrock and Tobagi have shown that [60]

$$E\{B\} = p + 2\tau - \frac{p}{G} (1 - e^{-G\tilde{\tau}}) \quad (4.100)$$

and

$$E\{I\} = \frac{p}{G}. \quad (4.101)$$

It can also be seen that

$$E\{U\} = p P_{capt}(z_0) \quad (4.102)$$

where $P_{capt}(\cdot)$ is the probability of receiver's capture and also it represents the probability of a successful transmission. Using the results of (4.100)-(4.102), the throughput can be written as

$$S = \frac{G P_{capt}(z_0)}{G(1 + 2\tilde{\tau}) + e^{-G\tilde{\tau}}} \quad (4.103)$$

κ - μ Fading Channel

The κ - μ fading model [19] considers clusters of multipath waves propagating in a nonhomogeneous environment. The probability density function (PDF) of the signal envelope r may be expressed as

$$f_R(r) = \frac{2\mu(\kappa+1)^{\frac{\mu+1}{2}}}{\hat{r}\kappa^{\frac{\mu-1}{2}}e^{\kappa\mu}} \left(\frac{r}{\hat{r}}\right)^\mu \exp\left[-\mu(\kappa+1)\left(\frac{r}{\hat{r}}\right)^2\right] I_{\mu-1}\left[2\mu\sqrt{\kappa(\kappa+1)}\frac{r}{\hat{r}}\right] \quad (4.104)$$

where $\hat{r} = \sqrt{E(R^2)}$ is the rms value of R , $I_\nu(\cdot)$ is the modified Bessel function of the first kind and ν -th order [21, Eq. 9.6.10], $\kappa > 0$ is the ratio between the total power of the dominant components and the total power of the scattered waves, $\mu > 0$ is given by $\mu \triangleq \frac{E^2(R^2)(2\kappa+1)}{V(R^2)(\kappa+1)^2}$, and $E(\cdot)$ and $V(\cdot)$ are the expectation and variance operator, respectively.

Let $W = R^2$ be the signal power and $\bar{w} = \hat{r}^2$ its average value. The signal power PDF may be expressed as

$$f_W(w) = \frac{\mu(\kappa+1)^{\frac{\mu+1}{2}}}{\bar{w}\kappa^{\frac{\mu-1}{2}}e^{\kappa\mu}} \left(\frac{w}{\bar{w}}\right)^{\frac{\mu-1}{2}} \exp\left[-\mu(\kappa+1)\frac{w}{\bar{w}}\right] I_{\mu-1}\left[2\mu\sqrt{\kappa(\kappa+1)}\frac{w}{\bar{w}}\right]. \quad (4.105)$$

Interference Signal

In a wireless system, interference typically results from signals arriving at the receiver's antenna from multiple transmitters. Depending on how these random signals combine during the observation interval, one of two scenarios might occur [1]: coherent addition or incoherent addition.

Coherent addition occurs if the carrier frequencies are equal and if the random phase fluctuations are small during the capture time t_w . The conditions for the coherent addition of signals to occur are difficult to meet, which makes it a rather unlikely scenario, and will not be considered at this moment.

Incoherent addition occurs if the phases of the individual signals fluctuate significantly due to mutually independent modulation [29, 64]. In this case, the interference power W_n experienced

during the observation interval is the sum of the individual signals' powers W_i , i.e.,

$$W_n = \sum_{i=1}^n W_i = \sum_{i=1}^n \overline{X_i(t)X_i^*(t)} \quad (4.106)$$

where $X_i^*(\cdot)$ is the complex conjugate of phasor $X_i(\cdot)$. Considering the current work, where the signal power is a random variable, the PDF of the joint interference power is therefore the convolution of the PDFs of all contributing signal powers. If the individual components are independent and identically distributed (i.i.d.), then the interference power is expressed as the n -fold convolution of the PDF of the individual signal power.

4.5.3 Results

For the calculations presented in this section, let (4.105) represent the desired signal power PDF as well as, with different parameters, the signal power PDF of an individual component of the interference signal. Also, for the remaining of this application example and wherever applicable, the subscripts s , i and n are used to represent the desired signal variables, the interference signal's individual component variables, and the joint interference signal variables, respectively. Finally, let \tilde{z}_0 be defined as $\tilde{z}_0 \triangleq z_0/(\bar{w}_s/\bar{w}_n)$ where the ratio \bar{w}_s/\bar{w}_n is commonly denoted as average SIR.

For the incoherent addition, assume that the interference signal is composed of n i.i.d. variables. As a result, the joint interference signal power PDF is the n -fold convolution of the individual signal power PDF which, on its turn, is expressed by (4.105). If the Laplace transform of the PDF is used, then the n -fold convolution can be converted to a n -times product. Using [21, Eqs. 29.2.12 and 29.3.81], the Laplace transform $F_W(s) = L[f_W(w)]$ of (4.105) can be calculated as

$$F_W(s) = e^{-\kappa\mu} \left(\frac{a}{s+a} \right)^\mu \exp \left(\frac{k}{s+a} \right) \quad (4.107)$$

where $a \triangleq \frac{\mu(\kappa+1)}{\bar{w}}$ and $k \triangleq \frac{\mu^2\kappa(\kappa+1)}{\bar{w}}$. Raising (4.107) to the n -th power and using [21, Eqs. 29.2.12 and 29.3.81] to calculate its inverse Laplace transform gives the joint interference signal power

Table 4.4: Relation between number of terms and accuracy in the infinite summation of (4.109).

Parameters					smallest J for accuracy of			
μ_s	μ_n	κ_s	κ_n	\tilde{z}_0	3-decimal-place	6-decimal-place		
0.5	0.5	0.01	0.01	0.1	3	5		
				1.0	9	19		
				5.0	34	70		
			1.0	1.0	8	15		
			10.0	1.0	5	9		
			1.0	0.01	1.0	15	31	
				1.0	1.0	13	24	
				10.0	1.0	8	13	
			10.0	0.01	1.0	70	145	
		1.0		1.0	54	103		
		10.0		1.0	26	41		
		0.5	1.0	0.01	0.01	1.0	7	13
					1.0	1.0	6	11
					10.0	1.0	5	8
				1.0	0.01	1.0	11	21
1.0	1.0				10	17		
10.0	1.0				7	11		
10.0	0.01			1.0	45	87		
	1.0			1.0	37	65		
	10.0			1.0	21	32		
10.0	1.0			1.0	1.0	6	10	
1.0	0.5			1.0	1.0	1.0	21	41
	1.0			1.0	1.0	1.0	15	28
	10.0	1.0	1.0	1.0	9	14		
10.0	0.5	1.0	1.0	1.0	178	345		
	1.0	1.0	1.0	1.0	114	207		
	10.0	1.0	1.0	1.0	40	60		

PDF, which can be expressed as

$$f_{W_n}(w_n) = \frac{\mu_n(\kappa_n + 1)^{\frac{\mu_n+1}{2}}}{\bar{w}_n \kappa_n^{\frac{\mu_n-1}{2}} e^{\kappa_n \mu_n}} \left(\frac{w_n}{\bar{w}_n} \right)^{\frac{\mu_n-1}{2}} \exp \left[-\mu_n(\kappa_n + 1) \frac{w_n}{\bar{w}_n} \right] \times I_{\mu_n-1} \left[2\mu_n \sqrt{\kappa_n(\kappa_n + 1)} \frac{w_n}{\bar{w}_n} \right]. \quad (4.108)$$

It can be seen that the joint interference signal power PDF and the individual signal power PDF follow the same distribution, with $\mu_n = n\mu_i$, $\kappa_n = \kappa_i$ and $\bar{w}_n = n\bar{w}_i$.

Using the appropriated expressions in (4.96), and after some manipulation (see Section 4.5.5), the signal-to-interference CDF may be expressed as

$$F_Z(\tilde{z}_0) = \frac{u^{\mu_n}}{e^{\kappa_n \mu_n}} \sum_{j=0}^{\infty} \frac{(1-u)^{j+\mu_s} Q(j+1, \kappa_s \mu_s)}{(j+\mu_s) B(j+\mu_s, \mu_n)} {}_1F_1(j+\mu_s+\mu_n, \mu_n, \kappa_n \mu_n u) \quad (4.109)$$

where $B(\cdot)$ is the beta function [21, Eq. 6.2.2], ${}_1F_1(\cdot)$ is the Kummer confluent hypergeometric function [21, Eq. 13.1.2], $Q(\cdot)$ is the regularized incomplete gamma function defined as $Q(a, b) \triangleq \frac{\Gamma(a, b)}{\Gamma(a)}$, $\Gamma(\cdot)$ is the gamma function [21, Eq. 6.1.1], $\Gamma(\cdot, \cdot)$ is the incomplete gamma function [21, Eq. 6.5.3], and

$$u = \frac{\mu_n(\kappa_n + 1)}{\mu_n(\kappa_n + 1) + \mu_s(\kappa_s + 1)\tilde{z}_0}. \quad (4.110)$$

If $\mu_s = 1$ and $\mu_n = n$, where $n > 0$ is an integer, the result in (4.109) simplifies to the case of Rice channel model described in [68]. In addition, if both κ_s and κ_n are set to zero in (4.109), the CDF simplifies to the Rayleigh channel model and it can be expressed as

$$F_Z(\tilde{z}_0) = 1 - \left(\frac{n}{n + \tilde{z}_0} \right)^n. \quad (4.111)$$

Finally, if the result above is further simplified by assuming that $\bar{w}_s = \bar{w}_i = \bar{w}_n/n$, then the same expression presented in [29] is found.

Although (4.109) includes an infinite summation, the evaluation of the CDF converges rapidly for most cases of interest. Let J be defined as the number of terms in a truncated summation, i.e., $0 \leq j < J$. Table 4.4 gives the value of J necessary to obtain a three-decimal-

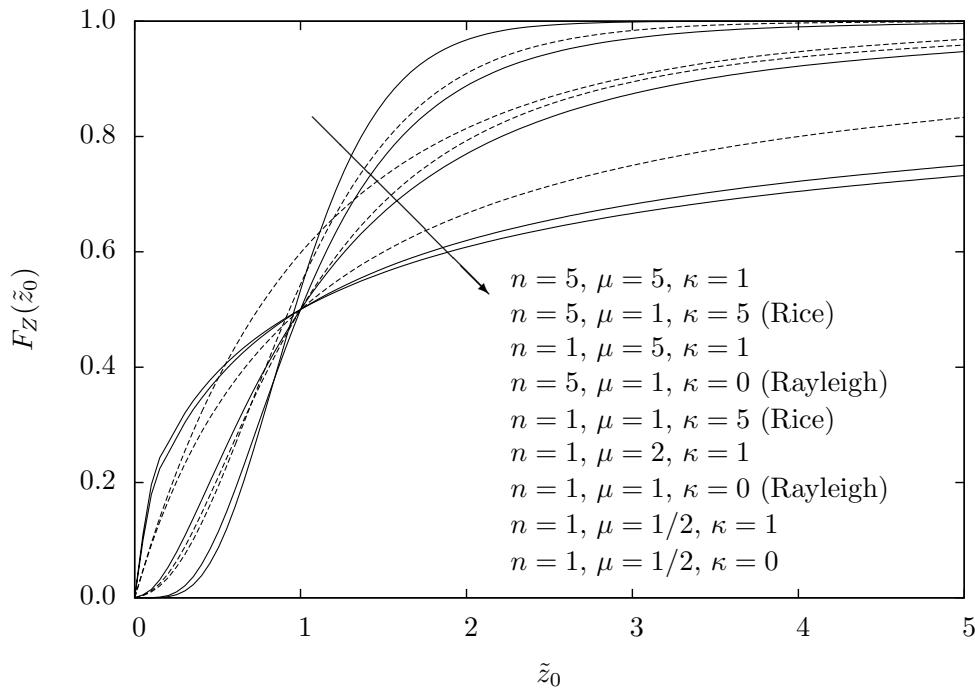


Figure 4.16: CDF of (4.109) with $\mu = \mu_s = \mu_i = \mu_n/n$ and $\kappa = \kappa_s = \kappa_i = \kappa_n$. The dashed lines correspond to the Rice and Rayleigh channels, as indicated.

place accuracy (error < 0.0005) and a six-decimal-place accuracy (error < 0.0000005) for the infinite summation of (4.109).

Fig. 4.16 depicts the CDF of (4.109) for $\mu = \mu_s = \mu_i = \mu_n/n$ and $\kappa = \kappa_s = \kappa_i = \kappa_n$ and a couple of values of n . The curves for Rice and Rayleigh channels are indicated. The Rayleigh channel is obtained when [19] $\mu = 1$ and $\kappa = 0$, and the Rice channel is obtained when $\mu = 1$ with the Ricean parameter k given by $k = \kappa$. First, it can be seen that larger values of μ concentrate the random outcomes around $\tilde{z}_0 = 1$. This is indicated by the sharp increase of the CDF around this value. Also, larger values of n tend to produce a distribution with lower variance. This is indicated by the steeper climb from zero that curves with larger n experience.

With the results obtained so far, using (4.98), (4.103) and (4.109), it is now possible to calculate the channel throughput, which are presented in Fig. 4.17. The graphics clearly indicate the important role the normalised worst case propagation delay $\tilde{\tau}$ plays to determine the channel throughput. Also, the higher the capture threshold is (indicated by higher \tilde{z}_0), the lower the throughput is, which is expected since it indicates a diminished ability of receiver detection of the intended signal among the interfering signals. The fading intensity may be the reason

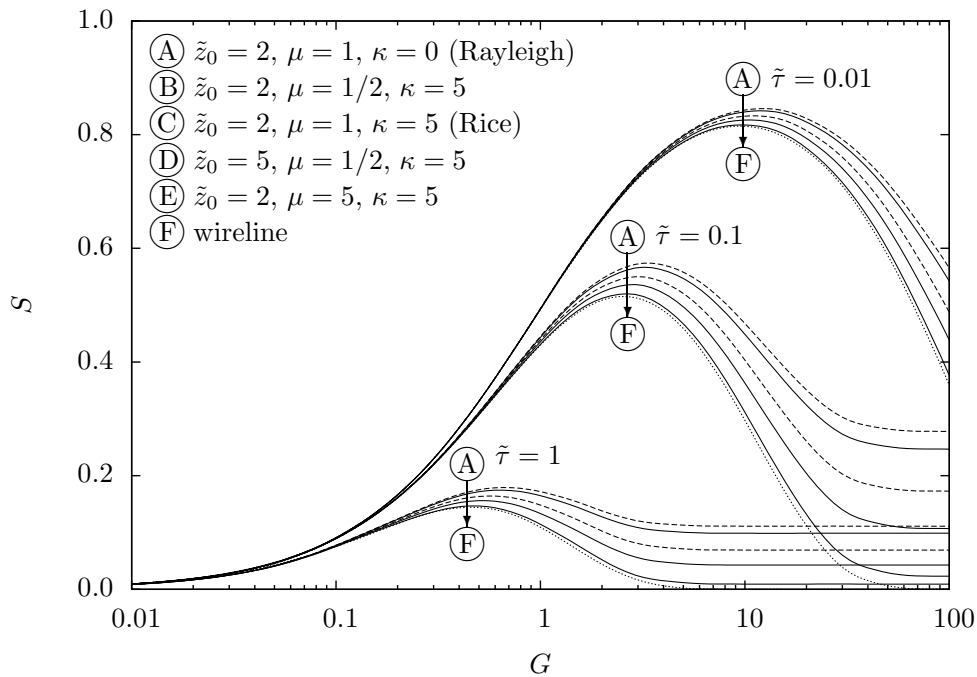


Figure 4.17: Throughput S for incoherent $\kappa - \mu$ channel with $\mu = \mu_s = \mu_i = \mu_n/n$ and $\kappa = \kappa_s = \kappa_i = \kappa_n$. The dashed lines correspond to the Rice and Rayleigh channels, as indicated. The dotted lines correspond to the wireline channel ($z_0 \rightarrow \infty$).

behind the influence of μ , where lower values of μ (i.e., higher fading intensity) produce higher throughput. The parameter κ plays a somewhat smaller influence on the throughput. It can be seen that lower values of κ produce higher fading intensity and, as a result, higher throughput.

4.5.4 Conclusion

This application example investigates the throughput performance of CSMA in a packet radio network and κ - μ fading environment. Analytical and numerical results are presented considering the signal capture model with incoherent addition of interfering signals. The approach used here includes the signal capture model with uniform attenuation for all terminals (or perfect power control). The results indicate that higher fading intensity, lower capture threshold or lower propagation delay contributes to higher channel throughput.

4.5.5 Calculation

The calculation presented below refers to the incoherent addition of n interfering signals. Let (4.105) and (4.108) be used to describe the desired signal power and the interference power, respectively. With (4.96), changing the integration order, using [21, Eq. 9.6.10] and integrating over z (see [48, Eqs. 3.381.1, 8.356.3]) leads to

$$F_Z(z_0) = \sum_{k=0}^{\infty} \int_0^{\infty} \frac{(\mu_s \kappa_s)^k \mu_n \kappa_n^{-\frac{\mu_n+1}{2}}}{k! e^{\kappa_n \mu_n + \kappa_s \mu_s}} \left(\frac{\kappa_n + 1}{\bar{w}_n} \right)^{\frac{\mu_n+1}{2}} y^{\frac{\mu_n-1}{2}} e^{-\frac{\kappa_n+1}{\bar{w}_n} \mu_n y} \times I_{\mu_n-1} \left(2\mu_n \sqrt{\kappa_n \frac{\kappa_n + 1}{\bar{w}_n}} y \right) \left[1 - Q \left(k + \mu_s, \frac{\kappa_s + 1}{\bar{w}_s} \mu_s z_0 y \right) \right] dy. \quad (4.112)$$

Applying [48, Eq. 8.356.2] recursively, and [21, Eqs. 6.5.3, 6.5.4, 6.5.29], it can be seen that

$$Q(\alpha + n, x) = Q(\alpha, x) + \frac{x^\alpha}{e^x} \sum_{j=0}^{n-1} \frac{x^j}{\Gamma(\alpha + j + 1)} = 1 - \frac{x^\alpha}{e^x} \sum_{j=n}^{\infty} \frac{x^j}{\Gamma(\alpha + j + 1)}. \quad (4.113)$$

Using (4.113) in (4.112) leads to

$$F_Z(z_0) = \sum_{k=0}^{\infty} \sum_{j=k}^{\infty} \int_0^{\infty} \frac{\mu_s^{j+k+\mu_s} \kappa_s^k \mu_n \kappa_n^{-\frac{\mu_n+1}{2}}}{k! \Gamma(j + \mu_s + 1) e^{\kappa_n \mu_n + \kappa_s \mu_s}} \left(\frac{\kappa_s + 1}{\bar{w}_s} z_0 \right)^{j+\mu_s} \left(\frac{\kappa_n + 1}{\bar{w}_n} \right)^{\frac{\mu_n+1}{2}} \times y^{j+\mu_s+\frac{\mu_n-1}{2}} e^{-\left(\frac{\kappa_s+1}{\bar{w}_s} \mu_s z_0 + \frac{\kappa_n+1}{\bar{w}_n} \mu_n\right) y} I_{\mu_n-1} \left(2\mu_n \sqrt{\kappa_n \frac{\kappa_n + 1}{\bar{w}_n}} y \right) dy. \quad (4.114)$$

Solving the integral over y (see [48, Eqs. 6.643.2, 9.220.2]) results

$$F_Z(z_0) = \sum_{k=0}^{\infty} \sum_{j=k}^{\infty} \frac{(\mu_s \kappa_s)^k (1-u)^{j+\mu_s} u^{\mu_n}}{k! e^{\kappa_n \mu_n + \kappa_s \mu_s}} \frac{\Gamma(j + \mu_s + \mu_n)}{\Gamma(j + \mu_s + 1) \Gamma(\mu_n)} \times {}_1F_1(j + \mu_s + \mu_n, \mu_n, \mu_n \kappa_n u) \quad (4.115)$$

where u is given by (4.110). Changing the summation order and using [48, Eq. 8.352.2] eliminates the summation on k . From here (4.109) is easily obtained.

4.6 Throughput of CSMA in a Rice-Signal with Hoyt-Interference Environment⁷

4.6.1 Introduction

Wireless local area networks (WLANs) have been experiencing rapid development in part stimulated by the deployment of systems compatible to the IEEE 802.11 standards. They offer data communication between terminals within radio range while allowing a certain degree of mobility. These networks are organized either with or without a central node. In either case, the aims are to provide complete connectivity among terminals and to efficiently and fairly dispense the available bandwidth while employing little or no central coordination.

In order to serve terminals exhibiting bursty traffic behaviour, WLANs make use of packet radio techniques with random access to a transmission channel shared by multiple users. Specifically, variations of carrier sense multiple access (CSMA) is generally used to access the wireless medium [54, 56, 57]. The capacity of the channel is then influenced by the probability of packet collision and by the signal degradation due to mutual interference and signal attenuation. In other words, it is influenced by the medium contention resolution algorithm and by the channel characteristics.

Intuitively, one might expect that original (wireline) CSMA systems show better system performance than wireless systems because of more hostile channel characteristics found in the latter. However, this is not necessarily the case. For instance, in a channel model that takes into account the effects of fading, competing packets arriving at a common radio receiver antenna will not always destroy each other because they may show different and independent fading and attenuation levels [58, 59]. This leads to expect that wireless systems may actually exhibit successful reception rate higher than that of wireline systems. In fact, Arnbak and Blitterswijk have shown this to happen with slotted Aloha over Rayleigh fading channels [29].

In this application example, we investigate the throughput performance of CSMA in a packet radio network with combined Rice and Hoyt fading environment. The performance of the

⁷This material was presented at [76].

wireline CSMA is presented in [60] and is here extended to this fading scenario. A number of formulations are found and, to the best of the authors' knowledge, these results are novel contributions. As an intermediate outcome of the calculation, results for the outage probability for these environments are also presented. Analysis of the outage probability for fading channels has been an active investigation topic for the last few years [70, 73, 74], in part because it may be used to estimate performance of spectrum sharing systems. The work presented here offers contributions in this area and introduces many original results.

The channel models considered in this work are among those commonly used to describe the short-term signal statistics of wireless communications links subject to fading [2].

This application example is organized as follows. Section 4.6.2 describes the analytical model. Section 4.6.3 considers the cases of incoherent signal addition at the receiver's antenna with uniform attenuation for all terminals (or perfect power control). Coherent signal addition and a model that includes spatial coverage such as in a cell is also explored. Numerical results and conclusions are given in Sections 4.6.4 and 4.6.5, respectively.

4.6.2 Analytical Model

Nonpersistent CSMA

For nonpersisting CSMA, a terminal ready to transmit first senses the channel. If it senses the channel idle, it transmits the packet. Otherwise, it schedules the (re)transmission of the packet to a later time according to some randomly distributed retransmission delay. After the retransmission delay has elapsed, the terminal repeats the procedure described above. In this application example, the channel is considered to be memoryless, i.e., failures to capture the channel and future attempts are uncorrelated. In addition, all packets are assumed to have fixed length and to require p seconds to transmit. Finally, each packet is assumed to have a single destination.

Probability of Capture

Given the transmission of an arbitrary test packet over a wireline channel, it is generally assumed that a successful reception can only occur if no other transmission attempt is made during the test packet reception, i.e., if there is no signal overlap at the receiver's end. However, in wireless systems the radio receiver may be able to be captured by a test packet, even in the presence of n interfering packets, provided the power ratio between the test signal and the joint interfering signal exceeds a certain threshold during a given portion of the transmission period t_w , $0 < t_w < p$, to lock the receiver [61, 62]. In such a case, a test packet is only destroyed if

$$\frac{w_s}{w_n} \leq z \quad \text{during } t_w, \text{ with } n > 0, \quad (4.116)$$

where z is the capture ratio, and w_s and w_n are the test packet power and the joint interference power at the receiver's antenna, respectively. Values for z and the capture window t_w depend on the modulation and the coding employed by the network, among other things. For a typical narrowband FM receiver, a z value of 6 dB is suggested in [63]. The details about estimation of the values of z and t_w are beyond the scope of this application example.

Let the random variable Z be defined as the signal-to-interference ratio (SIR)

$$Z \triangleq \frac{W_s}{W_n} \geq 0, \quad (4.117)$$

where $W_s \geq 0$ and $W_n \geq 0$ are random variables representing the desired signal power and the interference power, respectively. Assuming that W_s and W_n are statistically independent, the resulting cumulative density function (CDF) can be expressed as [47]

$$F_Z(z_0) = \int_0^{z_0} \int_0^\infty y f_{W_s}(zy) f_{W_n}(y) dy \quad (4.118)$$

where $f_{W_s}(\cdot)$ and $f_{W_n}(\cdot)$ are the probability density functions (PDFs) of the desired signal power and the interference power, respectively.

Let the number of packets generated in the network for new messages plus retransmissions

be Poisson distributed, with mean generation rate of λ packets per second. The mean offered traffic is then expressed as $G = p\lambda$ packets per transmission period. Given the transmission of an arbitrary test packet, the probability of it being overlapped by n other packets is given by [47]

$$R_n = \frac{(G\tilde{\tau})^n}{n!} e^{-G\tilde{\tau}} \quad (4.119)$$

where τ is the worst case propagation delay and $\tilde{\tau} = \tau/p$ its normalised version. Finally, the unconditional probability of a test packet being able to capture the receiver in an arbitrary transmission period may be expressed by

$$P_{capt}(z_0) = 1 - \sum_{n=1}^{\infty} R_n F_Z(z_0). \quad (4.120)$$

Outage Probability Defined

The CDF in (4.118) also represents another important measure of performance for wireless systems: the outage probability. It is defined as the probability that the SIR at the reference receiver falls below a certain specified threshold required for successful reception. Therefore

$$P_{out}(z_0) = F_Z(z_0) \quad (4.121)$$

where z_0 is the successful reception threshold.

Channel Throughput

Let U , B and I be random variables representing, respectively, the duration of the successful transmission, the duration of the busy period and the duration of the idle period. Let $E\{U\}$, $E\{B\}$ and $E\{I\}$ be their respective expected values. Clearly, the channel throughput can be expressed by [60]

$$S = \frac{E\{U\}}{E\{B\} + E\{I\}}. \quad (4.122)$$

For nonpersistent CSMA, Kleinrock and Tobagi have shown that [60]

$$E\{B\} = p + 2\tau - \frac{p}{G} (1 - e^{-G\bar{\tau}}) \quad (4.123)$$

and

$$E\{I\} = \frac{p}{G}. \quad (4.124)$$

It can also be seen that

$$E\{U\} = p P_{capt}(z_0) \quad (4.125)$$

where $P_{capt}(\cdot)$ is the probability of receiver's capture and also it represents the probability of a successful transmission. Using the results of (4.123)-(4.125), the throughput can be written as

$$S = \frac{GP_{capt}(z_0)}{G(1 + 2\bar{\tau}) + e^{-G\bar{\tau}}} \quad (4.126)$$

Rice Fading Channel

The Rice fading model assumes that the received signal is the result of a dominant component (such as a direct LOS signal) added to a large number of multipath scattered waves. Let X and Y be two independent Gaussian processes with zero mean and variances σ_X^2 and σ_Y^2 , respectively. The in-phase and quadrature components of the signal envelope in a Rice fading channel can be expressed as $X + a$ and Y , respectively, where the constant a represents the envelope of the dominant signal (also, the mean value for the in-phase component). Assuming that $\sigma^2 \triangleq \sigma_X^2 = \sigma_Y^2$, the PDF of the received signal envelope can be expressed as [2]

$$f_R(r) = \frac{r}{\sigma^2} e^{-\frac{r^2+a^2}{2\sigma^2}} I_0\left(\frac{ar}{\sigma^2}\right) \quad (4.127)$$

where $I_\nu(\cdot)$ is the modified Bessel function of the first kind and ν -th order [21, Eq. 9.6.10].

Let $\kappa \triangleq a^2/(2\sigma^2)$ be defined as power ratio between the dominant and scattered signals. It is easy to see that if κ is set to zero, thus eliminating the dominant component, the Rice distribution simplifies to the Rayleigh.

Let $W = R^2$ be the signal power and $\bar{w} = E\{R^2\}$ its average value, where $E\{\cdot\}$ represents expected value. The signal power PDF may be expressed as

$$f_W(w) = \frac{\kappa + 1}{\bar{w} e^\kappa} e^{-(\kappa+1)\frac{w}{\bar{w}}} I_0 \left[2\sqrt{\kappa(\kappa + 1)\frac{w}{\bar{w}}} \right]. \quad (4.128)$$

Hoyt Fading Channel

The Hoyt fading model assumes that the received signal is the result of the sum of a large number of multipath scattered waves, without the prevalence of a single component (for instance, the LOS signal). Let X and Y be two independent Gaussian processes with zero mean and variances σ_X^2 and σ_Y^2 , respectively. The PDF of the received signal envelope can be expressed as [17]

$$f_R(r) = \frac{r e^{-\frac{r^2}{4}\left(\frac{1}{\sigma_X^2} + \frac{1}{\sigma_Y^2}\right)}}{\sigma_X \sigma_Y} I_0 \left[\frac{r^2}{4} \left(\frac{1}{\sigma_Y^2} - \frac{1}{\sigma_X^2} \right) \right]. \quad (4.129)$$

Let $\eta \triangleq \sigma_X^2/\sigma_Y^2$ be defined as the power ratio between in-phase and quadrature signals. Also, let the parameters h and H be defined as

$$h \triangleq \frac{1}{4} \left(\frac{1}{\sqrt{\eta}} + \sqrt{\eta} \right)^2 \quad \text{and} \quad H \triangleq \frac{1}{4} \left(\frac{1}{\eta} - \eta \right). \quad (4.130)$$

Again, it is easy to see that if η is set to unity, thus $h = 1$ and $H = 0$ and Hoyt distribution simplifies to the Rayleigh distribution.

With $W = R^2$ and $\bar{w} = E\{R^2\}$ as defined earlier, the signal power PDF may be expressed as

$$f_W(w) = \frac{\sqrt{h}}{\bar{w}} e^{-h\frac{w}{\bar{w}}} I_0 \left(H\frac{w}{\bar{w}} \right). \quad (4.131)$$

Knowing that $\eta > 0$, it can be seen that the PDF in (4.131) is symmetrical around $\eta = 1$ [19]. Therefore, as far as the signal power distribution is concerned, considering either of the ranges $\eta \leq 1$ or $\eta \geq 1$ suffices.

Interference Signal

In a wireless system, interference typically results from signals arriving at the receiver's antenna from multiple transmitters. Depending on how these random signals combine during the observation interval, one of two scenarios might occur [1]: coherent addition or incoherent addition.

Coherent addition occurs if the carrier frequencies are equal and if the random phase fluctuations are small during the capture time t_w . For instance, coherent addition might happen when the deviation caused by the phase modulation is very small, and the observation interval is short compared to the modulation rate.

Let the phasor $x(t) = \text{Re}\{r(t) e^{j[w_c t + \theta(t)]}\}$ represent a signal reaching the receiver's antenna, where $r(t)$ and $\theta(t)$ are the random envelope and phase, respectively, and w_c is the carrier's angular frequency. For the coherent addition of n signals, the resulting phasor is [29]

$$x_n(t) = \sum_{i=1}^n x_i(t) \quad (4.132)$$

where the subscripts n and i represent the aggregate and individual variables, respectively.

Consider the Hoyt channel model described earlier, with its in-phase and quadrature Gaussian components. Since such channel is generated by the sum of Gaussian processes, further adding same-type phasors changes the parameters of the channel without changing its nature. In other words, the interference signal, assuming coherent addition, behaves as a Hoyt phasor, with the aggregate mean value equal to the sum of the individual mean values. As a result, the coherent addition of n uncorrelated Hoyt phasors produces a Hoyt phasor with mean value $\bar{w}_n = \sum_{i=1}^n \bar{w}_i$, in-phase signal power $\sigma_{X,n}^2 = \sum_{i=1}^n \sigma_{X,i}^2$, and quadrature signal power $\sigma_{Y,n}^2 = \sum_{i=1}^n \sigma_{Y,i}^2$. If the n phasors are independent and identically distributed (i.i.d.), the resulting phasor has $\bar{w}_n = n\bar{w}_i$, $\sigma_{X,n}^2 = n\sigma_{X,i}^2$, $\sigma_{Y,n}^2 = n\sigma_{Y,i}^2$, and $\eta_n = \eta_i$.

Incoherent addition occurs if the phases of the individual signals fluctuate significantly due to mutually independent modulation [29, 64]. In this case, the interference power w_n experienced

during the observation interval is the sum of the individual signals' powers w_i , i.e.,

$$w_n = \sum_{i=1}^n w_i = \sum_{i=1}^n \overline{x_i(t)x_i^*(t)} \quad (4.133)$$

where $x_i^*(\cdot)$ is the complex conjugate of phasor $x_i(\cdot)$. Considering the current work, where the signal power is a random variable, the PDF of the joint interference power is therefore the convolution of the PDFs of all contributing signal powers. If the individual components are i.i.d., then the interference power is expressed as the n -fold convolution of the PDF of the individual signal power.

4.6.3 Analytical Results

For the remaining of this application example and wherever applicable, the subscripts s , i and n are used to represent the desired signal variables, the interference signal's individual component variables, and the joint interference signal variables, respectively. For the calculations presented in this section, let (4.128) represent the desired signal power PDF and (4.131) the signal power PDF of an individual component of the interference signal. Also, for compactness, let \tilde{z}_0 be defined as $\tilde{z}_0 \triangleq z_0/(\bar{w}_s/\bar{w}_n)$ where the ratio \bar{w}_s/\bar{w}_n is commonly denoted as average SIR.

Coherent Addition

If coherent addition of phasors is assumed, then (4.131) should be used to represent the joint interference signal power PDF. Using the appropriate expressions in (4.118), and after some manipulation, the signal-to-interference CDF may be expressed as

$$F_Z(\tilde{z}_0) = \frac{u_1}{\sqrt{h_n}} \sum_{j=1}^{\infty} (1 - u_1)^j Q(j, \kappa_s) {}_2F_1 \left[\frac{j+1}{2}, \frac{j}{2} + 1, 1, \left(\frac{H_n}{h_n} u_1 \right)^2 \right] \quad (4.134)$$

where $Q(\cdot)$ is the regularized incomplete gamma function defined as $Q(a, b) = \Gamma(a, b)/\Gamma(a)$, $\Gamma(\cdot, \cdot)$ is the incomplete gamma function [21, Eq. 6.5.3], ${}_2F_1(\cdot)$ is the Gauss hypergeometric

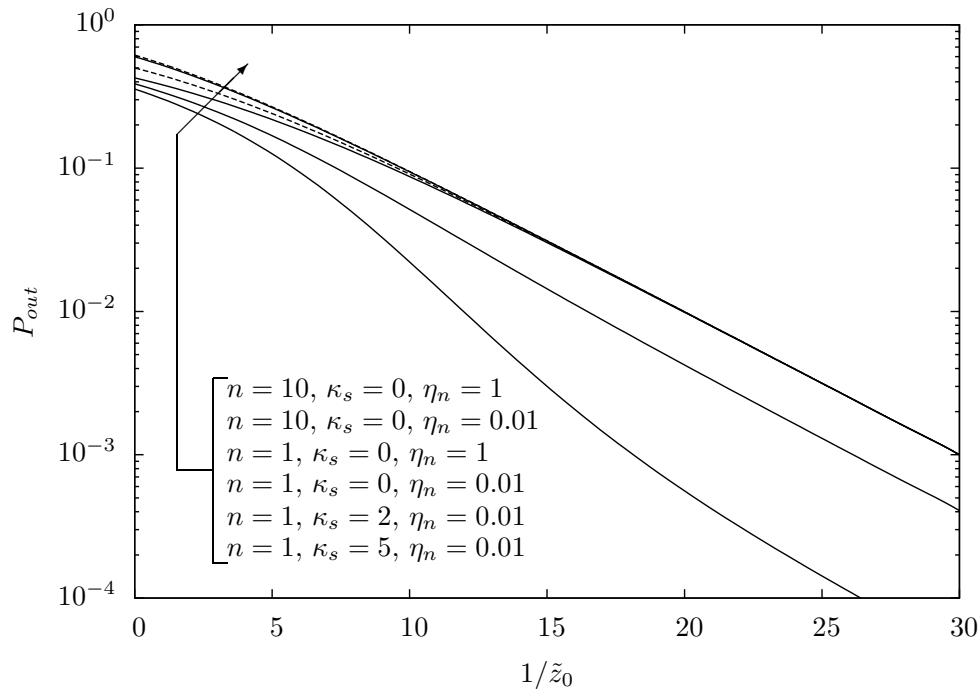


Figure 4.18: Outage probability for incoherent combined Rice and Hoyt channel. The dashed lines correspond to the Rayleigh channel ($\kappa_s = 0$ and $\eta_n = 1$).

function [21, Eq. 15.1.1], and

$$u_1 = \frac{h_n}{h_n + (\kappa_s + 1)\tilde{z}_0}. \quad (4.135)$$

It is interesting to note that (4.134) does not depend directly on the value of n . In other words, the statistics of the joint interference signal can be described using only the parameters η_n and \bar{w}_n , which is expected since this signal follows the Hoyt distribution.

Although (4.134) includes an infinite summation, the evaluation of the CDF converges rapidly for cases of interest. Let J be the maximum value of the index variable j in a truncated summation, i.e., $1 \leq j \leq J$. The entries for $n = 1$ in Table 4.5 give the value of J necessary to obtain a three-decimal-place accuracy (error < 0.0005) and a six-decimal-place accuracy (error < 0.000005) for the infinite summation of (4.134).

Incoherent Addition

For the incoherent addition, assume that the interference signal is composed of n i.i.d. variables. As a result, the joint interference signal power PDF is the n -fold convolution of the individual signal power PDF which, on its turn, is expressed by (4.131). This calculation gives

Table 4.5: Relation between number of terms and accuracy in the infinite summation of (4.134) and (4.137).

Parameters				smallest J for accuracy of	
n	κ_s	η_n	\tilde{z}_0	3-decimal-place	6-decimal-place
1	0.01	0.01	0.1	2	6
			1.0	9	25
			5.0	41	109
		0.5	0.1	2	4
			1.0	8	19
			5.0	31	78
	0.99	1.0	7	17	
		5.0	29	67	
	1.0	0.01	1.0	17	46
			5.0	80	211
		0.99	1.0	13	30
			5.0	55	128
	10.0	0.01	1.0	88	232
			5.0	431	1140
		0.99	1.0	60	140
			5.0	294	677
10	1.0	0.01	1.0	8	15
			5.0	29	50
		0.99	1.0	7	13
			5.0	24	39
	10.0	0.01	1.0	31	55
			5.0	141	243
		0.99	1.0	26	42
			5.0	115	178
50	1.0	0.01	5.0	21	32
		0.99	5.0	20	29
	10.0	0.01	5.0	94	130
		0.99	5.0	86	113

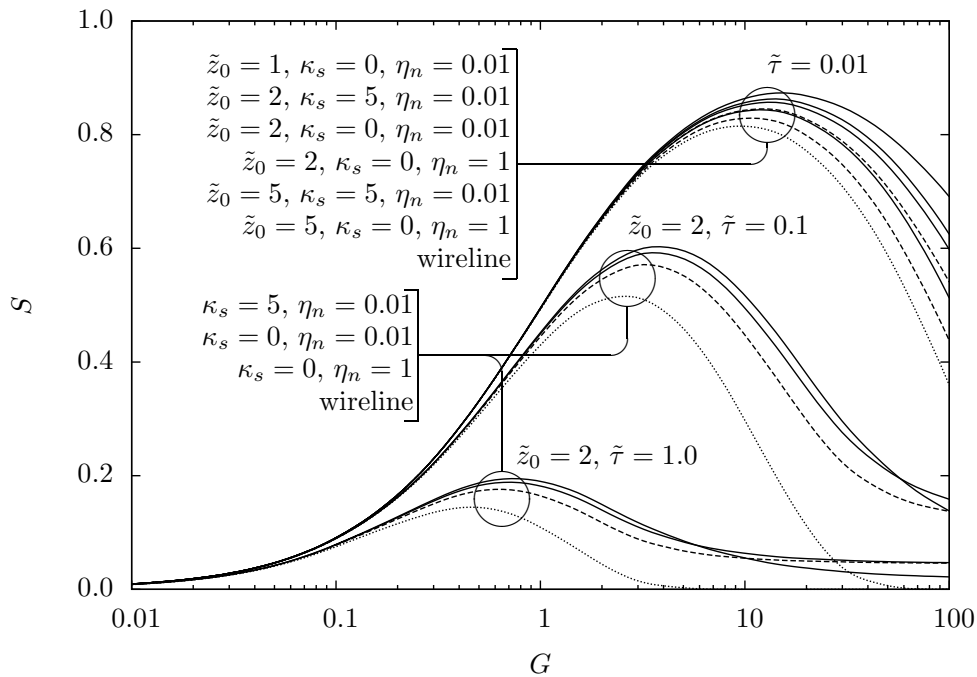


Figure 4.19: Throughput S for incoherent combined Rice and Hoyt channel with perfect power control. The dashed lines correspond to the Rayleigh channel ($\kappa_s = 0$ and $\eta_n = 1$). The dotted lines correspond to the wireline channel ($z_0 \rightarrow \infty$).

that

$$f_{W_n}(w_n) = \frac{\sqrt{\pi}}{\Gamma(\frac{n}{2})} n^{\frac{n+1}{2}} h_n^{\frac{n}{2}} \left(\frac{w_n}{2H_n \bar{w}_n} \right)^{\frac{n-1}{2}} \exp\left(-nh_n \frac{w_n}{\bar{w}_n}\right) I_{\frac{n-1}{2}}\left(nH_n \frac{w_n}{\bar{w}_n}\right) \quad (4.136)$$

where $\bar{w}_n = n\bar{w}_i$, $h_n = h_i$ and $H_n = H_i$. It can be seen that the n -fold convolution used to obtain (4.136) produced the $\eta - \mu$ distribution for $\mu = n/2$ [19].

Using the appropriate expressions in (4.118), and after some manipulation, the signal-to-interference CDF may be expressed as

$$F_Z(\tilde{z}_0) = \frac{u_n^n}{\sqrt{h_n^n}} \sum_{j=1}^{\infty} \frac{(1-u_n)^j Q(j, \kappa_s)}{jB(j, n)} {}_2F_1\left[\frac{j+n}{2}, \frac{j+n+1}{2}, \frac{n+1}{2}, \left(\frac{H_n}{h_n} u_n\right)^2\right] \quad (4.137)$$

where $B(\cdot)$ is the beta function [21, Eq. 6.2.2] and

$$u_n = \frac{nh_n}{nh_n + (\kappa_s + 1)\tilde{z}_0} \quad (4.138)$$

with $\bar{w}_n = n\bar{w}_i$, $\eta_n = \eta_i$, $h_n = h_i$ and $H_n = H_i$ since the n interfering signals are i.i.d..

Although (4.137) includes an infinite summation, the evaluation of the CDF converges rapidly for cases of interest. Let J be the maximum value of the index variable j (as defined earlier). Table 4.5 gives the value of J necessary to obtain a three-decimal-place accuracy (error < 0.0005) and a six-decimal-place accuracy (error < 0.0000005) for the infinite summation of (4.137).

4.6.4 Numerical Results

Outage Probability

The outage probabilities for the combined Rice and Hoyt channel, considering incoherent addition of interfering signals and perfect power control, is pictured in Fig. 4.18. In all cases the outage probability decreases with higher values of average SIR, as expected. In addition, using the results for the Rayleigh channel as a reference, the figures allow a comparison between these channels with regards to the outage probabilities. The figures show that higher fading intensity values translate into higher outage probabilities. Also, considering the average SIR value constant, the number of interfering signals n has only a minor influence on the outage probability.

Perfect Power Control

With the results obtained in the previous sections, using (4.120), (4.126) and (4.137), it is now possible to calculate the CSMA channel throughput for the combined Rice and Hoyt channel, assuming incoherent addition of interfering signals and perfect power control. Fig. 4.19 shows the throughput for various values of κ_s , η_n , \tilde{z}_0 and $\tilde{\tau}$.

The throughput graphs clearly indicate the important role the normalised worst case propagation delay $\tilde{\tau}$ plays to determine the channel throughput. Also, the higher the capture threshold is, the closer the curve is to the wireline results, which is expected since it indicates a diminished ability of receiver detection of the intended signal among the interfering signals. Examining same \tilde{z}_0 data, compared to the Rayleigh channel results, higher values of κ_s produce almost equal throughput when the throughput is around its maximum value, and slightly lower figures for

high mean offered traffic G . On the other hand, lower values of η_n produce slightly higher throughput when compared to Rayleigh channel results. In general, higher fading intensity values lead to higher throughput, in particular for heavier traffic (larger G).

4.6.5 Conclusions

This application example investigates the throughput performance of CSMA in a packet radio network and combined Rice and Hoyt fading environment. Analytical and numerical results are presented considering the signal capture model with coherent and incoherent addition of interfering signals. The approach considered includes the signal capture model with uniform attenuation for all terminals (or perfect power control). The results indicate that higher fading intensity, lower capture threshold or lower propagation delay contributes to higher channel throughput.

4.7 The Ratio of Independent Arbitrary α - μ Random Variables and its Application in the Capacity Analysis of Spectrum Sharing Systems⁸

4.7.1 Introduction

Many wireless communication performance measures (e.g., capacity, outage, interference, and others) involve the calculation of the ratio between signal powers. A relation typically of interest is the signal-to-interference ratio (SIR), i.e., the quotient of the desired signal power and the interference power, the latter one commonly found as the result of a sum of interfering signals. In addition, if the communication system is operating over a non-deterministic channel, such as a wireless fading channel, then the SIR involves the ratio of random variables (RVs), selected according to the channel model assumed. In such a case, the knowledge of the statistics of the SIR is key to assess the performance.

⁸This material was published in [77].

In this application example, general, simple, exact, closed-form expressions for the probability density function (PDF) and cumulative distribution function (CDF) for the ratio of independent non-identically distributed (i.n.i.d.) α - μ RVs [20] are derived. As an application example of our results, we provide a comprehensive capacity analysis of spectrum sharing systems undergoing α - μ fading. Although along the last years (see, for instance, [78, 79]) the capacity limits of spectrum sharing systems in traditional fading environments (i.e., Rayleigh, Nakagami- m) have been extensively investigated, such a study in a more generalized fading scenario, such as the α - μ model is still missing⁹. Relying upon the obtained results, a closed-form expression for the delay-limited capacity is derived. Furthermore, based on the power allocation related to the outage capacity, a closed-form expression for the corresponding minimum outage probability is attained. Finally, expressions for the ergodic capacity are also derived in closed-form considering an average interference power constraint. Numerical plots are shown in order to investigate the effect of the fading parameters in the system capacity. To the best of the authors' knowledge, these results are all unprecedented in the literature. Due to space constraint the derivations of our exact formulations are only, but clearly, hinted.

4.7.2 Ratio of Independent Arbitrary α - μ RVs

Let the RV $G \geq 0$ designate the instantaneous power, either the signal power or channel power gain, depending on the application. From [20, Eqs. (1) and (5)], the PDF of G can be expressed as

$$f_G(g) = \frac{\alpha \mu^\mu g^{\frac{\alpha}{2}\mu-1}}{2 \hat{g}^{\frac{\alpha}{2}\mu} \Gamma(\mu)} \exp \left[-\mu \left(\frac{g}{\hat{g}} \right)^{\frac{\alpha}{2}} \right], \quad (4.139)$$

in which $\alpha > 0$ denotes the non-linearity parameter, $\mu > 0$ is related to the number of multipath clusters, $\Gamma(\cdot)$ is the Gamma function [21, Eq. (6.1.1)], $\hat{g} \triangleq E\left(\sqrt[\frac{\alpha}{2}]{G}\right) = E(G)\mu^{\frac{2}{\alpha}}\Gamma(\mu)/\Gamma(\mu + \frac{2}{\alpha})$, and $E(\cdot)$ denotes expectation.

⁹In [80], the α - μ model has been considered, but the calculations were drastically facilitated since the links were assumed to be independent and identically distributed (i.i.d.).

Furthermore, let the RV X be defined as

$$X \triangleq \frac{G_N}{G_D}, \quad (4.140)$$

in which G_N and G_D are instantiations of the RV G . Assuming that G_N and G_D are statistically independent, the resulting PDF can be expressed as [47]

$$f_X(x) = \int_0^\infty t f_{G_N}(xt) f_{G_D}(t) dt, \quad (4.141)$$

with $f_{G_N}(\cdot)$ and $f_{G_D}(\cdot)$ denoting the PDFs of G_N and G_D , respectively.

Adding the appropriate subscripts in (4.139) and using it in (4.141), the PDF of X , $f_X(x)$, can be calculated after some algebraic manipulations [21, Eq. (4.2.1)], [48, Eq. (3.478.1)] as

$$f_X(x) = \frac{\alpha_D}{2x} \sum_{i=0}^{\infty} \frac{(-1)^i}{i!} \frac{(ux)^{-(\mu_D+i)\frac{\alpha_D}{2}}}{\beta\left(\frac{\alpha_D}{\alpha_N}, \mu_D, \mu_N, i\right)} \quad (4.142)$$

and, equivalently, as

$$f_X(x) = \frac{\alpha_N}{2x} \sum_{i=0}^{\infty} \frac{(-1)^i}{i!} \frac{(ux)^{(\mu_N+i)\frac{\alpha_N}{2}}}{\beta\left(\frac{\alpha_N}{\alpha_D}, \mu_N, \mu_D, i\right)}, \quad (4.143)$$

depending on which of the two exponential functions appearing in (4.141) the series expansion gets applied to. In the formulae, $\beta(r, m_0, m_1, i) = \Gamma(m_0)\Gamma(m_1)/\Gamma[(m_0 + i)r + m_1]$, and $u = (\mu_N)^{2/\alpha_N}/(\mu_D)^{2/\alpha_D} \times \hat{g}_D/\hat{g}_N$. Both (4.142) and (4.143) converge adequately and correctly, although because of their alternating series, convergence rate may rely upon the accuracy of the calculating machine. A useful and decisive alternative we propose here is to assume that $\alpha_N/\alpha_D = p/q$, for which $p \geq 1$ and $q \geq 1$ are co-prime integers, and then make use of [51, Eq. (2.3.2.13)].

Two situations are presented: for the case in which $p > q$, the result is given by

$$f_X(x) = \frac{\alpha_D}{2x} \sum_{i=0}^{p-1} \frac{(-1)^i}{i!} \frac{(ux)^{-(\mu_D+i)\frac{\alpha_D}{2}}}{\beta\left(\frac{q}{p}, \mu_D, \mu_N, i\right)} {}_{q+1}F_p \left[\Omega_{q,p}^{(1)}(\mu_D, \mu_N, i); \frac{q^q}{(-p)^p} (ux)^{-\frac{\alpha_D}{2}p} \right], \quad (4.144)$$

whereas if $p < q$, the result is given by

$$f_X(x) = \frac{\alpha_N}{2x} \sum_{i=0}^{q-1} \frac{(-1)^i}{i!} \frac{(ux)^{(\mu_N+i)\frac{\alpha_N}{2}}}{\beta\left(\frac{p}{q}, \mu_N, \mu_D, i\right)} {}_{p+1}F_q \left[\Omega_{p,q}^{(1)}(\mu_N, \mu_D, i); \frac{p^p}{(-q)^q} (ux)^{\frac{\alpha_N}{2}q} \right]. \quad (4.145)$$

In the formulae, ${}_pF_q(\cdot)$ represents the generalized hypergeometric function [48, Eq. (9.14.1)], $\Omega_{r_0, r_1}^{(1)}(m_0, m_1, i) = \{1, \Delta(r_0, (m_0+i)r_0/r_1+m_1); \Delta(r_1, i+1)\}$, and $\Delta(k, a) = \{a/k, (a+1)/k, \dots, (a+k-1)/k\}$.

If $p = q = 1$, thus making $\alpha_N = \alpha_D = \alpha$, and from [48, Eq. (3.381.4)], the PDF of X reduces to

$$f_X(x) = \frac{\alpha u(ux)^{\frac{\alpha}{2}\mu_N-1}}{2 B(\mu_N, \mu_D)} \left[1 + (ux)^{\frac{\alpha}{2}}\right]^{-\mu_N-\mu_D}, \quad (4.146)$$

for which $B(\cdot)$ denotes the beta function [21, Eq. (6.2.2)].

By its turn, the CDF of X can be calculated from (4.142), in closed-form, as

$$F_X(x) = 1 - \sum_{i=0}^{\infty} \frac{(-1)^i}{i!(\mu_D+i)} \frac{(ux)^{-\frac{\alpha_D}{2}(\mu_D+i)}}{\beta\left(\frac{\alpha_D}{\alpha_N}, \mu_D, \mu_N, i\right)}, \quad (4.147)$$

and, equivalently, using (4.143) as

$$F_X(x) = \sum_{i=0}^{\infty} \frac{(-1)^i}{i!(\mu_N+i)} \frac{(ux)^{(\mu_N+i)\frac{\alpha_N}{2}}}{\beta\left(\frac{\alpha_N}{\alpha_D}, \mu_N, \mu_D, i\right)}. \quad (4.148)$$

Now, let us use an approach similar to the one described above, with $\alpha_N/\alpha_D = p/q$ as already defined. Assuming $p > q$, the CDF of X can be expressed as

$$F_X(x) = 1 - \sum_{i=0}^{p-1} \frac{(-1)^i}{i!(\mu_D+i)} \frac{(ux)^{-\frac{\alpha_D}{2}(\mu_D+i)}}{\beta\left(\frac{q}{p}, \mu_D, \mu_N, i\right)} \\ {}_{q+2}F_{p+1} \left[\Omega_{q,p}^{(2)}(\mu_D, \mu_N, i); \frac{q^q}{(-p)^p} (ux)^{-\frac{\alpha_D}{2}p} \right]. \quad (4.149)$$

Equivalently, for $p < q$, the CDF of X can be expressed as

$$F_X(x) = \sum_{i=0}^{q-1} \frac{(-1)^i}{i!(\mu_N + i)} \frac{(ux)^{(\mu_N+i)\frac{\alpha_N}{2}}}{\beta\left(\frac{p}{q}, \mu_N, \mu_D, i\right)} \times {}_{p+2}F_{q+1} \left[\Omega_{p,q}^{(2)}(\mu_N, \mu_D, i); \frac{p^p}{(-q)^q} (ux)^{\frac{\alpha_N}{2}q} \right]. \quad (4.150)$$

In the formulae, $\Omega_{r_0, r_1}^{(2)}(m_0, m_1, i) = \{1, (m_0 + i)/r_1, \Delta(r_0, (m_0 + i)r_0/r_1 + m_1); (m_0 + i)/r_1 + 1, \Delta(r_1, i + 1)\}$.

If $p = q = 1$, thus making $\alpha_N = \alpha_D = \alpha$, the CDF of X reduces to

$$F_X(x) = \frac{(ux)^{\frac{\alpha\mu_N}{2}} {}_2F_1\left(\mu_N, \mu_N + \mu_D, \mu_N + 1, -(ux)^{\frac{\alpha}{2}}\right)}{\mu_N B(\mu_N, \mu_D)}, \quad (4.151)$$

in which ${}_2F_1(\cdot)$ denotes the Gauss hypergeometric function [21, Eq. (15.1.1)].

4.7.3 Application Example: Capacity Analysis of Spectrum Sharing Systems

System Model

Consider a spectrum sharing system over a block-fading channel in which a secondary user (SU) is allowed to use the spectrum licensed to the primary user (PU) as long as the interference power at the PU receiver remains below a certain threshold. Let G_0 and G_1 denote the instantaneous channel power gain from the SU transmitter (SU-Tx) to the PU receiver (PU-Rx) and SU receiver (SU-Rx), respectively, which are assumed to be independent, and of the flat fading type with channel coefficients following the α - μ distribution [20] and subject to additive white Gaussian noise (AWGN). In addition, the corresponding noise terms n_0 and n_1 are independent circularly symmetric complex Gaussian random variables with zero mean and variance N_0 [79]. Finally, perfect channel state information (CSI) on G_0 and G_1 is assumed to be available at the SU-Tx.

Let $P(G_0, G_1) \geq 0$ be the instantaneous transmit power at the SU-Tx for the channel gain

pair (G_0, G_1) . Also, since we consider as a constraint the interference power at the PU-Rx, let Q_{avg} and Q_{pk} denote the average and peak received power limits at the PU-Rx, respectively. Q_{avg} is a figure better suited for services in which the long-term Quality of Service (QoS) at the PU-Rx is more relevant, whereas Q_{pk} is more appropriate for services with an instantaneous QoS requirement. Clearly,

$$Q_{avg} \leq E[G_0 P(G_0, G_1)], \quad Q_{pk} \leq G_0 P(G_0, G_1). \quad (4.152)$$

Outage Capacity

Outage capacity is defined as the maximum constant rate that can be sustained with a given outage probability. Mathematically speaking, this is equivalent to minimize the outage probability for a given transmission rate R_0 . Assuming a peak interference power constraint Q_{pk} , our problem can be formulated as

$$\begin{cases} \text{minimize} & \Pr \left\{ \log_2 \left[1 + \frac{G_1 P(G_0, G_1)}{N_0} \right] < R_0 \right\}, \\ \text{subject to} & G_0 P(G_0, G_1) \leq Q_{pk}, \end{cases} \quad (4.153)$$

in which $\Pr\{\cdot\}$ denotes probability. It can be easily observed that (4.153) is minimized for $P(G_0, G_1) = Q_{pk}/G_0$, so that the outage probability can be expressed as

$$P_{out} = \Pr \left\{ \frac{G_1}{G_0} < \frac{N_0(2^{R_0} - 1)}{Q_{pk}} \right\}. \quad (4.154)$$

Note that the statistical distribution of the ratio G_1/G_0 is key for the calculation of (4.154). With $G_1 = G_N$ and $G_0 = G_D$ in (4.140), the PDF and the CDF of the ratio G_1/G_0 are already available. Therefore, the outage probability can be expressed in closed-form as

$$P_{out} = F_X \left(\frac{N_0(2^{R_0} - 1)}{Q_{pk}} \right), \quad (4.155)$$

with $F_X(\cdot)$ being either (4.147), (4.148), (4.149), (4.150) or (4.151).

Delay-Limited Capacity

The DLC is defined as the maximum constant transmission rate achievable over each of the fading blocks. Herein, we will analyze the DLC under the average interference power constraint Q_{avg} , because for the peak power case the DLC is easily proved to be zero. Our problem can therefore be formulated as

$$\begin{cases} \text{maximize} & \log_2 \left[1 + \frac{G_1 P(G_0, G_1)}{N_0} \right], \\ \text{subject to} & E[G_0 P(G_0, G_1)] \leq Q_{avg}. \end{cases} \quad (4.156)$$

In [79], it was shown that the optimal power allocation for this problem is given by

$$P(G_0, G_1) = \frac{Q_{avg}}{G_1 E(G_0/G_1)}. \quad (4.157)$$

Let again $G_1 = G_N$ and $G_0 = G_D$ in (4.140) and define $Y \triangleq G_0/G_1 = X^{-1}$. Using standard statistical procedures, the PDF of Y can be derived using the concepts of transformations of RVs [47] and calculated using the results presented in Section 4.7.2. The mean value of Y can be expressed by

$$E(Y) = \int_0^\infty \int_0^\infty y t f_{G_0}(yt) f_{G_1}(t) dt dy. \quad (4.158)$$

Changing the order of integration and using [48, Eq. (3.478.1)] to integrate first on y and then on t , the mean value of Y can be expressed now by

$$E(Y) = \frac{E(G_0)}{E(G_1)} \frac{\Gamma\left(\mu_1 + \frac{2}{\alpha_1}\right) \Gamma\left(\mu_1 - \frac{2}{\alpha_1}\right)}{\Gamma(\mu_1)^2}, \quad (4.159)$$

for $\mu_1 > 2/\alpha_1$. Noting that the constant transmission rate is maximized when $P(\cdot, \cdot)$ is maximized, the DLC can be attained in closed-form as

$$C_d = \log_2 \left[1 + \frac{E(G_1)}{E(G_0)} \frac{Q_{avg} \Gamma(\mu_1)^2}{N_0 \Gamma\left(\mu_1 + \frac{2}{\alpha_1}\right) \Gamma\left(\mu_1 - \frac{2}{\alpha_1}\right)} \right]. \quad (4.160)$$

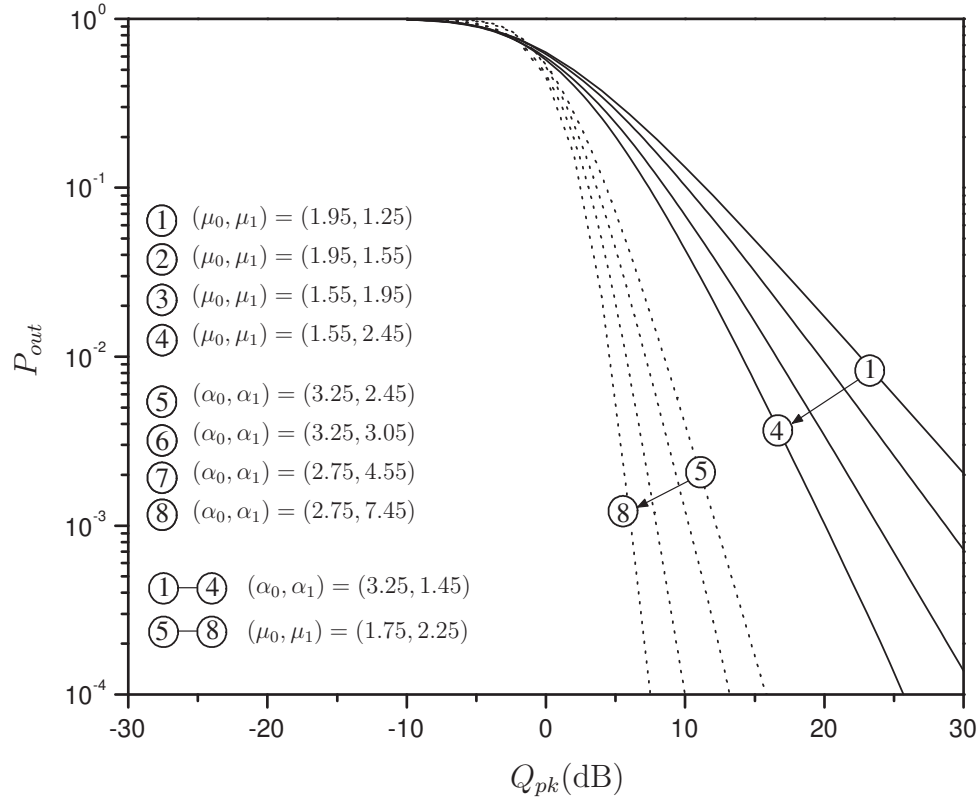


Figure 4.20: Outage probability versus Q_{pk} for different fading conditions.

Observe that, by setting $\mu_1 = 1$ and $\alpha_1 = 2$ (i.e., the Rayleigh case) in (4.160), the DLC equals zero. This is justified by the fact that, for the Rayleigh scenario, $E(Y)$ tends to infinity, being in accordance with the related results presented in the literature.

Ergodic Capacity

Ergodic capacity is defined as the maximum achievable rate averaged over all the fading blocks (long-term average). For the case of average interference power constraint, the optimization problem to be solved is

$$\begin{cases} \text{maximize} & E \left[\log_2 \left(1 + \frac{G_1 P(G_0, G_1)}{N_0} \right) \right], \\ \text{subject to} & E[G_0 P(G_0, G_1)] \leq Q_{avg}. \end{cases} \quad (4.161)$$

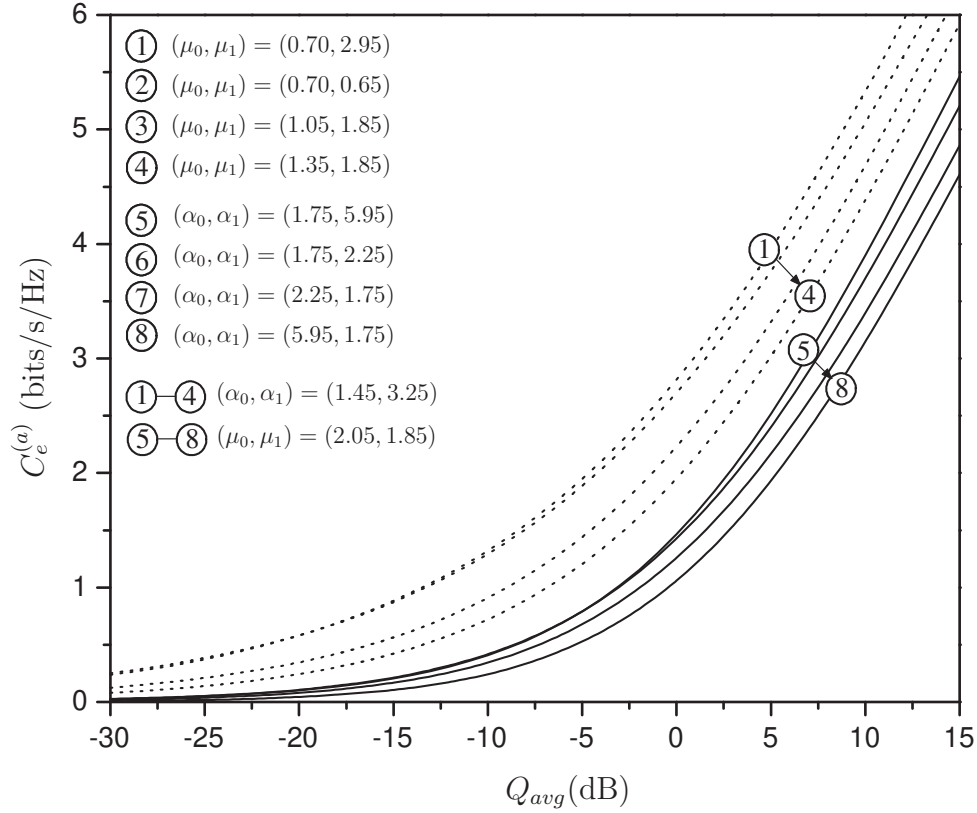


Figure 4.21: Ergodic capacity versus Q_{avg} for different fading conditions.

Then, employing a similar rationale to the one applied in [78, Sec. III], the ergodic capacity under average interference power constraint can be obtained as

$$C_e^{(a)} = \int_{\frac{1}{\gamma_0}}^{\infty} B \log_2(\gamma_0 x) f_X(x) dx, \quad (4.162)$$

in which B is the total available bandwidth, $\gamma_0 = 1/(\psi_0 N_0 B)$, and ψ_0 is calculated so that the average interference power in (4.162) equals Q_{avg} , i.e.,

$$\int_{G_0} \int_{G_1} \max\left(0, \frac{1}{\psi_0} - N_0 B \frac{G_0}{G_1}\right) f_{G_0}(g_0) f_{G_1}(g_1) dg_0 dg_1 = Q_{avg}, \quad (4.163)$$

in which $f_{G_i}(g_i)$, $i = 1, 2$ is the PDF given in (4.139).

Let $G_1 = G_N$ and $G_0 = G_D$ in (4.140). With an approach similar to that used earlier, the ergodic capacity under average interference power constraint, expressed by (4.162), can now be calculated. For some cases, however, the integral in (4.162) may diverge. A way to circumvent

this is to write (4.162) as

$$C_e^{(a)} = \widehat{C} - \int_0^{\frac{1}{\gamma_0}} B \log_2(\gamma_0 x) f_X(x) dx, \quad (4.164)$$

in which

$$\widehat{C} = \int_0^\infty B \log_2(\gamma_0 x) f_X(x) dx. \quad (4.165)$$

The introduction of \widehat{C} is decisive because it removes the infinity as one of the limits of integration in (4.162), thence convergence is always attained.

The value of \widehat{C} can be calculated using (4.141) in (4.165), changing the order of integration and using [48, Eq. (4.352.1)] to integrate first on x and then using [48, Eqs. (3.478.1) and (4.352.1)] to integrate on t . The result is given by

$$\widehat{C} = \frac{B}{\ln(2)} \left[\ln\left(\frac{\gamma_0}{u}\right) - \frac{2}{\alpha_0} \psi(\mu_0) + \frac{2}{\alpha_1} \psi(\mu_1) \right] \quad (4.166)$$

in which $\psi(\cdot)$ is the psi (digamma) function [21, Eq. (6.3.1)].

Using (4.162) with (4.142) and (4.164) with (4.143), the ergodic capacity can be expressed by

$$C_e^{(a)} = \frac{2B}{\alpha_0 \ln(2)} \sum_{i=0}^{\infty} \frac{(-1)^i}{i!(\mu_0 + i)^2} \frac{\left(\frac{\gamma_0}{u}\right)^{\frac{\alpha_0}{2}(\mu_0 + i)}}{\beta\left(\frac{\alpha_0}{\alpha_1}, \mu_0, \mu_1, i\right)}, \quad (4.167)$$

and

$$C_e^{(a)} = \widehat{C} + \frac{2B}{\alpha_1 \ln(2)} \sum_{i=0}^{\infty} \frac{(-1)^i}{i!(\mu_1 + i)^2} \frac{\left(\frac{u}{\gamma_0}\right)^{\frac{\alpha_1}{2}(\mu_1 + i)}}{\beta\left(\frac{\alpha_1}{\alpha_0}, \mu_1, \mu_0, i\right)}, \quad (4.168)$$

respectively. Applying an approach similar to the one described earlier, let $\alpha_1/\alpha_0 = p/q$ as already defined, and use this assumption to rewrite (4.167) and (4.168). For $p > q$, (4.167) is used and the result is given by

$$C_e^{(a)} = \frac{2B}{\alpha_0 \ln(2)} \sum_{i=0}^{p-1} \frac{(-1)^i}{i!(\mu_0 + i)^2} \frac{\left(\frac{\gamma_0}{u}\right)^{\frac{\alpha_0}{2}(\mu_0 + i)}}{\beta\left(\frac{q}{p}, \mu_0, \mu_1, i\right)} \times {}_{q+3}F_{p+2} \left[\Omega_{q,p}^{(3)}(\mu_0, \mu_1, i); \frac{q^q}{(-p)^p} \left(\frac{\gamma_0}{u}\right)^{\frac{\alpha_0}{2}p} \right]; \quad (4.169)$$

and for $p < q$, (4.168) is used and the result is given by

$$\begin{aligned}
 C_e^{(a)} &= \widehat{C} + \frac{2B}{\alpha_1 \ln(2)} \sum_{i=0}^{q-1} \frac{(-1)^i \left(\frac{u}{\gamma_0}\right)^{\frac{\alpha_1}{2}(\mu_1+i)}}{i!(\mu_1+i)^2 \beta\left(\frac{p}{q}, \mu_1, \mu_0\right)} \\
 &\times {}_{p+3}F_{q+2} \left[\Omega_{p,q}^{(3)}(\mu_1, \mu_0, i); \frac{p^p}{(-q)^q} \left(\frac{u}{\gamma_0}\right)^{\frac{\alpha_1}{2}q} \right].
 \end{aligned} \tag{4.170}$$

In the formulae, $\Omega_{r_0, r_1}^{(3)}(m_0, m_1, i) = \{1, (m_0+i)/r_1, (m_0+i)/r_1, \Delta(r_0, (m_0+i)r_0/r_1+m_1); (m_0+i)/r_1+1, (m_0+i)/r_1+1, \Delta(r_1, i+1)\}$. If $p = q = 1$, thus making $\alpha_0 = \alpha_1 = \alpha$, the ergodic capacity reduces to

$$\begin{aligned}
 C_e^{(a)} &= \frac{2B}{\alpha \ln(2)} \frac{1}{\mu_0^2 B(\mu_0, \mu_1)} \left(\frac{\gamma_0}{u}\right)^{\frac{\alpha}{2}\mu_0} \\
 &\times {}_3F_2 \left[\mu_0, \mu_0, \mu_0 + \mu_1; \mu_0 + 1, \mu_0 + 1; -\left(\frac{\gamma_0}{u}\right)^{\frac{\alpha}{2}} \right].
 \end{aligned} \tag{4.171}$$

4.7.4 Numerical Results and Discussions

This section shows some plots to illustrate the use of the exact expressions derived in this application example. Without loss of generality, it is assumed that $E(G_0) = E(G_1) = 1$. Fig. 4.20 shows the outage probability versus the peak interference power constraint assuming $N_0 = 1$ and $R_0 = 1$ bit/s/Hz, and varying fading parameters. First, note that the curves are close together when Q_{pk} is lower than 0 dB, indicating that the fading scenario does not affect considerably the outage capacity performance for small values of the peak interference power constraint. Interestingly, it can be noted that at 0 dB ($Q_{pk} = N_0 (2^{R_0} - 1)$), the outage is independent of the fading scenario, which is consistent with our analysis in Sec. III-B. As expected, the outage diminishes with the increase of Q_{pk} . Note also in Fig. 4.20 that, as the fading condition at the interfering link improves (higher α_0 or higher μ_0), the probability of outage increases, which is consistent with the fact that, in such a case, the peak power at the primary user receiver may have a higher chance of being reached. Fig. 4.21 shows the ergodic capacity as a function of the average interference power constraint for the various fading scenarios. Of course, the capacity increases as the interference power constraint is loosened

(higher Q_{avg}). The most interesting analysis, however, concerns how the fading scenarios affect the capacity. It can be seen that as α_0 or μ_0 increase, i.e. the fading condition of the interfering link improves, the ergodic capacity diminishes. In the same way, in Fig. 4.21, it can be seen that as α_1 or μ_1 increase, i.e. the fading condition of the target link improves, the ergodic capacity also increases. Both analysis are physically consistent, attesting the consistency of the exact formulations derived here. The curves for the DLC are not shown here, but the observations made for the ergodic capacity are also valid for DLC.

4.8 Exact Formulations for the Throughput of IEEE 802.11 DCF in Hoyt, Rice, and Nakagami- m Fading Channels¹⁰

4.8.1 Introduction

Wireless local area networks (WLANs) have been experiencing rapid development lately in part stimulated by the deployment of systems compatible with the IEEE 802.11 standards [82]. They offer data communication capability between terminals within radio range while allowing a certain degree of mobility. These networks are organized either with or without a central node. In the cellular topology, a central node is responsible for controlling the access to the wireless medium and forwarding data to the intended users. In ad-hoc topologies, the central node is absent and all terminals share similar capabilities and responsibilities; the terminals can communicate with each other either directly or by routing their data through intermediate nodes. In either case, the aims are to provide connectivity among terminals and to efficiently and fairly dispense the available bandwidth while employing little or no central coordination.

In order to serve terminals exhibiting bursty traffic behavior, WLANs make use of packet radio techniques with random access to a transmission channel shared by multiple users. Specifically, variations of carrier sense multiple access (CSMA) protocols and, in particular, of CSMA with collision avoidance (CSMA/CA), are generally used to access the wireless medium [57, 83, 84, 85, 86, 87, 88]. The capacity of the channel is then influenced by the probability of packet collision and by the signal degradation due to mutual interference and signal attenuation. In other words, it is influenced by the medium contention resolution algorithm and by the channel characteristics. Currently, it is fair to say that the use of CSMA/CA is wide, and it has been growing continually, with very recent adoption by some other IEEE standards [89, 90].

Intuitively, one might expect that original (wireline) CSMA systems show better performance than wireless ones because of the more hostile channel characteristics found in the latter.

¹⁰This material was submitted to [81].

However, this is not necessarily the case. For instance, in a channel model that takes into account the effects of fading, competing packets arriving at a common radio receiver antenna will not always destroy each other because they may show different and independent fading and attenuation levels [58, 59]. This leads to infer that wireless CSMA systems may actually exhibit successful reception rate higher than that of wireline ones. In fact, Arnbak and Blitterswijk have shown this to happen with slotted Aloha over Rayleigh fading channels [29].

A practical and more sophisticated implementation of the CSMA/CA protocol is the IEEE 802.11. Such a system specifies two operating modes: the Point Coordination Function (PCF) and the Distributed Coordination Function (DCF). The former is an access method planned to be implemented in an infrastructured network. The latter, which is similar to CSMA/CA, is the main focus of this work.

In this application example, we investigate the throughput performance of IEEE 802.11 DCF with Hoyt, Rice and Nakagami- m fading environments and capture effect. The performance of IEEE 802.11 DCF with unsaturated traffic and non-ideal channel is presented in [91] and it is here extended to these fading scenarios. The evolution of the performance analysis of IEEE 802.11 DCF has been conducted in the following steps. Bianchi [92] presented analytical results and simulation for the performance of IEEE 802.11 DCF assuming ideal channel conditions, finite number of terminals and saturated traffic. In [92], the MAC algorithm is modeled by a two dimensional Markov chain. Liaw *et al.* [93] added an idle state to the Markov chain of Bianchi's model, this way extending it to unsaturated traffic conditions, however keeping the channel ideal. Daneshgaran *et al.* [91] further extended the analysis to include non-ideal channel conditions and capture effect. In [91], the authors assume Rayleigh fading channel and they use simulation to validate their results.

The IEEE 802.11 DCF is a commercially available, widely used and practical system and it is interesting to see it evaluated with generic and potentially more realistic fading models. In addition, for the sake of comparison, results for CSMA/CA in similar fading conditions are also presented. The work presented here introduces a number of exact closed-form as well as exact series-based expressions. To the best of the authors' knowledge, unless otherwise cited, these

results are novel contributions. As an intermediate outcome of the calculation, novel results for the outage probability for these environments are also introduced. Analysis of the outage probability for fading channels has been an active investigation topic for the last few years [72, 35, 94, 73, 74, 39], in part because it may be used to estimate the performance of spectrum sharing systems. The work presented here offers contributions in this area and introduces many original results.

The channel models considered in this work are among those commonly used to describe the short-term signal statistics of wireless communications links subject to fading [2, 66, 67]. The Rice model (also known as Nakagami- n) is used when the random multipath signals are superimposed on a nonfading dominant signal, for instance, when a line-of-sight (LOS) component is present. The Hoyt model (also known as Nakagami- q) applies to the cases when no dominant signal is present and the in-phase and quadrature components of the received signal have non-identical powers or, otherwise, are correlated. Finally, the Nakagami- m model was inferred by Nakagami [18] from experimental data. Its distribution can approximate the Hoyt and Rice distributions, and it includes as special cases the one-sided Gaussian and the Rayleigh distributions.

In this application example, the channel is considered to be memoryless, i.e., failures to capture the channel and future attempts are uncorrelated. In addition, all packets are assumed to have fixed length and to require p seconds to transmit, and that the 2-way handshaking mechanism is used for the packet transmissions. The 4-way handshaking, with the “Request to Send” (RTS) and “Clear to Send” (CTS) messages is not considered here and might be a topic for future work. Also, the analysis makes distinction between usefull (data) traffic and overhead (control) traffic. Finally, each packet is assumed to have a single destination.

This application example is organized as follows. Sections 4.8.2 describes the framework used in this application example, while Section 4.8.3 applies it to the particular scenario assumed here. Section 4.8.4 considers the cases of incoherent signal addition at the receiver’s antenna with uniform attenuation for all terminals (or perfect power control). Coherent signal addition and a model that includes spatial coverage, such as in a cell, are also explored. Numerical results

and conclusions are given in Sections 4.8.5 and 4.8.6, respectively.

4.8.2 Framework

Consider a generic packet data communication system. If the transmission of an arbitrary test packet is performed over a wireline channel, it is generally assumed that a successful reception can only occur if no other transmission attempt is made during the test packet reception, i.e., if there is no signal overlap at the receiver's end. However, in wireless systems the radio receiver may be able to be captured by a test packet, even in the presence of n interfering packets, provided the power ratio between the test signal and the joint interfering signal exceeds a certain threshold during a given portion of the transmission period t_w , $0 < t_w < p$, to lock the receiver [61, 62]. In such a case, the test packet is only destroyed if

$$\frac{w_s}{w_n} \leq z \quad \text{during } t_w, \text{ with } n > 0, \quad (4.172)$$

where z is the capture ratio, and w_s and w_n are the test packet power and the joint interference power at the receiver's antenna, respectively. Values for z and the capture window t_w depend on, e.g., the modulation and the coding employed by the network. For a typical narrowband FM receiver, a z value of 6 dB is suggested in [63]. The details about estimating the values of z and t_w are beyond the scope of this application example. The interested reader can find further information about the capture effect in the literature, including [95, 96, 97, 98].

For the wireless channel, for which the signal assumes a random behavior, the capture phenomenon should, accordingly, be treated statistically. Let the random variable Z be defined as the signal-to-interference ratio (SIR)

$$Z \triangleq \frac{W_s}{W_n} \geq 0, \quad (4.173)$$

where $W_s \geq 0$ and $W_n \geq 0$ are random variables representing the desired signal power and the interference power at the receiver's antenna, respectively, with the latter one assumed to be an n -signal ensemble. If W_s and W_n are statistically independent, the resulting probability density

function (PDF) can be expressed as [47]

$$f_Z(z) = \int_0^\infty y f_{W_s}(zy) f_{W_n}(y) dy \quad (4.174)$$

where $f_{W_s}(\cdot)$ and $f_{W_n}(\cdot)$ are the PDFs of the desired signal power and the interference power, respectively. The cumulative distribution function (CDF) is then expressed as

$$F_Z(z_0) = \text{Prob} \left\{ \frac{W_s}{W_n} \leq z_0 \right\} = \int_0^{z_0} f_Z(z) dz. \quad (4.175)$$

If n is known and fixed, the resulting conditional capture probability may be expressed as

$$P_{cap}(z_0|n) = 1 - F_Z(z_0). \quad (4.176)$$

Of course, the statistics of W_s and W_n depend on the channel characteristics, and, in the current work, on the fading model used.

In order to produce the unconditional capture probability, let γ be defined as the probability that a station starts a transmission in a randomly chosen time slot, with γ assumed to be constant across all time slots. Considering a scenario in which there are N stations apt to transmit, the unconditional probability of a test packet being able to capture the receiver in an arbitrary transmission period may be expressed by

$$P_{cap}(z_0) = \sum_{n=1}^{N-1} \binom{N}{n+1} \gamma^{n+1} (1-\gamma)^{N-n-1} P_{cap}(z_0|n). \quad (4.177)$$

Hence, given the conditions described above, (4.177) yields the probability of successful reception.

Furthermore, let S represent the normalized channel throughput (or channel efficiency), defined as the fraction of time the channel is used to successfully transmit user information. It can be expressed as $S = G \times P_{cap}(z_0)$, where G is the offered traffic. In other words, S is evaluated as the portion of the offered traffic that is successfully received.

It is interesting to note that the CDF in (4.175) also represents another important measure of

performance for wireless systems: the outage probability. This is defined as the probability that the SIR at the reference receiver falls below a certain specified threshold required for successful reception. Therefore $P_{out}(z_0) = F_Z(z_0)$, where z_0 is the successful reception threshold.

Another relevant aspect of our investigation is how the interfering signal arises. In a wireless system, it typically results from signals arriving at the receiver's antenna from multiple transmitters. Depending on how these random signals combine during the observation interval, one of two scenarios might occur [1]: coherent addition or incoherent addition.

Coherent addition occurs if the carrier frequencies are equal and if the random phase fluctuations are small during the capture time t_w . For instance, coherent addition might happen when the deviation caused by the phase modulation is very small, and the observation interval is short compared to the modulation rate. In other words, coherent addition should be considered if the random phases of the individual interferers barely vary during the capture period. Incoherent addition occurs if the phases of the individual signals fluctuate significantly due to mutually independent modulation [29, 64].

Let the phasor $x(t) = \text{Re}\{r(t)e^{j[w_c t + \theta(t)]}\}$ represent a signal reaching the receiver's antenna, where $r(t)$ and $\theta(t)$ are the random envelope and phase, respectively, and w_c is the carrier's angular frequency. For the coherent addition of n signals, the resulting phasor is [29]

$$x_n(t) = \sum_{i=1}^n x_i(t) \quad (4.178)$$

where the subscripts n and i represent the aggregate and individual variables, respectively.

For the incoherent addition, the interference power w_n experienced during the observation interval is the sum of the individual signals' powers w_i , i.e.,

$$w_n = \sum_{i=1}^n w_i = \sum_{i=1}^n \overline{x_i(t)x_i^*(t)} \quad (4.179)$$

where $x_i^*(\cdot)$ is the complex conjugate of phasor $x_i(\cdot)$. Considering the current work, where the signal power is a random variable, the PDF of the joint interference power is therefore the convolution of the PDFs of all contributing signal powers. If the individual components are

independent and identically distributed (i.i.d.), then the interference power is expressed as the n -fold convolution of the PDF of the individual signal power.

In the next section, the concepts introduced here are tailored to the specific scenario of the current work.

4.8.3 System Model

Medium Access Mechanism

The IEEE 802.11 DCF standard [82] is the communication system considered in this work. It uses CSMA/CA as its medium contention resolution algorithm and, in essence, a terminal ready to transmit first senses the channel for a period of at least a Distributed Interframe Space (DIFS). If it senses the channel idle, it transmits its packet. Otherwise, it schedules the (re)transmission of the packet to a later time according to some randomly distributed retransmission delay. After the retransmission delay has elapsed, the terminal repeats the procedure described above. A binary exponential backoff algorithm is used to determine the retransmission delay. The delay is uniformly chosen in the interval $[0, CW_i - 1]$, where CW_i is the contention window size at the backoff stage i , $i = 0, \dots, m$. At the first transmission attempt ($i = 0$), the contention window size is set to its minimum value $CW_0 = CW_{min}$. After each unsuccessful transmission, the backoff stage i is incremented up to the value of m and the contention window is doubled up to its maximum value $CW_m = CW_{max} = 2^m CW_{min}$.

Consider a setting with unsaturated traffic generated by N contending stations, non-ideal transmission channel, capture effect, and that the number of packets generated in the network for new messages plus retransmissions follows the Poisson distribution, with mean generation rate of λ packets per second. For such a scenario, Daneshgaran *et al.* [91] use a two-dimensional Markov process to model the protocol's behavior and produces a channel throughput given by

$$S = \frac{P_t P_s (1 - P_e) E\{PL\}}{(1 - P_t)\sigma + P_t(1 - P_s)T_c + P_t P_s (1 - P_e)T_s + P_t P_s P_e T_e}, \quad (4.180)$$

in which: (i) P_t is the probability that, in the considered time slot, at least one of the contending

stations is transmitting; (ii) P_s is the probability that a packet transmission is successful; (iii) P_e is the probability that errors due to the channel may occur on a transmitted packet; (iv) $E\{PL\}$ is the average packet payload length; (v) σ is the duration of an empty time slot; and (vi) T_c , T_e and T_s are the average times a channel is sensed busy due to a collision, an error affected data frame transmission and a successful data frame transmission, respectively. In order to calculate the channel throughput in (4.180), the analysis leads to the set of equations given below, which should be treated as a nonlinear system and should be solved numerically [91]:

$$\begin{aligned}
P_t &= 1 - (1 - \gamma)^N; \\
P_s &= \frac{N\gamma(1 - \gamma)^{N-1} + P_{cap}(z_0)}{P_t} \\
P_{col} &= 1 - (1 - \gamma)^{N-1} - P_{cap}(z_0) \\
P_{eq} &= (1 - P_e)(1 - P_{col}) = P_e + P_{col} - P_e P_{col} \\
\gamma &= \frac{2(1 - 2P_{eq})q}{q[(CW + 1)(1 - 2P_{eq}) + CW P_{eq}(1 - (2P_{eq})^m)] + 2(1 - q)(1 - P_{eq})(1 - 2P_{eq})} \\
q &= 1 - e^{-\lambda E\{S_{ts}\}} \\
E\{S_{ts}\} &= (1 - P_t)\sigma + P_t(1 - P_s)T_c + P_t P_s(1 - P_e)T_s + P_t P_s P_e T_e,
\end{aligned} \tag{4.181}$$

in which: (i) P_{col} is the probability that collisions may occur on a transmitted packet; (ii) P_{eq} is the probability of failed transmission; (iii) q is the probability that there is at least one packet to be transmitted in the buffer; and (iv) $E\{S_{ts}\}$ is the expected time per slot.

In the current work, the Poisson model is used to describe the traffic generation process, i.e., the packet transmission requests from the upper layers. Accordingly, the resulting inter-arrival time is exponentially distributed. Although the Poisson model may not well represent bursty packet data traffic, it offers an approach that is simple, tractable and currently widely used [99, 100, 101, 102].

For the sake of comparison, the analysis of channel throughput for the CSMA/CA is also performed. In this case, a similar analysis to the one presented above for the IEEE 802.11 DCF is assumed, with a difference that for the former a single-stage backoff algorithm is used to determine the retransmission delay, i.e., $m = 0$, with $CW_{min} = CW_{max}$

Channel Models

For the calculations presented in this subsection, as well as for the remaining of this application example, let r represents the received signal envelope, $w = r^2$ the received signal power, and \bar{w} its average value.

Hoyt Fading Channel. The Hoyt fading model assumes that the received signal is the result of the sum of a large number of multipath scattered waves, without the prevalence of a single component (for instance, the LOS signal) [17]. Let x and y be two independent Gaussian processes with zero mean and variances σ_x^2 and σ_y^2 , respectively. The PDF of the received signal envelope can be expressed as [17]

$$f_R(r) = \frac{r}{\sigma_x \sigma_y} \exp \left[-\frac{r^2}{4} \left(\frac{1}{\sigma_x^2} + \frac{1}{\sigma_y^2} \right) \right] I_0 \left[\frac{r^2}{4} \left(\frac{1}{\sigma_y^2} - \frac{1}{\sigma_x^2} \right) \right] \quad (4.182)$$

where $I_\nu(\cdot)$ is the modified Bessel function of the first kind and ν -th order [21, Eq. 9.6.10].

The signal power PDF may be expressed as

$$f_W(w) = \frac{\sqrt{h}}{\bar{w}} \exp \left(-h \frac{w}{\bar{w}} \right) I_0 \left(H \frac{w}{\bar{w}} \right) \quad (4.183)$$

where $\bar{w} = \sigma_x^2 + \sigma_y^2$, $h \triangleq \frac{1}{4} \left(\frac{1}{\sqrt{\eta}} + \sqrt{\eta} \right)^2$, $H \triangleq \frac{1}{4} \left(\frac{1}{\eta} - \eta \right)$, and $\eta \triangleq \sigma_x^2 / \sigma_y^2$ is the power ratio between the in-phase and quadrature signals. Knowing that $\eta > 0$, it can be seen that the PDF in (4.183) is symmetrical around $\eta = 1$ [19]. Therefore, as far as the signal power distribution is concerned, considering either of the ranges $\eta \leq 1$ or $\eta \geq 1$ suffices. Also, it is easy to see that if η is set to unity, thus making $\sigma_x^2 = \sigma_y^2$, the Hoyt distribution simplifies to the Rayleigh one.

Considering the way the Hoyt phasor is produced, with its in-phase and quadrature Gaussian components, it is easy to see that the coherent addition of n uncorrelated Hoyt phasors also produces a Hoyt phasor with aggregate mean value $\bar{w}_n = \sum_{i=1}^n \bar{w}_i$, in-phase signal power $\sigma_{X,n}^2 = \sum_{i=1}^n \sigma_{X,i}^2$, and quadrature signal power $\sigma_{Y,n}^2 = \sum_{i=1}^n \sigma_{Y,i}^2$. If the n phasors are i.i.d., the resulting phasor has $\bar{w}_n = n\bar{w}_i$, $\sigma_{X,n}^2 = n\sigma_{X,i}^2$, $\sigma_{Y,n}^2 = n\sigma_{Y,i}^2$, and $\eta_n = \eta_i$.

Rice Fading Channel. The Rice fading model assumes that the received signal is the result of a dominant component (such as a direct LOS signal) added to a large number of multipath

scattered waves. Let x and y be two independent Gaussian processes with zero mean and equal variances σ^2 . The in-phase and quadrature components of the signal envelope in a Rice fading channel can be expressed as $x + a$ and y , respectively, where the constant a represents the envelope of the dominant signal (also, the mean value for the in-phase component). The PDF of the received signal envelope can be expressed as [2]

$$f_R(r) = \frac{r}{\sigma^2} \exp\left(-\frac{r^2 + a^2}{2\sigma^2}\right) I_0\left(\frac{ar}{\sigma^2}\right). \quad (4.184)$$

The signal power PDF may be expressed as

$$f_W(w) = \frac{\kappa + 1}{\bar{w} e^\kappa} \exp\left[-(\kappa + 1)\frac{w}{\bar{w}}\right] I_0\left(2\sqrt{\kappa(\kappa + 1)}\frac{w}{\bar{w}}\right) \quad (4.185)$$

where $\bar{w} = a^2 + 2\sigma^2 = 2\sigma^2(\kappa + 1)$, and $\kappa \triangleq a^2/(2\sigma^2)$ is the power ratio between the dominant and scattered signals. It is easy to see that if κ is set to zero, thus eliminating the dominant component, the Rice distribution simplifies to the Rayleigh one.

Similarly to the Hoyt case described above, the coherent addition of n uncorrelated Rice phasors produces a Rice phasor with aggregate mean value $\bar{w}_n = \sum_{i=1}^n \bar{w}_i$, dominant signal power $a_n^2 = \sum_{i=1}^n a_i^2$, and scattered signal power $\sigma_n^2 = \sum_{i=1}^n \sigma_i^2$. If the n phasors are i.i.d., the resulting phasor has $\bar{w}_n = n\bar{w}_i$, $a_n^2 = na_i^2$, $\sigma_n^2 = n\sigma_i^2$, and $\kappa_n = \kappa_i$.

Nakagami- m Fading Channel. In a Nakagami fading channel, PDF of the signal envelope is given by [18]

$$f_R(r) = \frac{2r^{2m-1}}{\Gamma(m)} \left(\frac{m}{\hat{r}^2}\right)^m \exp\left(-\frac{mr^2}{\hat{r}^2}\right) \quad (4.186)$$

where $\hat{r}^2 \triangleq E\{r^2\}$ is the mean square value, $m \geq 0$ is a fading parameter, and $\Gamma(\cdot)$ is the gamma function [21, Eq. 6.1.1]. For $m = 1/2$, the Nakagami distribution reduces to the one-sided Gaussian PDF; for $m = 1$, it reduces to the Rayleigh PDF while $m \rightarrow \infty$ corresponds to a non-fading situation. The signal power PDF may be expressed as

$$f_W(w) = \frac{w^{m-1}}{\Gamma(m)} \left(\frac{m}{\bar{w}}\right)^m \exp\left(-\frac{mw}{\bar{w}}\right). \quad (4.187)$$

For the Nakagami- m channel, treatment of coherent addition of signals is still under investigation by the authors. The main problem is that the exact analysis leads to very intricate formulation and the idea to use some approximation has not yet produced interesting results.

4.8.4 Analytical Results

For the remaining of this application example and wherever applicable, the subscripts s , i and n are used to represent the desired signal variables, the interference signal's individual component variables, and the joint interference signal variables, respectively. Also, for compactness, let \tilde{z}_0 be defined as $\tilde{z}_0 \triangleq z_0/(\bar{w}_s/\bar{w}_n)$ where the ratio \bar{w}_s/\bar{w}_n is commonly denoted as the average SIR.

Perfect Power Control

Hoyt Fading Channel. For the calculations presented in this subsection, let (4.183) represent the desired signal power PDF as well as, with different parameters, the signal power PDF of an individual component of the interference signal.

If coherent addition of phasors is assumed, then (4.183) should be used to represent the joint interference signal power PDF. With (4.174) and (4.175), changing the integration order, using [21, Eq. 9.6.10], integrating over z (see [48, Eq. 3.351.1]), and using [103], the integral solves to

$$F_Z(z_0) = 1 - \frac{v_1}{\sqrt{h_s h_n}} \sum_{i=0}^{\infty} \frac{(2i)!}{(i!)^2} \left(\frac{H_s}{2h_s} \right)^{2i} \sum_{j=0}^{2i} (1 - v_1)^j {}_2F_1 \left[\frac{j+1}{2}, \frac{j}{2} + 1, 1, \left(\frac{H_n}{h_n} v_1 \right)^2 \right] \quad (4.188)$$

where ${}_2F_1(\cdot)$ is the Gauss hypergeometric function [21, Eq. 15.1.1], and

$$v_1 = \frac{h_n}{h_n + h_s \tilde{z}_0}. \quad (4.189)$$

Changing the summation order, using [21, Eq. 6.1.18] and [103], the signal-to-interference CDF

may be expressed as

$$F_Z(\tilde{z}_0) = 1 - \frac{v_1}{\sqrt{\pi}\sqrt{h_s h_n}} \sum_{j=0}^{\infty} (1 - v_1)^j {}_2F_1 \left[\frac{j+1}{2}, \frac{j}{2} + 1, 1, \left(\frac{H_n}{h_n} v_1 \right)^2 \right] \left(\frac{H_s}{h_s} \right)^{2c_j} \quad (4.190)$$

$$\times \frac{\Gamma(c_j + \frac{1}{2})}{\Gamma(c_j + 1)} {}_2F_1 \left[1, c_j + \frac{1}{2}, c_j + 1, \left(\frac{H_s}{h_s} \right)^2 \right]$$

where $c_j = \lceil j/2 \rceil$, $\lceil \cdot \rceil$ is the ceiling function (defined as $\lceil x \rceil = k$, with $x \in \mathbb{R}$ and k being the smallest integer such that $x \leq k$).

Although (4.190) includes an infinite summation, the evaluation of the CDF converges rapidly for cases of interest. In order to estimate the error if the summation in (4.190) is truncated, all summands whose absolute value is larger than 10^{-20} are calculated, and those smaller than this value are discarded because it was observed that they do not affect the desired accuracy. The error of the truncated summation may now be estimated and, of course, these results vary depending on the given set of parameters used. Let J be defined as the number of terms in a truncated summation, i.e., $0 \leq j < J$. The entries for $n = 1$ in Table 4.6 give the value of J necessary to obtain a three-decimal-place accuracy (error < 0.0005) and a six-decimal-place accuracy (error < 0.0000005) for the infinite summation of (4.190).

For the incoherent addition, assume that the interference signal is composed of n i.i.d. variables. As a result, the joint interference signal power PDF is the n -fold convolution of the individual signal power PDF which, on its turn, is expressed by (4.183). This calculation gives

$$f_{W_n}(w_n) = \frac{\sqrt{\pi}}{\Gamma(\frac{n}{2})} \frac{n^{\frac{n+1}{2}} h_n^{\frac{n}{2}}}{\bar{w}_n} \left(\frac{w_n}{2H_n \bar{w}_n} \right)^{\frac{n-1}{2}} \exp \left(-nh_n \frac{w_n}{\bar{w}_n} \right) I_{\frac{n-1}{2}} \left(nH_n \frac{w_n}{\bar{w}_n} \right) \quad (4.191)$$

where $\bar{w}_n = n\bar{w}_i$, $\eta_n = \eta_i$, $h_n = h_i$ and $H_n = H_i$. It can be seen that the n -fold convolution used to obtain (4.191) produced the η - μ distribution for $\mu = n/2$ [19].

With (4.174) and (4.175), changing the integration order, using [21, Eq. 9.6.10], integrating

over z (see [48, Eq. 3.351.1]), and using [103], the integral solves to

$$F_Z(z_0) = 1 - \frac{v_n^n}{\Gamma(n)\sqrt{h_s h_n^n}} \sum_{i=0}^{\infty} \frac{(2i)!}{(i!)^2} \left(\frac{H_s}{2h_s}\right)^{2i} \times \sum_{j=0}^{2i} \frac{\Gamma(j+n)}{j!} (1-v_n)^j {}_2F_1 \left[\frac{j+n}{2}, \frac{j+n+1}{2}, \frac{n+1}{2}, \left(\frac{H_n}{h_n} v_n\right)^2 \right] \quad (4.192)$$

where

$$v_n = \frac{nh_n}{nh_n + h_s \tilde{z}_0}. \quad (4.193)$$

Changing the summation order, using [21, Eq. 6.1.18] and [103], the signal-to-interference CDF may be expressed as

$$F_Z(\tilde{z}_0) = 1 - \frac{v_n^n}{\sqrt{\pi}\sqrt{h_s h_n^n}} \sum_{j=0}^{\infty} \frac{(1-v_n)^j}{(j+n)B(j+1, n)} \left(\frac{H_s}{h_s}\right)^{2c_j} \frac{\Gamma(c_j + \frac{1}{2})}{\Gamma(c_j + 1)} \times {}_2F_1 \left[\frac{j+n}{2}, \frac{j+n+1}{2}, \frac{n+1}{2}, \left(\frac{H_n}{h_n} v_n\right)^2 \right] {}_2F_1 \left[1, c_j + \frac{1}{2}, c_j + 1, \left(\frac{H_s}{h_s}\right)^2 \right] \quad (4.194)$$

where $B(\cdot)$ is the beta function [21, Eq. 6.2.2], and c_j as already defined.

Although (4.194) includes an infinite summation, the evaluation of the CDF converges rapidly for cases of interest. Let J be the number of terms in a truncated summation (as defined earlier). Table 4.6 gives the value of J necessary to obtain a three-decimal-place accuracy (error < 0.0005) and a six-decimal-place accuracy (error < 0.0000005) for the infinite summation of (4.194).

Rice Fading Channel. For the calculations presented in this subsection, let (4.185) represent the desired signal power PDF as well as, with different parameters, the signal power PDF of an individual component of the interference signal.

If coherent addition of phasors is assumed, then (4.185) should be used to represent the joint interference signal power PDF. With (4.174) and (4.175), changing the integration order, using [21, Eq. 9.6.10], integrating over z (see [48, Eq. 3.351.1]), and using [103], the integral solves to

$$F_Z(z_0) = 1 - \frac{u_1}{e^{\kappa_s + \kappa_n}} \sum_{i=0}^{\infty} \frac{\kappa_s^i}{i!} \sum_{j=0}^i (1-u_1)^j {}_1F_1(j+1, 1, \kappa_n u_1) \quad (4.195)$$

where ${}_1F_1(\cdot)$ is the Kummer confluent hypergeometric function [21, Eq. 13.1.2], and

$$u_1 = \frac{(\kappa_n + 1)}{(\kappa_n + 1) + (\kappa_s + 1) \tilde{z}_0}. \quad (4.196)$$

Changing the summation order, using [48, Eqs. 1.211.1 and 8.352.2], and the signal-to-interference CDF may be expressed as

$$F_Z(\tilde{z}_0) = 1 - \frac{u_1}{e^{\kappa_n}} \sum_{j=0}^{\infty} (1 - u_1)^j [1 - Q(j, \kappa_s)] {}_1F_1(j + 1, 1, \kappa_n u_1) \quad (4.197)$$

where $Q(\cdot)$ is the regularized incomplete gamma function defined as $Q(a, b) = \Gamma(a, b)/\Gamma(a)$, and $\Gamma(\cdot, \cdot)$ is the incomplete gamma function [21, Eq. 6.5.3].

If both κ_s and κ_n are set to zero in (4.197), the CDF simplifies to the Rayleigh channel model. If this result is further simplified by assuming that $\bar{w}_s = \bar{w}_i = \bar{w}_n/n$ (hence making $\tilde{z}_0 = nz_0$), then the same expression presented in [29, Eq. 20.b] is produced.

Although (4.197) includes an infinite summation, the evaluation of the CDF converges rapidly for cases of interest. Let J be the number of terms in a truncated summation (as defined earlier). The entries for $n = 1$ in Table 4.7 give the value of J necessary to obtain a three-decimal-place accuracy (error < 0.0005) and a six-decimal-place accuracy (error < 0.0000005) for the infinite summation of (4.197).

For the incoherent addition, assume that the interference signal is composed of n i.i.d. variables. As a result, the joint interference signal power PDF is the n -fold convolution of the individual signal power PDF which, on its turn, is expressed by (4.185). This calculation gives

$$f_{W_n}(w_n) = \frac{n}{e^{n\kappa_n}} \left(\frac{\kappa_n + 1}{\bar{w}_n} \right)^{\frac{n+1}{2}} \left(\frac{w_n}{\kappa_n} \right)^{\frac{n-1}{2}} e^{-n(\kappa_n+1)\frac{w_n}{\bar{w}_n}} I_{n-1} \left(2n\sqrt{\kappa_n(\kappa_n + 1)\frac{w_n}{\bar{w}_n}} \right) \quad (4.198)$$

where $\bar{w}_n = n\bar{w}_i$, and $\kappa_n = \kappa_i$. It can be seen that the n -fold convolution used to obtain (4.198) produced the κ - μ distribution for integer values of $\mu = n$ [19].

With (4.174) and (4.175), changing the integration order, using [21, Eq. 9.6.10], integrating

over z (see [48, Eq. 3.351.1]), and using [103], the integral solves to

$$F_Z(z_0) = 1 - \frac{u_n^n}{e^{\kappa_s + n\kappa_n}} \sum_{i=0}^{\infty} \frac{\kappa_s^i}{i!} \sum_{j=0}^i \frac{\Gamma(j+n)}{\Gamma(n)j!} (1-u_n)^j {}_1F_1(j+n, n, n\kappa_n u_n) \quad (4.199)$$

where

$$u_n = \frac{n(\kappa_n + 1)}{n(\kappa_n + 1) + (\kappa_s + 1)\tilde{z}_0}, \quad (4.200)$$

Changing the summation order, using [48, Eqs. 1.211.1 and 8.352.2], and the signal-to-interference CDF may be expressed as

$$F_Z(\tilde{z}_0) = 1 - \frac{u_n^n}{e^{n\kappa_n}} \sum_{j=0}^{\infty} \frac{(1-u_n)^j [1 - Q(j, \kappa_s)]}{(j+n)B(j+1, n)} {}_1F_1(j+n, n, n\kappa_n u_n). \quad (4.201)$$

If both κ_s and κ_n are set to zero in (4.201), the CDF simplifies to the Rayleigh channel model. If this result is further simplified by assuming that $\bar{w}_s = \bar{w}_i = \bar{w}_n/n$ (hence making $\tilde{z}_0 = nz_0$), then the same expression presented in [29, Eq. 20.a] is found.

Although (4.201) includes an infinite summation, the evaluation of the CDF converges rapidly for cases of interest. Let J be the number of terms in a truncated summation (as defined earlier). Table 4.7 gives the value of J necessary to obtain a three-decimal-place accuracy (error < 0.0005) and a six-decimal-place accuracy (error < 0.0000005) for the infinite summation of (4.201).

Nakagami- m Fading Channel. For the calculations presented in this subsection, let (4.187) represent the desired signal power PDF as well as, with different parameters, the signal power PDF of an individual component of the interference signal.

For the incoherent addition, assume that the interference signal is composed of n i.i.d. variables. As a result, the joint interference signal power PDF is the n -fold convolution of the individual signal power PDF which, on its turn, is expressed by (4.187). This calculation yields

$$f_{W_n}(w_n) = \frac{w_n^{m_n-1}}{\Gamma(m_n)} \left(\frac{m_n}{\bar{w}_n}\right)^{m_n} \exp\left(-\frac{m_n w_n}{\bar{w}_n}\right) \quad (4.202)$$

where m_i and $m_n = nm_i$ are the individual and the joint fading parameters, respectively, and

$\bar{w}_n = n\bar{w}_i$ is the joint mean power. It can be seen from (4.187) and (4.202) that both signal power and interference power are described by the same distribution, except that they have distinct parameters.

Using the appropriate expressions in (4.174), and after some manipulation, the signal-to-interference PDF is found as

$$f_Z(z) = \frac{1}{B(m_s, m_n)} \frac{\bar{w}_n m_s}{\bar{w}_s m_n} b^{m_s-1} (1-b)^{m_n+1} \quad (4.203)$$

where

$$b = \frac{\bar{w}_n m_s z}{\bar{w}_n m_s z + \bar{w}_s m_n}. \quad (4.204)$$

The corresponding CDF may be expressed as [104, 30]

$$F_Z(\tilde{z}_0) = I_{b_n}(m_s, m_n) = 1 - I_{1-b_n}(m_n, m_s) \quad (4.205)$$

where $I_x(\cdot)$ is the regularized incomplete beta function [21, Eq. 6.6.2], and

$$b_n = \frac{m_s \tilde{z}_0}{m_s \tilde{z}_0 + m_n}. \quad (4.206)$$

Spatial Coverage

The analysis presented above for the incoherent addition of interferers assumes that the components of the interference signal have identical mean power \bar{w}_i , $i = 1, \dots, n$. This restriction limits the results to systems where perfect power control is employed or to terminals placed at a fixed distance from the receiving antenna (i.e., on a circular ring) and in an environment without any shadowing effects. Let us now extend the model presented above to include the case of packets arriving with different mean powers, e.g., from terminals with a given spatial distribution across the cell radius and at different transmission distances to the receiver's antenna. Therefore, the statistical behavior of the packet mean power needs to be specified and taken into account.

The mean power of a packet received from a terminal at a distance d is of the general form

[2]

$$\bar{w} = \Lambda d^{-\alpha} \quad (4.207)$$

where α gives the channel attenuation with the distance, and Λ is a value that depends on, e.g., the transmit power and the height and gain of the antennas. Typical values of the exponent α are $\alpha = 2$ in free space and $\alpha = 4$ in urban land mobile cellular systems. Using a similar approach to that presented in [29], let $\rho \triangleq d \Lambda^{-1/\alpha}$ be defined and used to rewrite (4.207) as

$$\bar{w} = \rho^{-\alpha}. \quad (4.208)$$

Let the offered traffic density function $G(\rho)$ be defined as the number of packets offered per transmission period per unit of area at distance ρ . The total offered traffic can be calculated by $G_t = 2\pi \int_0^\infty \rho G(\rho) d\rho$.

The spatial CDF of the offered traffic as a function of the distance ρ can be expressed as

$$F_G(\rho) = \text{Prob}\{\text{packet generated within distance } \rho\} = \frac{2\pi}{G_t} \int_0^\rho u G(u) du \quad (4.209)$$

and the corresponding PDF is

$$f_G(\rho) = \frac{2\pi}{G_t} \rho G(\rho). \quad (4.210)$$

The PDF of the received packet mean power $f_{\bar{W}}(\bar{w}) = f_G(\rho) \left| \frac{d\rho}{d\bar{w}} \right|$ is calculated using (4.208) and (4.210) and can be expressed as

$$f_{\bar{W}}(\bar{w}) = \frac{2\pi}{\alpha G_t \bar{w}^{1+2/\alpha}} G(\bar{w}^{-1/\alpha}). \quad (4.211)$$

The capture probability for spatial coverage is now considered. Given an arbitrary spatial traffic density $G(\rho)$, (4.211) can be used to calculate the PDF of the test packet mean power $f_{\bar{W}_s}(\bar{w}_s)$. The PDF of the mean interference power of n packets $f_{\bar{W}_n}(\bar{w}_n)$ is calculated by convolving (4.211) n times. With these results and assuming that the signal power and the interference power are statistically independent, the CDF of the signal-to-interference ratio can

be calculated as

$$F_Z(z_0) = \int_0^{z_0} dz \int_0^\infty d\bar{w}_n \int_0^\infty f_Z(z) f_{\bar{W}_n}(\bar{w}_n) f_{\bar{W}_s}(\bar{w}_s) d\bar{w}_s \quad (4.212)$$

where $f_Z(\cdot)$ is given by (4.174). With (4.177) and (4.212), the capture probability is then calculated. As an example, let us use the quasi-constant traffic density given in [29], expressed as

$$G(\rho) = \frac{G_t}{\pi} \sqrt{\xi} \exp\left(-\frac{\pi}{4}\xi\rho^4\right), \quad \xi > 0, \rho \geq 0. \quad (4.213)$$

It is possible to see that the traffic density is roughly constant inside the cell of radius $\rho = 1$, falling rapidly beyond the cell boundary. If we select $\alpha = 4$, it can be seen that

$$f_{\bar{W}_s}(\bar{w}_s) = \frac{\sqrt{\xi}}{2\bar{w}_s^{3/2}} \exp\left(-\frac{\pi\xi}{4\bar{w}_s}\right) \quad (4.214)$$

and

$$f_{\bar{W}_n}(\bar{w}_n) = \frac{n\sqrt{\xi}}{2\bar{w}_n^{3/2}} \exp\left(-\frac{n^2\pi\xi}{4\bar{w}_n}\right). \quad (4.215)$$

Using these results in (4.212), and considering the Nakagami- m channel, where $f_Z(\cdot)$ is given by (4.203), the signal-to-interference CDF is given by

$$F_Z(z_0) = \sec(m_s\pi) \left[\frac{c_0^{m_s}}{m_s} \frac{{}_2F_1(m_s, m_s + m_n, m_s + 1, c_0)}{B(m_s, m_n)} - 2\sqrt{c_0} \frac{\Gamma(m_n + \frac{1}{2})}{\Gamma(m_s)\Gamma(m_n)\Gamma(-m_s + \frac{3}{2})} {}_3F_2\left(\frac{1}{2}, 1, m_n + \frac{1}{2}, \frac{3}{2}, -m_s + \frac{3}{2}, c_0\right) \right] \quad (4.216)$$

where ${}_3F_2(\cdot)$ is a generalized hypergeometric function [48, Eq. 9.14.1], and

$$c_0 = n^2 z_0 \frac{m_s}{m_n}. \quad (4.217)$$

Note that the parameter ξ does not influence the results in (4.216). This is due to the fact that it appears as a multiplicative factor of the mean power (Eqs. 4.214 and 4.215), and in (4.212) the average is performed over the ratio of these powers. In physical terms, this parameter simply indicates more or less concentration of traffic within the center of the cell, which impacts equally on the effect of the desired signal as well as of the interference ones.

4.8.5 Numerical Results

This section presents numerical results assuming, wherever applicable and unless otherwise indicated, the networks parameters listed in Table 4.8. These parameters belong to the IEEE 802.11b protocol. However, the mathematical models used here hold for any wireless protocol with similar MAC functionality.

Outage Probability

The outage probabilities for the Hoyt, Rice and Nakagami- m channels, considering incoherent addition of interfering signals and perfect power control, are pictured in Figs. 4.22, 4.23 and 4.24, respectively. In all cases the outage probability decreases with higher values of average SIR, as expected. In addition, using the results for the Rayleigh channel as a reference, the figures allow a comparison between these channels with regards to the outage probabilities. Considering a line of decreasing fading intensity, the Rice channel spans from Rayleigh fading ($\kappa = 0$) to a no-fading situation ($\kappa \rightarrow \infty$); the Hoyt channel ranges from one-sided Gaussian fading ($\eta = 0$) to Rayleigh fading ($\eta = 1$); and the Nakagami- m channel varies from one-sided Gaussian fading ($m = 1/2$) to a no-fading situation ($m \rightarrow \infty$), with Rayleigh fading ($m = 1$) in-between. The figures show that higher fading intensity values translate into higher outage probabilities. Also, considering the average SIR value constant, the number of interfering signals n has only a minor influence on the outage probability.

Channel Throughput: Perfect Power Control

With the results obtained in the previous sections, using (4.177), (4.180), (4.201), (4.194) and (4.205), it is now possible to calculate the IEEE 802.11 DCF channel throughput for the Hoyt, Rice and Nakagami- m channels, assuming incoherent addition of interfering signals and perfect power control. Let τ be the worst case propagation delay and $\tilde{\tau} = \tau/p$ its normalized version. For the Hoyt channel, the throughput for various values of $\eta = \eta_s = \eta_n$, \tilde{z}_0 , $\tilde{\tau}$ and P_e is shown in Fig. 4.25. For the Rice channel, Fig. 4.26 depicts the throughput for various values of $\kappa = \kappa_s = \kappa_n$, \tilde{z}_0 , $\tilde{\tau}$ and P_e . For the Nakagami- m channel, considering various values

of $m = m_s = m_i$, \tilde{z}_0 , $\tilde{\tau}$ and P_e , the throughput is presented in Fig. 4.27.

The figures indicate that the behavior of the throughput S as a function of the packet rate λ consists, basically, of two regions: a linear growth region where S is a linear function of λ , and a saturation region where S remains almost constant. The transition between the two regions may be characterized by a peak in the throughput, in particular if the number of nodes N is high.

In addition, the throughput graphs clearly indicate the important role the normalized worst case propagation delay $\tilde{\tau}$ plays to determine the channel throughput. Also, higher normalized capture threshold \tilde{z}_0 values mean lower channel throughput, which is expected since it indicates a diminished ability of receiver detection of the intended signal among the interfering signals. Examining same- \tilde{z}_0 data, compared to the Rayleigh channel results, higher values of κ in Rice channels tend to produce slightly lower throughput. The reason behind it is that higher κ implies a more deterministic scenario, approaching that of the wireline case. On the other hand, lower values of η in Hoyt channels tend to produce slightly higher throughput when compared to Rayleigh channel results. The reason for this is that lower η implies a more random scenario which may increase the chance of capture. For the Nakagami- m channel, depending on the value of m , throughput results can be higher or lower than those seen for the Rayleigh channel. In all cases, higher fading intensity values tend to higher throughput, although the differences observed are rather marginal. Also, in all cases, higher probability of channel error P_e translates into lower throughput.

It is noteworthy that the Nakagami- m distribution approximates Hoyt and Rice and includes Rayleigh. The Hoyt channel is approximated if the parameter m is such that $1/2 < m < 1$, with [18]

$$\eta = \frac{1 - \sqrt{\frac{1}{m} - 1}}{1 + \sqrt{\frac{1}{m} - 1}}. \quad (4.218)$$

On the other hand, the Rice channel is approximated if $m > 1$, with [18]

$$\kappa = \frac{\sqrt{m^2 - m}}{m - \sqrt{m^2 - m}}. \quad (4.219)$$

Of course, $m = 1$ produces the Rayleigh channel. Fig. 4.28 illustrates these situations by showing the throughput for the Hoyt, Rice and Rayleigh channels and equivalent curves for the matching Nakagami- m channel. It can be seen that the original and the matching curves are indistinguishable. These results show that the formulation obtained for the spatial coverage for the Nakagami- m case can be directly applied to the Hoyt ($1/2 < m < 1$) and Rice ($m > 1$) cases, for which the exact formulations are mathematically intractable.

Channel Throughput: Spatial Coverage

With the results obtained in Section 4.8.4, using (4.177), (4.180) and (4.216), the throughput can be calculated for the Nakagami- m channel model. Fig. 4.29 presents the throughput for various values of $m = m_s = m_i$, \tilde{z}_0 and P_e . In addition, it shows how the IEEE 802.11 DCF compares against a simpler version of CSMA/CA. In this case, CSMA/CA is assumed to implement a single-stage backoff algorithm, i.e., $m = 0$, with $CW_{min} = CW_{max} = 256$. Similarly to the perfect power control scenario presented above, it can be seen that lower values of \tilde{z}_0 or P_e translates into higher throughput figures. However, it seems that the influence of the fading parameter m is somewhat weaker when compared to the results presented earlier. On the other hand, the results indicate that \tilde{z}_0 appears to play a more significant role in determining the channel performance. Also, the results, presented for $N = 4$, show that the IEEE 802.11 DCF outperforms the CSMA/CA although the difference seems narrower at the both ends of the curves, i.e., with low and high packet rates. Also, the transition between the linear and the saturation regions for CSMA/CA is not as sharp as the one observed for the IEEE 802.11 DCF.

Fig. 4.30 presents the throughput for various values of $m = m_s = m_i$ and average packet payload length $E\{PL\}$. As expected, the throughput is lower for shorter payload packets, although the relation between packet payload length and throughput is not a one-to-one. For instance, a reduction of 49% in the average packet payload length (from 1020 to 520 bytes) causes the saturated throughput to drop only about 8%, and an 87% reduction (from 1020 to 128 bytes) causes the saturated throughput to drop about 37%.

As already mentioned, it is important to note that since the Nakagami- m distribution ap-

proximates Hoyt and Rice, the former may be used to estimate the spatial coverage when the desired channel model is either one of the latter.

4.8.6 Conclusions

This application example investigates the throughput performance of IEEE 802.11 DCF in a packet radio network and Hoyt, Rice and Nakagami- m fading environments. Analytical and numerical results are presented considering the signal capture model with coherent and incoherent addition of interfering signals. The approach used here includes the signal capture model with uniform attenuation for all terminals (or perfect power control) and unequal average power levels (or spatial coverage). The results indicate that higher fading intensity, lower capture threshold or lower propagation delay contributes to higher channel throughput. Also, since the fading intensity values of the Nakagami- m channel model approximate those found in the Hoyt and Rice channels, the results presented for the former channel offer a good indication of what range the latter channels may exhibit. It is certainly of interest to extend these results to more general fading scenarios, such as those of κ - μ , η - μ and α - μ [20].

The IEEE 802.11 DCF algorithm and its corresponding Markov model as used here, and that has been extracted from [91], has already been fully validated in [91] by means of simulation. Apart from the new channel model statistics proposed here, which have no effect on the traffic model of [91], the formulations of [91] are kept intact. The new fading statistics added to the model of [91] have been fully validated by means of numerical integration. Therefore, the full model is validated.

Table 4.6: Relation between number of terms and accuracy in the infinite summation of (4.194).

n	Parameters			smallest J for accuracy of	
	η_s	η_n	\tilde{z}_0	3-decimal-place	6-decimal-place
1	0.01	0.01	0.1	27	59
			1.0	117	274
			5.0	167	423
		0.1	1.0	115	265
			5.0	169	421
		0.99	1.0	104	217
	5.0		179	415	
	0.1	0.01	1.0	14	31
			5.0	18	44
		0.99	1.0	13	26
			5.0	19	44
	0.99	0.01	1.0	1	3
			5.0	1	3
		0.99	1.0	1	3
			5.0	2	3
	10	0.01	0.01	1.0	67
5.0				186	337
0.99			1.0	57	86
			5.0	181	293
0.99		0.01	1.0	1	3
			5.0	1	3
		0.99	1.0	1	3
			5.0	1	3
50	0.01	0.01	5.0	170	243
		0.99	5.0	163	217
	0.99	0.01	5.0	1	3
		0.99	5.0	1	3

Table 4.7: Relation between number of terms and accuracy in the infinite summation of (4.201).

n	Parameters			smallest J for accuracy of		
	κ_s	κ_n	\tilde{z}_0	3-decimal-place	6-decimal-place	
1	0.01	0.01	0.1	2	2	
			1.0	2	3	
			5.0	2	3	
		1.0	1.0	2	3	
			5.0	2	3	
			10.0	1.0	2	3
	1.0	0.01	1.0	5	8	
			5.0	5	8	
		10.0	1.0	5	8	
			5.0	5	9	
	10.0	0.01	1.0	18	26	
			5.0	18	26	
		10.0	1.0	19	25	
			5.0	17	26	
	10	0.01	0.01	1.0	2	3
				5.0	2	3
10.0			1.0	2	3	
			5.0	1	3	
10.0		0.01	1.0	19	25	
			5.0	12	25	
		10.0	1.0	18	23	
			5.0	0	15	
50	0.01	0.01	5.0	1	3	
		10.0	5.0	1	3	
	10.0	0.01	5.0	0	18	
		10.0	5.0	0	0	

Table 4.8: Typical network parameters.

MAC header	34 bytes
PHY header	24 bytes
ACK frame	14 bytes + PHY header
packet payload	1020 bytes
channel bit rate	1 Mbps
DIFS	50 μs
SIFS	10 μs
ACK timeout	300 μs
σ	20 μs
m	5
CW_{min}	8

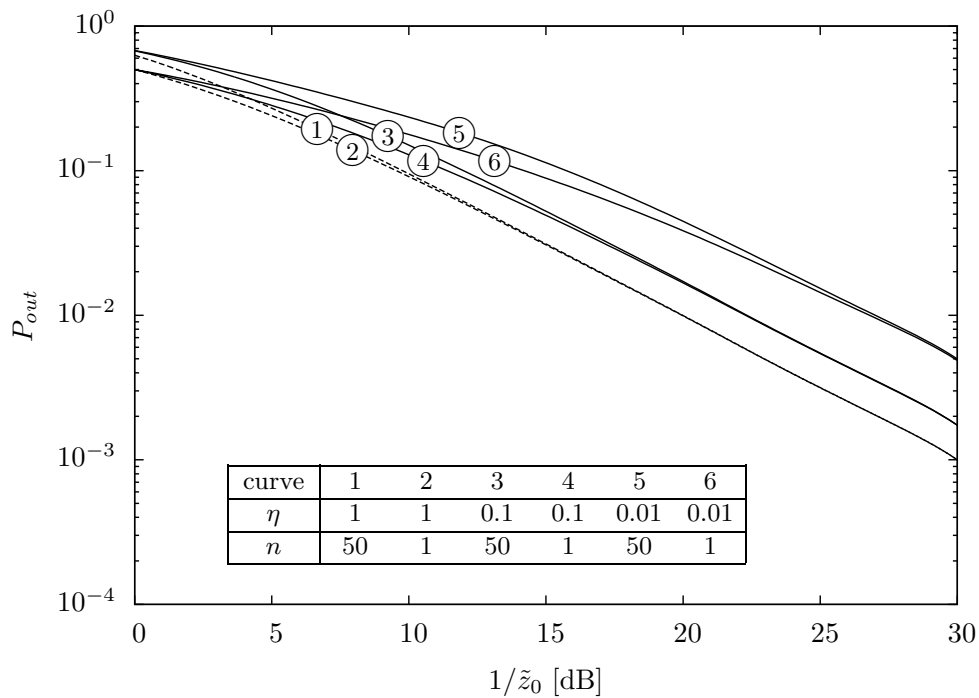


Figure 4.22: Outage probability for incoherent Hoyt channel with $\eta = \eta_s = \eta_n$. The dashed lines correspond to the Rayleigh channel ($\eta = 1$).

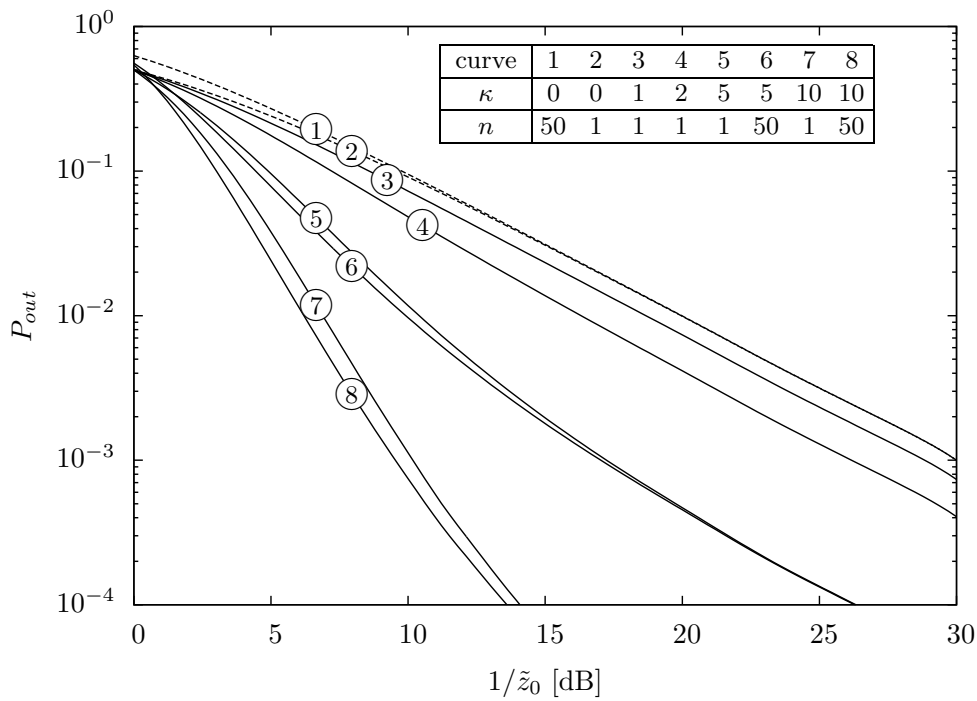


Figure 4.23: Outage probability for incoherent Rice channel with $\kappa = \kappa_s = \kappa_n$. The dashed lines correspond to the Rayleigh channel ($\kappa = 0$).

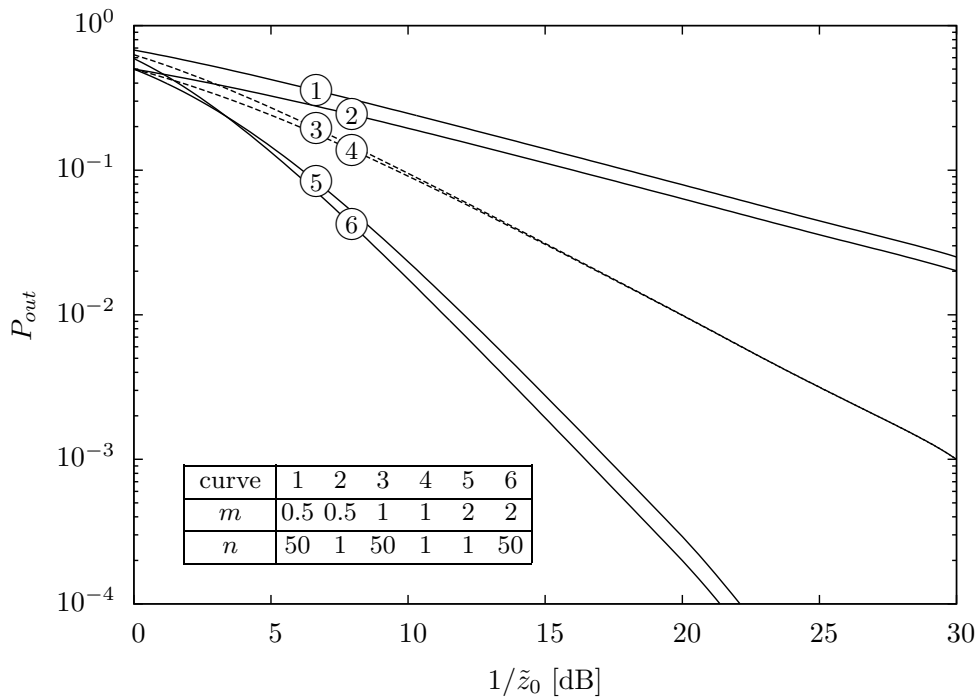


Figure 4.24: Outage probability for incoherent Nakagami- m channel with $m = m_s = m_i$. The dashed lines correspond to the Rayleigh channel ($m = 1$).

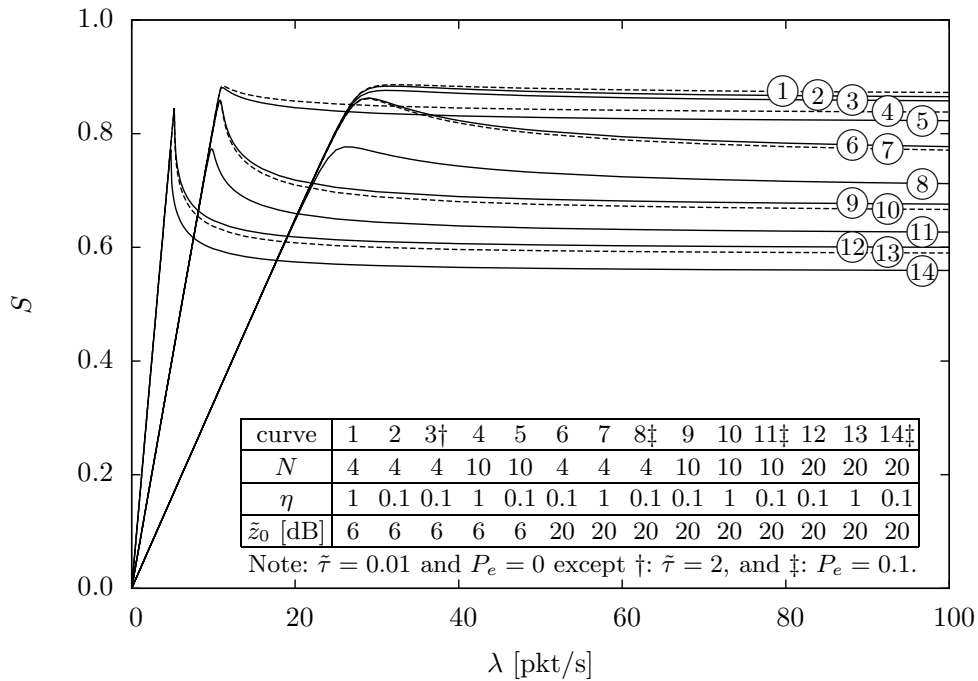


Figure 4.25: Throughput S for IEEE 802.11 DCF with 2-way handshake, incoherent Hoyt channel, perfect power control and $\eta = \eta_s = \eta_i = \eta_n$. The dashed lines correspond to the Rayleigh channel ($\eta = 1$)

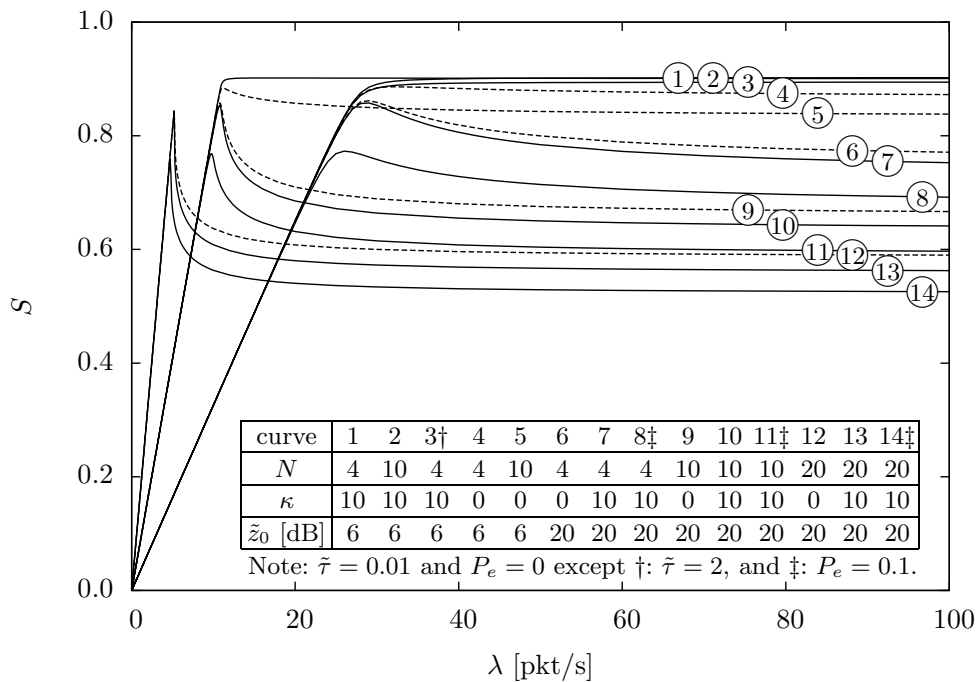


Figure 4.26: Throughput S for IEEE 802.11 DCF with 2-way handshake, incoherent Rice channel, perfect power control and $\kappa = \kappa_s = \kappa_i = \kappa_n$. The dashed lines correspond to the Rayleigh channel ($\kappa = 0$).

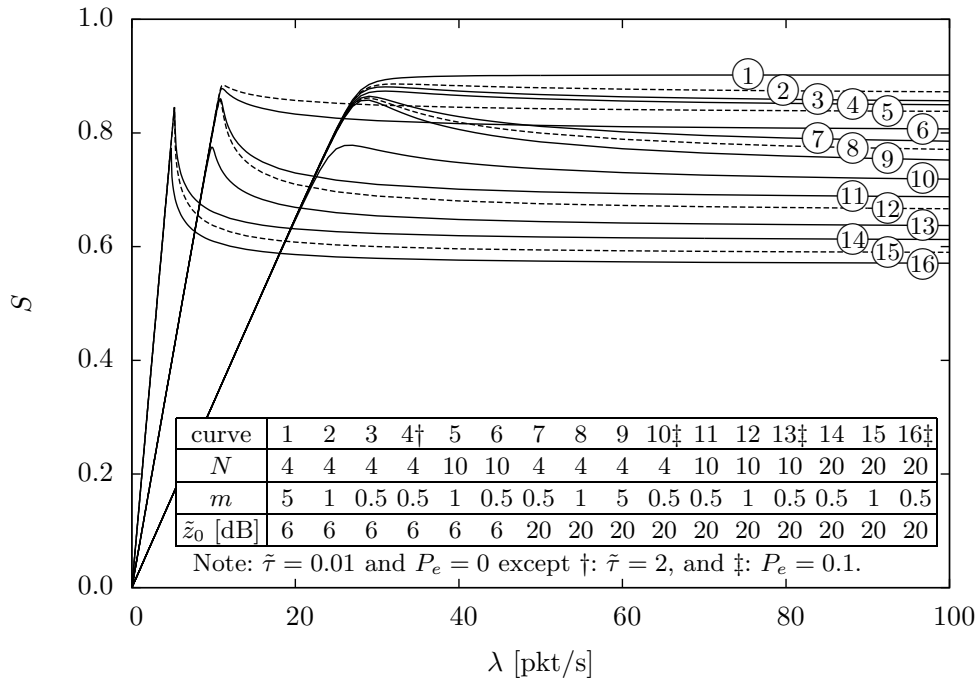


Figure 4.27: Throughput S for IEEE 802.11 DCF with 2-way handshake, incoherent Nakagami- m channel, perfect power control and $m = m_s = m_i = m_n/n$. The dashed lines correspond to the Rayleigh channel ($m = 1$).

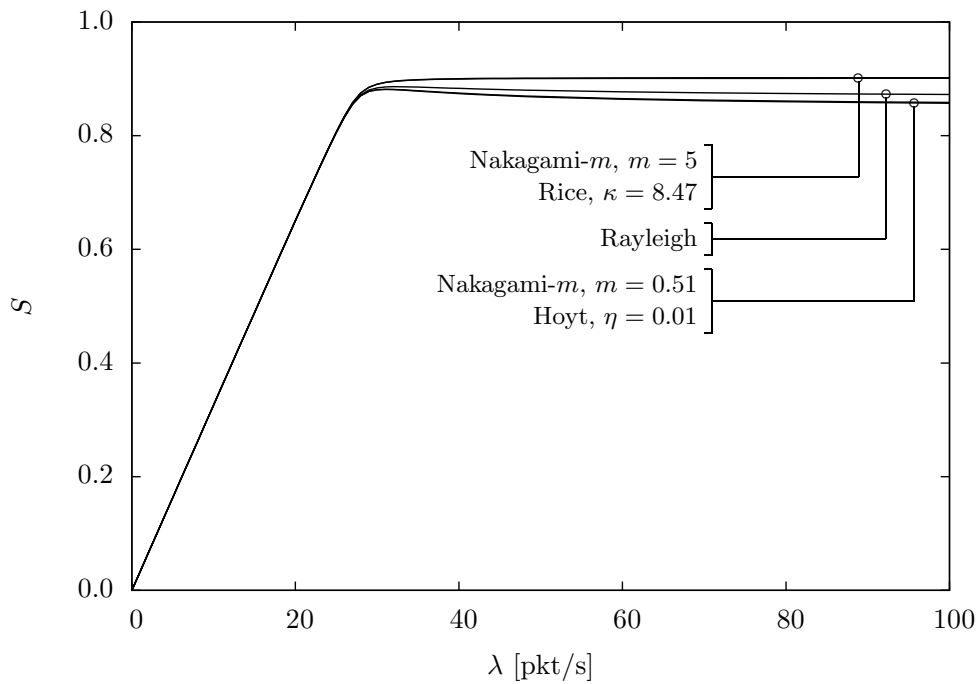


Figure 4.28: Throughput S for IEEE 802.11 DCF with 2-way handshake, incoherent Hoyt, Rice, Nakagami- m and Rayleigh channels with perfect power control, $\eta = \eta_s = \eta_i = \eta_n$, $\kappa = \kappa_s = \kappa_i = \kappa_n$ and $m = m_s = m_i = m_n/n$, $\tilde{\tau} = 0.01$, $N = 4$, $\tilde{z}_0 = 6$ dB and $P_e = 0$.

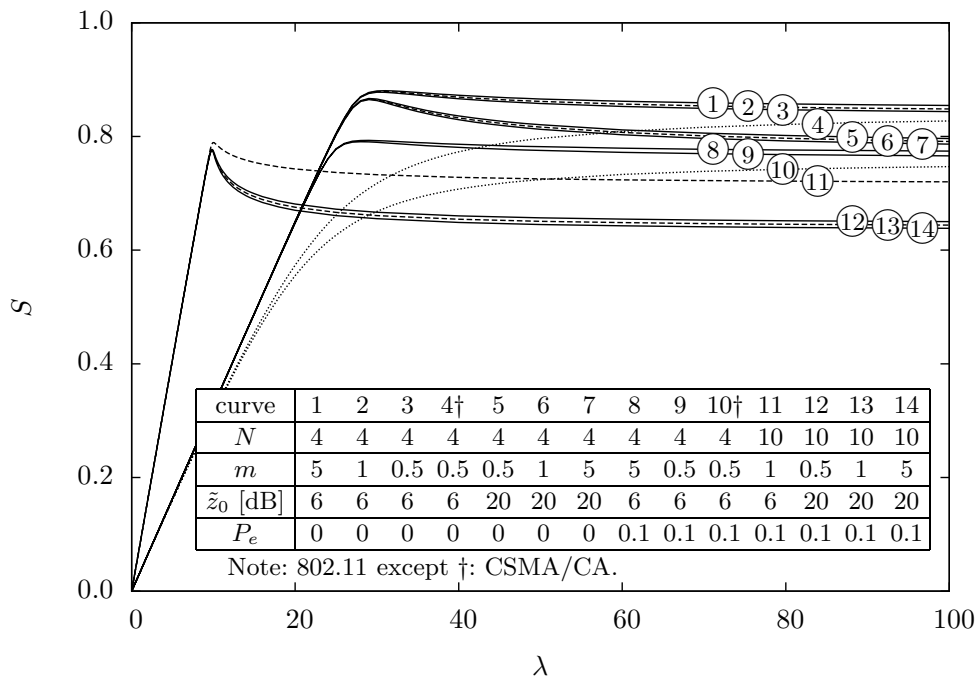


Figure 4.29: Throughput S for IEEE 802.11 DCF with 2-way handshake, incoherent Nakagami- m channel with spatial coverage, $m = m_s = m_i = m_n/n$ and $\tilde{\tau} = 0.01$. The dashed lines correspond to the Rayleigh channel ($m = 1$). The dotted lines correspond to CSMA/CA.

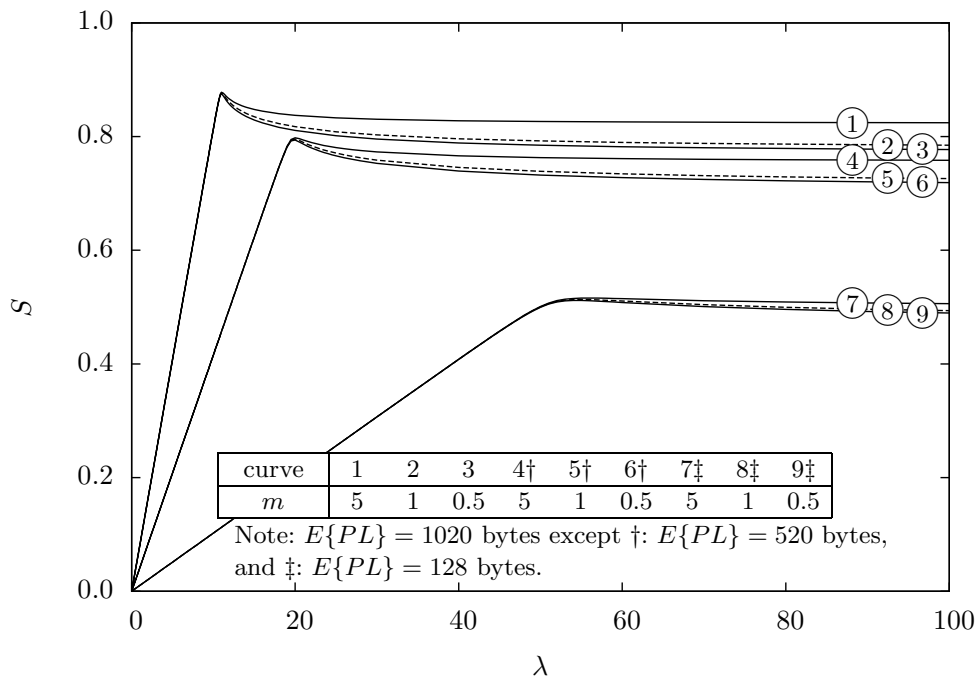


Figure 4.30: Throughput S for IEEE 802.11 DCF with 2-way handshake, incoherent Nakagami- m channel with spatial coverage, $m = m_s = m_i = m_n/n$, $\tilde{\tau} = 0.01$, $N = 10$, $\tilde{z}_0 = 6$ dB and $P_e = 0$. The dashed lines correspond to the Rayleigh channel ($m = 1$).

Conclusions and Perspectives

5.1 Contributions

The statistics of the ratio and the product of random variables (RVs) are important to characterize the wireless communication systems and it is key to assess their performance. In this work, general, simple, exact, closed-form and infinite series form expressions for the probability density function (PDF) and cumulative distribution function (CDF) for the ratio and the product of independent non-identically distributed (i.n.i.d.) fading RVs are derived. In particular, the statistical models considered in this research are among those commonly used to describe the short-term signal statistics of wireless communications links subject to fading. Furthermore, the focus has been on distributions that have been recently proposed: the α - μ [20], the κ - μ and the η - μ [19] distributions. Due to their flexibility, these distributions are adaptable to situations in which neither of the traditional distributions yields good fit.

The α - μ model is a general physical fading model which considers a signal composed of clusters of multipath waves propagating in a non-homogeneous environment. The distribution associated with this model includes as special cases other important distributions, such as Nakagami- m , Weibull, Rayleigh, Negative Exponential, and One-Sided Gaussian. As its name implies, the α - μ distribution is written in terms of two physical parameters, namely α and μ . The power parameter α is related to the nonlinearity of the environment, whereas the parameter $\mu > 0$ is associated to the number of multipath clusters.

The κ - μ fading environment is a general fading model that can be used to better represent the small-scale variation of the fading signal in the presence of a LOS component. The distribution has the Rice (Nakagami- n), the Nakagami- m , the Rayleigh, and the One-Sided Gaussian distributions as special cases. As its name implies, the κ - μ distribution is written in terms of the physical parameters κ and μ . The parameter κ is defined as the ratio between the total power of the dominant components and the total power of the scattered waves, and the parameter $\mu > 0$ is associated to the number of multipath clusters.

The η - μ fading environment is a general fading model that can be used to better represent the small-scale variation of the fading signal in a non-line-of-sight condition. The distribution has the Hoyt (Nakagami- q), the Nakagami- m , the Rayleigh, and the One-Sided Gaussian distributions as special cases. As its name implies, the η - μ distribution is written in terms of the physical parameters η and μ . The parameter η is defined as the scattered-wave power ratio between the in-phase and quadrature components, whereas the parameter $\mu > 0$ is associated to the number of multipath clusters.

In this thesis, the following ratio of RVs have been considered: Hoyt/ η - μ , Rice/ η - μ , Rice/ κ - μ , η - μ / η - μ , η - μ / κ - μ , κ - μ / κ - μ , κ - μ / η - μ , and α - μ / α - μ . Also, the following product of RVs are considered: η - μ \times η - μ , κ - μ \times κ - μ , η - μ \times κ - μ , and α - μ \times α - μ . In addition, a few application examples are presented. They include the analysis of the throughput of Carrier Sense Multiple Access (CSMA) in Rice, Hoyt, Nakagami- m , combined Ride and Hoyt, η - μ and κ - μ fading channels. In addition, it is presented the throughput of the Distributed Coordination Function (DCF) of IEEE 802.11 in Hoyt, Rice, and Nakagami- m Fading Channels. The ratio of independent alpha-mu random variables and its application in the capacity analysis of spectrum sharing systems is also presented.

5.2 Future Works

Recommendations for further study include the calculation of the moments of the ratios Z and the products W . Of special interest is the first moment (mean value) of these RVs.

Also, it is certainly of interest to extend these results to the cross ratios and products

involving the three distributions, α - μ , κ - μ and η - μ , that have not yet been calculated in this work.

Other interesting topics for future work are listed below.

- Calculation of the products for a generic n number of terms.
- Calculation of the ratios of generic products, i.e., the numerator is the product of m terms and the denominator is the product of n terms, with generic m and n .
- Assessment of closed formulations for special cases of interest.
- Evaluation of how close the calculated ratios are of the ratios of sum of η - μ , κ - μ and α - μ variates.

The last suggestion refers to applications where the ratio of sum of RVs is necessary; the goal is to use a single η - μ and κ - μ to approximate the sum of η - μ and κ - μ RVs.

Bibliography

- [1] J. P. Linnartz. *Narrowband Land-Mobile Radio Networks*. Artech House, 1993.
- [2] M. D. Yacoub. *Foundations of Mobile Radio Engineering*. CRC Press, 1993.
- [3] T. S. Rappaport. *Wireless Communications: Principles and Practice*. Prentice Hall, 1996.
- [4] B. Fleury. Characteristics of Radio Channels. In E. Damosso and L. M. Correia, editors, *Cost Action 231: Digital Mobile Radio Towards Future Generation Systems, Final Report*, pages 28–43. European Commission, 1999.
- [5] J. B. Andersen, P. Eggers, and B. L. Andersen. Propagation Aspects of Datacommunication over the Radio Channel: a Tutorial. pages 301–305. Proceedings on Area Communication, 8th. European Conference on Electrotechnics, 1988.
- [6] T. Kurner. Propagation Models for MacroCells. In E. Damosso and L. M. Correia, editors, *Cost Action 231: Digital Mobile Radio Towards Future Generation Systems, Final Report*, pages 134–148. European Commission, 1999.
- [7] G. L. Stuber. *Principles of Mobile Communications*. Kluwer Academic Publishers, second edition, 2001.
- [8] M. Gudmundson. Analysis of Handover Algorithms. pages 537–542. 41st. IEEE Vehicular Technology Conference, 1991.
- [9] S. Y. Seidel, T. S. Rappaport, S. Jain, M. L. Lord, and R. Singh. Path Loss, Scattering and Multipath Delay Statistics in Four European Cities for Digital Cellular and Microcellular Radiotelephone. *IEEE Transactions on Vehicular Technology*, 40(4):721–730, 1991.
- [10] M. J. Feuerstein, K. L. Blackard, T. S. Rappaport, S. Y. Seidel, and H. H. Xia. Path Loss, Delay Spread, and Outage Models as Functions of Antenna Height for Microcellular System Design. *IEEE Transactions on Vehicular Technology*, 43(3):487–498, 1994.
- [11] G. Durgin, T. S. Rappaport, and H. Xu. Measurements and Models for Radio Path Loss and Penetration Loss in and Around Homes and Trees at 5.85 GHz. *IEEE Transactions on Communications*, 46(11):1484–1496, 1998.
- [12] V. Erceg, L. J. Greenstein, S. Y. Tjandra, S. R. Parkoff, A. Gupta, B. Kulic, A. A. Julius, and R. Bianchi. An Empirically Based Path Loss Model for Wireless Channels in Suburban

- Environments. *IEEE Journal on Selected Areas in Communications*, 17(7):1205–1211, 1999.
- [13] T. Schwengler and M. Gilbert. Propagation Models at 5.8 GHz - Path Loss and Building Penetration. pages 119–124. IEEE Radio and Wireless Conference, RAWCON, 2000.
- [14] J. W. Porter, I. Lisica, and G. Buchwald. Wideband Mobile Propagation Measurements at 3.7 GHz in an Urban Environment. volume 4, pages 3645–3648. IEEE Antennas and Propagation Society International Symposium, 2004.
- [15] T. Rautiainen, K. Kalliola, and J. Juntunen. Wideband Radio Propagation Characteristics at 5.3 GHz in Suburban Environments. volume 2, pages 868–872. IEEE 16th International Symposium on Personal, Indoor and Mobile Radio Communications, PIMRC, 2005.
- [16] S. O. Rice. Mathematical Analysis of Random Noise. *Bell System Technical Journal*, 23(3):282–332, 1944.
- [17] R. S. Hoyt. Probability Functions for the Modulus and Angle of the Normal Complex Variate. *Bell System Technical Journal*, 26(2):318–359, 1947.
- [18] M. Nakagami. The m -distribution - A general Formula of Intensity Distribution of Rapid Fading. In W. C. Hoffman, editor, *Statistical Methods in Radio Wave Propagation*, pages 3–36. Pergamon Press, 1960.
- [19] M. D. Yacoub. The κ - μ Distribution and the η - μ Distribution. *IEEE Antennas and Propagation Magazine*, 49(1):68–81, 2007.
- [20] M. D. Yacoub. The α - μ Distribution: a Physical Fading Model for the Stacy Distribution. *IEEE Transactions on Vehicular Technology*, 56(1):27–34, 2007.
- [21] M. Abramowitz and I. A. Stegun. *Handbook of Mathematical Functions*. National Bureau of Standards, 10th. edition, 1972.
- [22] E. Mekic, M. Stefanovic, P. Spalevic, N. Sekulovic, and Ana Stankovic. Statistical Analysis of Ratio of Random Variables and Its Application in Performance Analysis of Multihop Wireless Transmissions. *Mathematical Problems in Engineering*, 2012:1–10, 2012. Hindawi Publishing.
- [23] K. D. Ward, C. J. Baker, and S. Watts. Maritime Surveillance Radar; I. Radar Scattering from the Ocean Surface. *IEE Proceedings F, Radar and Signal Processing*, 137(2):51–62, 1990.
- [24] P. Barsocchi. Channel Models for Terrestrial Wireless Communications: a Survey. Technical report, 2006.
- [25] D. Tse and P. Vishwanath. *Fundamentals of Wireless Communication*. Cambridge University Press, 2005.
- [26] Z. A. Lomnicki. On the Distribution of Products of Random Variables. *Journal of the Royal Statistical Society, Series B (Methodological)*, 29(3):513–524, 1967.

- [27] P. Galambos and I. Simonelli. *Products of Random Variables: Applications to Problems of Physics and to Arithmetical Functions*. Marcel Dekker, 2004.
- [28] S. Ahmed, L.-L. Yang, and L. Hanzo. Probability Distributions of Products of Rayleigh and Nakagami- m Variables Using Mellin Transform. pages 1–5. IEEE International Conference on Communications, ICC, 2011.
- [29] J. C. Arnbak and W. V. Blitterswijk. Capacity of Slotted ALOHA in Rayleigh-Fading Channels. *IEEE Journal on Selected Areas in Communications*, 5(2):261–269, 1987.
- [30] S. A. Al-Semari and N. Grami. A General Expression for the Capacity of Slotted ALOHA Under Nakagami Fading. volume 2, pages 849–853. IEEE Wireless Communications and Networking Conference, WCNC, 1999.
- [31] T. Pham-Gia and N. Turkkan. Distributions of Ratios of Random Variables from the Power-Quadratic Exponential Family and Applications. *Statistics*, 39(4):355–372, 2005. Taylor & Francis Journals.
- [32] B. M. G. Kibria and A. Nadarajah. Reliability Modeling: Linear Combination and Ratio of Exponential and Rayleigh. *IEEE Transactions on Reliability*, 56(1):102–105, 2007.
- [33] S. Pereira, A. Sezgin, A. Paulraj, and G. Papanicolaou. Interference Limited Broadcast: Role of Interferer Geometry. pages 757–761. IEEE International Symposium on Information Theory, ISIT, 2008.
- [34] R. Annavajjala, A. Chockalingam, and S. K. Mohammed. On a Ratio of Functions of Exponential Random Variables and Some Applications. *IEEE Transactions on Communications*, 58(11):3091–3097, 2010.
- [35] J. F. Paris and D. Morales-Jimenez. Outage Probability Analysis for Nakagami- q (Hoyt) Fading Channels under Rayleigh Interference. *IEEE Transactions on Wireless Communications*, 9(4):1272–1276, 2010.
- [36] S. Nadarajah. Distribution Properties and Estimation of the Ratio of Independent Weibull Random Variables. *Advances in Statistical Analysis, AStA*, 94(3):231–246, 2010.
- [37] S. Nadarajah. The Gamma Beta Ratio Distribution. *Brazilian Journal of Probability and Statistics*, 26(2):178–207, 2012. Brazilian Statistical Association.
- [38] M. F. Hanif, N. C. Beaulieu, and D. J. Young. Two Useful Bounds Related to Weighted Sums of Rayleigh Random Variables with Applications to Interference Systems. *IEEE Transactions on Communications*, 60(7):1788–1792, 2012.
- [39] J. Paris. Outage Probability in η - μ/η - μ and κ - μ/η - μ Interference-Limited Scenarios. *IEEE Transactions on Communications*, pages 1–9. Accepted for publication.
- [40] J. Salo, H. M. El-Sallabi, and P. Vainikainen. The Distribution of the Product of Independent Rayleigh Random Variables. *IEEE Transactions on Antennas and Propagation*, 54(2):639–643, 2006.

- [41] G. Karagiannidis, S. Nikos, and M. Takis. N*Nakagami: A Novel Stochastic Model for Cascaded Fading Channels. *IEEE Transactions on Communications*, 55(8):1453–1458, 2007.
- [42] J.-R. L. W.-B. Xu, K. Niu, and Z.-Q. Hea. Performance Analysis of ARQ Schemes with Code Combining over Nakagami- m Fading Channel. *Journal of China Universities of Posts and Telecommunications*, 16:14–19, 2009.
- [43] T. Betlehem and A. J. Coulson. Distribution of the Sum of a Complex Gaussian and the Product of Two Complex Gaussians. pages 126–129. Australian Communications Theory Workshop, AusCTW, 2012.
- [44] N. O’Donoghue and J. M. F. Moura. The complex Double Gaussian distribution. pages 3593–3596. IEEE International Conference on Acoustics, Speech and Signal Processing, ICASSP, 2012.
- [45] Y. Chen, G. K. Karagiannidis, H. Lu, and N. Cao. Novel Approximations to the Statistics of Products of Independent Random Variables and Their Applications in Wireless Communications. *IEEE Transactions on Vehicular Technology*, 61(2):443–454, 2012.
- [46] Z. Zheng, L. Wei, J. Hamalainen, and O. Tirkkonen. Approximation to Distribution of Product of Random Variables Using Orthogonal Polynomials for Lognormal Density. *IEEE Communications Letters*, 16(12):2028–2031, 2012.
- [47] A. Papoulis. *Probability, Random Variables, and Stochastic Processes*. McGraw-Hill, 3rd. edition, 1991.
- [48] I. S. Gradshteyn and I. M. Ryzhik. *Table of Integrals, Series, and Products*. Academic Press, 5th. edition, 1994.
- [49] A. P. Prudnikov, Y. A. Brychkov, and O. I. Marichev. *Integrals and Series: Special Functions*, volume 2. Gordon and Breach Science Publishers, 3rd edition, 1992.
- [50] Wolfram Research. Wolfram Functions Site, Dec. 2012. <http://functions.wolfram.com/>.
- [51] A. P. Prudnikov, Y. A. Brychkov, and O. I. Marichev. *Integrals and Series: Elementary Functions*, volume 1. Gordon and Breach Science Publishers, 4th edition, 1998.
- [52] A. P. Prudnikov, Y. A. Brychkov, and O. I. Marichev. *Integrals and Series: Special Functions, Additional Chapters (in Russian)*, volume 3. Fizmatlit, 2nd edition, 2003.
- [53] E. J. Leonardo and M. D. Yacoub. Capacity of CSMA under Nakagami Fading. pages 1–5. 7th. International Telecommunications Symposium, ITS, 2010.
- [54] R. Verdone, F. Fabbri, and C. Buratti. Area Throughput for CSMA based Wireless Sensor Networks. pages 15–18. 19th International Symposium on Personal, Indoor and Mobile Radio Communications, PIMRC, 2008.
- [55] L. Jiang and J. Walrand. A Distributed CSMA Algorithm for Throughput and Utility Maximization in Wireless Networks. pages 23–26. 6th. Annual Allerton Conference on Communications, Control, and Computing, 2008.

- [56] H. Kwon, H. Seo, S. Kim, and B.-G. Lee. Generalized CSMA/CA for OFDMA systems: Protocol Design, Throughput Analysis, and Implementation Issues. *IEEE Transactions on Wireless Communications*, 8(8):4176–4187, 2009.
- [57] C. W. Pyo and H. Harada. Throughput Analysis and Improvement of Hybrid Multiple Access in IEEE 802.15.3c mm-wave WPAN. *IEEE Journal on Selected Areas in Communications*, 27(8):1414–1424, 2009.
- [58] S. A. Qasbi and K. T. Wong. The Probability Distribution of the Carrier-to-Interference ratio (CIR) of a CSMA/CA Ad Hoc Wireless Network. volume 2, pages 996–1001. IEEE Military Communications Conference, MILCOM, 2005.
- [59] S. Choudhury and J. D. Gibson. Payload Length and Rate Adaptation for Throughput Optimization in Wireless LANs. volume 5, pages 2444–2448. IEEE 63rd. Vehicular Technology Conference, VTC-Spring, 2006.
- [60] L. Kleinrock and F. A. Tobagi. Packet Switching in Radio Channels: Part I — Carrier Sense Multiple-Access Modes and Their Throughput-Delay Characteristics. *IEEE Transactions on Communications*, 23(12):1400–1416, 1975.
- [61] J. H. Kim and J. K. Lee. Capture Effects of Wireless CSMA/CA Protocols in Rayleigh and Shadow Fading Channels. *IEEE Transactions on Vehicular Technology*, 48(4):1277–1286, 1999.
- [62] N. Zhang, B. Vojcic, M. R. Souryal, and E. G. Larsson. Exploiting Multiuser Diversity in Reservation Random Access. *IEEE Transactions on Wireless Communications*, 5(9):2548–2554, 2006.
- [63] J.-P. M. G. Linnartz, R. Hekmat, and R.-J. Venema. Near-far Effects in Land Mobile Random Access Networks with Narrow-band Rayleigh Fading Channels. *IEEE Transactions on Vehicular Technology*, 41(1):77–90, 1992.
- [64] R. Prasad and A. Kegel. Improved Assessment of Interference Limits in Cellular Radio Performance. *IEEE Transactions on Vehicular Technology*, 40(2):412–419, 1991.
- [65] E. J. Leonardo and M. D. Yacoub. Throughput of CSMA in Hoyt Fading Channels. pages 537–542. 13th. International Symposium on Wireless Personal Multimedia Communications, WPMC, 2010.
- [66] M. K. Simon and M.-S. Alouini. *Digital Communication over Fading Channels*. John Wiley & Sons, 2000.
- [67] M. A. Taneda, J. Takada, and K. Araki. The Problem of the Fading Model Selection. *IEICE Transactions on Communications*, E84-B(3):660–666, 2001.
- [68] E. J. Leonardo and M. D. Yacoub. Throughput of CSMA in Rice Fading Channels. pages 537–542. 4th. International Conference on Signal Processing and Communication Systems, ICSPCS, 2010.
- [69] E. J. Leonardo and M. D. Yacoub. Throughput of CSMA in η - μ Fading Channels. pages 537–542. 22nd. Annual IEEE International Symposium on Personal, Indoor and Mobile Radio Communications, PIMRC, 2011.

- [70] P. M. Shankar. Outage Analysis in Wireless Channels with Multiple Interferers Subject to Shadowing and Fading using a Compound PDF Model. *AEU - International Journal of Electronics and Communications*, 61(4):255–261, 2007.
- [71] M. Hadzialic, S. Colo, and A. Sarajlic. An Analytical Approach to Probability of Outage Evaluation in Gamma Shadowed Nakagami- m and Rice Fading Channel. pages 217–222. International Conference on Next Generation Mobile Applications, Services and Technologies, NGMAST, 2007.
- [72] I. Trigui, A. Laourine, S. Affes, and A. Stephenne. Performance Analysis of Mobile Radio Systems over Composite Fading/Shadowing Channels with Co-located Interference. *IEEE Transactions on Wireless Communications*, 8(7):3448–3452, 2009.
- [73] H. Tran, T. Q. Duong, and H.-J. Zepernick. Performance of a Spectrum Sharing System over Nakagami- m Fading Channels. pages 1–6. 4th International Conference on Signal Processing and Communication Systems, 2010.
- [74] R. Giacomelli, R. K. Ganti, and M. Haenggi. Outage Probability of General Ad Hoc Networks in the High-Reliability Regime. *IEEE/ACM Transactions on Networking*, 19(4):1151–1163, 2011.
- [75] E. J. Leonardo and M. D. Yacoub. Throughput of CSMA in κ - μ Fading Channels. pages 537–542. XXIX Simposio Brasileiro de Telecomunicacoes, SBrT, 2011.
- [76] E. J. Leonardo and M. D. Yacoub. Throughput of CSMA in a Rice-Signal with Hoyt-Interference Environment. pages 537–542. 2011 SBMO/IEEE MTT-S International Microwave and Optoelectronics Conference, IMOC, 2011.
- [77] E. J. Leonardo, D. B. da Costa, U. S. Dias, and M. D. Yacoub. The Ratio of Independent Arbitrary α - μ Random Variables and its Application in the Capacity Analysis of Spectrum Sharing Systems. *IEEE Communications Letters*, 16(11):1776–1779, 2012.
- [78] A. Ghasemi and E. S. Sousa. Fundamental Limits of Spectrum-Sharing in Fading Environments. *IEEE Transactions on Wireless Communications*, 6(2):649–658, 2007.
- [79] X. Kang, Y.-C. Liang, A. Nallanathan, H. K. Garg, and R. Zhang. Optimal Power Allocation for Fading Channels in Cognitive Radio Networks: Ergodic Capacity and Outage Capacity. *IEEE Transactions on Wireless Communications*, 8(2):940–950, 2009.
- [80] D. B. da Costa and U. S. Dias. On the Capacity of Spectrum Sharing Systems in Generalized Fading Scenarios. pages 17–20. IEEE Radio and Wireless Symposium, RWS, 2011.
- [81] E. J. Leonardo and M. D. Yacoub. Exact Formulations for the Throughput of IEEE 802.11 DCF in Hoyt, Rice, and Nakagami- m Fading Channels. *IEEE Transactions on Wireless Communications*. accepted for publication.
- [82] IEEE Standards. *IEEE Standard 802.11, Wireless LAN Medium Access Control (MAC) and Physical Layer (PHY) Specifications*. IEEE, 1999.
- [83] T. H. Kim, J. Ni, and N. H. Vaidya. A Distributed Throughput-Optimal CSMA with Data Packet Collisions. pages 1–6. 5th. IEEE Workshop Wireless Mesh Networks, 2010.

- [84] J. Ghaderi and R. Srikant. On the Design of Efficient CSMA Algorithms for Wireless Networks. pages 954–959. 49th. IEEE Conference on Decision and Control, 2010.
- [85] Y. Chang, C. P. Lee, and J. A. Copeland. Goodput Enhancement of VANETs in Noisy CSMA/CA Channels. *IEEE Journal on Selected Areas in Communications*, 29(1):236–249, 2011.
- [86] H. C. Lee. A MAC Throughput over Rayleigh Fading Channel in the 802.11a/g/n-based Mobile LAN. pages 1–7. International Conference Elect. Eng. and Inform., 2011.
- [87] J. Dai and Y. Yamao. CSMA/CA Performance under Fading Environment with Two-Dimensional Distribution of Hidden Terminal. pages 1–5. IEEE 63rd. Vehicular Technology Conference, VTC 2011-Fall, 2011.
- [88] H. Cheng and Y. Yamao. Performance Analysis of CSMA/CA Broadcast Relay Network for ITS V2V Communications. pages 1–5. IEEE 75th. Vehicular Technology Conference, VTC 2012-Spring, 2012.
- [89] IEEE Standards. *IEEE Standard 802.15.4, Local and Metropolitan Area Networks, Low-Rate Wireless Personal Area Networks (LR-WPANs)*. IEEE, 2011.
- [90] IEEE Standards. *IEEE Standard 802.15.6, Local and Metropolitan Area Networks, Wireless Body Area Networks*. IEEE, 2012.
- [91] F. Daneshgaran, M. Laddomada, F. Mesiti, and M. Mondin. Unsaturated Throughput Analysis of IEEE 802.11 in Presence of Non Ideal Transmission Channel and Capture Effects. *IEEE Transactions on Wireless Communications*, 7(7):1276–1286, 2008.
- [92] G. Bianchi. Performance Analysis of the IEEE 802.11 Distributed Coordination Function. *IEEE Journal on Selected Areas in Communications*, 18(3):535–547, 2000.
- [93] Y. S. Liaw, A. Dadej, and A. Jayasuriya. Performance Analysis of IEEE 802.11 DCF under Limited Load. pages 759–763. Asia-Pacific Conference on Communications, 2005.
- [94] D. Morales-Jimenez and J. F. Paris. Outage Probability Analysis for η - μ Fading Channels. *IEEE Communications Letters*, 14(6):521–523, 2010.
- [95] A. Kochut, A. Vasan, A. U. Shankar, and A. Agrawala. Sniffing out the Correct Physical Layer Capture Model in 802.11b. pages 252–261. 12th. IEEE International Conference on Network Protocols, 2004.
- [96] J. Lee, W. Kim, S.-J. Lee, D. Jo, J. Ryu, T. Kwon, and Y. Choi. An Experimental Study on the Capture Effect in 802.11a Networks. pages 19–26. 2nd. ACM Workshop on Wireless Network Testbeds, Experimental Evaluation and Characterization, 2007.
- [97] A. Iyer, C. Rosenberg, and A. Karnik. What is the Right Model for Wireless Channel Interference? *IEEE Transactions on Wireless Communications*, 8(5):2662–2671, 2009.
- [98] A. Chehri, P. Fortier, and P. M. Tardif. Throughput-Delay Trade-Off for Slotted Aloha Multiple Access with Capture Effect. *Journal of Computer Science*, 5(9):630–634, 2009.

-
- [99] A. Sunny, J. Kuri, and S. Aggarwal. Delay Modelling for a Single-hop Wireless Mesh Network under Light Aggregate Traffic. pages 271–275. International Conference on Communications and Signal Processing, 2011.
- [100] S. H. Nguyen, H. L. Vu, and L. L. H. Andrew. Performance Analysis of IEEE 802.11 WLANs With Saturated and Unsaturated Sources. *IEEE Transactions on Vehicular Technology*, 61(1):333–345, 2012.
- [101] I. McLean and K. Christensen. Reducing Energy Use: A Dual-Channel Link. *IEEE Communications Letters*, 16(3):411–413, 2012.
- [102] J. Misic, S. Rashwand, and V. B. Misic. Analysis of Impact of TXOP Allocation on IEEE 802.11e EDCA under Variable Network Load. *IEEE Transactions on Parallel and Distributed Systems*, 23(5):785–799, 2012.
- [103] Wolfram Research. Mathematica, 2003.
- [104] A. Wojnar. Unknown Bounds on Performance in Nakagami Channels. *IEEE Transactions on Communications*, 34(1):22–24, 1986.